Vibration based gear wear monitoring and prediction

Author:
Feng, Ke

Publication Date:
2021

DOI:
https://doi.org/10.26190/unsworks/2329

Vibration Based Gear Wear Monitoring and Prediction

Ke Feng

A thesis in fulfilment of the requirements for the degree of

Doctor of Philosophy

School of Mechanical and Manufacturing Engineering

Faculty of Engineering

University of New South Wales, Australia

August 2021

Thesis/Dissertation Sheet

Surname/Family Name	:	**Feng**
Given Name/s	:	**Ke**
Abbreviation for degree as give in the University calendar	:	**PhD**
Faculty	:	**Engineering**
School	:	**School of Mechanical and Manufacturing Engineering**
Thesis Title	:	**Vibration Based Gear Wear Monitoring and Prediction**

Abstract 350 words maximum:

Gear wear is an inevitable phenomenon during gear service life. Its propagation would impair the durability of gear tooth and reduce the remaining useful life of gear transmission system. Therefore, monitoring and predicting gear wear progression can bring significant benefits to industrial practice. Vibration analysis responds immediately to changes in the machine state (health and operating condition) and can therefore be used for gear monitoring. However, vibration-based techniques for gear wear monitoring are rather rare, even though techniques have been well established for detection and diagnosis of common gear faults such as gear tooth root cracks and tooth breakage. Therefore, in this research, a vibration-based integrated system is developed for gear wear monitoring and prediction. The developments were carried out in two stages: (i) wear mechanism identification using measured vibrations, and (ii) wear propagation monitoring and prediction using the integration of models, measurements and model updating approaches.

In the first stage, the correlation between surface features and vibration characteristics is investigated. Then, use of cyclostationary properties of vibrations, a vibration-based online gear wear mechanism identification methodology is developed. Moreover, the evolution of fatigue pitting and abrasive wear (micro-level) are tracked using an indicator of second-order cyclostationarity of vibrations in specific spectral bands.

In the second stage, a digital-twin system is developed by the integration of (i) a dynamic model to simulate the dynamic responses of gear system; (ii) two tribological (wear) models for estimation of wear depth and pitting density, and (iii) model updating through comparing simulation and measured vibrations. The integration of dynamic model and tribological models allow a knowledge-based wear prediction of the gear profile change (determined by the wear depth) and pitting density. With the regularly model updating using measured vibrations, the wear process can be well monitored, and the best possible prediction of remaining useful life can be achieved.

The above developments provide effective and efficient tools for monitoring and prediction of gear wear, in particular, the profile change and pitting density, which is critical for making appropriate maintenance decisions to maximise the useful life of gears and to avoid catastrophic failures and unexpected economic losses.

Thesis/Dissertation Sheet

Declaration relating to disposition of project thesis/dissertation

I hereby grant to the University of New South Wales or its agents a non-exclusive licence to archive and to make available (including to members of the public) my thesis or dissertation in whole or in part in the University libraries in all forms of media, now or here after known. I acknowledge that I retain all intellectual property rights which subsist in my thesis or dissertation, such as copyright and patent rights, subject to applicable law. I also retain the right to use all or part of my thesis or dissertation in future works (such as articles or books).

18/08/2021

……………………………………………

Date

……………………………………………………………

Signature

The University recognises that there may be exceptional circumstances requiring restrictions on copying or conditions on use. Requests for restriction for a period of up to 2 years can be made when submitting the final copies of your thesis to the UNSW Library. Requests for a longer period of restriction may be considered in exceptional circumstances and require the approval of the Dean of Graduate Research.

INCLUSION OF PUBLICATIONS STATEMENT

UNSW is supportive of candidates publishing their research results during their candidature as detailed in the UNSW Thesis Examination Procedure.

Publications can be used in their thesis in lieu of a Chapter if:

- The candidate contributed greater than 50% of the content in the publication and is the "primary author", ie. the candidate was responsible primarily for the planning, execution and preparation of the work for publication
- The candidate has approval to include the publication in their thesis in lieu of a Chapter from their supervisor and Postgraduate Coordinator.
- The publication is not subject to any obligations or contractual agreements with a third party that would constrain its inclusion in the thesis

Please indicate whether this thesis contains published material or not:

☐ This thesis contains no publications, either published or submitted for publication
(if this box is checked, you may delete all the material on page 2)

☒ Some of the work described in this thesis has been published and it has been documented in the relevant Chapters with acknowledgement
(if this box is checked, you may delete all the material on page 2)

☐ This thesis has publications (either published or submitted for publication) incorporated into it in lieu of a chapter and the details are presented below

CANDIDATE'S DECLARATION

I declare that:

- I have complied with the UNSW Thesis Examination Procedure
- where I have used a publication as a Chapter, the listed publication(s) below meet(s) the requirements to be included in the thesis.

Candidate's Name	Signature	Date (dd/mm/yy)
Ke Feng		18/08/2021

For each publication incorporated into the thesis, provide all of the requested details and signatures required

INCLUSION OF PUBLICATIONS STATEMENT

Details of publication #1: *Full title: Use of cyclostationary properties of vibration signals to identify gear wear mechanisms and track wear evolution* *Authors: Ke Feng, Wade A. Smith, Pietro Borghesani, Robert B. Randall and Zhongxiao Peng* *Journal or book name: Mechanical Systems and Signal Processing* *Volume/page numbers: 150: 107258* *Date accepted/ published:28 August 2020*						
Status	*Published*	✓	*Accepted and In press*		*In progress (submitted)*	
The Candidate's Contribution to the Work Ke Feng is the lead and the corresponding author. Ke Feng made a significant contribution to conceptualization, methodology, formal analysis, investigation, and writing to this work published in the best journal in the field of vibration.						
Location of the work in the thesis and/or how the work is incorporated in the thesis: Location: Chapter 4. The main content of Chapter 4 is identical to the above publication, while the structure has been arranged to ensure the consistency of the thesis.						
PRIMARY SUPERVISOR'S DECLARATION I declare that: • the information above is accurate • All of the co-authors of the publication have reviewed the above information and have agreed to its veracity by signing a 'Co-Author Authorisation' form.						
Primary Supervisor's name Zhongxiao Peng		**Primary Supervisor's signature**			**Date (dd/mm/yy)** 18/08/2021	

Details of publication #2: *Full title: Vibration-based updating of wear prediction for spur gears* *Authors: Ke Feng, Pietro Borghesani, Wade A. Smith, Robert B. Randall, Zhan Yie Chin, Jinzhao Ren, and Zhongxiao Peng* *Journal or book name: Wear* *Volume/page numbers: 426-427: 1410-1415* *Date accepted/ published: 03 January 2019*						
Status	*Published*	✓	*Accepted and In press*		*In progress (submitted)*	
The Candidate's Contribution to the Work Ke Feng is the first and the corresponding author. Being the lead author, Ke Feng made a major contribution to conceptualization, methodology, formal analysis, investigation, and writing to this publication in a top journal in the field of tribology.						
Location of the work in the thesis and/or how the work is incorporated in the thesis:						

INCLUSION OF PUBLICATIONS STATEMENT

Location: Chapter 5 and Chapter 6.

Compared with publication #2, more details on the model establishment and model validation are included in Chapter 5.

Some parts of Chapter 6 are from publication #2, and the structure has been re-arranged to ensure the consistency of the thesis.

PRIMARY SUPERVISOR'S DECLARATION

I declare that:

- the information above is accurate
- All of the co-authors of the publication have reviewed the above information and have agreed to its veracity by signing a 'Co-Author Authorisation' form.

Primary Supervisor's name	Primary Supervisor's signature	Date (dd/mm/yy)
Zhongxiao Peng		18/08/2021

Details of publication #3:

Full title: *Use of an improved vibration-based updating methodology for gear wear prediction*

Authors: *Ke Feng, Wade A. Smith and Zhongxiao Peng*

Journal or book name: *Engineering Failure Analysis*

Volume/page numbers: *120: 105066*

Date accepted/ published: *04 November 2020*

Status	Published	✓	Accepted and In press		In progress (submitted)	

The Candidate's Contribution to the Work

Ke Feng is the lead and the corresponding author. Ke Feng made a leading contribution on conceptualization, methodology, formal analysis, investigation, and writing - original draft.

Location of the work in the thesis and/or how the work is incorporated in the thesis:

Location: Chapter 6.

The main content of Chapter 6 is identical to publications #2 and #3, while the structure of this chapter has been arranged to ensure the consistency of the thesis.

PRIMARY SUPERVISOR'S DECLARATION

I declare that:

- the information above is accurate
- All of the co-authors of the publication have reviewed the above information and have agreed to its veracity by signing a 'Co-Author Authorisation' form.

Primary Supervisor's name	Primary Supervisor's signature	Date (dd/mm/yy)
Zhongxiao Peng		18/08/2021

INCLUSION OF PUBLICATIONS STATEMENT

Details of publication #4: *Full title: Vibration-based monitoring and prediction of surface profile change and pitting density in a spur gear wear process* *Authors: Ke Feng, Wade A. Smith, Robert B. Randall, Hongkun Wu and Zhongxiao Peng* *Journal or book name: Mechanical Systems and Signal Processing* *Volume/page numbers: 165: 108319* *Date accepted/ published: 10 August 2021*					
Status	*Published*	✓	*Accepted and In press*		*In progress (submitted)*

The Candidate's Contribution to the Work
Ke Feng is the lead and the corresponding author. Ke Feng made a significant contribution to the conceptualization, methodology, formal analysis, investigation, and writing of the research work.
Location of the work in the thesis and/or how the work is incorporated in the thesis: Location: Chapter 7. The main content of Chapter 7 is identical to the above publication, while the structure has been arranged to ensure the consistency of the thesis.
PRIMARY SUPERVISOR'S DECLARATION I declare that: • the information above is accurate • All of the co-authors of the publication have reviewed the above information and have agreed to its veracity by signing a 'Co-Author Authorisation' form.

Primary Supervisor's name	**Primary Supervisor's signature**	**Date (dd/mm/yy)**
Zhongxiao Peng		18/08/2021

ORIGINALITY STATEMENT

'I hereby declare that this submission is my own work and to the best of my knowledge it contains no materials previously published or written by another person, or substantial proportions of material which have been accepted for the award of any other degree or diploma at UNSW or any other educational institution, except where due acknowledgement is made in the thesis. Any contribution made to the research by others, with whom I have worked at UNSW or elsewhere, is explicitly acknowledged in the thesis. I also declare that the intellectual content of this thesis is the product of my own work, except to the extent that assistance from others in the project's design and conception or in style, presentation and linguistic expression is acknowledged.'

Signed ……………………………………………..............

Date ……………………………………………..............

COPYRIGHT STATEMENT

Signed ……………………………………………..........................

Date ……………………………………………..............................

AUTHENTICITY STATEMENT

‘I certify that the Library deposit digital copy is a direct equivalent of the final officially approved version of my thesis.’

Signed ……………………………………………..........................

Date ……………………………………………..............................

Abstract

Gear wear is an inevitable phenomenon during gear service life. Its propagation impairs the durability of gear teeth and reduces the remaining useful life of gear transmission systems. Therefore, monitoring and predicting gear wear progression can bring significant benefits to industrial practice. Machine vibration responses reflect immediately the changes in the machine state (health and operating condition) and therefore provide a promising tool for gear condition monitoring. However, there is a coupling effect between gear wear and system dynamics, which results in the generation of vibrations with high complexity and brings significant challenges to the development of specific vibration techniques for extracting wear-related vibration features (indicators). Thus, vibration-based techniques for gear wear monitoring are rather rare, although techniques have been well established for the detection and diagnosis of common gear faults such as gear tooth root cracks and tooth breakage. Therefore, in this research, a vibration-based integrated system is developed for gear wear monitoring and prediction. The developments are carried out in two stages: (i) wear mechanism identification using measured vibrations, and (ii) wear propagation monitoring and prediction using the integration of models, measurements and model updating approaches.

Different gear wear mechanisms have different impacts on the gear tooth surface and result in different vibration characteristics, therefore, identifying gear wear mechanisms is a necessary procedure for developing proper gear wear monitoring techniques. Thus, in the first stage of this research, a vibration-based gear wear mechanism identification methodology is presented. More specifically, with consideration of the underlying physics of the gear meshing process and the unique surface features induced by fatigue pitting and abrasive wear, the correlation between surface features and vibration characteristics is investigated. The connection between the spatial frequency of the gear surface and the spectral frequency of the measured vibrations is established. With this established connection as the basis, a vibration-based online gear wear mechanism identification methodology is developed using cyclostationary properties of vibrations. Moreover, the evolution of fatigue pitting and abrasive wear (micro-level) are tracked using an indicator of second-order cyclostationarity of vibrations in specific spectral bands. Differently from previous works, the carrier frequencies (spectral content) of the gearmesh-cyclic second-order cyclostationary components are analysed and used to distinguish and track the two wear phenomena in this research.

With the identified specific gear wear mechanisms/events in the first stage, in the second stage of this research, a digital-twin system is developed by the integration of (i) a dynamic model to simulate the dynamic responses of the gear system; (ii) two tribological (wear) models for estimation of wear depth and pitting density, and (iii) model updating through comparing simulated and measured vibrations. More specifically, a 21-degree-of-freedom dynamic model is developed to simulate a spur gearbox setup and produce simulated vibrations and contact forces between the meshing gear teeth. Using the contact pressure (calculated from the force) as an input, the wear depth and pitting density are then predicted by the tribological models and used to modify the gear geometry profile and contact area in the dynamic model. The integration of the dynamic model and tribological models allows a knowledge-based wear prediction of the gear profile change (determined by the wear depth) and pitting density. To guarantee accurate prediction results from the models, novel approaches are developed to update the wear coefficients in the tribological models by comparing simulated and measured vibrations. With regular model updating, the wear process can be well monitored, and the best possible wear prediction can be achieved, facilitating vastly improved estimates of the system's remaining useful life.

The effectiveness of the developed methods in gear wear monitoring and prediction is validated using vibration data collected in two tests: a lubricated test dominated by fatigue pitting and a dry test dominated by abrasive wear.

In summary, this thesis has made the following main contributions to the research field:

- A vibration-based method is proposed for identifying two common gear wear mechanisms (abrasion and surface fatigue). This development is based on the cyclostationary analysis technique, and it is applied for the first time to analyse wear-related low energy phenomena (friction, asperity contacts) in vibration signals.
- Another important contribution of this research is the development of vibration features coupled with wear information for identification of the dominant wear modes (abrasive wear and contact fatigue) and tracking of their evolution.
- A novel vibration-based scheme for updating and prediction of abrasive wear of gears is developed in this research.
- A new approach is proposed to calculate the wear depth distribution of gears. And gear wear under different lubrication conditions is accurately predicted.

- Novel gear surface degradation prediction models and schemes are proposed in this research. Through regular and intelligent use of measured vibration signals, the models can be updated as necessary, ensuring accurate predictions of gear wear (both abrasion and fatigue pitting) propagation can be delivered.

The above developments provide effective and efficient tools for the monitoring and prediction of gear wear, in particular, the profile change and pitting density, which is critical for making appropriate maintenance decisions to maximize the useful life of gears and to avoid catastrophic failures and unexpected economic losses.

List of publications

Journal papers:

- * **Ke Feng**, Pietro Borghesani, Wade A. Smith, Robert B. Randall, Zhan Yie Chin, Jinzhao Ren, and Zhongxiao Peng. “Vibration-based updating of wear prediction for spur gears.” *Wear* 426 (2019): 1410-1415.
- * **Ke Feng**, Wade A. Smith, Pietro Borghesani, Robert B. Randall, and Zhongxaio Peng. “Use of cyclostationary properties of vibration signals to identify gear wear mechanisms and track wear evolution.” *Mechanical Systems and Signal Processing* 150 (2021): 107258.
- * **Ke Feng**, Wade A. Smith, and Zhongxaio Peng. “Use of an improved vibration-based updating methodology for gear wear prediction.” *Engineering Failure Analysis* 120 (2021): 105066.
- * **Ke Feng**, Wade A. Smith, Robert B. Randall, Hongkun Wu, and Zhongxiao Peng. “Vibration-based monitoring and prediction of surface profile change and pitting density in a gear wear process.” *Mechanical Systems and Signal Processing* 165 (2022): 108319.

Conference paper:

- Yeujian Chen, **Ke Feng**, Robert B. Randall, Pietro Borghesani, Ming J Zuo. "Use of Autoregressive Conditional Heteroskedasticity Model to Assess Gear Tooth Surface Roughness." *2020 Asia-Pacific International Symposium on Advanced Reliability and Maintenance Modeling (APARM)* 20 (2020): 1-4.

Acknowledgements

To my supervisor, Prof. Zhongxiao Peng, for your invaluable mentorship. Thank you for offering me the opportunity to join the Tribology and Machine Condition Monitoring Group. From the PhD scholarship application to the thesis writing, you always provide strong support to me. Also, the weekly meeting helps me gain valuable academic knowledge. Thank you for your encouragement and patience to help me overcome the obstacles I encountered in my research project.

To my joint supervisor, Dr. Wade Smith, for your strong support and countless help. The discussions with you always benefit me so much. When I was stuck, you always be there to provide suggestions to me and help me out.

To my co-supervisor, Emeritus Professor Robert Randall, for your intelligent guidance, endless patience and insightful suggestions. I’ve learnt a lot from your modest and friendly attitude in both research and daily life, which will be a valuable treasure for the rest of my academic career.

To my co-supervisor, Dr. Pietro Borghesani, for your valuable suggestions on my research. With your help, there is no doubt that the quality of my research work has been improved significantly.

I am also grateful to all the members of our Tribology and Machine Condition Monitoring Group at UNSW for their help and support. We share tears and laughter, which is a cherished memory for me.

This work is dedicated to my family and my girlfriend, Miss Qing Ni. Thanks to them for their selfless support and care.

Contents

Abstract i

List of publications v

Acknowledgements vii

List of Figures xv

List of Tables xxiii

Abbreviations xxv

Chapter 1 Introduction 1

1.1 Background 1

1.2 Research goals 3

1.3 Structure of this thesis 4

Chapter 2 Literature review 7

2.1 Gear wear 7

2.1.1 Gear wear modes 7

2.1.2 Differences between abrasive wear and fatigue pitting 10

2.2 Gear wear effects on vibrations of gear systems 12

2.3 Use of vibration features for gear wear monitoring 15

2.3.1 Vibration feature-based wear evolution tracking 15

2.3.2 Vibration feature-based wear mechanism identification........................... 21

2.4 Model-based gear wear monitoring techniques... 22

2.4.1 Dynamic models of spur gearboxes 23

2.4.2 Tribological (wear) models for monitoring wear depth and pitting density 26

2.4.3 Integration of dynamic and tribological models for gear wear monitoring 30

2.5 Wear prediction techniques 31

2.5.1 Prediction of tooth profile change from abrasive wear 31

2.5.2 Prediction of surface pitting propagation... 35

2.5.3 Research gaps... 37

2.6 Summary 38

Chapter 3 Methodology 40

3.1 The overall strategy of the vibration-based integrated system for gear wear monitoring 41

3.2 Experimental research facilities and test programs 43

3.2.1 Spur gearbox at University of New South Wales 43

3.2.2 Wear tests and data collection ... 44

3.3 Gear wear mechanism identification and wear evolution tracking using cyclostationary properties of vibrations (objective 1) ... 49

3.4 Model-based gear wear monitoring and prediction methodology ... 52

3.4.1 Super gearbox dynamic model development (objective 2) ... 53

3.4.2 Monitoring and prediction of tooth profile changes from abrasive wear (objective 3) ... 54

3.4.3 Monitoring and prediction of surface pitting propagation and tooth profile change from abrasive wear using a digital twin approach (objective 4) ... 56

Chapter 4 Identification of gear wear mechanisms and tracking wear evolution using cyclostationary properties of measured vibrations ... 61

4.1 Introduction ... 62

4.2 Hypothesis and proposed vibration-based approach for gear wear identification ... 65

4.2.1 Surface feature differences and their effects on sliding vibrations ... 65

4.2.2 Hypothesis for wear mechanism identification ... 67

4.2.3 Proposed vibration-based approach for wear mechanism identification ... 70

4.3 Observations in gear systems ... 71

4.3.1 Tribological features used to describe fatigue pitting and abrasive wear propagation ... 71

4.3.2 Theory of vibration-based wear mechanism identification techniques ... 72

4.3.3 Observation results ... 75

4.4 A new vibration-based procedure for comprehensive gear wear monitoring: mechanism identification and severity tracking..87

4.5 Summary 96

Chapter 5 Dynamic model development 97

5.1 Introduction 97

5.2 Dynamic model structure 99

5.2.1 Meshing stiffness and damping coefficient of gear system 104

5.2.2 Geometric transmission error...107

5.2.3 Dynamic simulation process 108

5.3 Model validation and calibration...111

5.4 Summary 122

Chapter 6 Monitoring and prediction of tooth profile changes during wear progression 124

6.1 Introduction 125

6.2 Methodology for monitoring and predicting tooth profile change from wear 127

6.2.1 The proposed vibration-based approach for monitoring and predicting tooth profile change...127

6.2.2 Dynamic model 128

6.2.3 Wear model for simulating tooth profile change 129

6.2.4 Updating methodology...133

6.3 Tooth profile change prediction results 134

6.3.1 Dry test 135

6.3.2 Lubricated test 137

6.4 Summary 140

Chapter 7 Development of a digital twin approach for monitoring and prediction of surface pitting and tooth profile changes 142

7.1 Introduction 143

7.2 Relationships of vibration features and wear features 145

7.3 Methodology for monitoring and predicting surface pitting and tooth profile change 147

7.3.1 Structure of the proposed vibration-based surface degradation prediction methodology 147

7.3.2 Wear models: modelling surface pitting behaviours 150

7.3.3 Model updating procedures using measured vibrations 153

7.4 Test and Results 157

7.4.1 Monitoring and prediction of surface pitting and mild tooth profile change during the lubricated test 158

7.4.2 Monitoring and prediction of severe tooth profile change during the dry test 170

7.5 Summary 176

Chapter 8 Conclusions and future work 178

8.1 Summary of findings and contribution to research 178

8.2 Recommendations for future work 182

References 184

List of Figures

Figure 2.1 Extremely worn gear due to abrasive particles in lubricant [19] 8

Figure 2.2 Fatigue pitting [19] 9

Figure 2.3 Typical scuffing failure in gears [20]. Note: only one instance of scuffing is indicated in this figure for demonstration purposes 9

Figure 2.4 Corrosion damage [18]. Note: only one instance of corrosion damage is indicated in this figure for demonstration purposes 10

Figure 2.5 Deviations from ideal tooth profile due to abrasive wear [22] 11

Figure 2.6 Typical vibration spectrum due to wear [22] 13

Figure 2.7 Second-order cyclostationary (CS2) signal generation from varying sliding velocity in mating gears; (a) number of tooth pairs in contact; (b) approximate sliding velocity; (c) possible amplitude-modulated random signal (CS2) generated from varying sliding velocity (N = number of teeth on the gear) [15] 19

Figure 2.8 Dynamic model of a spur gearbox [54] 24

Figure 3.1 The schematic diagram of the research methodology 42

Figure 3.2 The spur gear test rig at University of New South Wales (UNSW): (a) Overall view; (b) Detail of the gearbox; (c) A schematic diagram of the setup [16] 44

Figure 3.3 The initial surface of the pinion gear that was artificially roughened using sandpaper before conducting the test with lubrication..46

Figure 3.4 Gear pair and mould making (in lubricated test)..47

Figure 3.5 Gear surfaces after the lubricated test: (a) Appearance of the pinion; (b) An image of a mould of a pinion tooth surface with fatigue pitting....................................47

Figure 3.6 The initial pinion surface before the dry test..47

Figure 3.7 Gear pair and adhesive paper (in dry test)..48

Figure 3.8 Gear surfaces after the dry test: (a) Appearance of the pinion; (b) An image of a mould of a pinion tooth surface with abrasive wear 48

Figure 3.9 The schematic diagram of the vibration-based wear mechanism identification and evolution tracking...51

Figure 3.10 The skeleton of the model-based gear wear monitoring and prediction......53

Figure 3.11 Basic procedures of the proposed vibration-based updating scheme for tooth profile change (from abrasive wear) predictions 56

Figure 3.12 Basic procedures of the proposed vibration-based updating scheme for fatigue pitting propagation predictions 58

Figure 3.13 Basic procedures of the proposed digital twin approach for monitoring and prediction of surface pitting and tooth profile changes from abrasive wear..................59

Figure 4.1 Changes to gear surface morphologies in abrasive wear process and in the micro-scale: (a) a new surface; (b) a worn surface subjected to abrasive wear.............66

Figure 4.2 Changes to gear surface morphologies in a fatigue pitting process and the micro-scale: (a) a new surface; (b) a pitted surface 66

Figure 4.3 The fatigue pitting induced sliding vibration characteristics 69

Figure 4.4 The abrasive wear induced sliding vibration characteristics 69

Figure 4.5 Diagram of vibration-based gear wear mechanism identification approach . 70

Figure 4.6 Diagram to illustrate the hypothesis: increase in second-order cyclostationarity due to an increase in surface roughness (induced by fatigue pitting or abrasive wear) .. 73

Figure 4.7 Lubricated test: (a) Carrier frequency distribution at gear mesh (cyclic) frequency; (b) Top view 75

Figure 4.8 Lubricated test: ICS2-based band selection results 77

Figure 4.9 Figure pitting evolution on the dedendum of pinion tooth [128] 78

Figure 4.10 3D images of fatigue pitting propagation in the lubricated test................... 79

Figure 4.11 PSD analysis results of the scanned images of the lubricated test in Figure 4.10 80

Figure 4.12 Carrier frequency distribution at gear mesh (cyclic) frequency at different speeds (top views) of lubricated test: (a) input speed: 10 Hz; (b) input speed: 16 Hz; (c) input speed: 20 Hz 82

Figure 4.13 Mean carrier frequency with different rotating speeds of lubricated test: (a) frequency range: 0-30 kHz; (b) frequency range: 0-50 kHz 83

Figure 4.14 Dry test: (a) Carrier frequency distribution at gear mesh (cyclic) frequency; (b) Top view 84

Figure 4.15 Dry test: ICS2-based band selection result 85

Figure 4.16 3D images of abrasive wear propagation in the dry test....86

Figure 4.17 PSD analysis results of the 3D images shown in Figure 4.16....87

Figure 4.18 Proposed guideline of vibration-based comprehensive gear wear monitoring....88

Figure 4.19 Performance of ICS2 in wear severity tracking....89

Figure 4.20 Classical indicators performance in the lubricated test: (a) RMS of raw signal; (b) kurtosis of raw signal; (c) RMS of residual signal; (d) kurtosis of residual signal; (e) 1st gear mesh frequency....91

Figure 4.21 Lubricated test: correlation between ICS2 and pitted area....92

Figure 4.22 Dry test: correlation between ICS2 and surface roughness....93

Figure 4.23 Classical indicators performance in the dry test: (a) RMS of raw signal; (b) kurtosis of raw signal; (c) RMS of residual signal; (d) kurtosis of residual signal; (e) 1st gear mesh frequency....94

Figure 4.24 Performance of RMS of raw signal in tracking wear depth change (obtained from wear particle)....95

Figure 5.1 Spur gearbox test rig with each labelled modelling component....100

Figure 5.2 21 DOFs lumped dynamic model of UNSW test rig....100

Figure 5.3 Single tooth pair meshing stiffness....106

Figure 5.4 Gear systems: (a) gear contact mechanism; (b) deflections between mating teeth; (c) gear dynamic contact force....107

Figure 5.5 Gear state-space dynamic model....109

Figure 5.6 Dynamic model in Simulink® simulation environment: overall structure .109

Figure 5.7 Dynamic model in Simulink® simulation environment: gear contact part . 110

Figure 5.8 Dynamic model in Simulink® simulation environment: single tooth pair contact 110

Figure 5.9 Measured vibration during the spur gearbox ramp test: (a) rotational speed; (b) measured vibrations 112

Figure 5.10 PSD analysis of the vibrations of the spur gear system 112

Figure 5.11 Demonstration of quadrature picking method [168] 114

Figure 5.12 Harmer test on gearbox's foundation 115

Figure 5.13 The first four mode shapes of the gearbox's foundation 116

Figure 5.14 Frequency Response Function (FRF) of the gearbox's foundation 117

Figure 5.15 Meshing stiffness curve 118

Figure 5.16 Vibration signal: (a) experiment and (b) simulation 120

Figure 5.17 Five-gearmesh teeth: (a) experiment and (b) simulation 120

Figure 5.18 Dynamic contact force (from gear root to tip) 122

Figure 6.1 Basic procedures of the proposed vibration-based scheme for updating wear predictions 128

Figure 6.2 The wear depth at contact point #6: including the effects coming from adjacent contact points 131

Figure 6.3 Wear depth distribution 132

Figure 6.4 Contact pressure distribution: there are some peaks corresponding to each contact point 132

Figure 6.5 Dry test: RMS (in mm/s) versus the number of wear cycles from the experimental testing and the results from simulations (after updating)........................136

Figure 6.6 Wear depth comparison results of dry test: experiment (from wear particles) and model (after updating)..136

Figure 6.7 Lubricated test: RMS (in mm/s) versus the number of wear cycles from the experimental testing and the results from simulations (after updating)........................138

Figure 6.8 3D image of the mould profile collected from pinion (SAP: start of active profile, EAP: end of active profile)..138

Figure 6.9 The tooth profiles of pinion (SAP: start of active profile, EAP: end of active profile)..139

Figure 6.10 Wear depth comparison results of lubricated test: experiment (from moulding technique) and model (after updating) 139

Figure 7.1 Basic procedure of vibration-based updating methodology for gear wear prediction...149

Figure 7.2 3D image of the mould profile collected from pinion at 0.35 million cycles (SAP: start of active profile, EAP: end of active profile) during the lubricated test 159

Figure 7.3 Lubricated test: The average profiles of pinion at different running cycles (see the locations of SAP and EAP in Figure 7.2)...159

Figure 7.4 Lubricated test: Pitting density of pinion obtained from moulds: red dots represent: 0.12 million cycles, when surface pitting was detected; 2.12 million cycles, the point of maximum pitting density; and 3.25 million cycles, the end of the test...........160

Figure 7.5 Changes in gear mesh harmonics of measured vibrations during the lubricated test (the first ten gear mesh harmonics) 161

Figure 7.6 Lubricated test: $\mathrm{RMS_{SA}}$ $(\mathrm{N}=2)$ of measured vibrations and wear depth change obtained from mould images as shown in Figure 7.3 162

Figure 7.7 Lubricated test: $\mathrm{RMS_{SA}}$ $(\mathrm{N}=2)$ of measured vibrations and measured pitting density as shown in Figure 7.4 163

Figure 7.8 $\mathrm{RMS_{SA}}$ (N=2) comparison results of the lubricated test: experiment and model 164

Figure 7.9 Mean wear depth comparison results of the lubricated test: experiment and model. Note: grey dashed lines indicate when updates are executed 165

Figure 7.10 Lubricated test: Optical images of pinion tooth surfaces taken from moulds by optical microscope with a 5× magnification objective lens. Image size: 2.8mm ×2.11 mm (a) 0.1296 million cycles, (b) 0.8178 million cycles, (c) 1.7175 million cycles [142] 166

Figure 7.11 Diagram of pitting density calculation using surface pitting model: pitch line is at 0 rad and indicated by red vertical dash line 167

Figure 7.12 Comparison results: ICS2 of measured vibration and predicted pitting density based on model (after updating)... 169

Figure 7.13 Pitting density comparison results: experiment and model-based prediction. Note: grey dashed lines indicate when updates are executed 170

Figure 7.14 Gear tooth profile and surface morphology of the dry test at 0 and 0.04 million cycles (SAP: start of active profile, EAP: end of active profile) 171

Figure 7.15 Changes in gear mesh harmonics during the dry test (the first ten gear mesh harmonics).. 173

Figure 7.16 Dry test: measured $\mathrm{RMS}_{\mathrm{SA}}$ $(\mathrm{N} = 6)$ and measured wear depth based on collected wear particles 173

Figure 7.17 $\mathrm{RMS}_{\mathrm{SA}}$ comparison results of the dry test: experiment and model (after updating) 174

Figure 7.18 Mean wear depth comparison results of the dry test: experiment and model. Note: grey dashed lines indicate when updates are executed 174

Figure 7.19 Dry test: ICS2 of measured vibrations.. 175

List of Tables

Table 2.1 Differences between abrasive wear and fatigue pitting 11

Table 2.2 Effects of wear on vibrations [14, 15, 22, 29]... 14

Table 2.3 Studies of vibration feature-based gear wear evolution tracking................... 20

Table 3.1 Settings of lubricated test and dry test 49

Table 4.1 Correlation analysis results of vibration indicators with tribological parameter for the lubricated test... 92

Table 4.2 Correlation analysis results of vibration indicators with the surface roughness of the dry test.. 95

Table 5.1 Basic parameters of the spur gearbox test rig 99

Table 5.2 Mass and inertia of the dynamic model of spur gearbox systems 103

Table 5.3 Stiffness and damping of the dynamic model of spur gearbox systems 104

Table 5.4 Identified natural frequencies from the PSD analysis of experimental measurements 113

Table 5.5 Natural frequency comparison results of dynamic model and experimental data 118

Abbreviations

AGMA	American Gear Manufacturing Association
ALR	Averaged logarithmic ratio
ANN	Artificial neural network
AR	Auto-gressive
BP	Back propagation
CS2	Second-order cyclostationary
DT	Digital twin
DOF	Degree-of-freedom
DTE	Dynamic transmission error
EAP	End of active profile
EHL	Elastohydrodynamic lubrication
EMP	Electromagnetic particle
ER	Energy ratio

FEM	Finite element model
FM0	Zero-order figure of merit
FRF	Frequency Response Function
GA	Genetic algorithm
GTE	Geometric transmission error
ICS2	Indicator of second-order cyclostationarity
LSCM	Laser scanning confocal microscope
LTI	Linear Time-Invariant
mALR	Moving averaged logarithmic ratio
MPE	Model prediction error
PE	Parameter estimation
PHM	Prognostics and Health Management
PSD	Power spectral density
PSO	Particle swarm optimization
RMS	Root mean square
RUL	Remaining useful life
SAP	Start of active profile
SBR	Sideband ratio
SES	Squared enveloped spectrum
STE	Static transmission error
TE	Transmission error

TSA	Time synchronous averaging
UICA	Ultra-complete independent component analysis
UNSW	University of New South Wales
VFD	Variable frequency drive

Chapter 1 Introduction

1.1 Background

Gearboxes are critical elements in many rotating machines and are characterised by high transmission efficiency, reliable operation and an exact constant transmission ratio. Thanks to the above-mentioned merits, gearboxes are widely used in different transmission systems in many industries. Due to material degradation during operation and especially in a harsh working environment, gearboxes are subject to wear - a progressive material loss when two gear tooth surfaces contact with relative motions [1-3]. Wear can lead to the formation of stress concentrations, which may serve as initiation sites for other modes of gear failure such as spalling, gear root crack, and gear tooth breakage [4-6]. Thus, monitoring the gear wear process and scheduling required maintenance in advance accordingly, can avoid the occurrence of catastrophic failures and improve the availability of the gear system [7].

Abrasive wear and fatigue pitting are the two most common wear mechanisms during gear service life [8]. Abrasive wear, caused by a lack of or contaminated lubrication [9], is often associated with a high material removal rate of the gear surface, resulting in gear tooth profile change. Tooth profile changes can reduce the thickness of the gear tooth, which increases the risk of tooth breakage significantly. In comparison, fatigue pitting, due to repetitive rolling-sliding contact, has a slower rate in tooth profile change and can be identified by observing pits on the gear surface [4]. Fatigue pitting could promote the generation of surface spalls across the entire tooth width, resulting in a reduction in gear tooth surface durability and/or even tooth breakage. Thus, identifying abrasive wear and fatigue pitting and monitoring the surface degradation process (e.g., gear tooth profile change and surface pitting propagation) are very important topics in the area of wear analysis. Also, monitoring and predicting the wear propagation process can ensure timely maintenance being scheduled to avoid catastrophic failure, which benefits the Prognostics and Health Management (PHM) significantly. Therefore, a crucial component in machine condition monitoring, which is briefly overviewed below.

Machine condition monitoring includes detection, diagnosis, and prognosis of an abnormal condition of a machine. Prognostics is the least developed yet potentially most lucrative of the three phases. There are several main techniques of machine condition monitoring [10]: performance analysis, vibration analysis, lubricant/wear debris analysis, thermography, and acoustic emission analysis. Among these techniques, wear debris (part of lubricant analysis) and vibration analysis are the two most commonly used techniques for gear condition monitoring. In practice, wear particle analysis is a widely used methodology for gear wear monitoring. In particular, wear particle concentration, size, and size distribution are good indicators of the overall wear condition of a machine. Also, particle size, shape, and surface morphologies are useful features in revealing wear mechanisms. Nevertheless, wear particle analysis is often carried out offline, which can be time-consuming and costly [10, 11]. In contrast, gear vibration signals are the reflection of gear dynamic features at the moment they are measured and can be easily obtained online. It is now well established that vibration signals contain gear tooth profile information in their deterministic components (gearmesh harmonics and sidebands) [12, 13], and some recent preliminary studies have suggested a link between gear surface morphology and random vibration components [14, 15]. Vibration analysis is thus the more promising tool for efficient real-time gear wear monitoring. To date, vibration analysis techniques are widely used for gear fault detection, diagnosis and prognostics, but with very limited attempts to monitor wear because wear-related vibration signals are of high complexity and thus not easy to be extracted. To utilize wear-related information contained in vibrations and to develop vibration-based techniques for multiple purposes including online gear wear monitoring and prediction, much more research is needed to establish techniques that are suitable for practical applications.

1.2 Research goals

The ultimate goal of this research is to develop vibration-based techniques for wear monitoring and prediction of remaining useful life (RUL) of gear systems, complementing existing capabilities in fault detection and diagnosis. The specific objectives of this research project include:

1. To study the wear induced vibration characteristics and identify wear-related vibration features for identification of abrasive wear and fatigue pitting, the two common gear wear mechanisms/events.
2. To develop an online method for monitoring gear wear processes using the vibration indicators/characteristics.

3. To develop an integrated system for monitoring and predicting gear wear propagation by utilizing the power of computer simulation and empirical wear models together with the specific and unique responses in the vibrations of operating machines.

1.3 Structure of this thesis

This thesis commences with a literature review of relevant topics (Chapter 2), followed by designing the methodology for achieving the above objectives in Chapter 3. The developments of vibration-based techniques for wear mechanism identification and evaluation tracking (objectives 1 and 2) are presented in Chapter 4. Objective 3 is achieved in 3 steps: step 1 - the establishment of a lumped parameter dynamic model of the gearbox transmission system, step 2 - the methodology development in monitoring and prediction of wear induced tooth profile change, and step 3 - the methodology development in monitoring and prediction of tooth profile change and surface pitting propagation simultaneously. The developments of the gear wear monitoring and prediction system in these three steps are reported in Chapter 5, Chapter 6 and Chapter 7, respectively. The thesis ends in making the conclusions and recommendations in Chapter 8.

This thesis consists of 8 chapters. Summaries of the chapters are given below:

Chapter 1: Introduction

Chapter 2: This chapter reviews the progress of vibration-based gear wear monitoring, including gear wear modes, relationships between gear wear and dynamic responses of gear system, and vibration-based techniques (vibration features and models) for gear wear monitoring.

Chapter 3: This chapter describes the methodology used in this research project, including the research facilities, data acquisition system, and how the research objectives were achieved.

Chapter 4: This chapter introduces wear mechanisms and methods to identify and track the evolution of wear using the characteristic of cyclostationarity of vibrations. The impacts of different wear mechanisms (abrasive wear and fatigue pitting) on gear systems are also presented, that is, profile change and surface pitting of gear teeth.

Chapter 5: This chapter describes the development of a lumped parameter dynamic model of the gearbox test rig at the University of New South Wales (UNSW). The technical details and results of dynamic model validation and calibration are presented.

Chapter 6: This chapter introduces the developed methodology for gear tooth profile change monitoring and prediction. A run-to-failure test was conducted using the gearbox test rig at UNSW, where the gear teeth were not lubricated (dry test), resulting in wear of the gear teeth caused by abrasion.

Chapter 7: This chapter introduces the surface pitting and gear tooth profile change simultaneous monitoring and prediction. This chapter is a further improvement of Chapter 6, including another wear event: surface pitting. A test was conducted using the UNSW gearbox test rig, where the gear teeth were lubricated (lubricated test), resulting in both tooth surface pitting and mild tooth profile change during this run-to-failure test.

Chapter 8: This chapter summarises the key findings and articulates the new contribution to knowledge in this research field. Recommendations for future work are given.

Chapter 2 Literature review

This chapter reviews the existing studies, developments and challenges of gear wear monitoring using vibration analysis, including wear modes, the relationship between gear wear and the dynamic response of a gear system, vibration features/models for gear wear monitoring and prediction.

2.1 Gear wear

2.1.1 Gear wear modes

Surface wear is a common but inevitable phenomenon during the whole service life of a gearbox [16]. When gear pairs mesh with each other, the tooth flanks will be loaded to maintain contact. The motion of the gear tooth surfaces is a combination of rolling motion and sliding motion. The sliding component is present where the surface velocities of the two contacting teeth are different [17]. The sliding motion can cause material removal from the gear teeth, which results in gear mass reduction, that is, gear wear. Gear wear can be sorted based on the wear mechanisms as follows:

- Abrasive wear: Particle contamination or lack of lubrication, which could lead to sliding contact resulting in abrasive wear. Abrasive wear leaves radial scratches on the gear surface and causes changes to the geometry of the gear teeth [18], as shown in Figure 2.1.

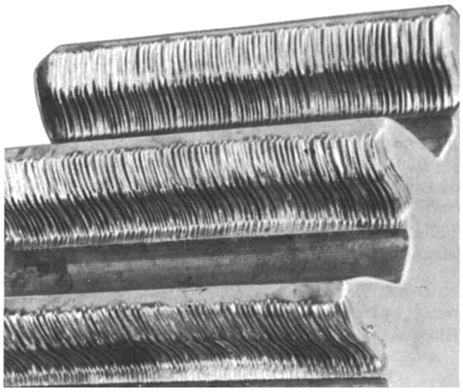

Figure 2.1 Extremely worn gear due to abrasive particles in lubricant [19]

- Fatigue: Surface fatigue results in the removal of material and it will leave cavities on the flank of the gear tooth. Normally, surface fatigue includes pitting and case crushing [18]. Case crushing often occurs in heavily loaded case-hardened gears. Compared with case crushing, fatigue pitting is more common during gear service life. Fatigue pitting is caused by cyclic loading conditions, resulting in fatigue cracks either at the surface of the gear tooth or shallow depth below the surface. The initial crack usually propagates for a short distance in a direction roughly parallel to the tooth surface before turning or branching to the surface. When the cracks have grown long enough to separate a piece of the surface material, fatigue pitting is formed [19], as shown in Figure 2.2.
- Scuffing: When there is substantial sliding motion between mating teeth under lubrication conditions, the excessive temperature at the sliding asperity contacts can result in all protective lubricating films breaking down. As a consequence, the softer asperities can deform plastically and transfer to the mating surface. This is

usually accompanied by a rapid increase in wear rate or even seizing of the sliding pair [20]. This phenomenon is known as scuffing, as shown in Figure 2.3.

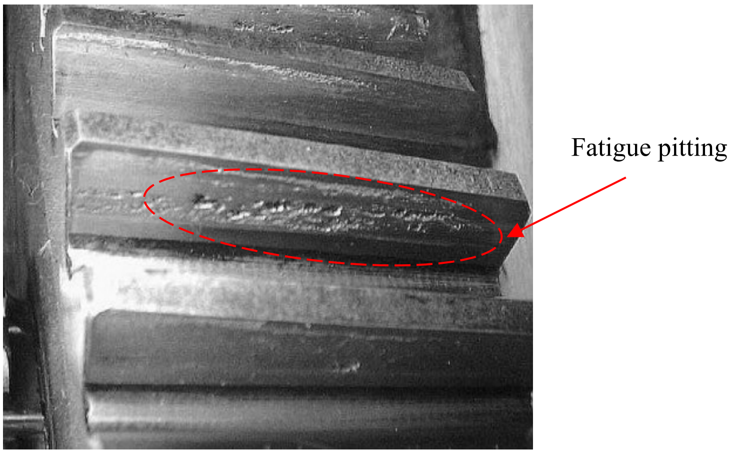

Figure 2.2 Fatigue pitting [19]

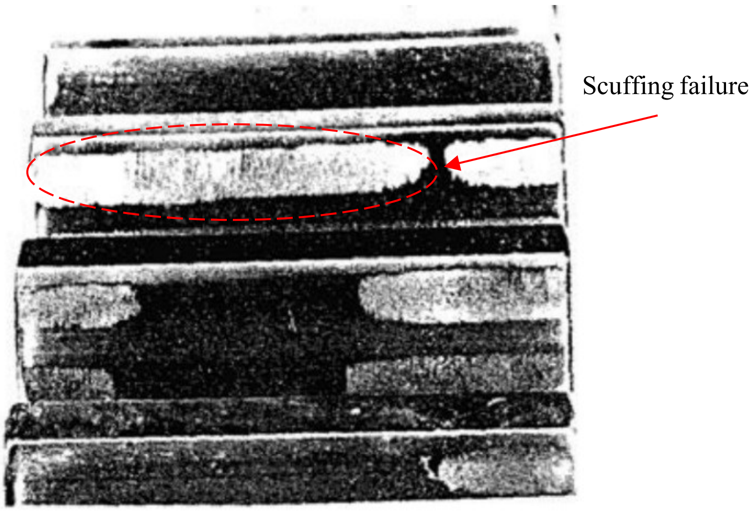

Figure 2.3 Typical scuffing failure in gears [20]. Note: only one instance of scuffing is indicated in this figure for demonstration purposes

- Corrosive wear: Corrosive wear is a visible wear type as a surface deterioration, as shown in Figure 2.4. It is mainly caused by chemical reactions with active ingredients in the lubricant [18]. Corrosive mild wear in gears is usually introduced by lubricant additives intended for preventing scuffing failure, such as extreme pressure additives [20].

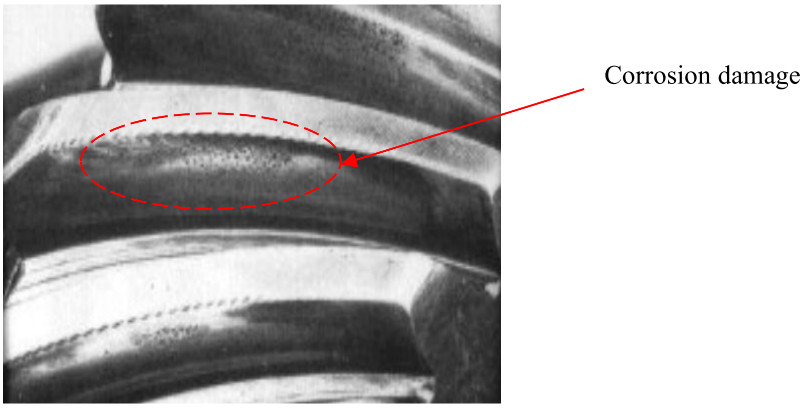

Figure 2.4 Corrosion damage [18]. Note: only one instance of corrosion damage is indicated in this figure for demonstration purposes

In practical applications, abrasive wear and fatigue pitting are the most common wear phenomena in gear systems [8], and therefore, in this research, the two are chosen as the objective of the study.

2.1.2 Differences between abrasive wear and fatigue pitting

Based on the comparison of abrasive wear and fatigue pitting shown in Figure 2.1 and Figure 2.2, there are two major differences between these two surface degradation mechanisms. First, abrasive wear often has a high wear rate and can result in noticeable accumulated material removal in the gear tooth thickness, i.e., changing the gear tooth profile over a certain period. Normally, tooth profile change is in millimetres and can be named to be macro-level wear, which is illustrated in Figure 2.5. In Figure 2.5, it can be seen that the maximum tooth profile change caused by abrasive wear occurs at the addendum and dedendum of the gear tooth, while the profile change is minimal at the pitch line. Consequently, the worn tooth has a double-scalloped tooth profile. The reason is that the sliding velocity, which is proportional to the wear depth in the Archard wear model, is theoretically zero (and zero wear depth) at the pitch line and reaches the maximum sliding speed (and wear depth) at the addendum and dedendum. This phenomenon has also been observed in gear wear simulation [21] and gear wear tests [19].

In contrast, fatigue pitting has a low wear rate in the tooth thickness direction, which makes it has negligible effects on gear tooth profile geometry, unless it is extremely severe. Therefore, these two wear mechanisms can often be differentiated in macro-scale for abrasive wear vs micro-scale for fatigue pitting.

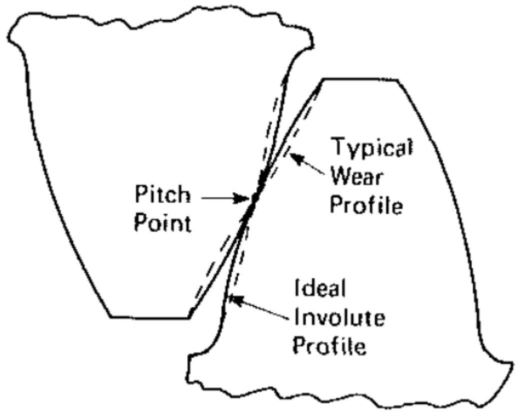

Figure 2.5 Deviations from ideal tooth profile due to abrasive wear [22]

Second, in view of gear surface morphology, it can be found that compared with fatigue pitting, abrasive wear tends to produce a surface with a relatively short wavelength in the direction of sliding direction, which results in a high spatial frequency [23]. As for fatigue pitting, the detachment of material fragments from the gear tooth surface results in localized valleys with long-wavelength which corresponds to the relatively low spatial frequency.

The differences in the features/characteristics of abrasive wear and fatigue pitting are summarized in Table 2.1.

Table 2.1 Differences between abrasive wear and fatigue pitting

Wear types	Wear rate	Morphology (spatial frequency)	Final form
Abrasive wear	High	High	Tooth profile change (together with a rough gear surface)
Fatigue pitting	Low	Low	Valleys on the certain region of gear tooth (between gear root and pitch line)

2.2 Gear wear effects on vibrations of gear systems

There is a two-way relationship between the wear process and gear dynamic characteristics. In general, gear wear can result in the alteration of gear tooth profile geometry or reduction of contact area, which will change the geometric transmission error (GTE) and meshing stiffness of gear system, then the dynamic characteristics will be affected, including the dynamic contact force and its distribution. As a consequence, the level of vibration and harmful noise will increase [24]. In turn, the change of dynamic contact force could alter and accelerate the gear wear process. The two-way relationship between gear wear and gear dynamics will produce complex gear dynamic responses and vibration features, which brings huge challenges in condition monitoring on gear wear progression compared with other failures, such as gear tooth root crack, tooth surface spalling, and tooth breakage.

With consideration of the contact patterns, abrasive wear and fatigue pitting have different impacts on the vibrations of the gear system in two different scales, existing studies and understanding of gear wear effects on vibrations are presented in the macro-level and micro-level below.

Macro-level wear (gear tooth profile change) is a kind of geometric deviation of the ideal gear tooth profile, which is serviced as a geometric transmission error to gear system. The macro-level wear can lead to an increase in the strength of gear meshing harmonics in the vibration signal [25, 26]. Meanwhile, due to the wear-induced gear tooth profile change, the load distribution on the tooth surface will also be altered, therefore, the dynamic characteristics of mating gears will change. The effect of macro-level wear on vibrations can be illustrated in Figure 2.6.

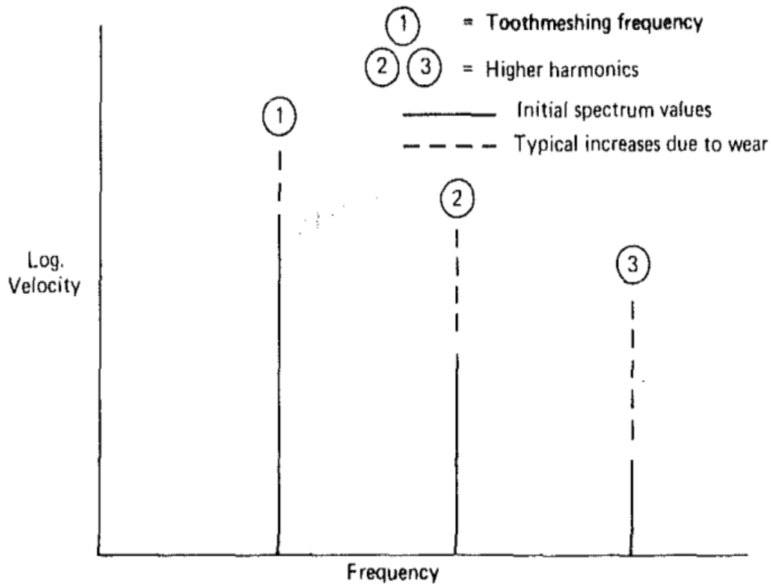

Figure 2.6 Typical vibration spectrum due to wear [22]

As explained in Section 2.1, abrasive wear can easily result in the gear tooth profile change, while fatigue pitting usually will not modify the gear tooth profile if gears are lubricated with a relatively low wear rate. However, both abrasive wear and fatigue pitting have significant impacts on the micro-geometry of the gear tooth surface. Abrasive wear and fatigue pitting can induce different surface morphologies, which are at the micro-level. Abrasive wear can lead to a creation of protrusions (i.e., lumps) distributed from gear root to tip uniformly, while fatigue pitting induces the occurrences of valleys on the gear surface, normally distributed from gear root to pitch line.

The micro-level wear generates a rough gear surface, which increases the friction force between the mating gears, increasing the overall vibrations level and its frequency characteristics [27]. The energy induced by micro-level wear might be very low in comparison with the macro-geometry of the gear surface, and the micro-level wear would induce a random vibration, namely sliding vibrations [14], so it won't be represented in the gear meshing harmonics (deterministic signals), thus it is not easy to distinguish and extract micro-level wear information from other effects in original measured vibration [28].

The effects of abrasive wear and fatigue pitting, in both macro-scale and micro-scale, on vibrations are summarized in Table 2.2.

Table 2.2 Effects of wear on vibrations [14, 15, 22, 29]

Wear type	Macro-level	Micro-level
	Gear meshing harmonics (deterministic components) change	Sliding induced vibration (random components) change
		Magnitude
Abrasive wear	Significant	Increase
Fatigue pitting	Slight	Increase

From Table 2.2, it can be found that these two wear mechanisms have distinct impacts on different vibrations features. In practice, when fatigue pitting propagates, abrasive wear may also co-exist due to oil contamination. The abrasive wear could help to remove high asperities, then lead to a smooth gear surface and good lubrication, which can help prevent the occurrence of fatigue pitting. While, the occurrence of fatigue pitting can break the oil film, and lead to a contact pressure concentration, which could promote the abrasive wear process [8]. This is a coupling effect between abrasive wear and fatigue pitting, which results in complex vibration characteristics and makes it difficult in extracting wear-related vibration features and developing specific vibration-based indicator(s) for wear mechanism identification and evolution tracking. Therefore, the vibration-based techniques for gear wear monitoring are rather rare. In the following, the existing vibration-based gear wear monitoring methodology, using vibration features and models, will be reviewed and summarized.

2.3 Use of vibration features for gear wear monitoring

Current wear monitoring work (using vibration features) mainly focuses on gear wear evolution tracking [13-15, 22, 29-35]. Moreover, most of this research aims to monitor gear tooth profile change (at the macro-level) [13, 22, 29-34]. In contrast, only a handful of studies are designed for micro-level wear monitoring, such as detecting surface roughness changes [14, 15] or monitoring fatigue pitting propagation [35]. Compared with wear evolution tracking techniques, up to date, the vibration-based techniques for wear mechanisms identification are rarer. Therefore, in the following, the existing vibration-based researches for wear evolution tracking are presented first, then, inspired by these researches, the potential researches for wear mechanism identification will be discussed and summarized.

2.3.1 Vibration feature-based wear evolution tracking

As discussed in Section 2.2, abrasive wear (or extreme severe fatigue pitting) could lead to gear tooth profile change (macro-level wear) with an increase in the overall energy of vibration signal and the magnitude of gear meshing harmonics. Therefore, the relationship between signal energy or gear meshing harmonics and gear wear severity were investigated.

Root mean square (RMS) (Eq. (2.1)) is widely used for reflecting the amplitude (or power) of the vibration signal. Considering the worn gear would bring in geometric deviation from ideal gear tooth involute, then results in a stronger vibration, there are some researchers in Refs. [30, 31] using RMS to monitor the gear wear process. It was found that the RMS value has a positive relationship with the gear wear severity. In addition, to improve the sensibility and reliability of RMS for detecting gear wear change, a sample parameter, named matched filtered RMS, was reported in reference [32], this parameter was defined to be the logarithmic value (expressed in dB) of the averaged power ratio between components of the current vibration signal and those of the reference signal. Compared with classical parameters such as RMS and peak values, it is easy to trend and performs better in tracking the gear wear process [13].

$$\mathrm{RMS_x} = \sqrt{\frac{1}{N}\left[\sum\nolimits_{i=1}^{N}(x_i)^2\right]} \tag{2.1}$$

As an extended version of RMS, an indicator named energy ratio (ER) was proposed in Ref. [29]. It was defined in Eq. (2.2) as the difference signal d divided by the RMS of the signal containing only the regular meshing components $\mathrm{y_d}$.

$$\mathrm{ER} = \frac{\mathrm{RMS_d}}{\mathrm{RMS_{y_d}}} \tag{2.2}$$

ER increases with wear severity when it occurs uniformly on the tooth surface since it would be expected that in this case $\mathrm{RMS_d}$ would increase while $\mathrm{RMS_{y_d}}$ would decrease.

However, RMS and its extended versions mainly focus on the changes in signal power, and thus may not be able to reflect the changes in the signal spectral distribution, which is also closely related to gear wear. Therefore, some studies start to focus on the signal spectral distribution change due to the gear wear processes.

With consideration of the wear pattern, the uniform wear effects on gear mesh harmonics were investigated in reference [22]. In reference [22], the author stated that systematic wear would tend to give a kind of profile deviation which is indicated in exaggerated form in Figure 2.5. Consequently, the higher harmonics of the tooth meshing will increase. Therefore, the amplitude of higher-order meshing harmonics could be a reliable way of detecting uniform wear at its early stage. With this knowledge as a basis, the first three gear mesh harmonics of the spectrum and quefrencies of the cepstrum were used in reference [33] to monitor the gear wear process.

However, in the gear wear process, the average gear tooth working profile/surface will steadily deviate further from the ideal involute geometry profile of the gear tooth, but the changes in the gear tooth meshing harmonics are not determined. That is, all the gear meshing harmonics could vary differently, and each gear meshing harmonic may increase in a certain period but decrease in the following period. Due to this complex situation, using only one or several specific meshing harmonics may not be sufficient to monitor the gear wear process. Therefore, all the gear meshing harmonics with significant energy are taken into consideration in reference [13], then the sideband ratio (SBR) proposed in reference [36] was extended and modified into two new indicators: averaged logarithmic ratio (ALR) and moving averaged logarithmic ratio (mALR). ALR can be used to reflect the wear effects on the gear degradation state. mALR shows immediate changes in the gear degradation state within each short time interval. The performance of the two developed indicators was evaluated by two sets of tests with different initial gear tooth surfaces.

In theory, surface wear will cause a gradual change in the mechanical properties of the gear transmission system (most notably in the gear tooth geometry profile and gear meshing stiffness) and therefore, a gradual change in the gear contact mechanism that generates the gear vibration signal. Thus, the difference between vibrations with healthy gears and vibrations with worn gears can be used to represent the gear wear propagation process.

In reference [34], an indicator named Model Prediction Error (MPE) was used to track the gear wear process (tooth geometry profile change). Auto-regressive (AR) model was used to predict the current state of the vibration signal based on the historical data, then "prediction error" is the difference between the predicted signal and the current measured signal, which can be used for indicating the gear wear process. A comparison with classical indicators was made, such as the FM0, FM4, NA4 and RMS. It proves that MPE has a better performance than those indicators in gear wear propagation monitoring.

Compared with the above-mentioned researches for macro-level wear severity assessment, researches for micro-level wear monitoring are quite rare. The reason is that the micro-level wear induced vibration is a random vibration with low energy, which is not easy to distinguish micro-level wear information from other effects in the original measured vibration. In the following, the existing researches for micro-level wear assessment will be introduced.

Recent developments [14, 15] show that the gear tooth surface roughness (induced by abrasive wear or fatigue pitting) information can be detected using a cyclostationary based approach. And the cyclostationarity of vibration is caused by the unique kinematic characteristics of gear transmission systems, as depicted in Figure 2.7. In the study [15], an indicator to measure the degree of second-order cyclostationarity (namely ICS2), proposed in reference [37], was used to monitor the gear surface roughness change. In the experimental part, an approximate positive correlation was found between the degree of second-order cyclostationary indicator (ICS2) of vibration and roughness. However, the connection was found to be more complex by a later investigation [14], based on a wider range of roughness values and a longer experimental duration. To date, insufficient conclusions can be drawn.

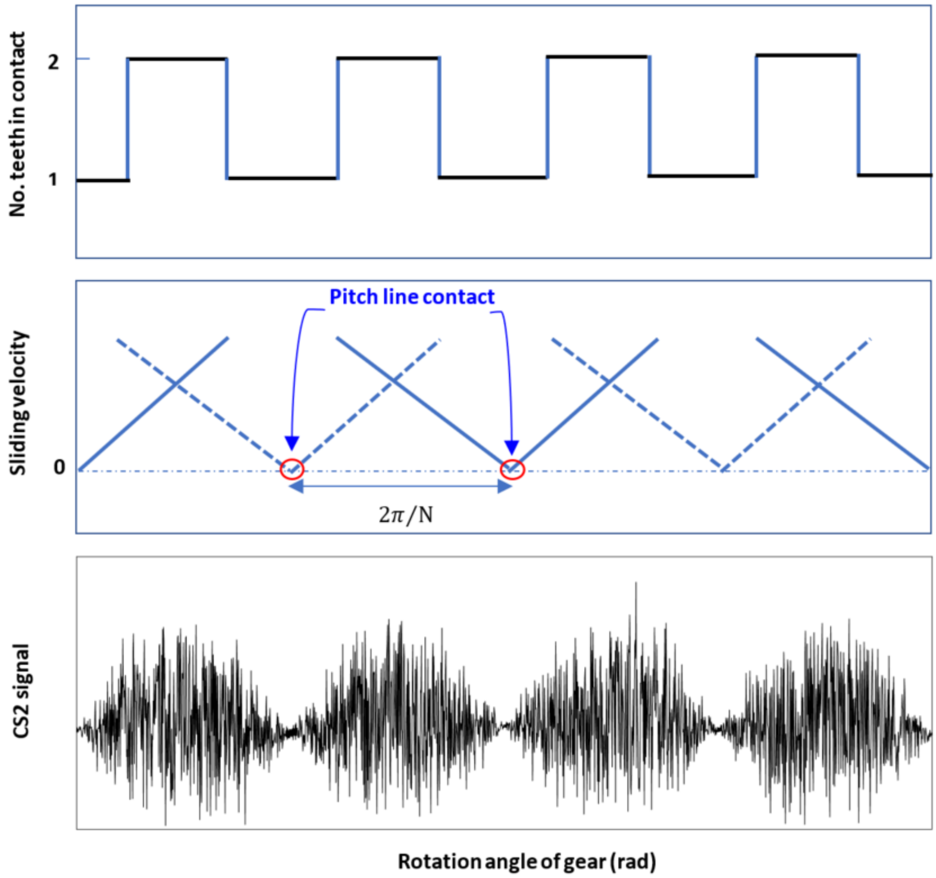

Figure 2.7 Second-order cyclostationary (CS2) signal generation from varying sliding velocity in mating gears; (a) number of tooth pairs in contact; (b) approximate sliding velocity; (c) possible amplitude-modulated random signal (CS2) generated from varying sliding velocity (N = number of teeth on the gear) [15]

In reference [35], the authors assumed that the strength of amplitude and frequency modulation is correlated to the gear wear severity, and used a correlation coefficient to quantify the difference between the reference signal (vibrations with healthy gears) and current measured vibrations, then linked it to gear wear severity. The difference with the work conducted in reference [34] is that the correlation coefficient used in Ref. [35] is for monitoring fatigue pitting propagation (micro-level wear), whose information is hard to detect in the deterministic part of vibration signal. Therefore, a residual signal, after removing gear meshing and shaft harmonics, is used for correlation coefficient calculation. Five natural pitting propagation tests were conducted in the laboratory to be used for verifying the effectiveness of this approach.

Table 2.3 Studies of vibration feature-based gear wear evolution tracking

References	Main techniques	Purpose
[13, 29-32]	RMS, ER	Accumulated gear wear evolution tracking (at macro-level)
[22, 33]	Gear mesh harmonics or quesfrencies	Accumulated gear wear evolution tracking (at macro-level)
[13, 33]	Sideband energy ratio, sidebands	Accumulated gear wear evolution tracking (at macro-level)
[34]	Auto-regressive model, then prediction error	Accumulated gear wear evolution tracking (at macro-level)
[35]	Correlation coefficient-based approach	Fatigue pitting propagation monitoring (at micro-level)
[14, 15]	ICS2 to monitor roughness change	Gear surface roughness monitoring (at micro-level)

Based on the above literature review, the existing vibration feature-based technique for gear wear evolution monitoring can be summarised in Table 2.3. From Table 2.3, it can be found that the vibration feature-based techniques for gear monitoring are quite limited and general. Most of the studies focus on tracking macro-level wear progression (gear tooth profile change), which can be easily detected and monitored in deterministic components of vibrations. In contrast, studies for micro-level wear, such as fatigue pitting or abrasive wear induced surface roughness change, are rather rare. The reason is that the vibration characteristics of micro-level wear are weak, and most of them are contained in the random components of vibrations, which are easily masked by unrelated signals from other vibration generating mechanisms or white noise. This challenge brings huge difficulties to extract useful vibration features and monitor micro-level gear wear evolution. Therefore, researches on investigating the internal relations between micro-level gear wear and measured vibration features, which could benefit the development of vibration-based fatigue pitting propagation, are in vital need and of great importance.

2.3.2 Vibration feature-based wear mechanism identification

Up to date, there is very limited work on vibration-based wear mechanism identification, and the existing approaches for wear mechanism identification mainly rely on visual inspection of a worn surface and/or its wear particles generated from the surface. Based on the literature review, there are several researches suggesting their potentials to wear mechanism identification, which will be presented as follows.

A phenomenon was found in the reference [38], that is, fatigue pitting information is in the low-frequency range of vibrations. In Ref. [38], artificial pits were introduced to all the teeth of the pinion with different sizes to simulate different pitting severities, then the mean frequency variation of a scalogram was used to detect the pitting damage. The experimental results showed that the mean frequency decreased when the severity of pitting increases. This suggested that pitting has effects on the low-frequency part of vibrations.

Even though insufficient conclusions can be drawn in references [14, 15], these two suggested the surface morphology information could be detected in sliding induced vibration. Reference [14] also mentioned that the wavelength of surface asperities might have an impact on the surface roughness monitoring results. This information can be used to separate abrasive wear and fatigue pitting.

Based on the findings in references [14, 15, 38, 39], the carrier frequency information of sliding induced vibrations might have the potential in identifying abrasive wear and fatigue pitting.

From the above literature review, it can be found that the unique surface features induced by different gear wear mechanisms have not been well explored and investigated, which will restrict the potential of vibration-based techniques for gear wear mechanism identification. Therefore, vibration feature-based techniques for gear wear monitoring with consideration of special vibration characteristics induced by different gear wear mechanisms are needed.

2.4 Model-based gear wear monitoring techniques

Gear wear simulation has significant benefits to gear wear monitoring and prediction. The gear wear simulation mainly uses the gear meshing mechanism, gear wear mechanism, and vibration characteristics to establish dynamic models, tribological (wear) models, and their interactions. Then, with the help of the established models, responses in different health conditions can be simulated and evaluated, and fault symptoms can be disclosed and concluded for fault diagnostics and prognostics [40-42]. In the gear wear simulation, gear dynamic models are concerned with the relationship of dynamic properties (stiffness, transmission error, friction, etc) and system responses such as vibration responses (dynamic contact forces and vibration signals). Tribological models rely on wear mechanism theory or experimental data to establish a damage propagation model, in which contact pressure distribution, oil film thickness and/or wear rate are studied based on certain inputs including the load, lubricant viscosity, sliding velocity and surface roughness. In the following sections, the research progress on gear wear model developments will be presented.

2.4.1 Dynamic models of spur gearboxes

Contact force is an important input for the tribological model [43-45]. By calculating the contact force, then contact pressure can be calculated based on Hertzian contact theory [46, 47], and the gear wear propagation behaviours can be simulated using tribological (wear) models. There are a lot of researches using empirical equations or finite element models to evaluate gear contact force and its distribution between meshing gear pairs [48-53], however, most of them are effective under quasi-static conditions. Without considering the inertia effects due to the dynamics of the gear system, the quasi-static contact force can be easily simulated using empirical equations and finite element models. However, in industrial practices, the gear transmission system is usually operated under dynamic operating conditions, the corresponding responses (e.g., contact force) are quite different from those under quasi-static conditions. Normally, because of inertia effects, the dynamic meshing forces are typically larger than the corresponding quasi-static forces and their magnitudes and waveforms are quite different [21]. Therefore, the dynamic contact force and its distribution should be properly evaluated to guarantee i) gear wear propagation behaviours can be simulated, and ii) accurate wear induced dynamic responses can be exhibited.

To obtain proper/accurate dynamic contact force during the gear wear process, a dynamic model of the gear transmission system, which can also generate wear induced dynamic responses (such as vibrations) for wear analysis, is required. In general, the dynamic model includes many parameters. Figure 2.8 shows a typical gear dynamic model, reproduced from reference [54]. In the dynamic model, there are two main excitations to generate vibrations of the gear pair. The external excitations are the fluctuation of the applied load and input operating speed, while the internal excitations are generated from time-varying cyclic meshing stiffness, $k(t)$, and geometric transmission error, $e(t)$ [55]. The occurrence of gear tooth surface wear can affect the GTE (part of internal excitations) significantly, then correspondingly the responses will change, which can represent different fault symptoms with different wear severities.

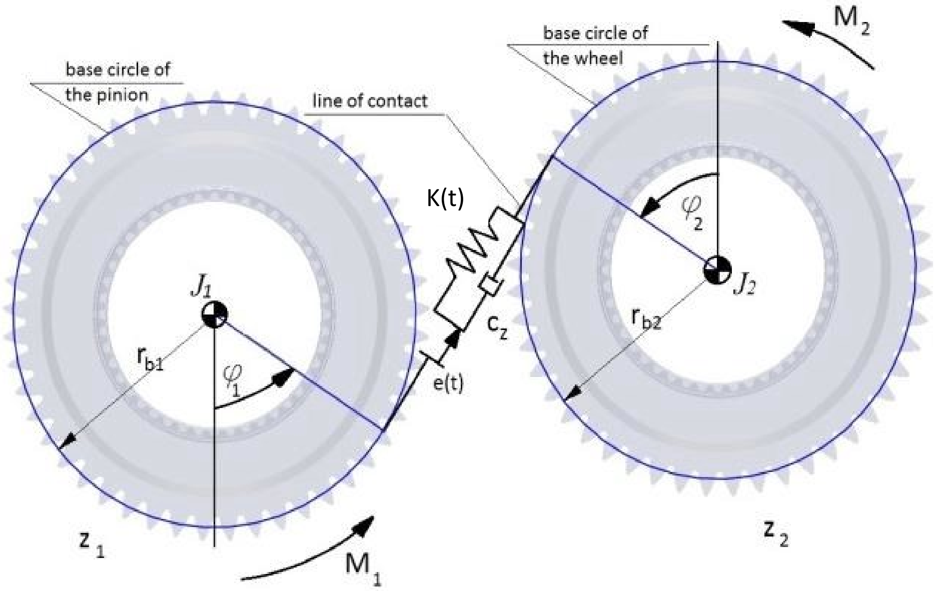

Figure 2.8 Dynamic model of a spur gearbox [54]

Generally, when gear wear occurs, the contact patterns between mating gear pairs can be substantially modified, that is, tooth profile change (induced by abrasive wear) and contact area reduction (induced by fatigue pitting). Tooth profile change is one kind of GTE. Both tooth profile change and contact area reduction can alter the gear meshing stiffness. However, considering the scale of gear wear, the meshing stiffness change induced by gear wear can be neglected as it is significantly less important than the transmission error effect [25]. Therefore, only the researches on wear induced transmission error of the dynamic model will be reviewed.

Owing to the wear induced GTE, the dynamic load and its distribution between the meshing gear pairs will be altered, which could lead to a dynamic transmission error (DTE) and thus result in changes in vibration and noise level. Different from the other parameters in the dynamic model, such as backlash, manufacturing error and tooth relief, gear wear will cause a tooth profile change with certain distribution, which is almost zero around the pitch line and has a maximum value at the root or tip of the gear tooth generally [56]. Different tooth profile changes will cause different corresponding dynamic characteristics and responses, therefore, to acquire accurate wear induced dynamic characteristics and responses, GTE should be properly obtained or simulated according to the characteristics of wear caused tooth profile changes. There are two possible approaches to obtain wear-induced GTE: one is the simulation-based method and the other one is the experimental method. In the following, researches involving GTE study for gear wear analysis will be introduced.

Experimentally, GTE can be measured used a special device. For example, researchers in Ref. [57] used a designed gear coordinate measurement machine to obtain a large number of lead traces, each containing around 200 measurement points that are aligned using a single profile trace to obtain a three-dimensional measurement of the actual gear tooth surface. This approach can acquire wear-induced GTE accurately. However, when measuring and evaluating the tooth surface changes, the gearbox should be stopped and dismantled, which maybe bring other failure modes into the gearbox, such as shaft misalignment. Therefore, many researchers chose the simulation-based approach. Since wear induced tooth profile change is complex, therefore, it is not easy to use simple equations such as sine/cosine functions to represent it accurately. Considering that, there are some researchers [21, 58-60] who use the tribological (wear) models to obtain the wear induced tooth profile changes. This approach can be regarded as an integration of dynamic model and tribological models, and it will be introduced in Section 2.4.3. In the following, tribological models to simulate wear propagation behaviours will be presented first.

2.4.2 Tribological (wear) models for monitoring wear depth and pitting density

There are different approaches to establish tribological models with consideration of wear modes (abrasive wear, scoring, corrosive wear, etc). Since abrasive wear and fatigue pitting are the objectives of this study, therefore, tribological models of these two wear mechanisms will be reviewed in this section.

As for abrasive wear, the Archard wear model [61] is the most accepted and widely used. The theoretical basis of the Archard wear model is the Archard wear equation, given by:

$$h = \int K_{\mathrm{wear}} P v dt \tag{2.3}$$

where h denotes the wear depth on gear tooth, v is the sliding velocity of mating gear pairs at time t, P represents the contact pressure and K_{wear} is a dimensional wear coefficient. The values for v and P can be determined by the parameters of the gearbox and dynamic model. In contrast, K_{wear} will be different in different lubrication conditions, therefore, the wear coefficient K_{wear} is a major unknown factor and it is usually determined from experiments [62] or by an approximate wear coefficient model, which is based on the effect of oil film thickness and gear surface roughness [63]. It is extremely difficult to measure the wear coefficient directly from experiments [64]. Therefore, the widely used approach is to evaluate and determine the wear coefficient using empirical models/equations.

In the determination of wear coefficient using empirical models/equations, lubrication plays an important role and its effect is considered based on the oil film thickness-to-roughness amplitude ratio defined as $\lambda = h_{\min}/R$. The minimum oil film thickness $h_{\min}$ can be determined by empirical equations with consideration of thermal effects [65]. And $R = (R_1 + R_2)/2$, where R_1 and R_2 are root mean square values of surface roughness on the pinion and gear [66]. Based on the value of the calculated λ, three lubrication regimes are considered in the simulations to represent the level of interaction between the mating gear surfaces, and the wear coefficient K_{wear} is calculated as follows:

a) if $\lambda > 4$, it means the oil film thickness is sufficient to avoid direct contact between the gear tooth surfaces, wear is neglected and K_{wear} is set to be zero.

b) if $\lambda \leq 0.5$, it indicates a strong interaction, wear is maximum and K_{wear} is usually determined based on experimental results.

c) in the intermediate zone, K_{wear} is supposed to be estimated by linear interpolations based on λ.

In conclusion, the relationship between the λ and K_{wear} can be summarized in Eq. (2.4) [21], given by:

$$K_{\text{wear}} = \begin{cases} k_{0,} & \lambda < \dfrac{1}{2} \\ \dfrac{2}{7}k_0(4-\lambda), & \dfrac{1}{2} < \lambda < 4 \\ 0, & \lambda > 4 \end{cases} \tag{2.4}$$

It can be seen that the values of K_{wear} depend on the oil film thickness and surface roughness, which are used to determine λ. Note that k_0 is an initial value of the wear coefficient.

In a gearbox, the interacting gear teeth are always rolling and sliding against each other under high contact pressure, which means that the lubrication state is most likely in the mixed or boundary regime [67]. Therefore, tribological models to simulate abrasive wear behaviours are almost always under boundary lubrication or mixed elastohydrodynamic lubrication (EHL). In the following paragraph, researches on abrasive wear models under boundary lubrication or mixed EHL will be briefly introduced.

As introduced in Eq. (2.4), surface roughness is an important factor to determine the empirical wear coefficient K_{wear}. However, initially, tribological models for abrasive wear were built with no consideration of surface roughness update, in other words, wear coefficient K_{wear} is a constant value during the whole abrasive wear propagation process [57, 58, 68-72]. In these researches, to achieve a gear wear profile that is close to real worn gear, authors in Refs. [57, 58] used a comprehensive finite element model to calculate the contact pressure between meshing gear pairs. However, the wear coefficient K_{wear} has not been updated based on Eq. (2.4), which means surface roughness remains to be a fixed value without updating, which is not true during the real gear wear process. The surface roughness update issue was addressed in the work conducted as part of references [73-75]. Time-varying contact parameters (the normal load, radii of curvature, surface velocities, and slide-to-roll ratio) and wear coefficient K_{wear} updating based on surface roughness was considered in a proposed transient mixed EHL model [73], then the transient behaviour of this model was studied and a fatigue model for a spur gear in combination with the dynamic model was proposed to study the wear induced characteristics. Then the model proposed in Ref. [73] was employed in references [74, 75] to establish a fatigue model, but for tooth crack failure rather than fatigue pitting. With consideration of surface roughness update during the wear process, a more accurate wear assessment result can be achieved, compared with the model without updating surface roughness.

From the above literature review, it can be found that the wear coefficient K_{wear} in most existing tribological models is an empirical value, even with consideration of surface roughness updating during the gear wear process. However, in actual practice, except the surface roughness, lots of other factors can also affect wear coefficient K_{wear}, such as contamination of the lubricant, operation condition change, surface morphology change, etc. Therefore, to accurately simulate wear propagation behaviours, it is necessary to obtain the real accurate wear coefficient K_{wear} based on actual measurements using efficient and reliable tools.

Compared with abrasive wear, studies on simulating surface pitting propagation behaviours are more sparse, although there are plenty of publications focusing on explaining the process of surface pitting initiation [74, 76-78]. In reference [79], a multi-axial fatigue criterion and an EHL model [73] were combined to develop a fatigue pitting model. With the developed model, the progression of micro-pits on the tooth surface is simulated. Similarly, with help of the fatigue formula and EHL model, simulation of fatigue pitting propagation behaviours under mixed elastohydrodynamic lubrication conditions is achieved in Ref. [8]. Different from Ref. [79], the competition behaviours between fatigue pitting and abrasive wear induced mild wear were also investigated. Both references [8] and [79] involved the EHL model, which is time-consuming due to its high complexity and high-level expert knowledge is required for model establishment. It will bring huge challenges to application in industrial practices. Therefore, it is vital to develop more efficient models/tools to simulate fatigue pitting behaviours. To address this issue, based on the Lundberg-Palmgren model [80], a modified fatigue model with high computational efficiency was proposed in reference [81], and results of test rig trials and material analyses were presented to demonstrate the effectiveness of the proposed fatigue pitting model.

2.4.3 Integration of dynamic and tribological models for gear wear monitoring

As mentioned in Section 2.4.1, GTE is a key parameter of the gear dynamic model for gear wear analysis. However, it is challenging to acquire an accurate tooth wear profile purely relying on experimental or simple analytical approaches. The tribological (wear) model can be used to generate the wear curve on the tooth flank, and then the generated wear curve can be incorporated into the gear dynamic model to generate vibrations induced by gear wear. This integration of dynamic and tribological models can help reveal the connection between gear wear and vibration characteristics, which can bring significant benefits to gear wear monitoring.

However, until this point, there are only limited references [21, 59, 60] using the integration of tribological and dynamic models for gear wear monitoring. Among them, authors in references [21, 60] combined the tribological model and dynamic model together, aimed at studying the coupling effects between surface wear and gear dynamics (such as meshing stiffness, contact force and vibrations). Then this approach was extended to the planetary gearbox in Ref. [59]. The reference [21] employed a torsional model with a single degree of freedom and then integrated it with a wear prediction model [57] to investigate the interactions between the tooth surface wear and spur gear system's dynamic characteristics. However, an accurate prediction for gear dynamics relies on a comprehensive dynamic model that can simulate the behaviours of the actual running rig. Reference [21] only included the torsional deflections in gear-shaft systems, the translational effects coming from the shaft bending and bearing radial deflections were not considered, which may degenerate the accuracy of the wear analysis. To solve this problem, later, a 4-degree-freedom model including translational motions of gears was introduced in reference [60] and a new dynamic wear analysis method was proposed to study the interactions between tooth surface wear and gear dynamics. However, in reference [60], the authors used simple sine/cosine functions to represent the meshing stiffness and GTE, which is very different from the actual application. An inaccurate evaluation of meshing stiffness and GTE of the gear dynamic model will also cause degeneration of the accuracy of the wear analysis.

Based on the discussion of the research publications in the previous sections, it can be seen that studies on the interaction between tribological and dynamic models for assessing gear wear processes are still needed with consideration of a comprehensive dynamic model together with a proper evaluation of parameters (stiffness and GTE). Therefore, the establishment of a comprehensive dynamic model with proper meshing stiffness and GTE is necessary, which could simulate realistic wear-induced vibrations (compared with actual running rig) for further wear analysis.

2.5 Wear prediction techniques

Having the capability to predict the gear wear process would bring enormous benefits in cost and safety to a wide range of industries. In the following, existing studies of vibration-based gear wear prediction techniques will be reviewed.

2.5.1 Prediction of tooth profile change from abrasive wear

In reference [82], the wear distribution on gear tooth was predicted using the Archard wear model for an unlubricated system. Their observations from experiments validated the prediction results, that is, the maximum wear occurs in the dedendum and addendum regions of gears. However, a gear system usually operates with substantial lubrication, as it reduces wear on the gear teeth, reduces noise and vibration, and improves the power conversion efficiency as less energy is irrecoverably lost to wear mechanisms. To address this issue, an EHL model was applied in Ref. [83] to simulate the wear propagation behaviours and predict the accumulated wear depth under lubrication conditions. But the applied EHL model in reference [83] is time-consuming and requires a high-expert knowledge for establishment. To reduce the computational cost of the EHL model, a simplified EHL model was developed in reference [84], where temperature factors were considered, and the predicted results of gear wear were validated against those obtained by isothermal formulas defined in reference [85]. However, in references [82-84], the contact force was calculated using empirical equations, without consideration of the real worn tooth profile geometry, which could degrade the accuracy of prediction results.

Several studies [86-88] used an empirical formula to estimate the contact force between gears, which was used to estimate the worn tooth profile. The accuracy of these estimates can be improved by using the finite element method to determine the contact force. A gear surface wear prediction methodology for spur and helical gears was proposed in reference [57]. In the proposed methodology, a finite element model of the gear contact mechanics, in conjunction with Archard's wear equation, was employed to predict gear wear. To guarantee the accuracy of prediction results, a special measurement machine was used to acquire the real worn tooth profile during the gear wear process. This measured worn tooth profile was set as an input of the finite element model to predict the wear propagation progression. And, the prediction results were validated through comparison with experimental ones. However, in the approach proposed in reference [57], the gearbox should be stopped and dismantled when measuring the worn tooth profile. The stoppage and subsequent dismantling could introduce other failure modes or affect the progression of existing ones. Researchers in references [89-91] have also used the finite element method to estimate the contact force between gears, which was used as an input into the Archard wear model, and subsequently used to predict the wear depth of spur and planetary gears. To obtain a more accurate contact force and reduce the computational cost, efforts on improving the finite element model were made in references [92, 93]. The results showed that the wear predictions were improved with help of the improved finite element model. However, there is a drawback of using a finite element model, in that it is difficult to properly represent the dynamic characteristics induced by inertia. With the finite element models employed in references [92, 93], the simulated contact force is under quasi-static conditions. However, in actual practice, the gearbox is running under dynamic operating conditions, and the dynamic contact force is different from the quasi-static contact force in both magnitude and waveform [21]. To include the dynamic effects into the finite model, the boundaries and mesh generation should be well defined, both of which require high-level expert knowledge, along with increased computational costs. Therefore, the use of a simple finite element model could bring noticeable errors to wear prediction, unless the worn tooth profile can be regularly corrected using actual measurement, as in reference [89]. Thus, a dynamic model is needed to provide the dynamic contact force, which is closest to the actual running test rig. Note that the finite element model mentioned in this thesis refers in particular to the simple finite element model without well-defined boundary conditions and mesh generations.

Except for physical model-based gear wear prediction, there are some other approaches that were proposed to monitor and predict the change of the profile of a gear tooth due to wear. For example, an integrated prognostics method was proposed in Ref. [24] for wear prediction in terms of wear depth change. In this hybrid approach, the Archard wear model was used to simulate wear behaviours, and the Bayesian update process was implemented to determine the wear coefficient during the wear process. The predicted results were compared with experimental results from tests using a planetary gearbox that was run-to-failure. Compared with the wear prediction purely relying on physics models or experiments, the results suggested that the integration of the wear model and actual measurements could achieve more reliable and accurate wear prediction. The relationship between gear hobbing processing technique and gear geometric deviation was modelled by applying the improved Particle Swarm Optimization (PSO) and Back Propagation algorithm (BP) to determine the optimal model parameters in reference [94]. The accuracy of both algorithms was evaluated by the Root Mean Square Error between the predicted and experimental values. The result shows that the gear geometric deviations were well predicted and were in reasonably good agreement with experimental data. A statistical model with statistical parameters was proposed in Ref. [95] to monitor and predict the gear behaviours with extreme tooth profile alteration induced by abrasive wear, the effects of the Sic concentration, applied load and sliding distance was statistically and physically analyzed in detail. Besides, a fusion of ultra-complete independent component analysis (UICA) and parameter estimation (PE) was developed in reference [96] to monitor and predict the severity of gear wear. Even though promising prediction results were achieved in references [94-96], these statistical model-based approaches could not reveal the wear behaviours and gear dynamic responses change during the gear wear process, which has significant benefits to the understanding of wear mechanism and its consequences to the gear system. Also, the statistical model-based approach heavily relies on a huge amount of experimental data, which limits its capability of applying in industrial practice. Therefore, a vibration-based tool, which can reveal the gear wear and dynamic behaviours also requires a small amount of experimental data for model parameter updating/calibration, is in vital need and it could bring significant benefits to gear wear monitoring and prediction in industrial practice.

2.5.2 Prediction of surface pitting propagation

The focus of the research described in the previous sections was on the prediction of the change in the profile of gear teeth caused by abrasive wear. Some research [8, 81] involved predicting the propagation of fatigue pitting. In reference [8], an EHL model and fatigue equation were combined to simulate the propagation behaviours of fatigue pitting propagation and mild tooth profile change (caused by abrasive wear), under mixed elastohydrodynamic lubrication conditions. In this approach, the competitive behaviours between abrasive wear and fatigue pitting were successfully simulated during the gear wear propagation progression. However, as for this approach, high computational cost and high-level expert knowledge are required to realize the EHL model. Compared with research described in reference [8], a more efficient approach was proposed by the researchers in Ref. [81], where the Archard wear model and empirical fatigue pitting formula were used to predict both the abrasive wear (in terms of wear depth) and fatigue pitting (in terms of surface pitting) propagation. Also, a statistical formulation was proposed in reference [97] to depict the evolution of asperity shape induced by wear and plastic deformations under mixed lubrication, and an asperity strain-hardening model was developed to predict the surface roughness change and fatigue pitting propagation. Although the model predictions were in almost perfect agreement with the experimental reference measurements in Ref. [97], the predictions must be subjected to a larger number of experimental evaluations for a more decisive validation and a final judgment on their precision, which brings huge challenges to the application in industrial practices. Moreover, in references [8, 81, 97], none of their propagation processes was timely examined and calibrated by actual measurements to accommodate changes in operating and lubrication conditions as well as wear conditions and rates.

In practice, the abrasive wear and fatigue pitting propagation rate would be affected by contamination of the lubricant, change in roughness, changes in the operating conditions, etc. Therefore, without real-time examination and updating, the accuracy of predictions is uncertain and will decrease significantly as wear progresses. Therefore, reliable, effective and efficient simulation methods are needed to predict the propagation of gear wear, with consideration of experimental/industrial measurements.

Besides, except for the above-mentioned physical model-based approaches, other kinds of techniques were also developed and proven to be effective for fatigue pitting prediction. For example, the artificial neural network (ANN) was used in Ref. [98] to predict the severity of gear fatigue pitting. Based on some well-known standards, there are some methodologies developed for predicting fatigue pitting severity in references [99, 100]. American Gear Manufacturing Association (AGMA) design standard was employed in Ref. [99] to predict pitting and bending fatigue crack initiation along the gear tooth profile. With help of the ISO standard of gear micropitting (ISO/TR 15144-1:2020) and considering the operating load and speed conditions, a theoretical study was carried out in Ref. [100] to assess the risk of gear micropitting by determining the gear contact stress, sliding parameter, local contact temperature and lubricant film thickness along the line of action of gear tooth contact. Note that a large set of experimental data is required to train the ANN or determine/optimize the parameters in the AGMA and ISO standards. In real applications and industry practice, it is hard to obtain significant historical data for training or parameter optimization. Also, having the ability to demonstrate the fatigue pitting propagation behaviours can help the analyst to well understand the fatigue mechanisms. However, ANN, AGMA or ISO standards cannot reveal and exhibit the fatigue pitting propagation behaviours with details.

2.5.3 Research gaps

From the above literature review on gear wear (abrasive wear and fatigue pitting) prediction techniques, it can be seen that most of the existing wear prediction techniques are designed for predicting abrasive wear induced tooth profile change. In contrast, the researches for fatigue pitting prediction are rare. The reason might be that i) there are few effective and efficient models/tools for simulating fatigue pitting propagation behaviour; and ii) abrasive wear usually co-exists during the fatigue pitting propagation progression, which brings in complex surface degradation process and surface morphology; iii) the fatigue pitting induced vibration feature is extremely complex, weak and difficult to extract. These challenges restrict the development of vibration-based fatigue pitting propagation monitoring and prediction. Therefore, a reliable, effective, and efficient fatigue pitting model/tool is required to reveal and represent fatigue pitting propagation behaviours.

From the review of the existing research on gear wear prediction, it can also be found that the physical-based approach is widely used. Compared with the statistical model-based approach, artificial intelligence-based approach and standard-based approach, the physical (wear) model has its unique advantage, which is that the surface degradation behaviours can be represented for helping understand the wear mechanism and its consequences to the gear system. However, the existing model-based wear prediction methodology has not been timely examined and calibrated using actual measurements, which could degrade the wear prediction accuracy. Therefore, it is necessary to develop a vibration-based tool for gear wear prediction, in which, the wear model is developed with a complete understanding of the wear mechanism and models parameters can be timely calibrated and updated with a reasonable amount of experiment data.

The digital twin (DT) is a virtual representation (mirror) of a physical structure or a system in real space along its lifecycles [101]. Through real-time interaction between the virtual model and physical structure, the degradation status of the system and its RUL can be reflected and evaluated effectively. Thanks to its unique speciality, DT has received considerable attention from the research community over the last decades. However, due to the complex structures and harsh operation conditions, research of DT-based gearbox transmission system RUL prediction is rather rare. And existing conceptual approaches [101-103] have limitations in indicating the specific contact statuses and providing insights on degradation stages of gearbox transmission systems, all of which are of high value to RUL prediction. Therefore, the development of a systematic and practical digital twin technology for gear wear monitoring and RUL prediction and will benefit the research community and industrial practices significantly. It is the main research goal of this thesis.

2.6 Summary

This chapter presents the review for vibration-based gear wear monitoring. From the literature review of vibration feature-based gear wear monitoring, it was found that most of the existing research focuses on tracking the abrasive wear-induced tooth profile change, which is at the millimetre level (macro-level wear). The researches for fatigue pitting monitoring (micro-level wear) and wear mechanism identification are rather rare and deserve more attention from the research community.

In reviewing the progress of vibration model-based gear wear monitoring, it can be seen that the Archard wear equation still plays an important role in modelling the abrasive wear behaviours. In contrast, models for fatigue pitting are limited, and the combination of the EHL model and fatigue criterion is the main approach to simulate fatigue pitting propagation behaviours, which is time-consuming and requires a high level of knowledge for the model establishment. Therefore, more effective and efficient models/tools for simulating fatigue pitting propagation behaviours are required.

Moreover, in practice, abrasive wear and fatigue pitting can both occur in the gear surface degradation process, simultaneously or appear at different times on the same gear. Therefore, it is important that both the gear tooth profile change and surface pitting density can be monitored and predicted. To do so, there is a vital need to quantify the wear induced tooth profile change (in terms of wear depth) and the surface pitting density in situations when these two wear events take place separately or simultaneously.

Chapter 3 Methodology

This chapter presents and demonstrates the rationalities of the overall approaches and technical strategies to achieve the ultimate goal of this research. More specific information on the approaches is presented in Chapters 4-7.

The structure of this chapter is arranged as follows. An introduction to the overall strategy to implement the vibration-based integrated system for gear wear monitoring and prediction is introduced in Section 3.1, and the procedures to achieve the specified project goals are presented. The experimental research facilities and test programs to realize the objectives of this research are presented in Section 3.2. Then, Section 3.3 and Section 3.4 give the skeletons of the proposed methodology for the specified research objectives in stages. More specifically, approaches used to identify gear wear mechanisms and to track wear evolution using vibrations are presented in Section 3.3. With the identified wear mode(s), model-based gear wear monitoring and prediction methodologies are introduced in Section 3.4, including dynamic model, tribological (wear) models and the corresponding updating procedures with help of measured vibrations.

3.1 The overall strategy of the vibration-based integrated system for gear wear monitoring

The developed vibration-based gear wear monitoring and prediction integrated system consists of two stages:

- **Stage 1:** Wear mechanism identification using vibration-based techniques
- **Stage 2:** Wear propagation monitoring and prediction using vibration-based approaches

This project can be further divided into four specific research objectives: objective 1 belongs to stage 1, and objectives 2-4 belong to stage 2.

- **Objective 1:** Identification of gear wear mechanism and tracking wear evolution using cyclostationary properties of measured vibrations
- **Objective 2:** Dynamic model development
- **Objective 3:** Monitoring and prediction of tooth profile changes during wear progression
- **Objective 4:** Development of a digital twin approach for monitoring and prediction of surface pitting and tooth profile changes

Objective 3 only focuses on monitoring and predicting one wear phenomenon, which is tooth profile change (e.g., from abrasive wear). Objective 4 is a further improvement in objective 3 by monitoring and predicting two wear phenomena/events, that is, tooth profile change and surface pitting. In practice, it is common that multiple wear events co-exist during gear wear progression. Therefore, these two common wear phenomena, surface pitting propagation and tooth profile change, are taken into consideration in objective 4. To show the connections of the above-mentioned objectives of this project, a schematic diagram of the overall strategy for gear wear monitoring and prediction is given in Figure 3.1. The specific techniques utilized to realize each objective will be introduced in Sections 3.3 and 3.4 below. Also, the congruent relationship between each objective and the following chapters of this thesis is shown in Figure 3.1.

To conduct the research stated in stage 1 and also to demonstrate and validate the effectiveness of the developed vibration-based integrated system in gear wear monitoring and prediction, two endurance tests were conducted on a spur gearbox at UNSW under different lubrication conditions to generate different dominant wear phenomena/events. The experimental research facilities and test programs to realize and accomplish the above-mentioned objectives of this research project will be introduced in the following section.

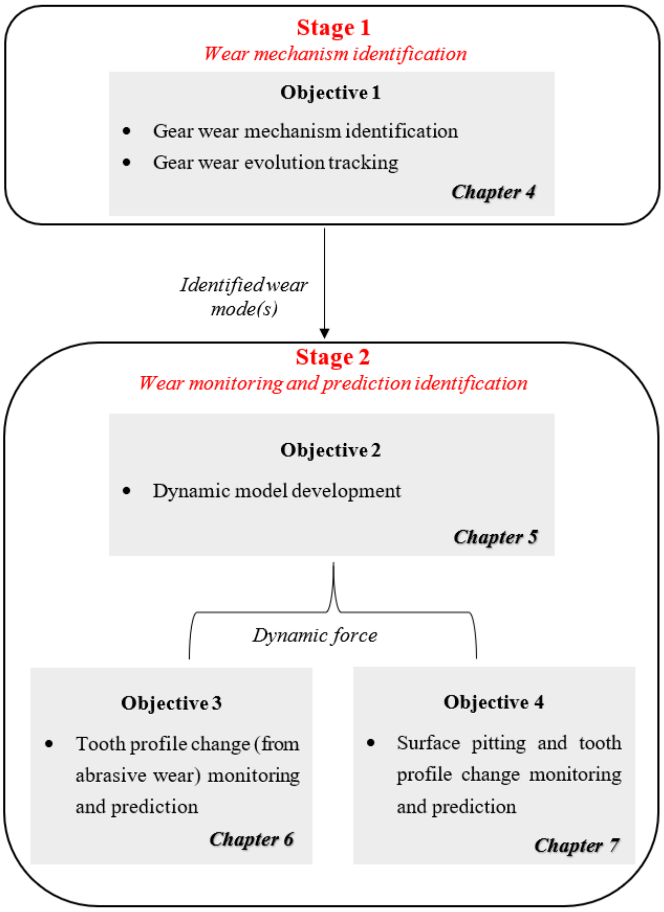

Figure 3.1 The schematic diagram of the research methodology

3.2 Experimental research facilities and test programs

3.2.1 Spur gearbox at University of New South Wales

A single-stage spur gearbox rig, shown in Figure 3.2, was used to conduct gear wear tests. The gearbox is composed of an input shaft and an output shaft, which carry two modular gears (module 2) with 19 and 52 teeth, respectively. To achieve an accelerated wear rate, gears made of mild steel (JIS S45C) were used. The gears have not been processed with heat treatment and the hardness is less than 194 HB. The precision grade of the gears is JIS grade 4 (JIS B1702:1976), and gear teeth are with standard full depth. The input shaft is powered by a 4-kW electric motor, whose instantaneous rotational speed is controlled by a variable frequency drive (VFD) and connected to a torque meter that can monitor the instantaneous torque of the gear transmission system. An electromagnetic particle (EMP) brake is connected to the output shaft (at the end) and is used to control the torque transmitted by the gear transmission system. Two encoders are installed at the remaining free ends of the shafts. The connections of the gearbox shafts with the motor, brake and encoders are achieved using couplings with high torsional stiffness and low bending stiffness.

Two vibration sensors (B&K 4396 and B&K 4394 accelerometers) are mounted on the top of the gearbox casing in the positions shown in Figure 3.2(b). The sensitivity of the B&K 4396 accelerometer is $10.0\ \mathrm{mV/ms^{-2}}$ and its nominal frequency range is 1 to 14000 Hz, while for the B&K 4394, its sensitivity and frequency range are $1.00\ \mathrm{mV/ms^{-2}}$ and 1 to 25000 Hz, respectively. The lubrication is provided by an oil bath and the kinematic viscosity of the oil is 146 (40 °C, Shell Spirax S2 A 80 W-90). Before the lubricated test and unlubricated test were conducted, three teeth on each gear (hence a total of 6 teeth) were chosen randomly and marked to be used for monitoring the evolution of wear on the surface of the gear teeth. The moulding procedure consisted of applying Microset 101 thixotropic silicone polymer to a series of marked gear teeth at each stoppage during the endurance tests. The moulds were then tagged with the collection time (cycles) and stored for further analysis.

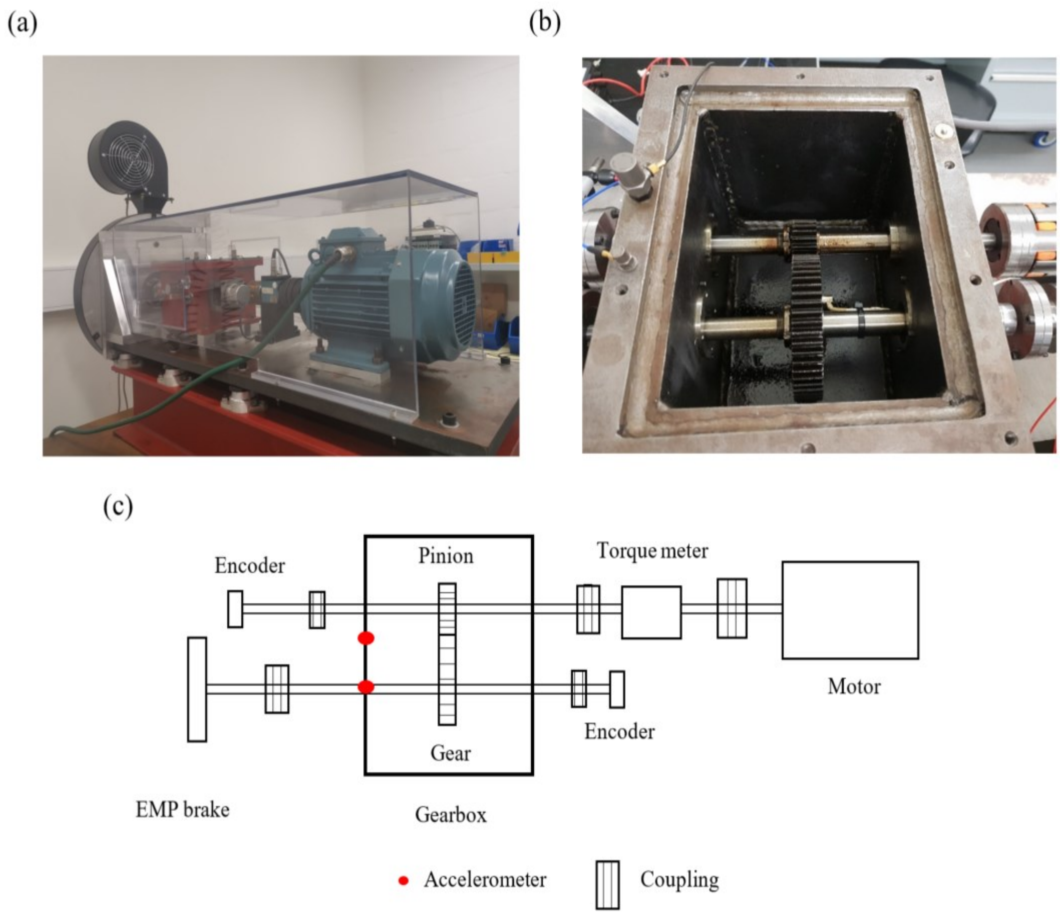

Figure 3.2 The spur gear test rig at University of New South Wales (UNSW): (a) Overall view; (b) Detail of the gearbox; (c) A schematic diagram of the setup [16]

3.2.2 *Wear tests and data collection*

Two run-to-failure tests were carried out to simulate gear wear progression behaviours under different lubrication conditions. A test with lubrication was conducted to generate fatigue pitting on the gear surfaces, and mild tooth profile change co-exists due to the abrasive wear. Next, a test without lubrication was conducted to create abrasive wear, and the tooth profile change is severe but no/rare surface pitting was observed. Further details of these two tests are presented below.

The test with lubrication was performed to simulate the natural fatigue pitting propagation progression. The lubricated test was performed with a pre-roughened gear pair to accelerate the degradation process and abrasive wear occurred at the beginning of the test when the gear tooth surface was rough; the initial gear surface condition/morphology is shown in Figure 3.3. The lubricated test ran for a total of 3.25 million cycles of the pinion (the driving gear). The test rig was stopped roughly every 0.1 million cycles for the lubricated test to record the surface condition of the six gears by using a moulding technique, as shown in Figure 3.4. During this endurance test, the motor torque was set to 20 Nm for the entire duration, which is around 9-times the pinion's rated torque for surface durability, guaranteeing the occurrence of surface pitting. During short specific intervals within the test campaign (mostly before each stoppage), the input shaft rotational speed was adjusted to 2 Hz, 6 Hz, 10 Hz, 16 Hz and 20 Hz from the pre-set operating speed to record vibration and tacho/encoder signals. Each speed adjustment lasted around 10 seconds, after which the input shaft speed was changed back to the pre-set operating speed. This speed adjustment was intended to generate different types of transmission error signals, with the relevant investigations reported in reference [104]. Vibration signals were acquired regularly (around every 6000 cycles) within the test campaign, with a record length of 10 seconds and a corresponding sampling rate of 100 kHz. Figure 3.5 shows a picture of the pinion and an image of a pinion tooth surface after the test with lubrication, which shows the occurrence of fatigue pitting.

The test without lubrication (dry test) was conducted with a new pair of gears over approximately 38,000 cycles of the pinion. The test rig was stopped roughly every 5000 cycles for the dry test to record the surface condition with the moulding technique. Figure

3.6 shows the surface of a tooth on the pinion and was not artificially worn before commencing the test. The dry test intended to create an environment conducive to high rates of abrasive wear, leading to rapid tooth profile changes, but without substantial levels of pitting. To achieve this, the motor torque was set to 5 Nm and the input shaft speed to 10 Hz for the entire duration of the test. Similarly, during short specific intervals within the test campaign (mostly before each stoppage), the input shaft rotational speed was adjusted to 2 Hz from the pre-set operating speed to record vibration and tacho/encoder signals. The vibration signals were sampled at 100 kHz and for a duration of 10 seconds. Wear particles were collected during the dry test using adhesive paper, as shown in Figure 3.7, and their mass has been used to calculate average wear depth. Figure 3.8 shows the appearance of the pinion and its gear surface after the test.

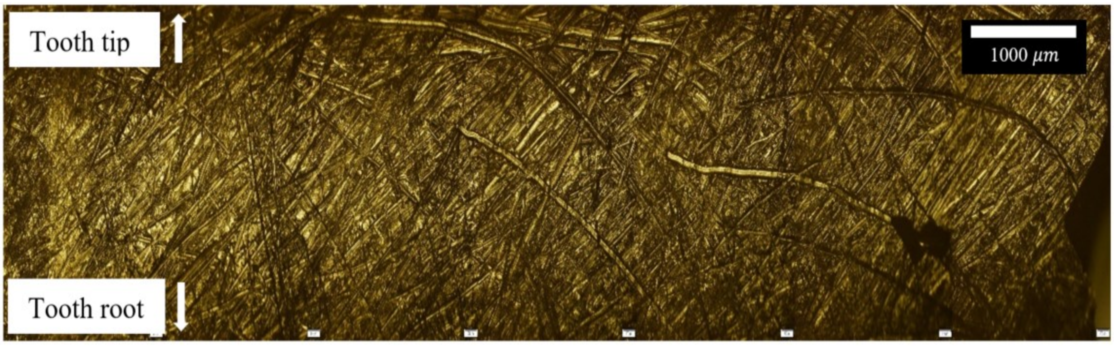

Figure 3.3 The initial surface of the pinion gear that was artificially roughened using sandpaper before conducting the test with lubrication

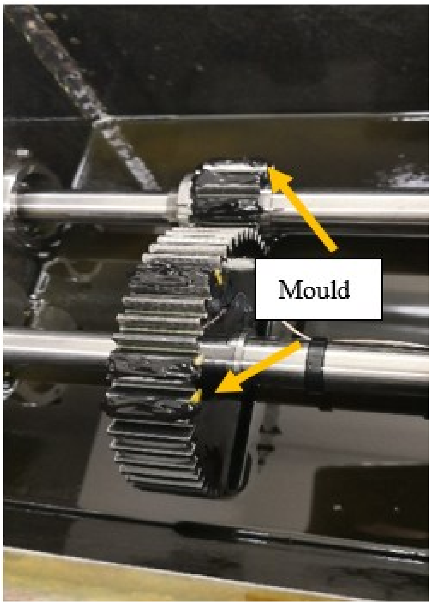

Figure 3.4 Gear pair and mould making (in lubricated test)

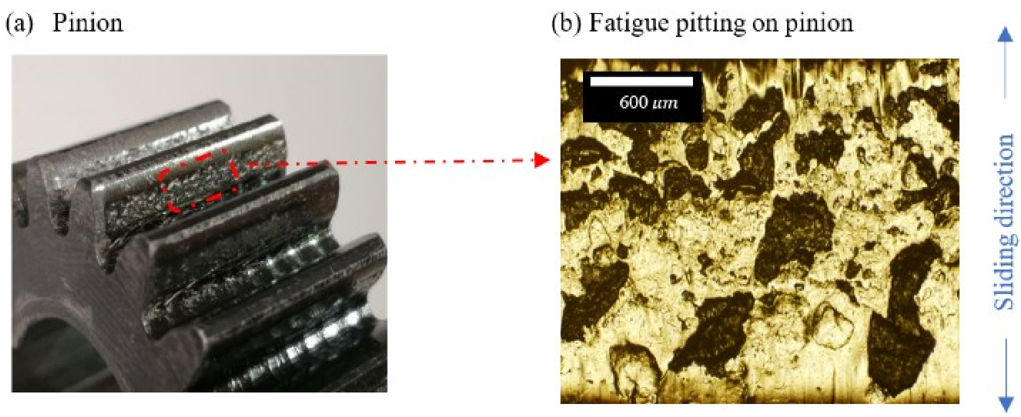

Figure 3.5 Gear surfaces after the lubricated test: (a) Appearance of the pinion; (b) An image of a mould of a pinion tooth surface with fatigue pitting

Figure 3.6 The initial pinion surface before the dry test

It should be highlighted that the aim of the two tests is not to conduct the most realistic wear progression possible. Nor is it to investigate the effect of speed and load on wear (rates). The objective is rather to generate lots of abrasive wear in one test and lots of fatigue pitting in the other, so that techniques for monitoring and predicting the progression of these wear types can be developed and tested.

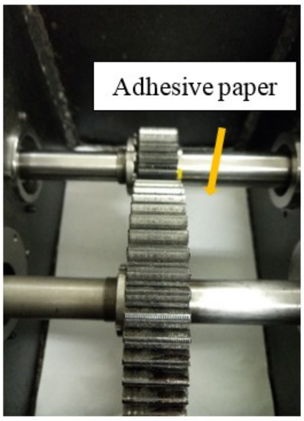

Figure 3.7 Gear pair and adhesive paper (in dry test)

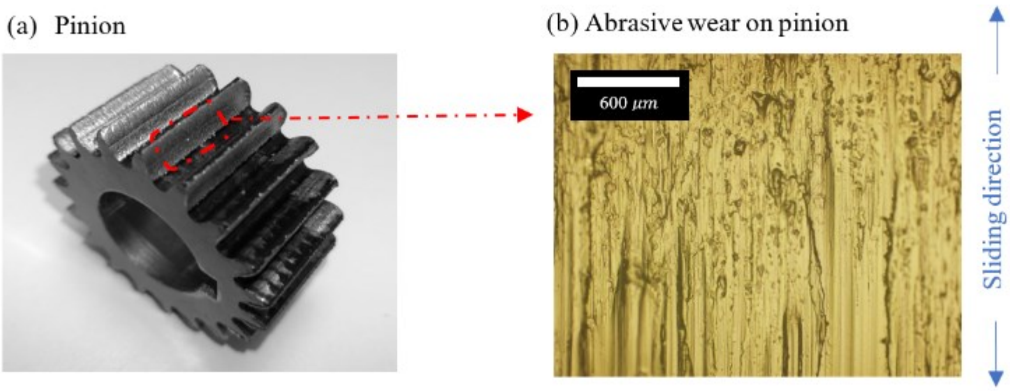

Figure 3.8 Gear surfaces after the dry test: (a) Appearance of the pinion; (b) An image of a mould of a pinion tooth surface with abrasive wear

The lubricated test and dry test are used in this research to help realize the above-mentioned objectives 1, 3 and 4. More specifically, two different dominant wear mechanisms/events occurred in the lubricated test and dry test respectively: fatigue pitting and abrasive wear. The measured vibrations in the two tests can be utilized to help develop the vibration-based techniques for wear mechanism identification, which corresponds to objective 1 of this research. Also, as for objectives 2, 3 and 4, the measured vibrations are used to conduct model calibration and compare with simulations to update model parameters for gear wear progression prediction, which will be introduced in Section 3.3 and Section 3.4. The details and differences of the lubricated test and dry test are summarized in Table 3.1.

Table 3.1 Settings of lubricated test and dry test

	Test 1	Test 2
Lubricated	Yes	No
Pre-worn	Yes	No
Max cycles	3,250,000 cycles	38,000 cycles
Stop intervals	100,000 cycles	5,000 cycles
Load	20 Nm	5 Nm
Input shaft speed (constant)	10 Hz	10 Hz
Short-term input shaft speed changes (constant; not used in this study)	2 Hz, 6 Hz, 16 Hz, 20 Hz	2 Hz

3.3 Gear wear mechanism identification and wear evolution tracking using cyclostationary properties of vibrations (objective 1)

It is necessary to identify the gear wear mechanism and understand its impacts on gear tooth before monitoring and predicting the wear propagation so that the corresponding maintenance strategies for specific wear events can be developed and scheduled. According to the literature review of Section 2.3, it can be found that the existing approaches for wear mechanism identification are off-line techniques. For instance, the widely used approach is the visual inspection of a worn surface and/or the wear particles generated from the surface. This approach requires either interruption of the operation (in the case of visual inspection) or a delay in analysing wear debris, and the operating status of gearboxes cannot be timely reflected. Therefore, it is necessary to identify wear mechanisms (abrasive wear and fatigue pitting) using an efficient and effective online approach and track its wear evolution.

In general, changes in the profile of gear teeth cause changes in the deterministic component of vibrations. In contrast, the sliding induced random vibration from the asperity contacts between two mating gears is closely related to the surface morphology [105, 106]. From the surface feature view, abrasive wear tends to introduce a change to the gear tooth profile, while fatigue pitting has negligible effects on the gear tooth profile unless the fatigue pitting is extremely severe [19]. However, both abrasive wear and fatigue pitting change the micro-geometry of gear tooth surfaces. Therefore, the sliding-induced random vibrations have the information of both abrasive wear and fatigue pitting.

However, in the measured vibrations, the sliding induced random vibration is usually mixed with the signals from other unrelated vibration generating mechanisms or white noise, which brings difficulties in extracting surface morphology related information for wear mechanism identification and wear severity tracking, and also leads to the traditional indicators (e.g., RMS and kurtosis) lose their effectiveness in gear wear monitoring. To effectively extract the sliding vibration from background noise (i.e, the signals from other unrelated vibration generating mechanisms or white noise), the special characteristics of sliding vibrations were investigated in references [14, 15], and it was found that the sliding vibration has second-order cyclostationarity (CS2) due to the time-varying sliding velocity and contact force on the tooth pairs. Therefore, cyclostationary properties of vibrations and the relevant techniques such as spectral coherence map and indicator of CS2 are used and further explored in this research to identify the wear mechanism and then track its propagation.

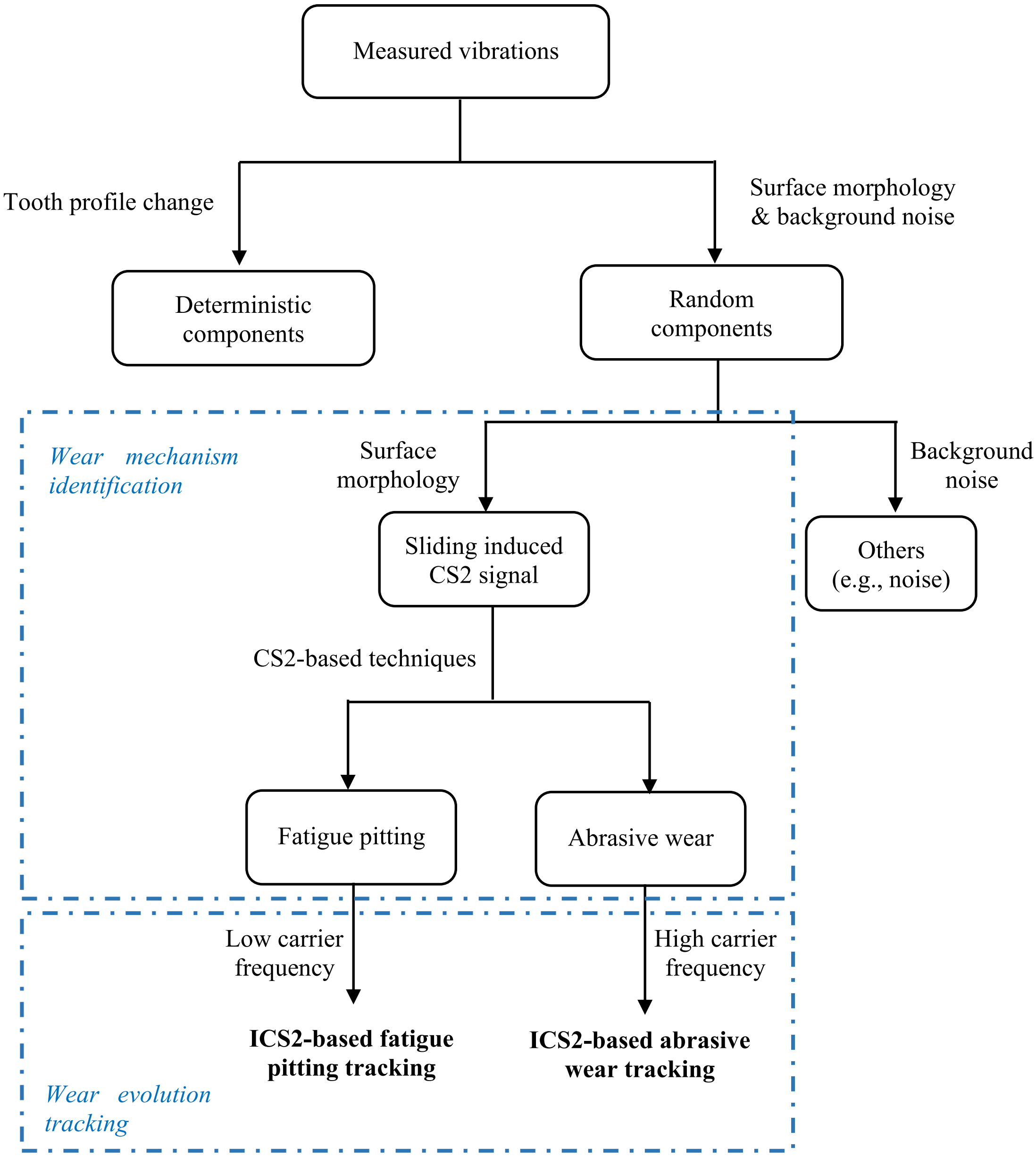

Figure 3.9 The schematic diagram of the vibration-based wear mechanism identification and evolution tracking

The main procedures to achieve objective 1 in this research are as follows. Firstly, the relationship between the spatial frequency of the surface morphology and the frequency of sliding vibration is investigated and established. Then the fatigue pitting and abrasive wear are identified and separated using the carrier frequency of measured vibrations and ICS2 of vibrations [37] (an indicator of CS2): fatigue pitting information is carried in the low-frequency range, while abrasive wear information is carried in the high-frequency range. Finally, the fatigue pitting and abrasive wear propagation are monitored and tracked using ICS2 in the proper frequency bands. A schematic diagram of the vibration-based wear mechanism identification and evolution tracking is shown in Figure 3.9. More details of this development can be found in Chapter 4.

3.4 Model-based gear wear monitoring and prediction methodology

Once the wear mechanism is identified, the gear wear propagation can be monitored and predicted using the corresponding approach/technique so that the remaining useful life of the gear system can be estimated. As reviewed in Section 2.4, compared with statistical models and artificial intelligence, the physical model-based wear monitoring methodology has many merits such as fewer measurements are required for training or calibration purpose and an in-depth understanding of the wear mechanism can be provided. Therefore, model-based techniques are utilized in this research for monitoring and predicting gear wear propagation.

However, in practice, during gear wear progression, the wear propagation rate tends to change due to factors such as oil contamination, changes in operating conditions, changes in surface roughness, etc. Therefore, to ensure accurate prediction results, regular comparison between simulations and actual measurements is scheduled in this project to update the model parameters if necessary. This updating procedure can address the wear rate shift issue and guarantee the best possible prediction of RUL can be achieved at any particular time. The skeleton of the model-based wear prediction proposed in this project is shown in Figure 3.10. In the following sections, specific models and techniques for monitoring different wear phenomena will be introduced. It should be emphasized here that the main novelty of this model-based gear wear monitoring scheme is that regular comparisons between simulations and actual measurements are conducted to update the model parameters whenever necessary so that an accurate prediction of wear propagation can be achieved. Also, compared with wear particle measurements or images obtained through scanning the worn tooth profile, vibration has a unique advantage in that it can be easily and quickly obtained for updating purposes, without interrupting the operation of the gearbox.

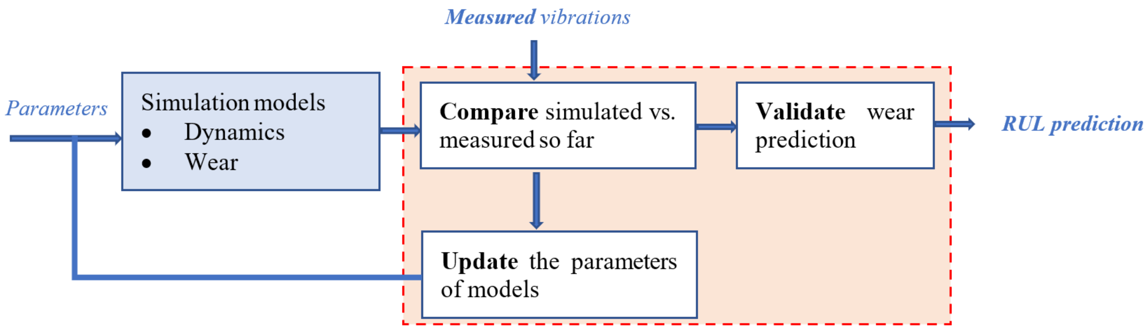

Figure 3.10 The skeleton of the model-based gear wear monitoring and prediction

3.4.1 Super gearbox dynamic model development (objective 2)

From the literature review of Section 2.4.1, modelling the contact force is a critical procedure for gear wear monitoring and prediction due to it is an important input of tribological (wear) models. Most of the existing researches use finite element models and empirical equations to calculate the contact force between the meshing gears, and the obtained contact force is under quasi-static conditions. However, in practice, the gear system is usually operating under dynamic conditions, and due to the inertial effects, dynamic meshing forces are typically larger than the corresponding quasi-static forces and their waveforms are quite different [21]. Therefore, the use of quasi-static force could bring noticeable errors to the subsequent wear prediction. Compared with the simple finite element model and empirical equations, the dynamic model can give a contact force under dynamic conditions which consider the inertia effects [18, 41, 107]. Therefore, the dynamic model is chosen to provide necessary inputs to wear models and generate simulated vibrations in this research.

To achieve objective 2 of this research, a 21 degree-of-freedom (DOF) lumped parameter dynamic model is established based on the UNSW gearbox test bench (as shown in Figure 3.2). The model includes the motor, shafts, gears, casing and couplings. The basic motion equations of the dynamic model are established based on Newton's Second Law of Motion.

To guarantee the outputs (such as dynamic contact forces and vibrations) from the dynamic model are close enough to the measurements from the experimental rig, the model has been validated and calibrated through a series of tests, including impact tests, speed ramp tests and several constant speed tests. More details of the dynamic model development can be found in Chapter 5. Note that the 21 degree-of-freedoms (DOFs) lumped parameter dynamic model is developed based on the fixed-axis spur gearbox test rig shown in Figure 3.2, whose structure and properties are different from the spur gearbox test rig shown in previously published work [18, 41, 107].

3.4.2 Monitoring and prediction of tooth profile changes from abrasive wear (objective 3)

With the dynamic contact force from the established dynamic model, the wear progression can be monitored and predicted through specific tribological (wear) models. Tooth profile change is one common wear phenomenon and it is usually caused by abrasive wear [19]. The tooth profile alteration can cause stress concentration, which increases the risk of tooth breakage significantly. Therefore, it is necessary to monitor and predict the tooth profile change from abrasive wear.

The physical-model based approach is chosen in this research to monitor the tooth profile change from abrasive wear, therefore, a tribological (wear) model which can represent the abrasive wear propagation behaviours and its induced tooth profile change is needed. From the literature review of Section 2.4.2, although many advanced wear models have been proposed using different methodologies and parameter sets, the Archard wear model [61] remains the most commonly used for practical applications, and is chosen in this research. However, none of the previously published research [21, 57, 62, 68, 108] considered the contribution of adjacent contact points to the wear depth accumulation with the Archard wear model, which can affect the wear distribution and then impair the wear prediction accuracy. Therefore, in this research, the Archard wear model is improved to calculate the wear depth on gear tooth, with consideration of the effect of Hertzian deformation, giving a contact area rather than a line, and the effects from adjacent contact points are included.

To solve the previously discussed wear propagation rate change issue, simulation and measured vibrations are compared regularly to update the model parameters if necessary, and a vibration-based scheme for updating gear wear prediction is proposed in this research project. The whole basic procedure of the proposed methodology is shown in Figure 3.11. The modelling component of this proposed methodology is composed of two interacting simulation models: a dynamic model and an Archard wear model. Based on the input of the gear tooth profile geometry, the dynamic model predicts gear tooth dynamic contact forces, which are passed on to the Archard wear model to estimate the gear wear distribution and consequently modify the gear tooth profile geometry, which is then fed back into the dynamic model. This iterative loop allows a knowledge-based prediction of gear wear propagation. To address the issue of changing wear rates (due to factors such as oil contamination, changes in operating conditions, changes in surface roughness, etc.), the vibrations from the gearbox dynamic model are compared to measured vibrations to track the quality of the wear model predictions and, if necessary, update the gear wear model parameters. This updating procedure is shown on the right of Figure 3.11, which is marked in red. As will be shown in the results presented in Chapter 6, the vibration-based updating scheme can deliver a reliable and accurate gear tooth profile change monitoring and prediction result from abrasive wear. More details of the development can be found in Chapter 6.

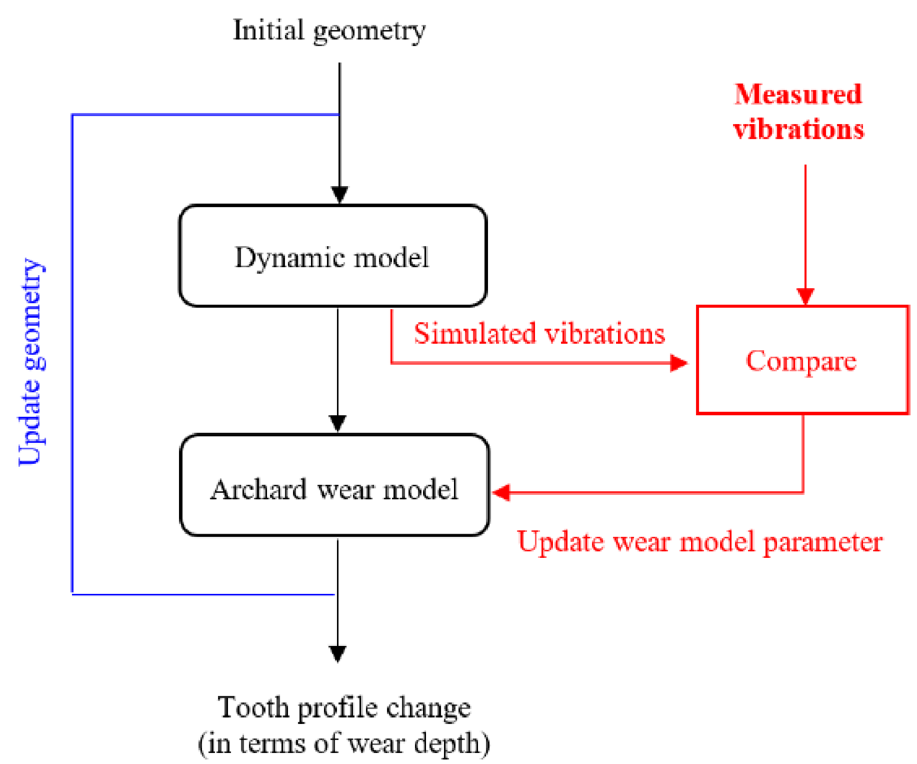

Figure 3.11 Basic procedures of the proposed vibration-based updating scheme for tooth profile change (from abrasive wear) predictions

3.4.3 Monitoring and prediction of surface pitting propagation and tooth profile change from abrasive wear using a digital twin approach (objective 4)

Fatigue pitting is another common wear phenomenon during the gear service life, it is caused by fatigue under cyclic loading, can result in large valleys on the gear tooth surface, but the effective working tooth profile (considered across the entire face width) often remains unchanged, unless pitting is extremely severe [19]. Therefore, fatigue pitting is very different from abrasive wear. Also, fatigue pitting could promote the generation of surface spalls across the entire tooth width, resulting in a reduction in gear tooth surface durability and/or even tooth breakage [4]. Therefore, it is necessary to monitor and predict the surface pitting propagation, which benefits the remaining useful life prediction of the gear system.

From the literature review of Section 2.5.2, most of the existing approaches for modelling surface pitting propagation are combinations of an elastohydrodynamic lubrication (EHL) model and fatigue criteria [8], which requires substantial computational resources and detailed knowledge of the surface micro-geometry and lubrication conditions due to the incorporation of surface roughness, prohibiting its widespread application in practice. To address this issue, in this research, a simple and efficient surface pitting model is derived to simulate and predict the pitting propagation behaviours based on the Lundberg-Palmgren model [80].

However, as with the previously discussed issue of changes in the abrasive wear rate, the surface pitting propagation rate would also be affected by a variety of factors – e.g., lubrication quality and quantity, contact pressure distribution, surface roughness and operating conditions, all of which may change significantly – and so without frequent checking and, if necessary, updating of the wear model parameters, the accuracy of the prediction results cannot be guaranteed and is likely to decrease significantly during the surface pitting propagation.

To accurately monitor and predict the surface pitting propagation, a similar vibration-based updating scheme as introduced in Section 3.4.2 is used in this research, as shown in Figure 3.12. In the proposed vibration-based updating scheme, contact pressure from the dynamic model is provided to the developed fatigue pitting model, and the surface pitting propagation can be predicted in terms of pitting density. The occurrence and progression of surface pitting could reduce the contact area of the mating gear tooth, then alter its contact pressure, which could impact the further surface pitting propagation. This knowledge-based surface pitting propagation is marked in black and blue as shown in Figure 3.12. To guarantee accurate predictions, regular updating of the pitting coefficients is implemented by comparing with measured vibrations (ICS2), when available, as marked in red in Figure 3.12. More details of the development of fatigue/surface pitting propagation prediction can be found in Chapter 7.

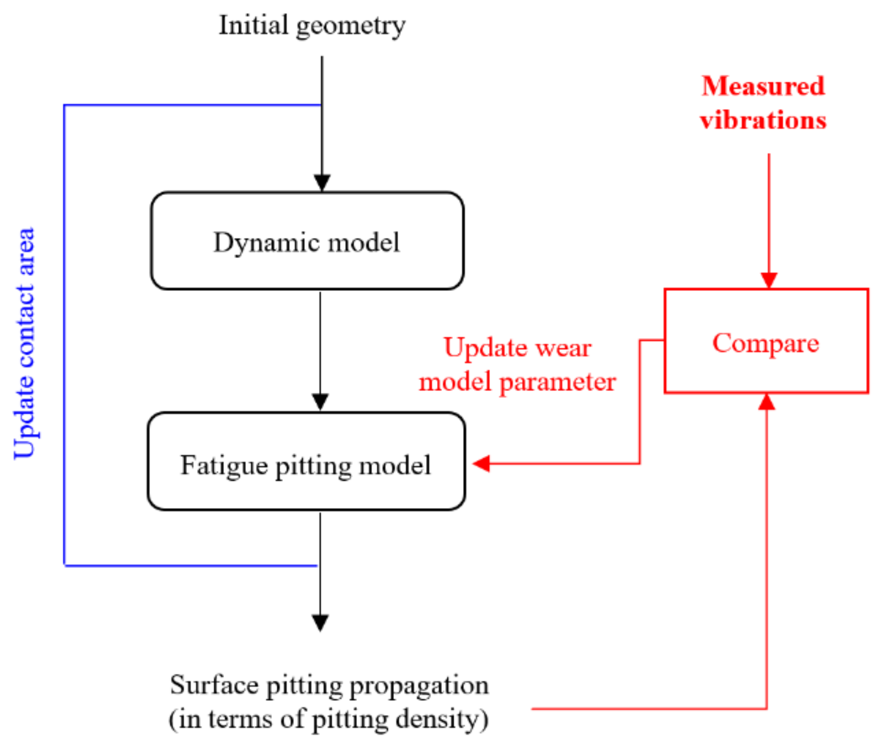

Figure 3.12 Basic procedures of the proposed vibration-based updating scheme for fatigue pitting propagation predictions

In practice, when fatigue pitting propagates, abrasive wear may co-exist due to oil contamination, thus, abrasive wear induced tooth profile changes and surface pitting can both occur as part of the surface degradation process in the same gear, either simultaneously or at different times, and these processes can strongly affect one another, Therefore, it is necessary to develop a reliable and efficient tool, which can utilise the capability of efficient physics-based models and measurements for predicting the surface pitting propagation and the tooth profile change caused by the co-exist abrasive wear.

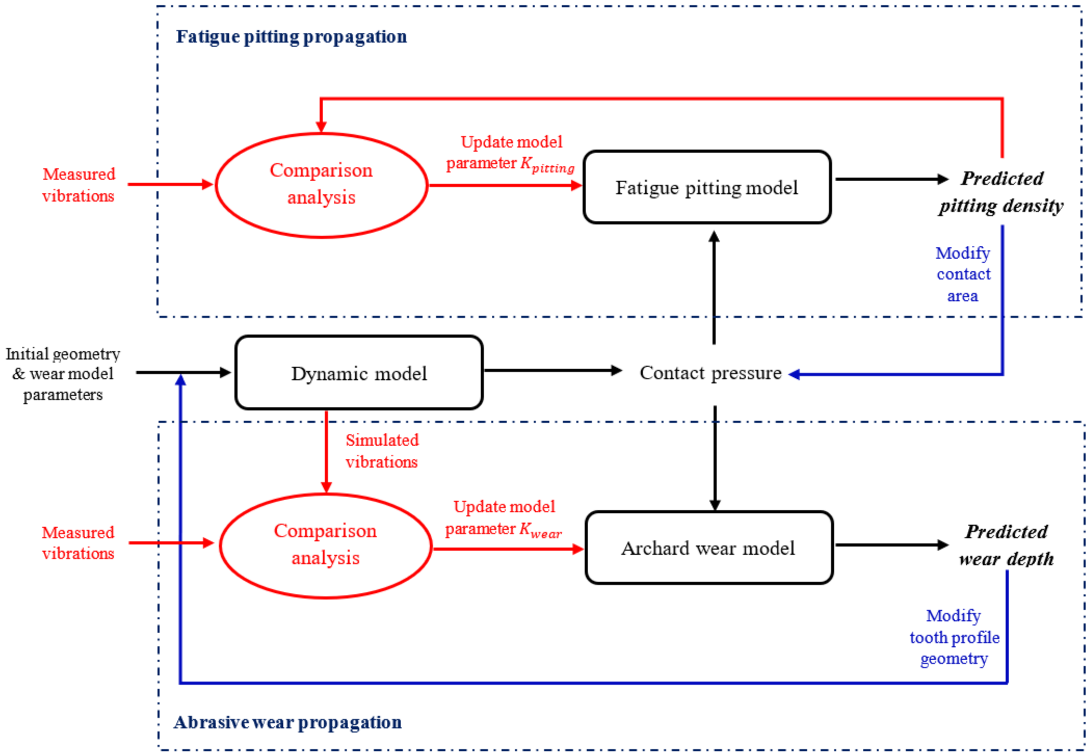

Figure 3.13 Basic procedures of the proposed digital twin approach for monitoring and prediction of surface pitting and tooth profile changes from abrasive wear

To address the above-mentioned issue, in this research, a digital twin approach for monitoring and prediction of surface pitting and tooth profile changes from abrasive wear is developed, whose skeleton is shown in Figure 3.13. Based on the inputs of gear tooth profile geometry and operating conditions, the dynamic model can provide dynamic contact forces and simulated vibrations of the gear system. The contact pressure can then be calculated using the Hertzian contact theory. With the contact pressure as an input, the Archard wear model can estimate the abrasive wear rate and consequently predict the gear tooth profile geometry at a specified future point in time, and this is then fed back into the dynamic model. Meanwhile, the contact pressure is passed on to a surface pitting model to predict the surface pitting density, which consequently modifies the contact area and then alters the Hertzian contact pressure. To obtain accurate predictions, regular updating of the wear coefficients is implemented by comparing measured vibrations, when available, with the simulations, as marked in red. More details of the development of the digital twin approach for monitoring and predicting both surface pitting propagation and tooth profile change can be found in Chapter 7.

Chapter 4 Identification of gear wear mechanisms and tracking wear evolution using cyclostationary properties of measured vibrations

The work presented in this chapter is devoted to achieving **objective 1** of this research: **identification of gear wear mechanism and tracking wear evolution using cyclostationary properties of measured vibrations**. This chapter is a modified version of the paper titled "*Use of cyclostationary properties of vibration signals to identify gear wear mechanisms and track wear evolution*", which was published in the journal of *Mechanical Systems and Signal Processing* (150: 107258, 2021). The main content of this chapter is identical to the above publication, while the structure has been arranged to ensure the consistency of the thesis.

This chapter is organized as follows. In Section 4.1, a brief introduction to this study is presented. Section 4.2 presents the relationship between tribological features and sliding induced vibration characteristics and introduces the hypothesis for wear mechanism identification. Section 4.3 presents the observations found in the experiments to validate the proposed hypothesis. A new vibration-based procedure for gear wear mechanism identification and wear tracking is proposed and applied in Section 4.4. A summary is given in Section 4.5.

4.1 Introduction

Fatigue pitting is a fatigue-induced material loss, after which the effective working tooth profile (considered across the entire face width) often remains unchanged (unless pitting is extremely severe). In general, fatigue pitting originates from a subsurface crack and occurs initially at the dedendum of the gear tooth or near the pitch line, due to the repetitive rolling-sliding contact and high contact stress [4, 109]. In contrast, abrasive wear, usually caused by particle contamination or lack of lubrication [9], is the removal of material (often across the entire face width) induced by sliding contact, and every piece of material removed contributes to a change in the profile [19]. Fatigue pitting and abrasive wear have different effects on the gear tooth surface and profile geometry. Therefore, it is necessary to identify and monitor fatigue pitting and abrasive wear separately for wear prediction, so that appropriate maintenance decisions can be made to avoid catastrophic failures, unexpected economic losses and serious accidents.

Vibration analysis is an effective approach to monitor the health state of machines [10, 110-112], and it has been well established for detection and diagnosis of common gear faults such as gear tooth root cracks [113-115], surface spalls [116-119] and tooth breakage [120-123]. However, vibration-based techniques for wear analysis, including wear mechanism identification and wear tracking, are rather rare. One reason for this is that there is a coupling effect between gear wear and gear dynamic characteristics, which produces complex gear dynamic characteristics/vibration features [21, 124], making it difficult to extract wear-related vibration features and develop specific vibration-based indicator(s) for wear identification and monitoring.

From the literature review of Section 2.3, it can be found that most of the existing vibration-based gear wear monitoring techniques were designed for detecting and tracking gear tooth profile change (accumulated gear wear), which is usually caused by abrasive wear. More specifically, the existing vibration-based techniques use gear meshing harmonics or signal "power", which is mainly based on the deterministic components of vibration, to monitor the gear wear process in terms of tooth profile change. Since fatigue pitting does not change the tooth profile noticeably (unless pitting is extremely severe) [19], it has a negligible effect on the deterministic components of vibration, which are closely related to gear macro-geometry, i.e., the tooth profile. Therefore, these proposed techniques in processing deterministic components of vibration have very limited ability to identify gear wear mechanisms and track fatigue pitting severity.

In contrast, the random signal components induced by varying sliding motions and contact forces contain useful information for gear wear mechanism identification and wear severity tracking because they are closely related to gear surface morphology characteristics [105, 106]. Furthermore, even though gear wear (fatigue pitting and abrasive wear) is usually likely to be uniform around the gear, it is still random from tooth to tooth. Therefore, studying the random signal components could bring benefits with respect to gear wear mechanism identification and the development of wear severity monitoring techniques. However, there is very limited research on the random signal components modulated by gear mesh behaviours and on how these components might be used to wear monitoring.

In recently published research [14, 15], the relationship between gear surface roughness and sliding induced random vibration was investigated. In the gear transmission system, all gear operations involve some form of sliding contact between the mating gear surfaces, and this sliding contact can produce random vibrations from the asperity contacts between the gears, the nature of which is dependent on a number of factors, such as the speed and load, the lubrication conditions and the micro-geometry of the surfaces. Therefore, the sliding induced vibrations have random characteristics. With this as a basis, second-order cyclostationarity was found in the sliding induced vibrations due to the time-varying sliding velocity [125] and contact force on the gear tooth pairs in reference [15]. A positive relationship between gear tooth surface roughness level and the degree of second-order cyclostationarity (CS2) of vibration was found. However, the connection was found by a later investigation [14] to be more complex, based on a wider range of roughness values and a longer experimental duration. To date, insufficient conclusions could be drawn in evaluating the cyclostationary features for vibration-based gear wear mechanism identification and wear severity tracking.

Even though the cyclostationarity of vibration signals has been widely studied, most published works have focused on signal modulation characteristics, using the 'degree' of cyclostationarity (for example a measure of the level of amplitude modulation) to correlate with fault severity [28, 126, 127], while studies on the spectral frequency of cyclostationary vibration at gear mesh cyclic frequency are rare. In other words, properties associated with the cyclic frequency α have been widely studied, while those of the carrier (spectral) frequency f have not, despite both having clear physical underpinnings. In Ref. [14], the authors used the mean carrier frequency to investigate the impacts of speed on the vibration signals modulated at the gearmesh frequency. Although a direct ratio between the mean carrier frequency and running speed was found, no further investigation was undertaken; for instance, the relationship between the carrier frequency and gear surface morphology was not investigated.

Inspired by the achievements reported in Refs. [14, 15], this study aims to develop a vibration-based approach for gear wear mechanism identification, and then to track wear evolution with the help of a cyclostationary indicator, the combination of which was not investigated previously. This work is based on the observation that sliding vibration signals are strongly influenced by the surface features induced by different wear mechanisms and also affected by modulation effects caused by sliding velocity.

4.2 Hypothesis and proposed vibration-based approach for gear wear identification

In this section, the surface feature differences arising from fatigue pitting and abrasive wear are introduced and summarised, followed by a brief description of micro-level gear surface feature effects on sliding induced vibrations. A hypothesis for gear wear mechanism identification will then be presented, after which a vibration-based wear mechanism identification approach is presented.

4.2.1 Surface feature differences and their effects on sliding vibrations

As mentioned before, from a macro-scale point of view, abrasive wear tends to introduce a change to the gear tooth profile, while fatigue pitting has negligible effects on the gear tooth profile unless the fatigue pitting is extremely severe [19]. Both abrasive wear and fatigue pitting change the micro-geometry of gear tooth surfaces, that is, the surface morphologies in a micrometre scale, as demonstrated in Figure 4.1 (abrasive wear) and Figure 4.2 (fatigue pitting). The images were obtained using a moulding procedure outlined in Ref. [128]. Abrasive wear causes scratches or gouges on the tooth surface that are oriented in the direction of sliding. As a result, the worn, rough surfaces have micro-scaled morphological features in short wavelengths and high spatial frequencies [23], while profile changes are long wavelengths. Fatigue pitting will instead introduce large valleys on the gear tooth surface, which contain longer wavelengths and lower spatial frequencies [20] in comparison with surface roughness changes associated with the abrasive wear process. These surface feature differences can help in separating fatigue pitting and abrasive wear.

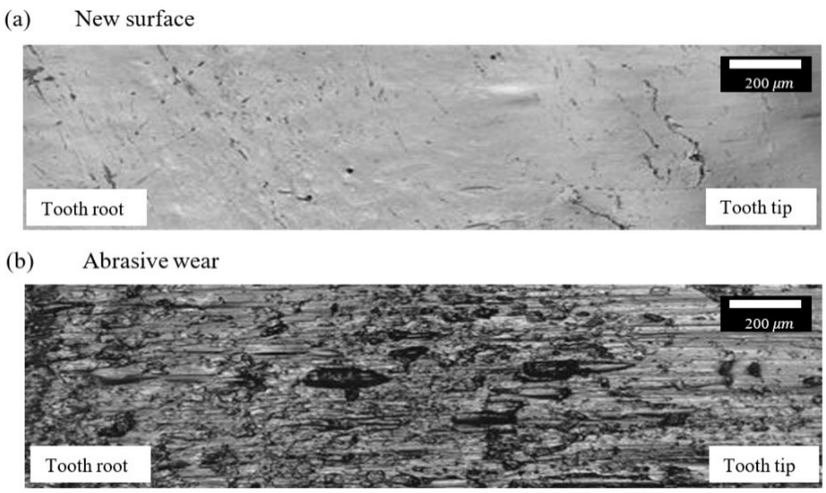

Figure 4.1 Changes to gear surface morphologies in abrasive wear process and in the micro-scale: (a) a new surface; (b) a worn surface subjected to abrasive wear

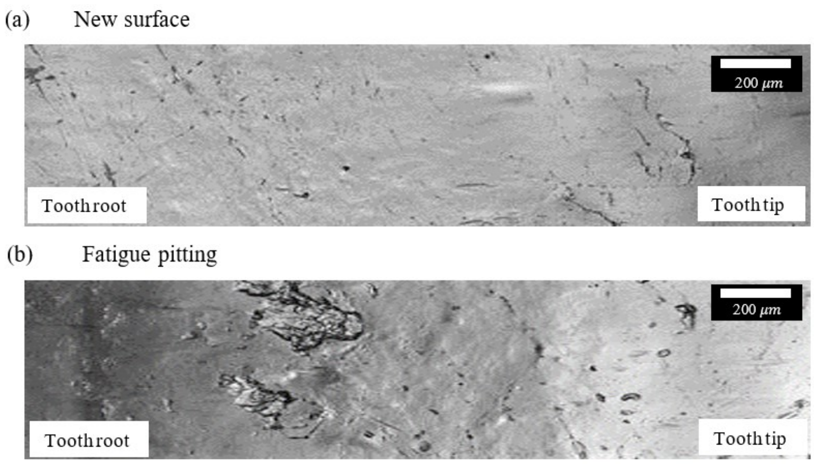

Figure 4.2 Changes to gear surface morphologies in a fatigue pitting process and the micro-scale: (a) a new surface; (b) a pitted surface

For gear systems, the surfaces of contacting gear teeth are subject to combined rolling and sliding action as the gears rotate. Since rolling resistance is considerably smaller than the sliding resistance [129], usually, its contribution to the total tooth friction is ignored, and only the sliding induced friction is considered. During the gear meshing process, the sliding induced tooth friction will result in the generation of vibration, which is a random signal and is closely related to the gear surface morphology [106]. Even though the sliding induced vibration might have very low energy compared with the vibration induced by macro-geometric effects (such as tooth profile change) of gears, it contains rich information about the surface morphology. It has been proposed that the surface morphology information can be detected and extracted through cyclostationary tools as demonstrated in Ref. [15]. Therefore, the use of cyclostationary properties of sliding induced vibration should be able to identify different wear mechanisms and then track their evolution. In the following sections, this possibility will be further explored and investigated.

4.2.2 Hypothesis for wear mechanism identification

The sliding induced vibration from the asperity contacts between two mating gears is closely related to the surface morphology. Different surface morphologies will result in different frequency components of sliding induced vibration. The relationship between the spatial frequency of the surface morphology and the frequency of sliding vibration can be assumed to follow the relationship

$$f_v \propto v_s \cdot f_s \tag{4.1}$$

where f_v (Hz) is the dominant sliding induced vibration frequency, v_s $(\mathrm{m/s})$ is the sliding velocity of the mating gear surface and f_s $(1/\mathrm{m})$ is the dominant spatial frequency of the roughness of the mating surfaces. Despite the presence of multiple phenomena (e.g., the dependency of power on load, transfer function effects), it is at least expected that, even if not quantitatively following this relationship, the frequency range characterising vibration due to sliding will grow with sliding velocity and spatial frequency of the roughness of the mating surfaces. The sliding velocity v_s is determined by the gear kinematics and remains virtually unchanged under mild/medium wear (micro-level). Surfaces modified in an abrasive wear process or fatigue pitting process have different spatial frequencies, as shown in Figure 4.3 and Figure 4.4 respectively. This is expected to affect the spectral content (carrier frequency band) of the resulting gearmesh-cyclic CS2 components. Based on the above assumptions, we expect that:

1) sliding of fatigue pitted surfaces, exhibiting low spatial frequency, should generate gearmesh-cyclic CS2 components with low spectral frequencies (Figure 4.3), and
2) sliding of worn surfaces subject to abrasion, characterised by surface morphologies with high spatial frequency, should result in gearmesh-cyclic CS2 components with high spectral frequencies (Figure 4.4).

It should be noted that in the above discussion, Eq. (4.1) and Figure 4.3 and Figure 4.4 are used to describe the manner of *excitation*, and that the measured response would be shaped by a system transfer function, and so the observed dominant carrier frequencies in the CS content of the measured signal would also depend on system resonances, as well as the cyclostationary tool used for their detection. While the theoretical excitation frequency (band) would be directly proportional to speed and surface spatial frequency, the observed vibration carrier frequency (band) is likely to appear to move discretely between dominant resonances. The fact that system resonances are generally not of uniform strength further complicates this phenomenon. To mitigate this issue, “normalised” cyclostationary tools such as cyclic-coherence [130] can be chosen to investigate the spectral content of the signals.

Based on this physical intuition, analysing the relative carrier frequency range of sliding induced vibrations is a promising approach for identifying fatigue pitting and abrasive wear. This hypothesis will be validated using experimental data in Section 4.3.

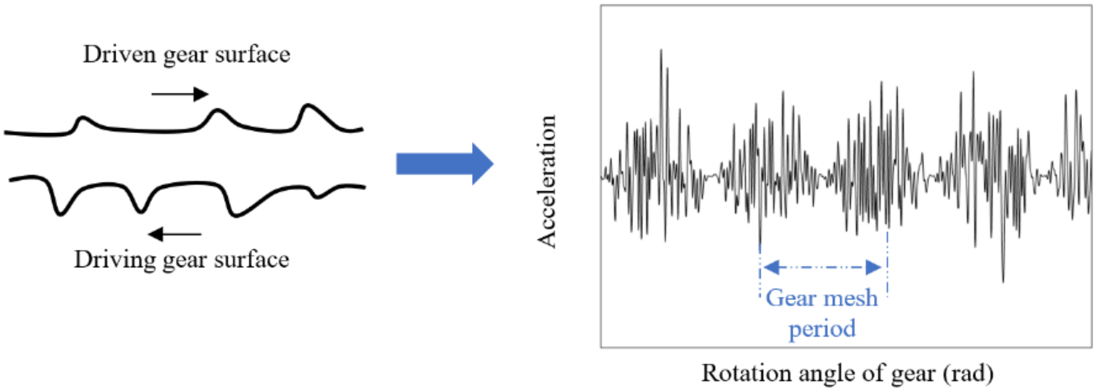

Figure 4.3 The fatigue pitting induced sliding vibration characteristics

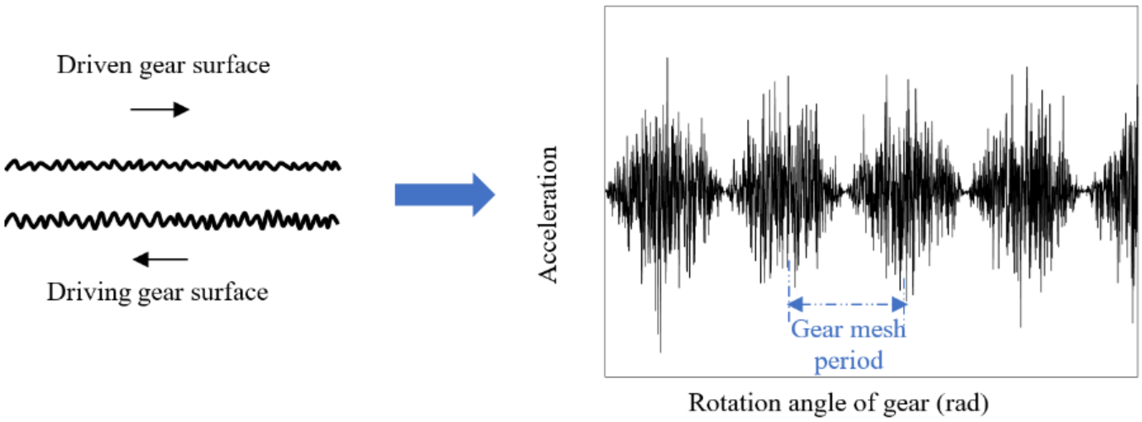

Figure 4.4 The abrasive wear induced sliding vibration characteristics

4.2.3 Proposed vibration-based approach for wear mechanism identification

To summarise the previous discussion, it is expected that (i) the CS2 vibration components with gearmesh cyclic frequency are symptomatic of changes in tooth surface morphology; and, (ii) the dominant spectral (carrier) frequency f of those CS2 components can be used to determine the key wavelengths of surface alterations and therefore the dominant wear mechanism.

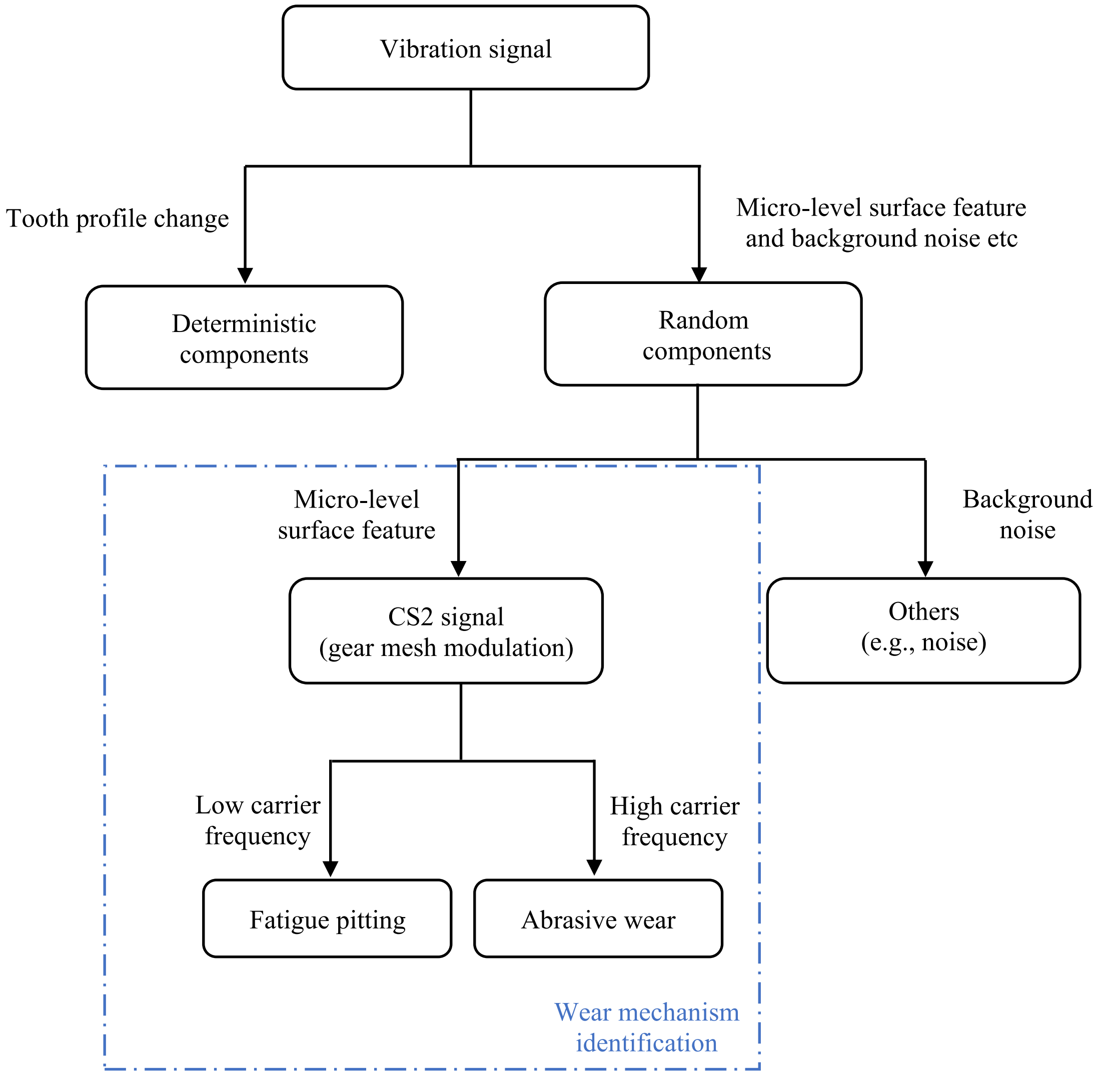

Figure 4.5 Diagram of vibration-based gear wear mechanism identification approach

With these hypotheses, a vibration-based approach for gear wear mechanism identification is illustrated in Figure 4.5. In the vibration signal, only the random components with second-order cyclostationarity (CS2), with a cyclic frequency corresponding to a particular gearmesh, are considered for gear wear (fatigue pitting and abrasive wear) identification. The deterministic ones are expected to be instead correlated to macroscopic profile changes (more severe wear effects). The proposed vibration-based wear identification approach is validated using experimental data in the following section.

It must be noted that the scope of this work has been restricted to micro-surface alteration and therefore to the random components of vibration, but future developments could then combine this information with that extracted from the deterministic component for a full picture of the tooth degradation.

4.3 Observations in gear systems

4.3.1 Tribological features used to describe fatigue pitting and abrasive wear propagation

It was observed through visual inspection that wear (fatigue pitting and abrasive wear) occurred quite uniformly on the gears and that the pinion was worn much more severely than the driven (big) gear due to the gear ratio. An optical microscope with a 5× magnification objective lens was used to capture 2D images of the gear moulds to monitor the wear progress qualitatively. A laser scanning confocal microscope (LSCM) was used to capture 3D images of the gear moulds for quantitative analysis. The captured 3D images contain the height and spatial information of the gear tooth surfaces for numerical characterisations of changes in the surface morphologies during the wear processes.

For fatigue pitting, initially, both the number and size of the pits increase, until the pitting becomes quite severe, at which point nearby pits tend to join and the actual number of pits may decrease. Thus the most robust indicator to describe pitting severity is probably the pitted area, and in Section 4.4 this is used to assess the performance of the proposed technique in monitoring pitting propagation.

For abrasive wear, a high wear rate often results in a surface deviation from a perfect involute (macroscopic profile change). Meanwhile, at the micro-level, the gear tooth surfaces tend to become rougher when abrasive wear propagates (very short wavelength) [131]. Surface roughness S_a, the arithmetic average of absolute values of surface deviation from the mean surface level, is often used to characterise the surface change in the micro-meter level. In this work, surface roughness S_a is applied as the tribological reference to help check the capability of the vibration-based indicators/techniques in monitoring the abrasive wear induced micro-surface feature change, which will be introduced in Section 4.4.

4.3.2 Theory of vibration-based wear mechanism identification techniques

In this section, the hypothesis and proposed approach in Sections 4.2.2 and 4.2.3 for wear mechanism identification are introduced in detail.

To obtain the sliding induced vibrations, the deterministic/random signal separation technique, time synchronous averaging (TSA) or discrete/random separation (DRS) [132-136] is applied to remove the deterministic components of the vibrations. The remainder is referred to as the residual signal. Spectral coherence, defined in reference [130], is employed to qualitatively explore the spectral frequency distribution of sliding induced vibration at gear mesh cyclic frequency, and to compute what will be referred to as "mean carrier frequency" (i.e., the first moment of the spectral-coherence along the spectral frequency axis). The definition of spectral coherence is

$$\gamma_x(\alpha, f) = \frac{S_x(\alpha, f)}{\sqrt{S_x(0, f)S_x(0, f-\alpha)}} \tag{4.2}$$

where $S_x(\alpha, f)$ represents the ordinary power spectral density at frequency f. I.e., the CS content at frequency f is normalised by the power at frequencies f and $f-\alpha$ in the stationary part of the signal.

Even though the deterministic components of vibrations are removed using TSA, in the residual signal, the sliding induced vibration is still mixed with the background noise, which brings difficulties in extracting surface morphology related information for wear mechanism identification and wear severity tracking.

CS2 signals have a close relationship with surface morphology [14, 15, 137, 138]. The general hypothesis is that when the surface roughness increases due to the occurrence of fatigue pitting or abrasive wear, the friction between the mating gear surfaces will increase, resulting in a stronger sliding induced vibration, while the gear mesh modulation pattern remains unchanged. Therefore, it is hypothesised that the second-order cyclostationarity of the sliding induced vibration will increase correspondingly, as qualitatively depicted in Figure 4.6.

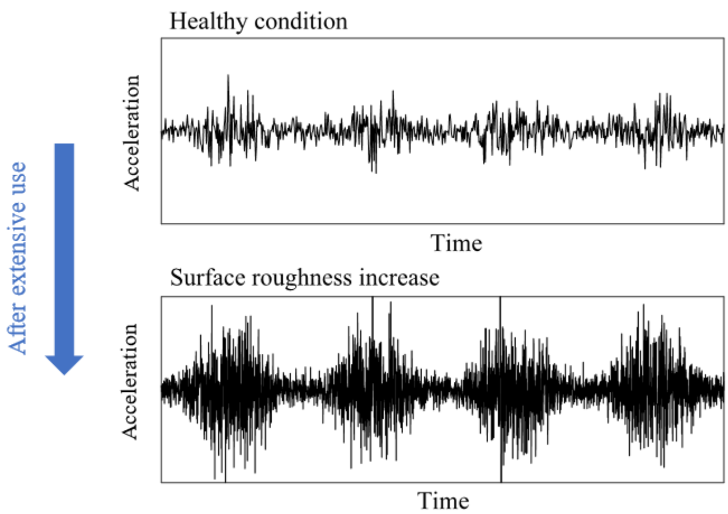

Figure 4.6 Diagram to illustrate the hypothesis: increase in second-order cyclostationarity due to an increase in surface roughness (induced by fatigue pitting or abrasive wear)

ICS2 [37, 139], an indicator to measure the degree of second-order cyclostationarity, can be used to assess the phenomenon illustrated in Figure 4.6, relative to stationary background noise. The definition of ICS2 is

$$\mathrm{ICS2}^{\mathcal{A}_\mathrm{h},\mathrm{H}} = \frac{\sum_{\mathrm{h}=1:\mathrm{H}} \max\limits_{\mathrm{n}\in\mathcal{A}_\mathrm{h}} (\mathrm{SES}[\mathrm{n}]^2)}{\mathrm{SES}[0]^2} \tag{4.3}$$

where $\mathcal{A}_\mathrm{h}$ with $h = 1$ is a set of cyclic frequencies of interest (with a tolerance band in the case of expected cyclic frequency deviations), and $\mathcal{A}_h$ ($h = 2, \ldots, \mathrm{H}$) represents the equivalent sets for the corresponding harmonics. H indicates the maximum gear mesh harmonics to be taken into consideration. In the case of gears, to monitor gear wear progression, $\mathcal{A}_1$ is set as the gear mesh frequency with 3 times the cyclic resolution as the tolerance band. SES is the squared envelope (amplitude) spectrum [110]. Note that the background noise is a stationary signal because any signal value (event) is equally probable to happen given any other signal value (another event) at any two time instances no matter how far apart they are.

With the use of a $1/3$ -binary tree filter bank (or other similar decomposition representation) [140], ICS2 can be used to select one band with maximum cyclostationarity, in which the influences of background noise become less significant and the vibration characteristics related to surface morphology are enhanced [139].

Based on the hypothesis in Section 4.2.2, the ICS2-based frequency band selection results will be different for fatigue pitting and abrasive wear, and can be used to separate them. Further, because background noise is minimised in the selected frequency band, the ICS2 level within the selected band should have better performance in tracking the evolution of fatigue pitting/abrasive wear severity compared with the full-band ICS2 level. The effectiveness of ICS2-based wear mechanism identification and wear monitoring is validated in Section 4.3.3 and Section 4.4, respectively, using experimental data measured from gear systems.

4.3.3 Observation results

In this section, the observation results in gear systems using the above-mentioned techniques, spectral coherence map and ICS2-based band selection, are presented to validate the hypothesis for wear mechanism identification proposed in Section 4.2 and Section 4.3.2.

Observation results of the lubricated test

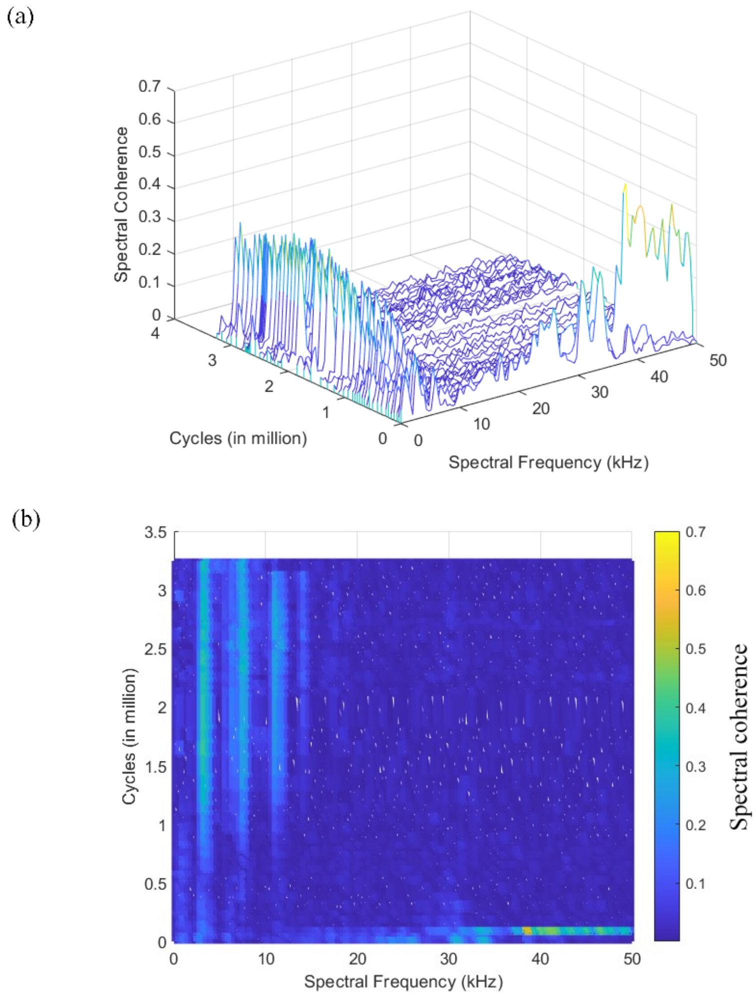

Figure 4.7 Lubricated test: (a) Carrier frequency distribution at gear mesh (cyclic) frequency; (b) Top view

Figure 4.7 shows the distribution in the spectral coherence of the gearmesh-cyclic CS2 component (cyclic frequency) for the lubricated test at 10 Hz, in which fatigue pitting is the dominant wear mechanism. The spectral coherence software developed in Ref. [141] was used for this analysis. From Figure 4.7, it can be found that the carrier frequency distribution is quite different before and after 0.23 million wear cycles. Before this point, the spectral coherence is highest for carrier frequencies around 30-50 kHz, this being interpreted as being caused by the initial rough surface prepared using sandpaper, which exhibits high spatial frequency content. The initial high carrier frequency with high spectral coherence, therefore, supports the hypothesis of Section 4.2.2 that the gearmesh-modulated CS2 carrier frequency range is closely connected with the spatial frequency of the gear tooth surfaces.

After the run-in period (i.e., after the 0.23 million cycles), the roughening marks were worn away, and fatigue pitting started propagating. During this process, the dominant carrier frequency band jumps to the low-frequency range, below 15 kHz. This phenomenon matches with the hypothesis (in Section 4.2.2) that sliding surfaces with low spatial frequency content, such as from fatigue pitting, will induce CS2 vibrations with lower carrier frequencies. Note that the distinctive vertical parallel bands shown in Figure 4.7 are indicating the resonances of the gear system. This phenomenon will be further explained with the spectral coherence maps under different rotational speeds.

The ICS2-based selection results at 10 Hz are demonstrated in Figure 4.8. Similar to Figure 4.7, before 0.23 million cycles, a high carrier frequency range is selected. After 0.23 million cycles, the selected frequency band jumps to the low-frequency range. This again supports the hypothesis connecting surface spatial frequency and CS2 carrier frequency, suggesting strong potential for differentiating between abrasive wear and fatigue pitting. Note that there is an abrupt change in [2.30~3.00] million cycles. During this period, there is a decrease in the total pitted area, which has been described in Ref. [128]. The cause of decreased pitted area might be that the generation of new pits achieves balance with the filling-in of existing cavities, perhaps from wear debris pressed into the cavities under the meshing load [142]. Thus, during this period, the excitation has changed, and so a different resonance(s) becomes dominant in the response. The ICS2 based band selection results are affected, resulting in the occurrence of abrupt changes. After this 'abnormal' period, the ICS2 based band selection shift back to the low frequency again, still indicating a low spatial frequency of pits. To help the reader obtain an intuitive understanding of this phenomenon, the gradual fatigue pitting propagation process is demonstrated in Figure 4.9.

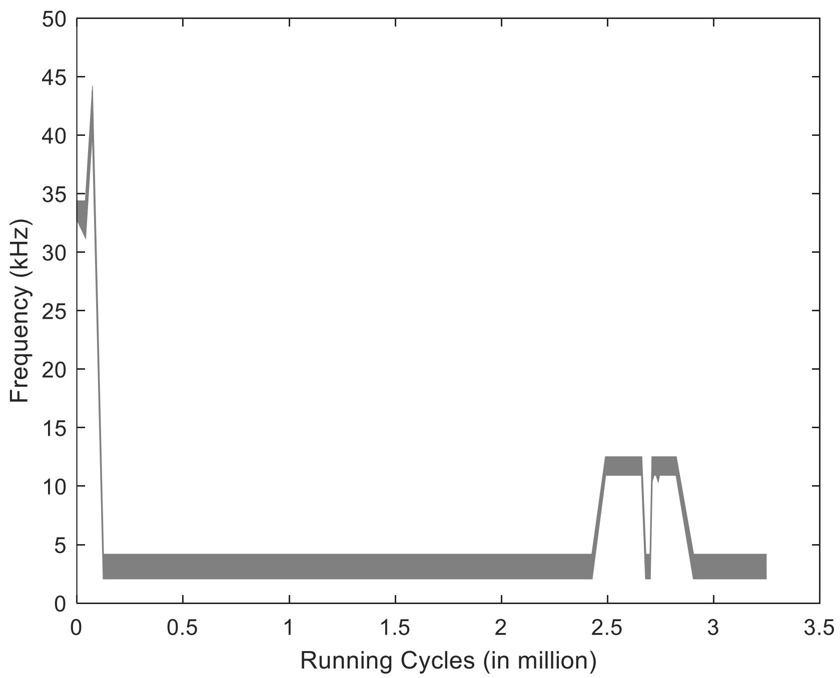

Figure 4.8 Lubricated test: ICS2-based band selection results

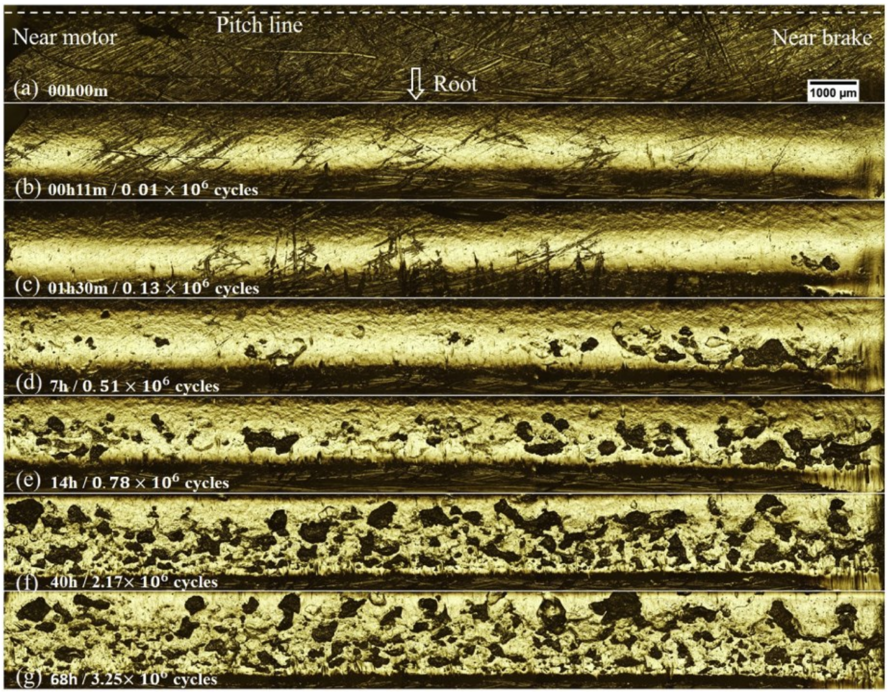

Figure 4.9 Figure pitting evolution on the dedendum of pinion tooth [128]

To validate the fatigue pitting related carrier frequency range, power spectral density (PSD) analysis [143-145] was applied on the scanned images (see Figure 4.10) to find the spatial frequency affected by fatigue pitting initiation and propagation. Note that even though the images in Figure 4.10 were captured at the same location of the same tooth, some features disappear due to new pits filling in existing cavities, resulting in some dissimilarities and a non-monotonic trend in the overall pitted area; however, the spatial frequencies it represents during fatigue pitting propagation are still reliable. The PSD function provides a representation of the density of the squared amplitude (height from a fixed reference) of a surface's morphology as a function of the spatial frequency of the morphology (units $\mu m^2 / \frac{1}{\mu m} = \mu m^3$). Spatial frequency is the inverse of the wavelength of the morphology features. The PSD analysis results are depicted in Figure 4.11, which shows that the spatial frequency range affected by fatigue pitting is [0.0012~0.0146] (1/μm). The sliding velocity (absolute value) range is [0~0.4461] (m/s) according to the dynamic model used in Ref. [124]. Based on Eq. (4.1), taking the central value of this sliding velocity range, the fatigue pitting related vibration frequency range is expected to be around [0.27~3.27] kHz. The upper part of this range matches very closely the results shown in Figure 4.7 and Figure 4.8. The hypothesis for fatigue pitting from Section 4.2.2 – that fatigue pitting induces CS2 signals with low carrier frequencies – is therefore at least qualitatively supported by the lubricated test results. It is important to note that Eq. (4.1) is expected to be only qualitatively matching with the results, given the effect of transfer functions and background-noise distribution which could bias the choice of the ICS2 indicator, for instance towards an area where background noise is lower.

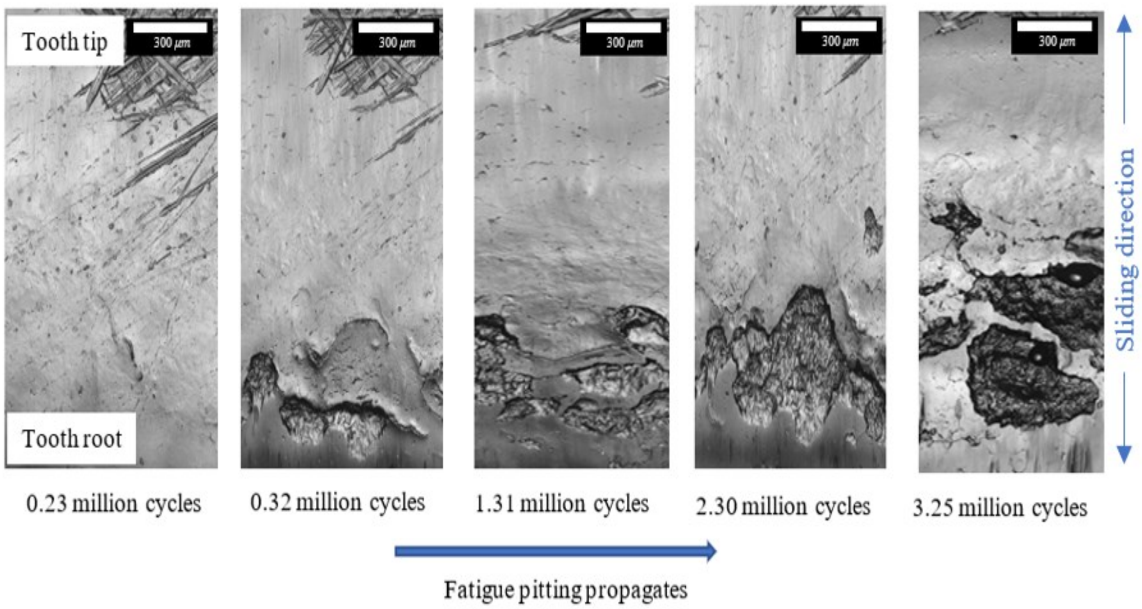

Figure 4.10 3D images of fatigue pitting propagation in the lubricated test

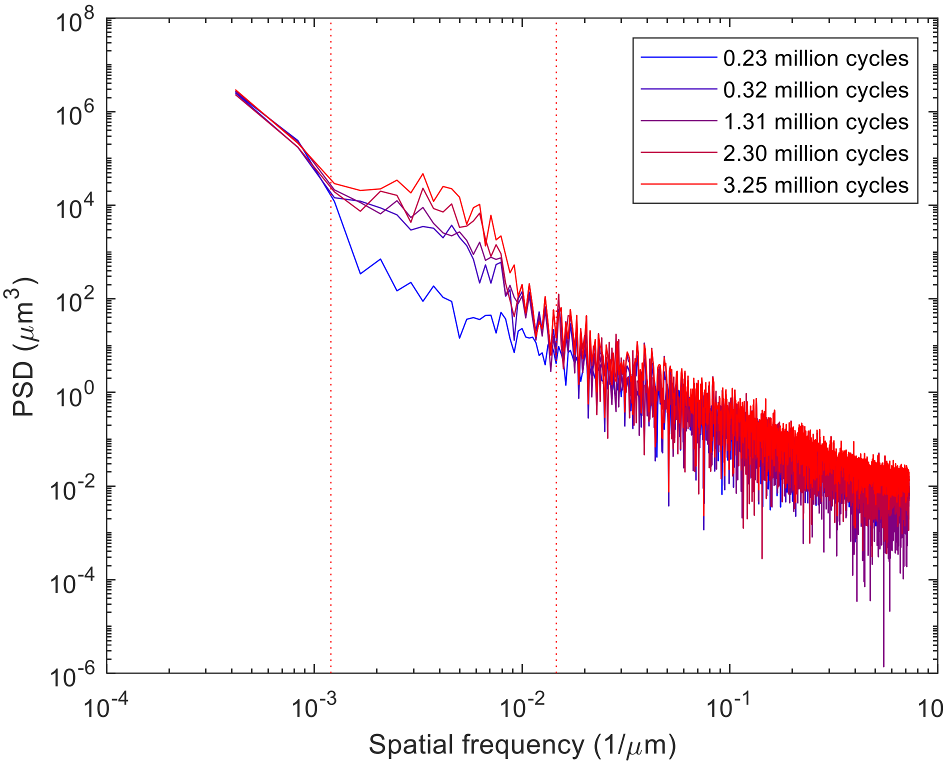

Figure 4.11 PSD analysis results of the scanned images of the lubricated test in Figure 4.10

In the above discussion, the relationship between the carrier frequency of the vibration and spatial frequency of the gear surface has been investigated and the hypothesis supported. In the following, the sliding velocity effects on the carrier frequency are investigated.

Figure 4.12 shows the spectral coherence maps for different speeds: 10, 16 and 20 Hz. Next, a mean carrier frequency at gear mesh cyclic frequency was calculated for different speeds (Figure 4.13) over two frequency ranges. The mean carrier frequency was obtained based on the distribution of the spectral coherence along the spectral axis, for the cyclic component at gearmesh frequency. Figure 4.13(a) is averaged over the range 0-30 kHz, and Figure 4.13(b) over the range 0-50 kHz. Even though Figure 4.12 shows that the dominant CS2 part (with highest spectral coherence) is below 30 kHz at all speeds, the range of 0-50 kHz was included for unbiased comparison with the results, shown later, for dry wear (Figure 4.14). Figure 4.12 and Figure 4.13 show that an increase in sliding velocity (induced by increasing rotating speed) basically leads to an increase in mean carrier frequency, in accordance with Eq. (4.1). The fact that the calculated mean carrier frequency does not match with the raw product of the quantities on the right-hand side of Eq. (4.1) can be explained. It is largely due to background noise (most evident in the difference between Figure 4.13(a) and (b), with the uniform noise above 30 kHz giving a bias to a higher mean frequency in particular for the 10 Hz result), and the use of spectral coherence rather than actual spectral power. The choice of spectral coherence, itself a measure of cyclostationarity, will bias the position of the dependent mean carrier frequency, but it was necessary to amplify the fairly weak CS2 content, in particular near modulated resonances, where the signal/noise ratio is higher, yet still limit the strong effects of resonances. Despite this limitation, the fixed resonances are clearly evident in Figure 4.12 at the different speeds, and rather than the mean frequency directly obeying Eq. (4.1), as for the expected *excitation* band, which would move gradually (on a continuum) depending on speed and spatial frequency, the dominant carrier frequency in the *response* would tend to move discretely between dominant bands. Nonetheless, the qualitative effect of sliding velocity on the vibration carrier frequency is clearly seen to be supported.

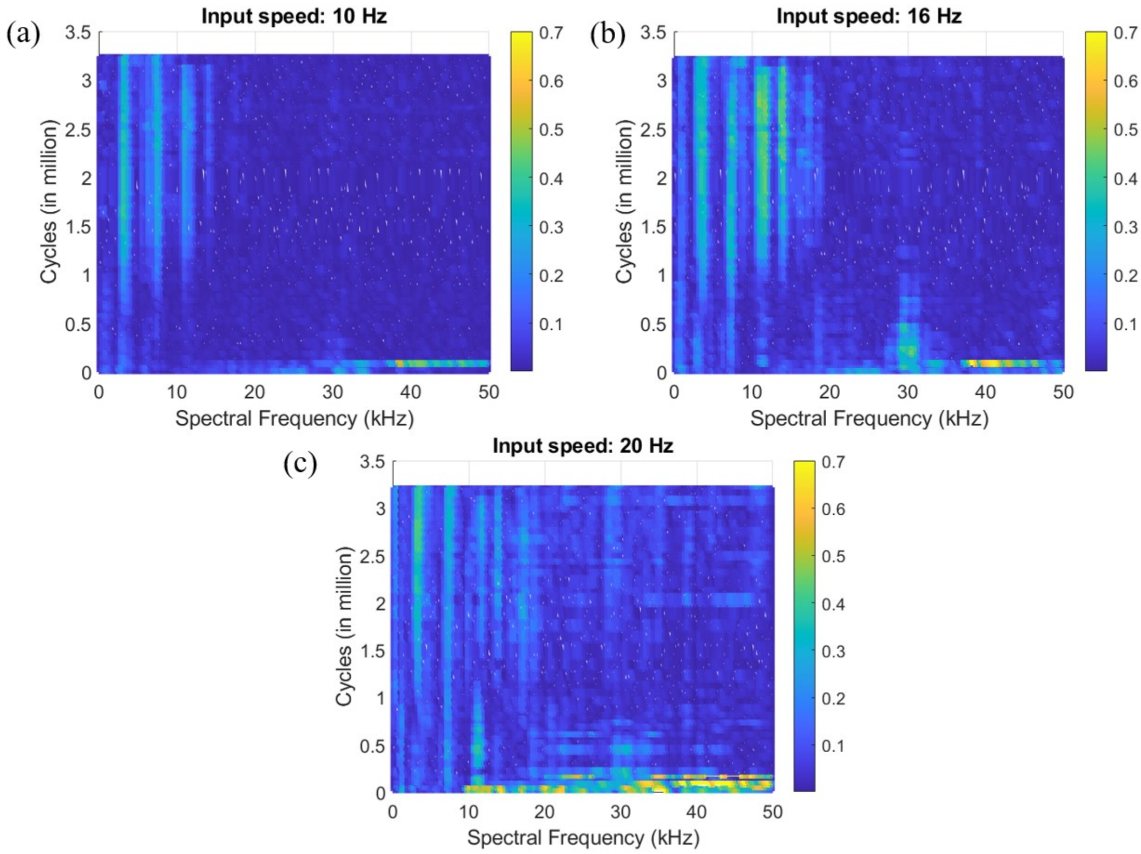

Figure 4.12 Carrier frequency distribution at gear mesh (cyclic) frequency at different speeds (top views) of lubricated test: (a) input speed: 10 Hz; (b) input speed: 16 Hz; (c) input speed: 20 Hz

When ICS2-based band selection results, as in Figure 4.8, were compared for the three different speeds, despite them all indicating carrier frequencies within the range up to 20 kHz (as indicated in Figure 4.12, at least after the initial run-in period), the variation with speed was not monotonic, but this can also be explained. The ICS2 value is much more sensitive to resonances than the spectral coherence, and is also a sum over a number of harmonics of gearmesh frequency (rather than just the first as for Figure 4.12). It is quite possible that at low speed a high harmonic of the gearmesh frequency will be greatly amplified by a high-frequency resonance and bias the effective carrier frequency. The ICS2 parameters are more directly affected by the amount of modulation, and are used later (Section 4.4) as indicators of the severity of wear.

(a)

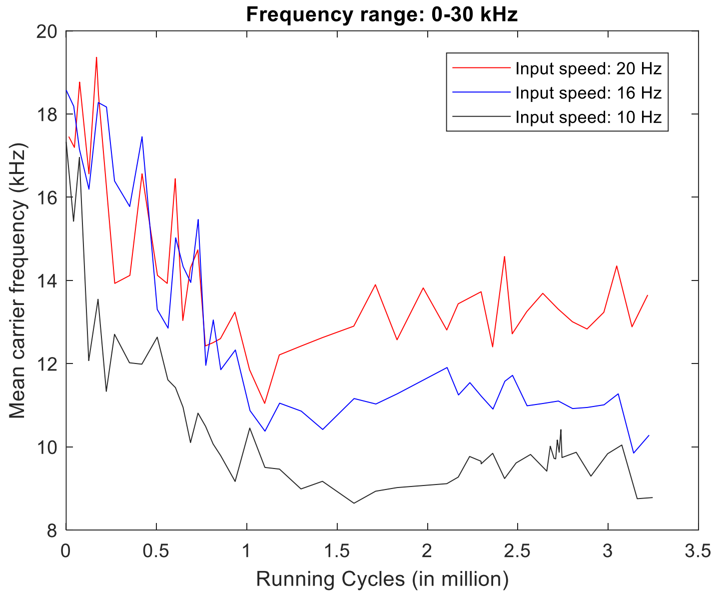

(b)

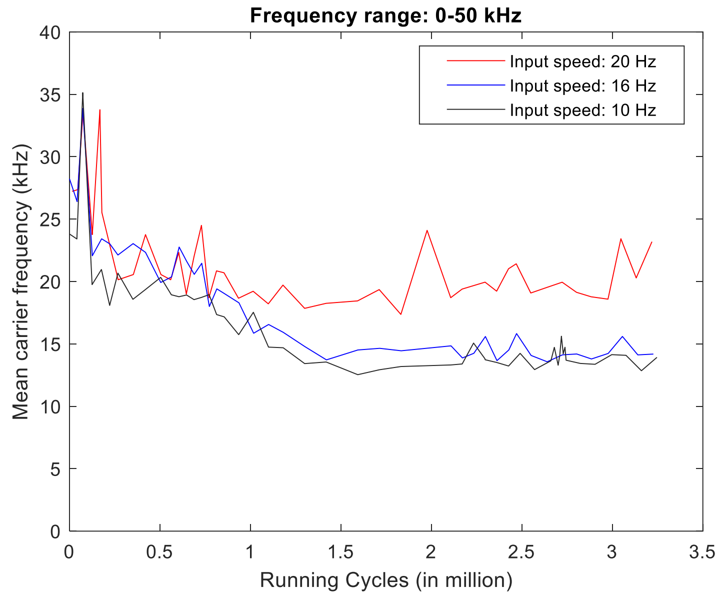

Figure 4.13 Mean carrier frequency with different rotating speeds of lubricated test: (a) frequency range: 0-30 kHz; (b) frequency range: 0-50 kHz

Observation results of dry test

Again, spectral coherence analysis is applied to the dry test to investigate the carrier frequency distribution with abrasive wear. The carrier frequency distribution (in terms of spectral coherence) at the gear mesh (cyclic frequency) for the dry test records is illustrated in Figure 4.14.

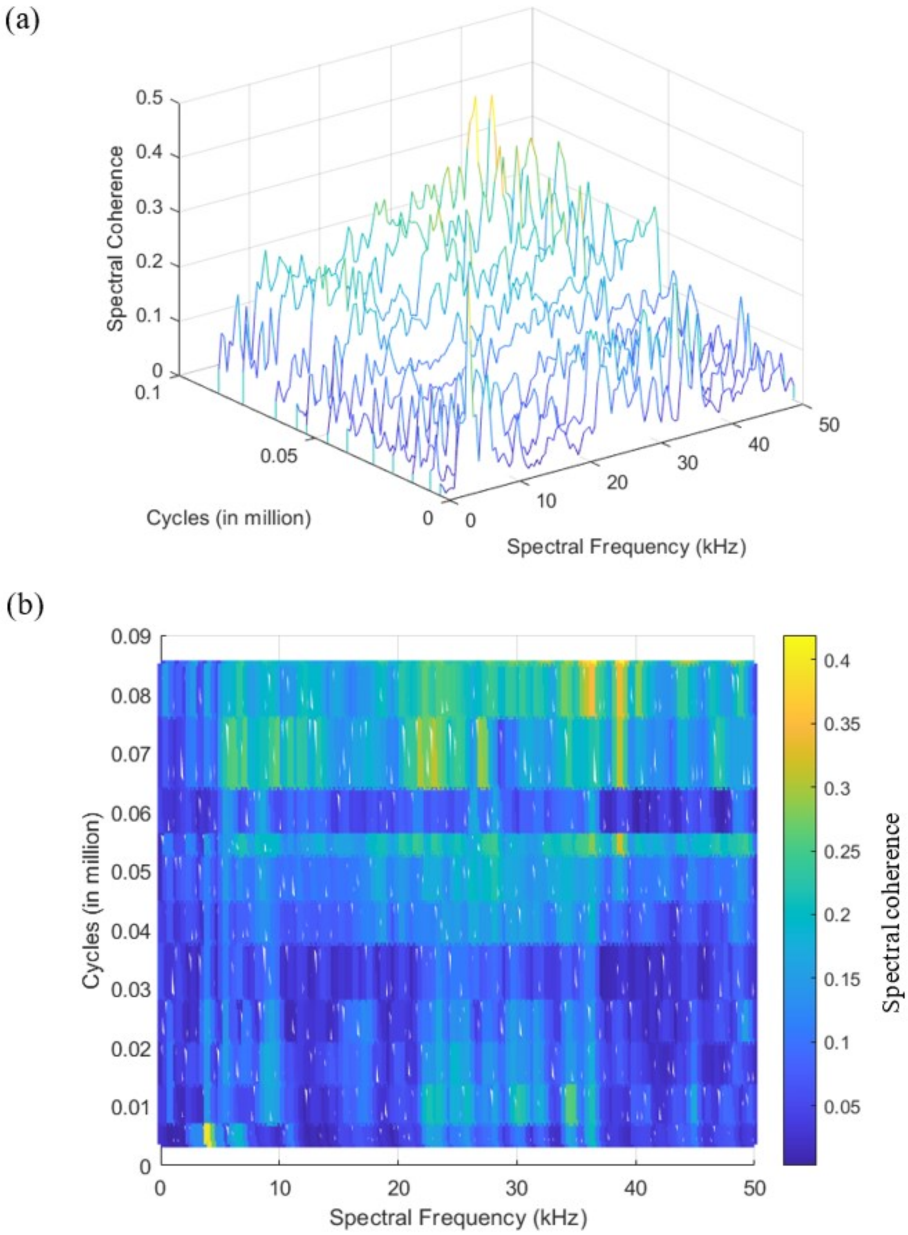

Figure 4.14 Dry test: (a) Carrier frequency distribution at gear mesh (cyclic) frequency; (b) Top view

Unlike fatigue pitting, the abrasive wear propagation results in an increasing spectral coherence of the high carrier frequency part. It suggests that abrasion, and the corresponding high spatial frequency surfaces, generate higher carrier frequencies. This phenomenon is also proved by the ICS2-based band selection in Figure 4.15. Note that the initial surfaces were smooth for this test, and hence a low carrier frequency was induced initially (unlike with the lubricated test). To verify the abrasive wear-related carrier frequency range, PSD analysis was applied on the scanned images (see Figure 4.16). Figure 4.17 shows the PSD analysis results, from which it can be found that the spatial frequency range affected by abrasive wear is [0.0283~0.0946] (1/μm). The sliding velocity (absolute value) range is around [0~0.4461] (m/s). Based on the right-hand side of Eq. (4.1), taking the average sliding velocity, the abrasive wear-related vibration frequency should be [6.31~21.10] kHz. It is in the high-frequency range. Figure 4.14 and Figure 4.15 show that the spectral coherence of the high carrier frequency part increases with an increase in abrasive wear, giving strong support to this hypothesis made in Section 4.2.2.

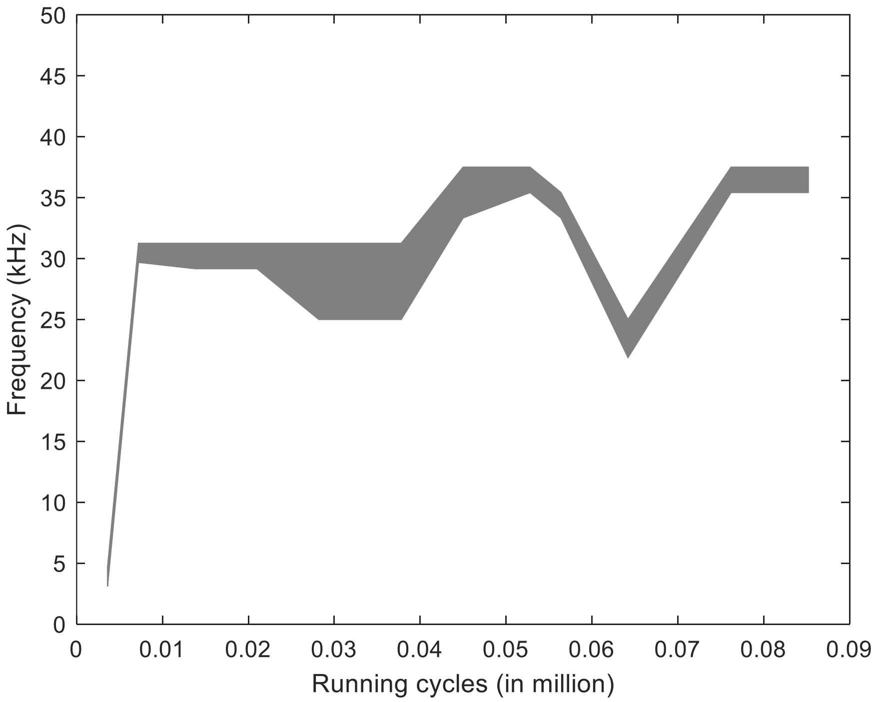

Figure 4.15 Dry test: ICS2-based band selection result

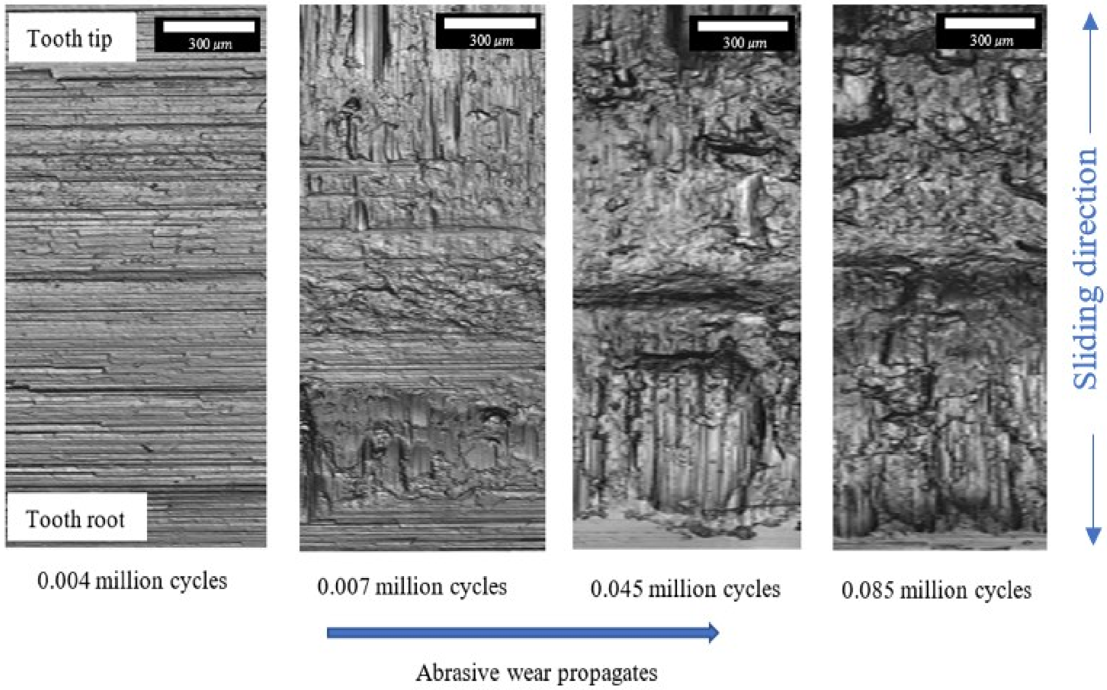

Figure 4.16 3D images of abrasive wear propagation in the dry test

An important comment must be added regarding the different lubrication conditions of the two tests. These could have also affected the frequency range of the CS2 content, and future tests will be required to analyse the extent of this bias. However, the fact that the initial (healthy) cases for both dry and lubricated tests showed an opposite trend vs the corresponding worn cases is an initial indication that the bias is not likely to compromise the procedure. In fact, dry tests with smooth surfaces resulted in low-frequency vibrations like the worn lubricated cases and the initial lubricated tests (with the artificially roughened surface) were comparable to worn dry tests. Albeit based on a low number of observations, this supports the hypothesis that the wavelength of surface roughness has a strong impact on the vibration spectral support, and that this effect seems fairly consistent with different lubrication conditions.

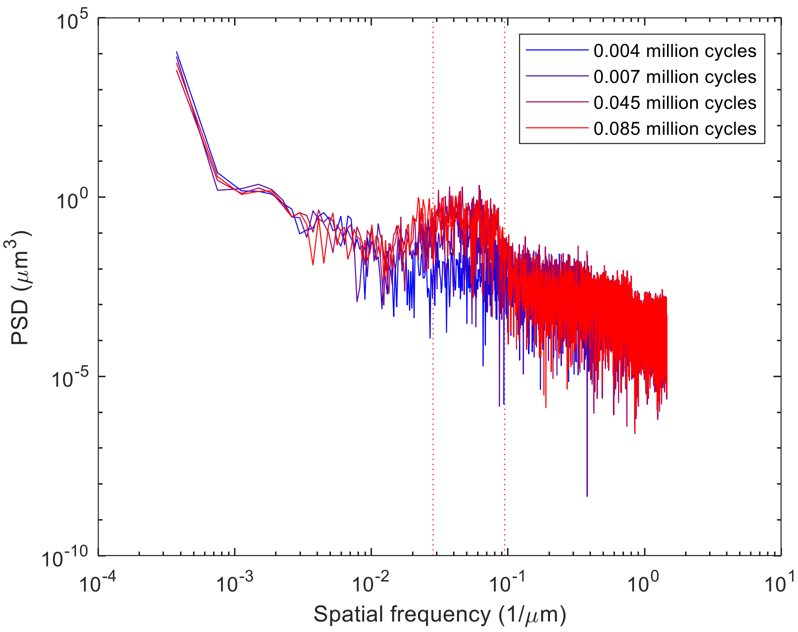

Figure 4.17 PSD analysis results of the 3D images shown in Figure 4.16

4.4 A new vibration-based procedure for comprehensive gear wear monitoring: mechanism identification and severity tracking

In Section 4.3, the hypothesis for fatigue pitting and abrasive wear identification was supported by the analysis of the spectral frequency distribution in the spectral coherence map and the ICS2-based band selection results. However, even though fatigue pitting and abrasive wear can be identified by observing the spectral coherence map and ICS2-based band selection results, the wear evolution (fatigue pitting and abrasive wear) cannot be monitored. A vibration-based approach/indicator is therefore still needed, which can distinguish the two wear mechanisms and track their evolution. In the following, a new vibration-based procedure for comprehensive gear wear monitoring is introduced and presented.

The ability of ICS2 to monitor fatigue pitting and abrasive wear propagation is likely to be improved in the selected frequency band, which enhances CS2 content over background noise. Therefore, an ICS2-based approach can help to comprehensively monitor gear wear progression: wear mechanism identification and wear severity tracking. The basic procedure of the proposed vibration-based approach for comprehensive gear wear monitoring is illustrated in Figure 4.18.

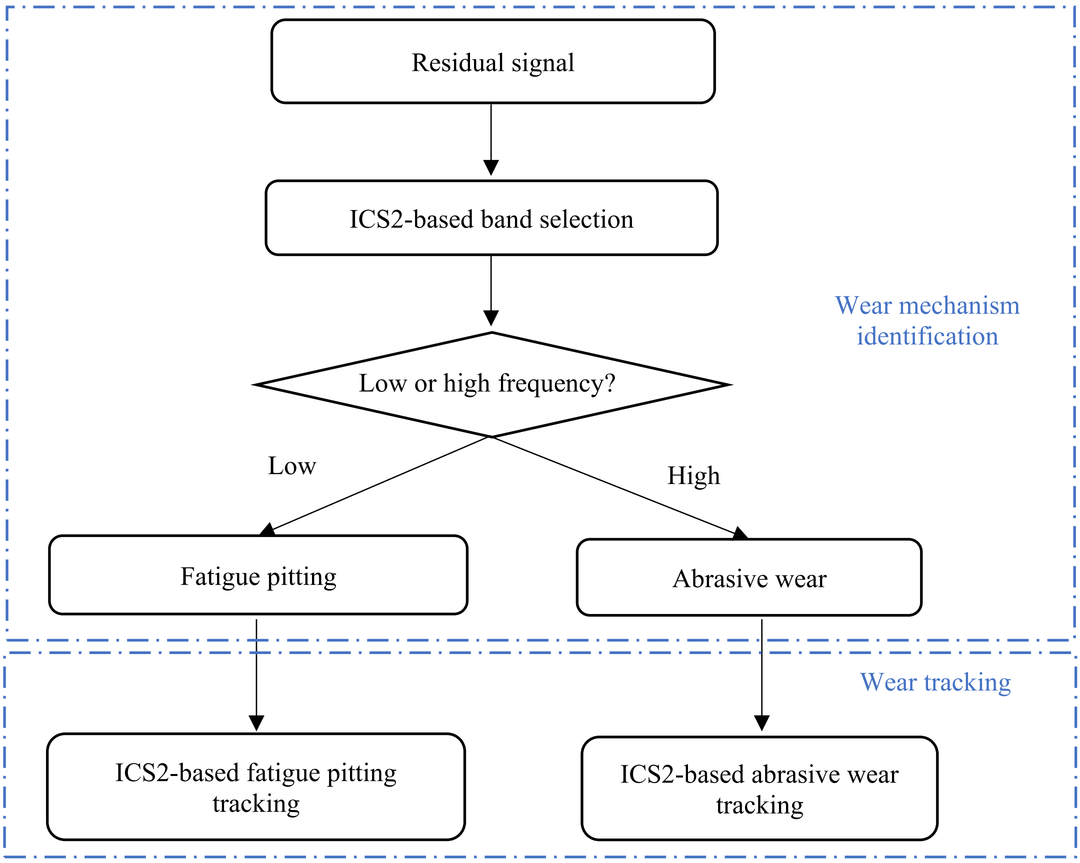

Figure 4.18 Proposed guideline of vibration-based comprehensive gear wear monitoring

In the following, the performance of this developed procedure for gear wear monitoring is demonstrated step by step, using the experimental data from the designed lubricated and dry tests.

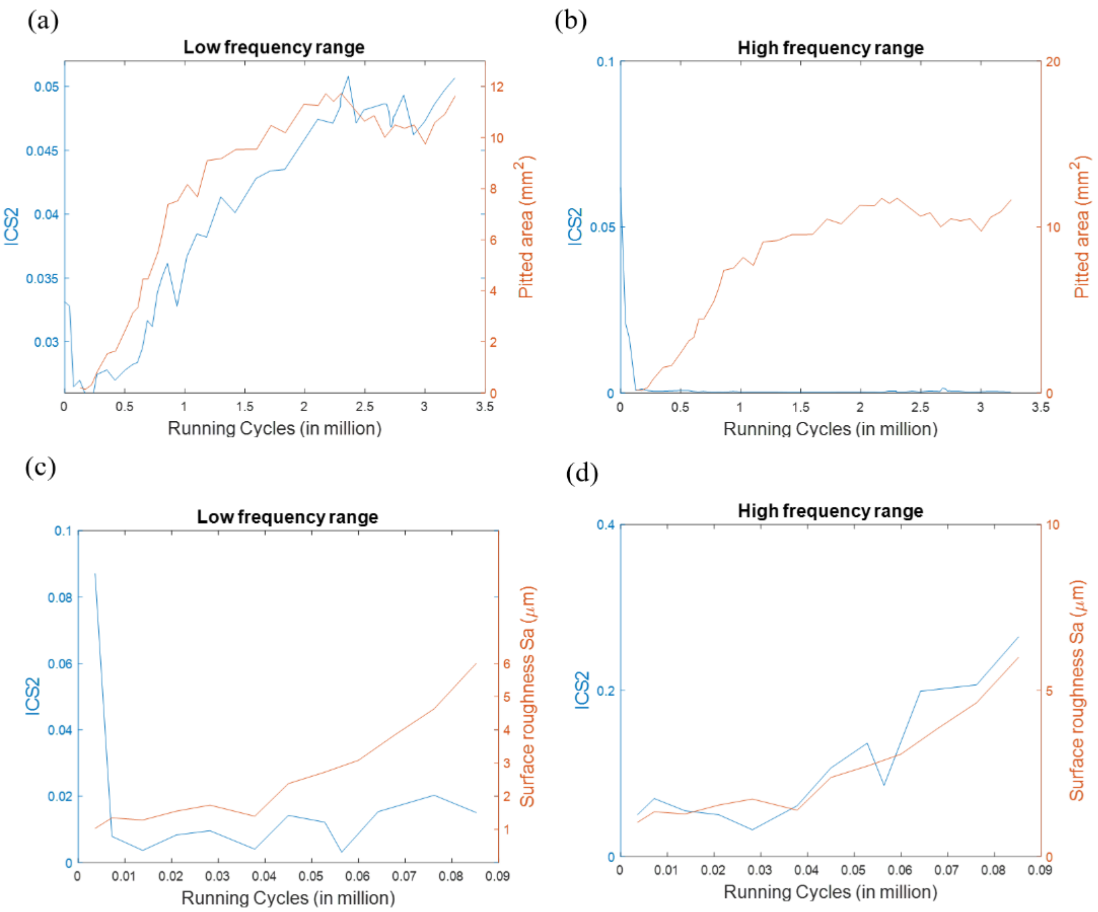

Figure 4.19 Performance of ICS2 in wear severity tracking

Firstly, ICS2-based band selection for identifying fatigue pitting ([2~13] kHz) and abrasive wear ([20~37] kHz) was illustrated in Figure 4.8 and Figure 4.15, and shows that fatigue pitting induces low carrier frequencies, and abrasive wear induces high carrier frequencies. Figure 4.19 shows that the ICS2 band selection results can assist the vibration-based wear mechanism identification and wear monitoring, by tracking the evolution of fatigue pitting and abrasive wear (at the micro-level), with a low-frequency range (2~13 kHz) and high-frequency range (20~37 kHz) indicators, respectively. From the comparison of Figure 4.19 (a) and (b), it can be found that only the ICS2 with low-frequency carrier tracks fatigue pitting propagation (in terms of pitted area). In contrast, in Figure 4.19 (c) and (d), only the ICS2 with a high-frequency carrier tracks the change in abrasive wear micro-scale features (in terms of surface roughness). Therefore, with an approximate frequency band (suggested by the ICS2-based band selection result), ICS2 can track wear severity for fatigue pitting and abrasive wear (at the micro-scale). Meanwhile, the performance of ICS2 in the low- and high-frequency ranges can also suggest different wear mechanisms. If ICS2 has a monotonic trend in the low-frequency range, but not in the high-frequency range, it indicates fatigue pitting propagation, while a monotonic trend in the high-frequency range, but not in the low-frequency range, suggests abrasive wear propagation.

To quantify the performance of ICS2 in the low-frequency range in fatigue pitting severity tracking, the pitted area was used as a reference to perform correlation analysis. Correlation analysis was also applied comparatively on a number of other classical vibration indicators, such as RMS and kurtosis, to demonstrate the performance of band selected ICS2 to monitor fatigue pitting progression, see Figure 4.20.

Figure 4.21 shows that the ICS2 of vibration with the low-frequency carrier has a high correlation coefficient with the total pitted area, this being 0.9085, and can thus track the severity of fatigue pitting. The correlation analysis results for other classical indicators are summarised in Table 4.1. These show that ICS2 of vibration in the low-frequency range has the best performance in tracking the fatigue pitting propagation. Although the RMS value of the raw vibration signal also has a high correlation with the total pitted area, it mainly indicates the energy change of deterministic components of vibration, which have less physical relevance with fatigue pitting propagation (induced micro-level surface feature change). Notably, the amplitude of the 1st gear mesh harmonics of vibration has a low correlation coefficient with fatigue pitting propagation, supporting the earlier point that fatigue pitting has negligible effects on the gear tooth profile, and so this indicator should not have the ability to track fatigue pitting propagation. It should be pointed out that the sidebands were used in some references [13, 22, 33] to indicate damage, but they can only pick up non-uniform effects and are not useful for the more typical uniform wear case studied here. From the comparisons, ICS2 in the low-frequency range has the best performance in tracking fatigue pitting severity.

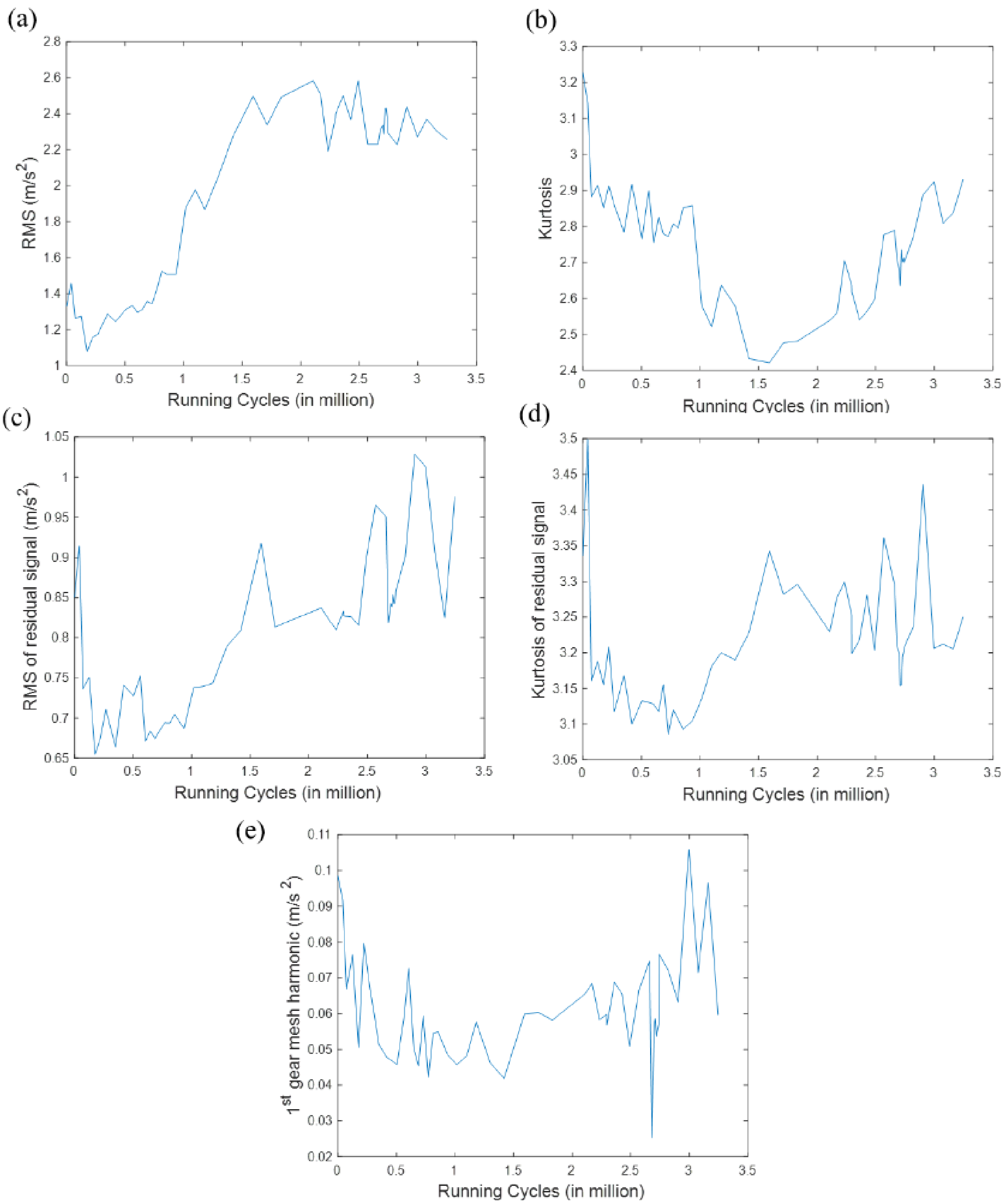

Figure 4.20 Classical indicators performance in the lubricated test: (a) RMS of raw signal; (b) kurtosis of raw signal; (c) RMS of residual signal; (d) kurtosis of residual signal; (e) 1st gear mesh frequency

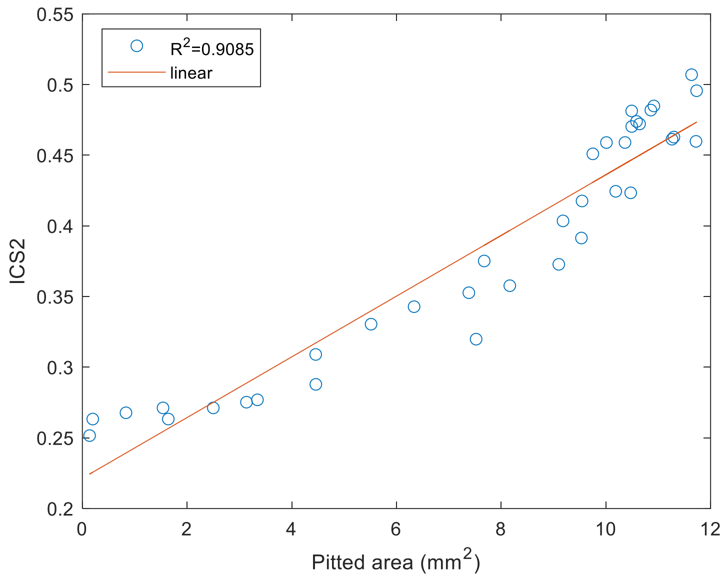

Figure 4.21 Lubricated test: correlation between ICS2 and pitted area

Table 4.1 Correlation analysis results of vibration indicators with tribological parameter for the lubricated test

Indicators	Correlation with pitted area: R^2
ICS2 (high frequency range)	0.0215
ICS2 (low frequency range)	0.9085
RMS (raw signal)	0.8146
Kurtosis (raw signal)	0.1237
RMS (residual signal)	0.6984
Kurtosis (residual signal)	0.6718
1st gear mesh frequency amplitude	0.2476

Similarly, surface roughness S_a was used as the tribological parameter to assess the effectiveness of ICS2 with the high-frequency carrier in monitoring abrasive wear propagation (at the micro-scale), as shown in Figure 4.22. The high correlation coefficient of 0.9086 shows that it can track this wear indicator very well. Note that compared with existing studies [14, 15], restricting the spectral band of the ICS2 to the high-frequency range, instead of the full frequency band, makes ICS2 a much better index to track surface roughness changes.

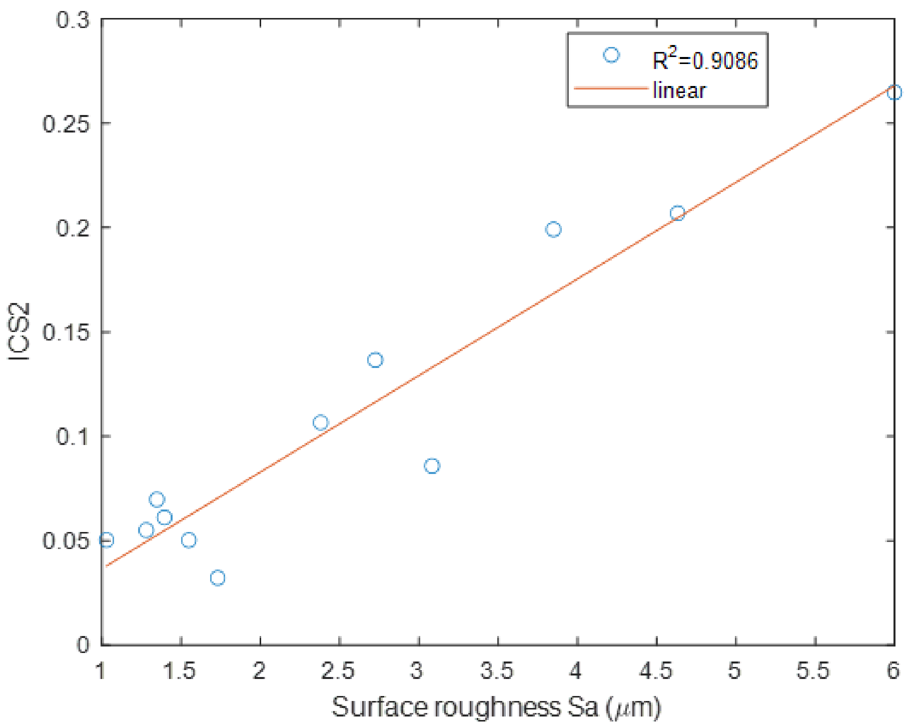

Figure 4.22 Dry test: correlation between ICS2 and surface roughness

Compared with other classical indicators (in Figure 4.23), ICS2 also has the best performance in monitoring the abrasive wear induced micro-level surface feature changes, as shown in Table 4.2. Even though the RMS value of the raw signal has a low correlation with the surface roughness, it should have a strong relationship with tooth profile changes induced by abrasive wear, which is tested in Figure 4.24. However, even though Figure 4.24 shows that the RMS value has a high correlation ($R^2 = 0.9816$) with the wear depth before 0.045 million cycles, it deviates widely after that. In the light of the findings of Ref. [104], it seems that the vibrations only respond to deviations of the tooth profile around the mean wear, and measurement of "absolute TE" is required to determine the overall wear depth. This will be tested in future work, but the total wear in this test was extreme, and that corresponding to 0.045 million cycles here would often be considered as being at the limit.

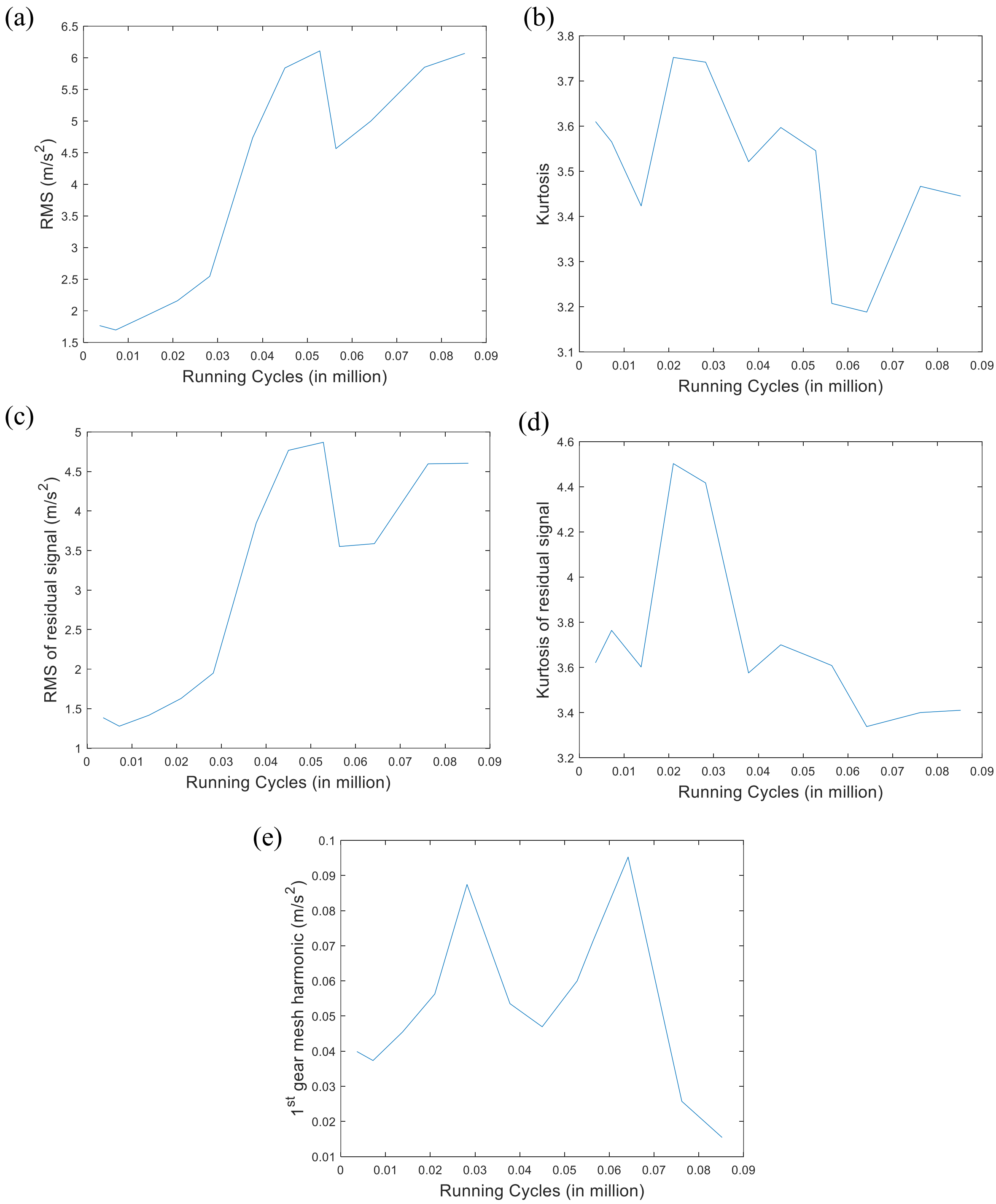

Figure 4.23 Classical indicators performance in the dry test: (a) RMS of raw signal; (b) kurtosis of raw signal; (c) RMS of residual signal; (d) kurtosis of residual signal; (e) 1st gear mesh frequency

Table 4.2 Correlation analysis results of vibration indicators with the surface roughness of the dry test

Indicators	Correlation with surface roughness: R^2
ICS2 (high frequency range)	0.9086
ICS2 (low frequency range)	0.0240
RMS of the raw signal	0.5590
Kurtosis of the raw signal	0.2313
RMS of the residual signal	0.4895
Kurtosis of the residual signal	0.2611
1st gear mesh frequency amplitude	0.0661

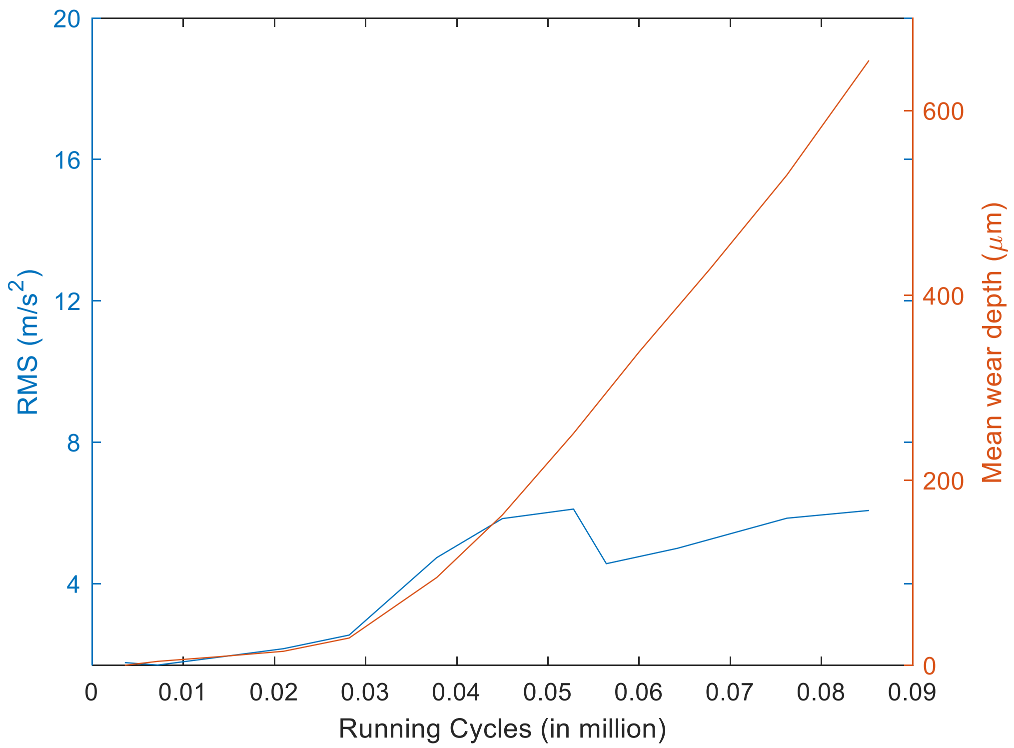

Figure 4.24 Performance of RMS of raw signal in tracking wear depth change (obtained from wear particle)

4.5 Summary

With consideration of the underlying physics of the gear meshing process and the unique surface features induced by fatigue pitting and abrasive wear, this chapter has investigated vibration-based methods to identify these two wear mechanisms and then track their evolution. This development is based on the cyclostationary analysis technique, which is applied for the first time to analyse wear-related low energy phenomena (friction, asperity contacts) in vibration signals. Differently from existing studies for wear mechanism identification (such as analysing wear particles or images captured from gear tooth surface), the proposed approach can be done online, making it more efficient than wear debris analysis techniques. In the proposed method, an indicator of second-order cyclostationarity of the vibration signal, ICS2, is calculated for low and high carrier spectral frequencies, and then used to separate fatigue pitting and abrasive wear. Moreover, the use of specific spectral bands for the calculation of the ICS2 increases the indicator's capability to track the evolution of fatigue pitting and abrasive wear (micro-level). As discussed in Section 4.1, none of the existing vibration-based gear wear monitoring research involved two wear mechanism/phenomena identification and monitoring. The ICS2-based wear monitoring result can offer useful information for the monitoring and prognostics of gear systems. Experimental data support the effectiveness of the proposed vibration-based method.

However, it should be noted that the spectral frequency distribution of measured vibration can be affected by lots of factors such as load, speed, especially lubrication. Therefore, further work on investigating the effects of operational conditions on spectral frequency distribution should be taken into consideration.

Chapter 5 Dynamic model development

The work presented in this chapter is devoted to achieving **objective 2** of this research: **dynamic model development**. This work has been presented in a paper titled "*Vibration-based updating of wear prediction for spur gears*", which was published in the journal of *Wear* (426-427: 1410-1415, 2019). Compared with this publication, more details on the model establishment and model validation are included in this chapter.

This chapter is organized as follows. In Section 5.1, a brief introduction to this study is given. Section 5.2 presents the dynamic model structure. After that, procedures of model validation and calibration are introduced in Section 5.3. A summary is given in Section 5.4.

5.1 Introduction

The dynamic model, developed with the key dynamic properties including gear meshing stiffness, transmission error, damping, can simulate and represent gear system responses under different failure modes and severities. Its time and cost-efficiency can bring significant benefits to gear wear analysis. As an output of the dynamic model, the dynamic contact force is a very important parameter and a crucial input to the tribological/wear model for wear analysis. Therefore, modelling the contact force is vital for analysing gear wear characteristics and further predicting its propagation.

From the literature review of Section 2.4.1, various approaches, such as the finite element model (FEM) [146-148] and empirical equations [48-53], have been developed/applied to estimate contact force, which is used as an input into tribological (wear) models. However, there is a common drawback existing in both FEM (without extra efforts in defining boundary conditions and mesh generations) and empirical equations, that is, only the contact force under quasi-static conditions can be produced and represented. However, in engineering practices, the gear transmission system is usually operated under dynamic operating conditions, and the corresponding responses are quite different from those under quasi-static conditions. Normally, owning to the inertia effects, the dynamic meshing forces are typically larger than the corresponding quasi-static forces and their magnitudes and waveforms are quite different [21]. Therefore, to guarantee reliable wear analysis and prediction through tribological (wear) models, the dynamic contact force with inertia effects should be properly evaluated, thus a 21-degree-of-freedom (DOF) dynamic model is established in this research based on the University of New South Wales (UNSW) gearbox test bench. To guarantee the outputs (such as dynamic contact forces and vibrations) from the dynamic model are close enough to the measurements from the experimental rig, the developed dynamic model has been validated and calibrated through a series of tests, including impact tests, speed ramp tests and several constant speed tests. The development of this comprehensive dynamic model will be introduced with details in the following. It should be pointed out that the 21 degree-of-freedoms (DOFs) lumped parameter dynamic model developed in this project is based on the fixed-axis spur gearbox test rig shown in Figure 3.2, whose structure and properties are different from the previously published research [18, 41, 107]. Also, as introduced in Chapter 3, the developed dynamic model will be integrated with tribological models that can be updated according to vibrations to predict gear wear propagation. This overall integration architecture is the main novelty of this thesis work, instead of the dynamic model development itself.

5.2 Dynamic model structure

The layout of the UNSW spur gearbox test rig and each labelled modelling component (such as coupling, motor and brake) are shown in Figure 5.1. The major parameters that are included in the dynamic model are summarised in Table 5.1. A 21 DOFs lumped parameter dynamic model is developed based on the spur gearbox test rig (shown in Figure 5.1), whose skeleton is shown in Figure 5.2.

Table 5.1 Basic parameters of the spur gearbox test rig

Parameters	Pinion	Gear
Gear type	Standard involute	
Modulus of elasticity, E (GPa)	205	
Poisson's ratio, υ	0.29	
Face width, W (mm)	20	
Module, m	2	
Pressure angle, φ (deg)	20	
Addendum (mm)	1.00	
Dedendum (mm)	1.25	
Number of teeth	19	20
Pitch radius, r (mm)	19	20

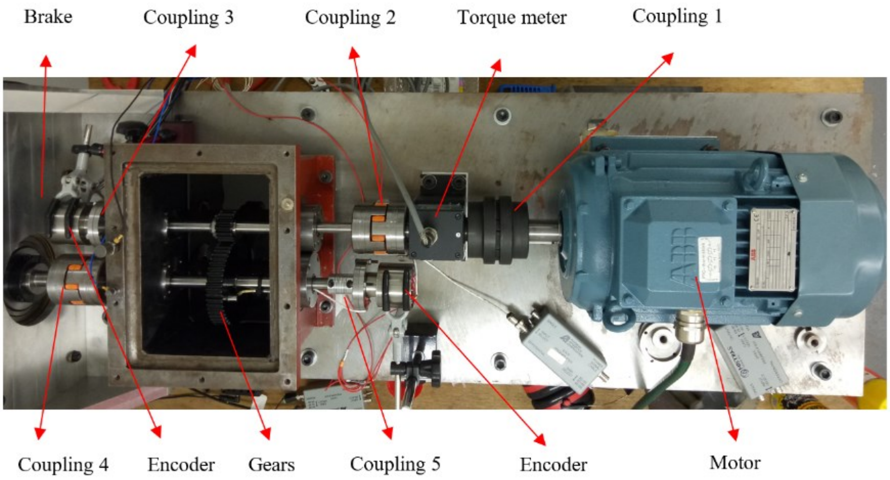

Figure 5.1 Spur gearbox test rig with each labelled modelling component

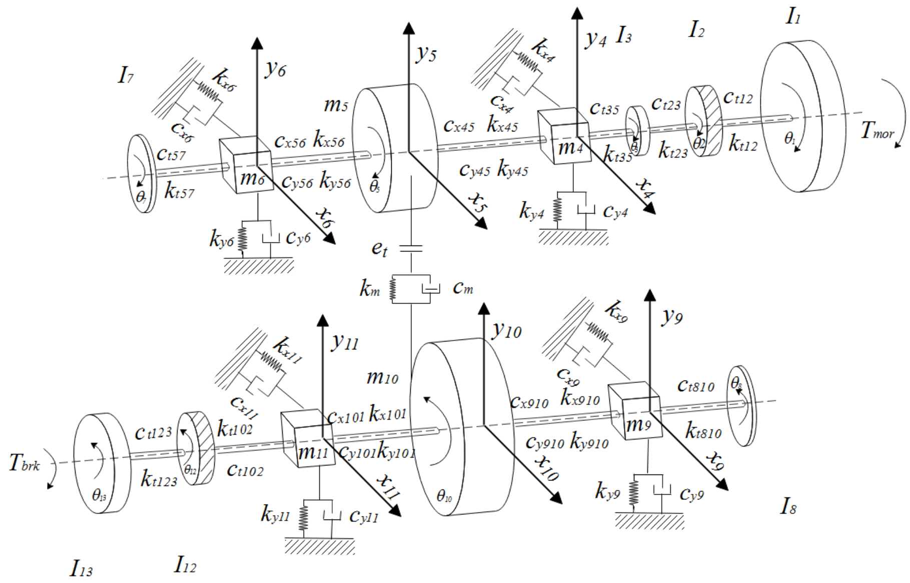

Figure 5.2 21 DOFs lumped dynamic model of UNSW test rig

There is a total of 21 DOFs of this dynamic model, including 9 torsional DOFs and 12 translations DOFs. The mass, stiffness, damping and inertia parameter information of this developed dynamic model are summarized in Table 5.2 and Table 5.3. The basic motion equations describing the coupled torsional and translational model are described as

$$\mathbf{M}\ddot{\mathbf{x}} + \mathbf{C}\dot{\mathbf{x}} + \mathbf{K}\mathbf{x} = \mathbf{f} \tag{5.1}$$

where

$$\mathbf{x} = [\theta_1, \theta_2, \theta_3, \theta_5, \theta_7, \theta_8, \theta_{10}, \theta_{12}, \theta_{13}, y_4, y_5, y_6, y_9, y_{10}, y_{11}, x_4, x_5, x_6, x_9, x_{10}, x_{11}]^T \tag{5.2}$$

represents the translational (x_i, y_i) and angular displacements θ_i of the different nodes of the system in the plane perpendicular to the shaft axes, and $\mathbf{C}$, $\mathbf{K}$ and **f** are the corresponding damping, stiffness and force matrixes. The absence of bearing torsional DOFs $(\theta_4, \theta_6, \theta_9, \theta_{11})$ is due to the absence of torsional stiffness at the bearings, whereas the missing translational displacement DOFs (all the nodes outside the gearbox) is a result of the low bending stiffness of the joints, effectively isolating the linear displacements of the gearbox.

The force vector **f** includes the input and output torques $\mathrm{T_{mot}}$ and $\mathrm{T_{brk}}$ provided by the motor and brake (on θ_1 and θ_{13}, respectively), and the contact forces between the two gears, modelled as $\mathrm{F_k}$ and $\mathrm{F_c}$ (elastic and viscous components). These are simulated by combining a gear meshing stiffness k_m, damping coefficient c_m and geometric transmission error (GTE) e_t:

$$\mathrm{F_k} = k_m(R_{b1}\theta_5 - R_{b2}\theta_{10} - y_5 cos\varphi + y_{10} cos\varphi + x_5 sin\varphi - x_{10} sin\varphi + e_t) \quad (5.3)$$

$$\mathrm{F_c} = C_m\left(R_{b1}\dot{\theta_5} - R_{b2}\dot{\theta_{10}} - \dot{y_5} cos\varphi + \dot{y_{10}} cos\varphi + \dot{x_5} sin\varphi - \dot{x_{10}} sin\varphi + \dot{e_t}\right) \quad (5.4)$$

where R_{b1} and R_{b2} are the basic radius of pinion and gear, and φ is the contact pressure angle.

The contact force is applied at nodes 5 and 10, considering the radius of the two gears and the contact angle

$$\mathbf{f} = [T_{mor}, 0,0, -R_{b1}(F_k + F_c), 0,0, R_{b2}(F_k + F_c), 0,0,0, cos\varphi(F_k + F_c), 0,0, \\ -cos\varphi(F_k + F_c), 0,0, -sin\varphi(F_k + F_c), 0,0, sin\varphi(F_k + F_c), 0]^T \quad (5.5).$$

The whole torsional and translation motion equations are given as follows

<u>Torsional DOFs:</u>

$$I_1\ddot{\theta_1} = T_{mot} - k_{t12}(\theta_1 - \theta_2) - C_{t12}\left(\dot{\theta_1} - \dot{\theta_2}\right) \quad (5.6\text{-a})$$

$$I_2\ddot{\theta_2} = k_{t12}(\theta_1 - \theta_2) + C_{t12}\left(\dot{\theta_1} - \dot{\theta_2}\right) - k_{t23}(\theta_2 - \theta_3) - C_{t23}\left(\dot{\theta_2} - \dot{\theta_3}\right) \quad (5.6\text{-b})$$

$$I_3\ddot{\theta}_3 = k_{t23}(\theta_2 - \theta_3) + C_{t23}(\dot{\theta}_2 - \dot{\theta}_3) - k_{t35}(\theta_3 - \theta_5) - C_{t35}(\dot{\theta}_3 - \dot{\theta}_5) \tag{5.6-c}$$

$$I_5\ddot{\theta}_5 = k_{t35}(\theta_3 - \theta_5) + C_{t35}(\dot{\theta}_3 - \dot{\theta}_5) + k_{t57}(\theta_7 - \theta_5) + C_{t57}(\dot{\theta}_7 - \dot{\theta}_5) \\ -R_{b1}(F_k + F_c) \tag{5.6-d}$$

$$I_7\ddot{\theta}_7 = k_{t57}(\theta_5 - \theta_7) + C_{t57}(\dot{\theta}_5 - \dot{\theta}_7) \tag{5.6-e}$$

$$I_8\ddot{\theta}_8 = k_{t810}(\theta_{10} - \theta_8) + C_{t810}(\dot{\theta}_{10} - \dot{\theta}_8) \tag{5.6-f}$$

$$I_{10}\ddot{\theta}_{10} = R_{b2}(F_k + F_c) - k_{t102}(\theta_{10} - \theta_{12}) - C_{t102}(\dot{\theta}_{10} - \dot{\theta}_{12}) + k_{t810}(\theta_8 - \theta_{10}) \\ +C_{t810}(\dot{\theta}_8 - \dot{\theta}_{10}) \tag{5.6-g}$$

$$I_{12}\ddot{\theta}_{12} = k_{t102}(\theta_{10} - \theta_{12}) + C_{t102}(\dot{\theta}_{10} - \dot{\theta}_{12}) - k_{t123}(\theta_{12} - \theta_{13}) - C_{t123}(\dot{\theta}_{12} - \dot{\theta}_{13}) \tag{5.6-h}$$

$$I_{13}\ddot{\theta}_{13} = k_{t123}(\theta_{12} - \theta_{13}) + C_{t123}(\dot{\theta}_{12} - \dot{\theta}_{13}) - T_{brk} \tag{5.6-i}$$

Translational DOFs:

$$m_4\ddot{y}_4 + k_{y4}y_4 + C_{y4}\dot{y}_4 + k_{y45}(y_4 - y_5) + C_{y45}(\dot{y}_4 - \dot{y}_5) = 0 \tag{5.7-a}$$

$$m_5\ddot{y}_5 + k_{y56}(y_5 - y_6) + C_{y56}(\dot{y}_5 - \dot{y}_6) + k_{y45}(y_5 - y_4) + C_{y45}(\dot{y}_5 - \dot{y}_4) = (F_k + F_c)cos\varphi \tag{5.7-b}$$

$$m_6\ddot{y}_6 + k_{y6}y_6 + C_{y6}\dot{y}_6 - k_{y56}(y_5 - y_6) - C_{y56}(\dot{y}_5 - \dot{y}_6) = 0 \tag{5.7-c}$$

$$m_9\ddot{y}_9 + k_{y9}y_9 + C_{y9}\dot{y}_9 + k_{y910}(y_9 - y_{10}) + C_{y910}(\dot{y}_9 - \dot{y}_{10}) = 0 \tag{5.7-d}$$

$$m_{10}\ddot{y}_{10} + k_{y910}(y_{10} - y_9) + C_{y910}(\dot{y}_{10} - \dot{y}_9) + k_{y101}(y_{10} - y_{11}) + C_{y101}(\dot{y}_{10} - \dot{y}_{11}) = (-F_k - F_c)cos\varphi \tag{5.7-e}$$

$$m_{11}\ddot{y}_{11} + k_{y11}y_{11} + C_{y11}\dot{y}_{11} - k_{y101}(y_{10} - y_{11}) - C_{y101}(\dot{y}_{10} - \dot{y}_{11}) = 0 \tag{5.7-f}$$

$$m_4\ddot{x}_4 + k_{x4}x_4 + C_{x4}\dot{x}_4 + k_{x45}(x_4 - x_5) + C_{x45}(\dot{x}_4 - \dot{x}_5) = 0 \tag{5.7-g}$$

$$m_5\ddot{x_5} + k_{x56}(x_5 - x_6) + C_{x56}(\dot{x_5} - \dot{x_6}) + k_{x45}(x_5 - x_4) + C_{x45}(\dot{x_5} - \dot{x_4}) = (-F_k - F_c)sin\varphi \quad (5.7\text{-h})$$

$$m_6\ddot{x_6} + k_{x6}x_6 + C_{x6}\dot{x_6} - k_{x56}(x_5 - x_6) - C_{x56}(\dot{x_5} - \dot{x_6}) = 0 \quad (5.7\text{-i})$$

$$m_9\ddot{x_9} + k_{x9}x_9 + C_{x9}\dot{x_9} + k_{x910}(x_9 - x_{10}) + C_{x910}(\dot{x_9} - \dot{x_{10}}) = 0 \quad (5.7\text{-j})$$

$$m_{10}\ddot{x_{10}} + k_{x910}(x_{10} - x_9) + C_{x910}(\dot{x_{10}} - \dot{x_9}) + k_{x101}(x_{10} - x_{11}) + C_{x101}(\dot{x_{10}} - \dot{x_{11}}) = (F_k + F_c)sin\varphi \quad (5.7\text{-k})$$

$$m_{11}\ddot{x_{11}} + k_{x11}x_{11} + C_{x11}\dot{x_{11}} - k_{x101}(x_{10} - x_{11}) - C_{x101}(\dot{x_{10}} - \dot{x_{11}}) = 0 \quad (5.7\text{-l})$$

Table 5.2 Mass and inertia of the dynamic model of spur gearbox systems

Inertia (kgm^2)		Mass (kg)	
I_1	Inertia of motor, inertia of motor shaft and $1/2$ inertia of coupling 1	m_4	Mass of pedestal and bearing
I_2	$1/2$ inertia of coupling 1, $1/2$ inertia of coupling 2 and inertia of torque meter shaft	m_5	Mass of pinion
I_3	$1/2$ inertia of coupling 2 and inertia of input shaft to bearing (not including bearing)	m_6	Mass of pedestal and bearing
I_5	Inertia of pinion, inertia of input shaft (whole shaft section through casing)	m_9	Mass of pedestal and bearing
I_7	Inertia of slip ring (rotor part), adapter, coupling 3 and shaft section outside casing (free end)	m_{10}	Mass of gear
I_8	Inertia of slip ring (rotor part), adapter, coupling 5 and shaft section outside casing (free end)	m_{11}	Mass of pedestal and bearing
I_{10}	Inertia of gear, inertia of whole output shaft section through casing		
I_{12}	$1/2$ inertia of coupling 4 and output shaft section to bearing (not including bearing)		
I_{13}	Inertia of brake, inertia of brake shaft and $1/2$ inertia of coupling 4		

Table 5.3 Stiffness and damping of the dynamic model of spur gearbox systems

Stiffness and damping			
k_{t12}, C_{t12}	Torsional stiffness and damping of coupling 1	k_{y56}, C_{y56}	Vertical stiffness and damping of shaft
k_{t23}, C_{t23}	Torsional stiffness and damping of coupling 2	k_{y101}, C_{y101}	Vertical stiffness and damping of shaft
k_{t35}, C_{t35}	Torsional stiffness and damping of shaft (from coupling 2 to pinion)	k_{y910}, C_{y910}	Vertical stiffness and damping of shaft
k_{t57}, C_{t57}	Torsional stiffness and damping of shaft (from pinion to slip ring)	k_{x45}, C_{x45}	Horizontal stiffness and damping of shaft
k_{t810}, C_{t810}	Torsional stiffness and damping of shaft (from gear to slip ring)	k_{x56}, C_{x56}	Horizontal stiffness and damping of shaft
k_{t102}, C_{t102}	Torsional stiffness and damping of shaft (from gear to coupling 4)	k_{x101}, C_{x101}	Horizontal stiffness and damping of shaft
k_{t123}, C_{t123}	Torsional stiffness and damping of coupling 4	k_{x910}, C_{x45}	Horizontal stiffness and damping of shaft
k_{y45}, C_{y45}	Vertical stiffness and damping of shaft	k_{y4}, k_{y6}, k_{y9}, k_{y11}	Vertical stiffness of pedestal/bearing

5.2.1 Meshing stiffness and damping coefficient of gear system

In the developed dynamic model, the internal excitation of the gear systems is from the gear meshing contact [149-151], therefore, properly modelling the contact properties of mating gear teeth can facility a better understanding of the coupling effects between gear wear and gear dynamic characteristics, and then provide useful information for wear monitoring and prediction.

Three major parameters are characterizing the gear contact, that is, meshing stiffness k_m, damping coefficient c_m and geometric transmission error e_t. In this study, the meshing stiffness k_m is considered as a function of the angular rotation of the pinion θ_5. The shape of the dependency $k_m(\theta_5)$ is derived based on the potential energy which considers the strain energy and Hertzian contact [152-154]. The strain energy consists of bending, shear and axial compressive potential energies stored in the meshing teeth, which are expressed below [155-157]

$$U_b = \frac{F^2}{2k_b} \tag{5.8}$$

$$U_s = \frac{F^2}{2k_s} \tag{5.9}$$

$$U_a = \frac{F^2}{2k_a} \tag{5.10}$$

where F is gear contact force, k_b, k_s and k_a are bending stiffness, shear stiffness and axial compressive stiffness.

The stiffness of the Hertzian contact between tooth pairs can be approximated by [158]

$$k_h = \frac{\pi E W}{4(1-\nu^2)} \tag{5.11}$$

The Hertzian stiffness is dependent on the width of contact between two teeth widths W and the material properties: Poisson's ratio and elastic modulus, ν and E, respectively. With Hertzian, bending, shear and axial compressive stiffness, the gear mesh stiffness for one tooth pair can be obtained by using [155, 159-161]

$$\frac{1}{k_m} = \frac{1}{k_h} + \sum_{j=1}^{2}\left[\frac{1}{k_{b,j}} + \frac{1}{k_{s,j}} + \frac{1}{k_{a,j}}\right] \tag{5.12}$$

where $j = 1{,}2$ represents the pinion and gear, respectively. The mesh stiffness of one tooth pair is demonstrated in Figure 5.3.

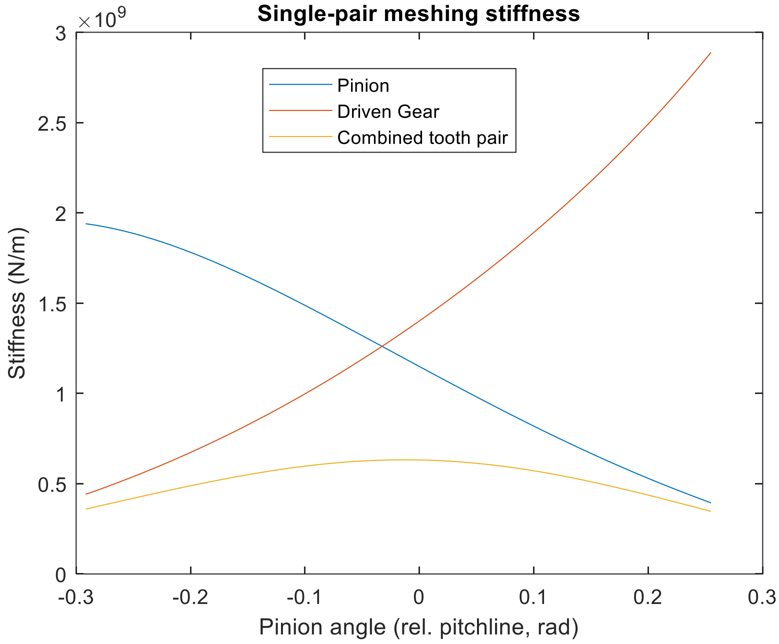

Figure 5.3 Single tooth pair meshing stiffness

It is assumed that the gear system has a constant damping ratio and the meshing damping coefficient is proportional to the gear meshing stiffness [162]

$$c_m = \mu k_m \tag{5.13}$$

where μ (s) is the scale constant.

To determine the value of μ, k_{ave} and c_{ave} are defined as the mean meshing stiffness and damping coefficient in one mesh period, and the damping ratio can be calculated through

$$\zeta = \frac{c_{ave}}{2\sqrt{k_{ave} m}} \tag{5.14}$$

where m represents the effective mass of pinion and gear, which can be derived as

$$m = \frac{m_5 m_{10}}{m_5 + m_{10}} \quad (5.15).$$

From Eq. (5.14) and Eq. (5.15), the average meshing damping coefficient c_{ave} is

$$c_{ave} = 2\zeta\sqrt{k_{ave}\frac{m_5 m_{10}}{m_5 + m_{10}}} \quad (5.16).$$

Therefore, based on Eqs. (5.13-5.16), the damping ratio μ together with the meshing damping coefficient c_m can be calculated.

5.2.2 Geometric transmission error

The GTE, e_t (geometric deviation from perfect involute), makes *kinematic* (inertia and loading independent) contribution to the transmission error of the gear system [25]. It can be used to represent gear surface wear, but could also include initial profile errors, that can be estimated based on manufacturing quality or measured.

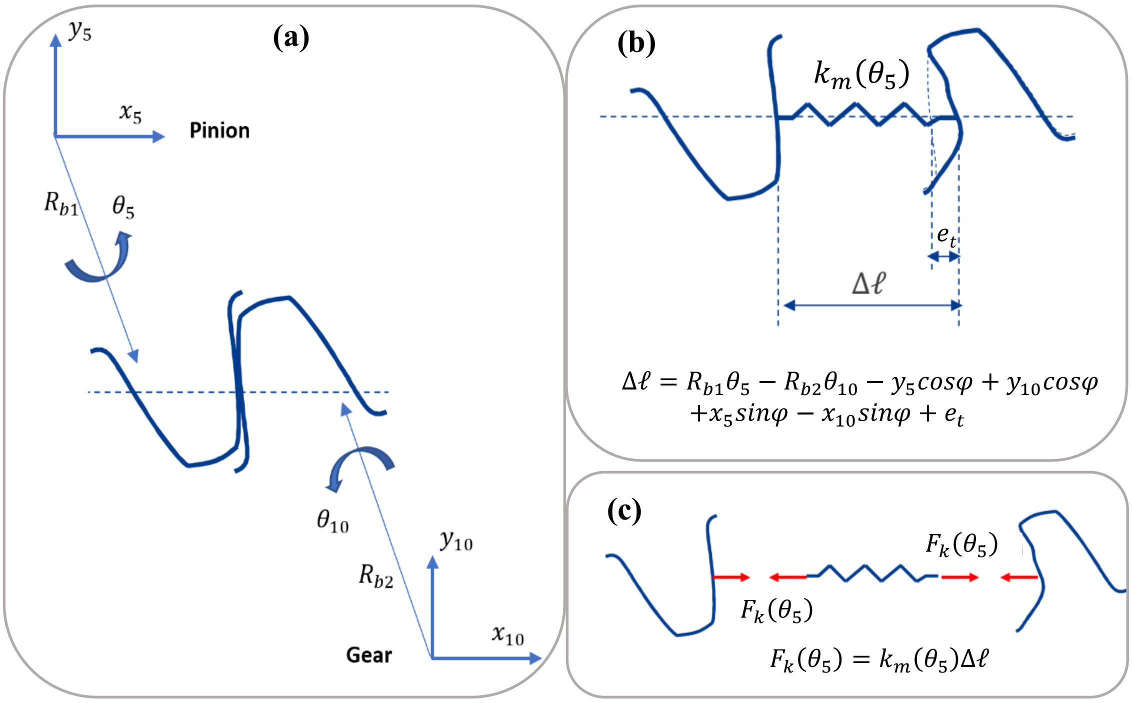

Figure 5.4 Gear systems: (a) gear contact mechanism; (b) deflections between mating teeth; (c) gear dynamic contact force

The shape and severity of GTE impact the contact mechanism of gear pairs significantly. Figure 5.4 demonstrates the effects of GTE on gear dynamic contact force F_k. The deflections $\Delta\ell$ between the mating gear teeth are shown in Figure 5.4(b), it consists of the stiffnesses related deformation and the geometric working surface deviations from the ideal gear tooth profile, which is GTE. Note that in the gear wear case, meshing stiffness change can be neglected as it is significantly less important than the transmission error effect [18]. Therefore, the assessment of gear wear induced GTE is vital for analyzing the coupling effects between gear wear and gear dynamic, and the further wear prediction. The evaluation of wear induced GTE will be introduced in Chapter 6.

5.2.3 Dynamic simulation process

In this study, the dynamic model is established using Simulink@ environment. To solve this developed gear system, the state space theory is used to represent the gear dynamic system in a useful mathematical way [163-165], as shown in Figure 5.5. Linear Time-Invariant (LTI) component is a linear representation of a dynamic gear system in either discrete or continuous time. With the LTI component, the eigenfrequencies can be easily obtained for validating the dynamic model. Also, the time-varying variables, such as meshing stiffness, damping coefficient, and geometric transmission error, are taken into consideration, using the lookup tables with cubic spline interpolation, so that the dynamic characteristics of the gear system can be realized and simulated. To clearly show the differences between this work and previously published research [18, 41, 107, 166], more details of the dynamic model in the Simulink® simulation environment are demonstrated in Figure 5.6, Figure 5.7, and Figure 5.8.

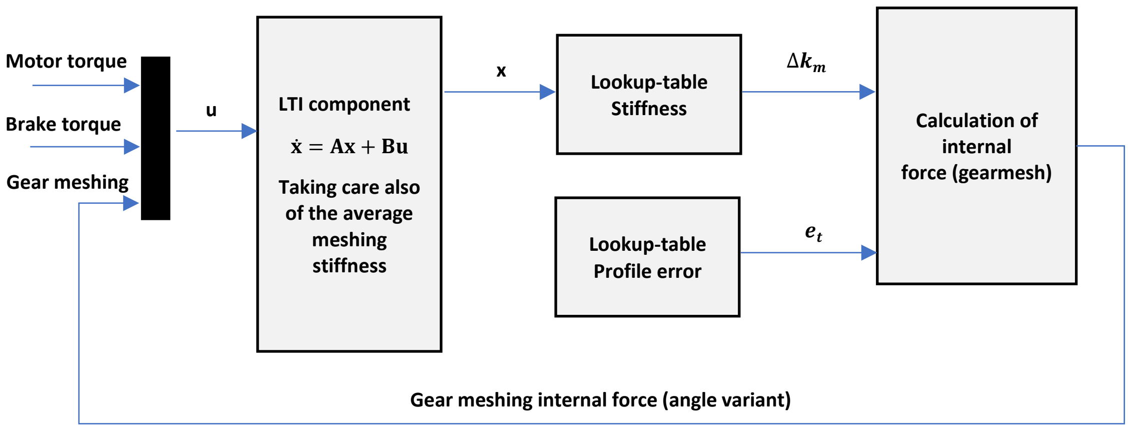

Figure 5.5 Gear state-space dynamic model

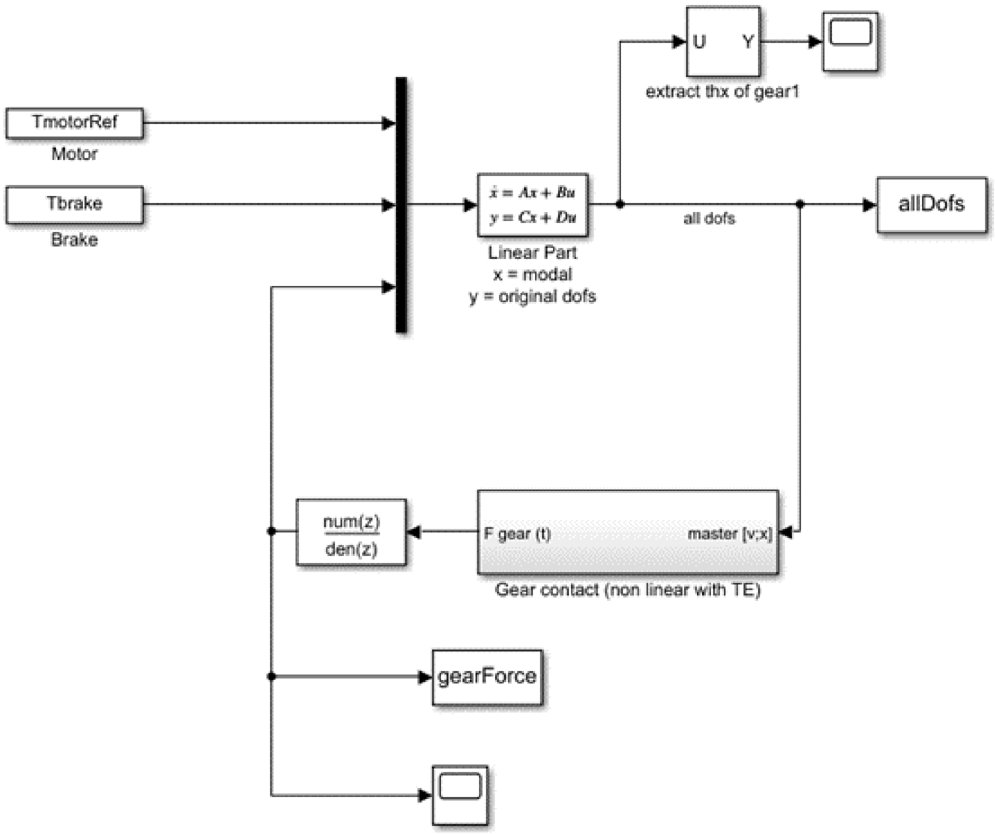

Figure 5.6 Dynamic model in Simulink® simulation environment: overall structure

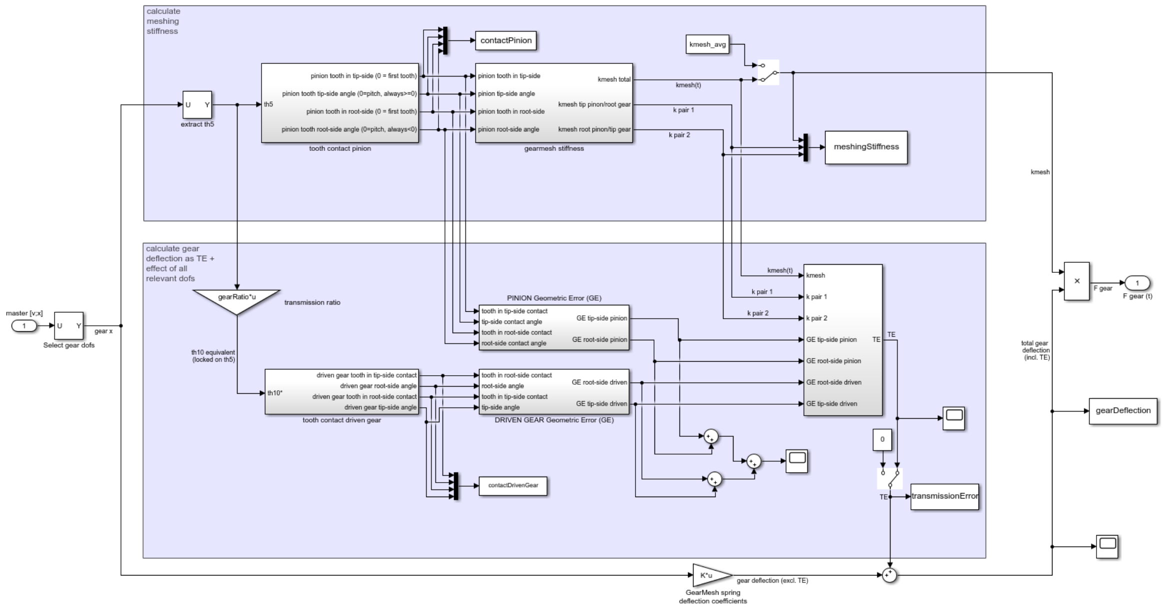

Figure 5.7 Dynamic model in Simulink® simulation environment: gear contact part

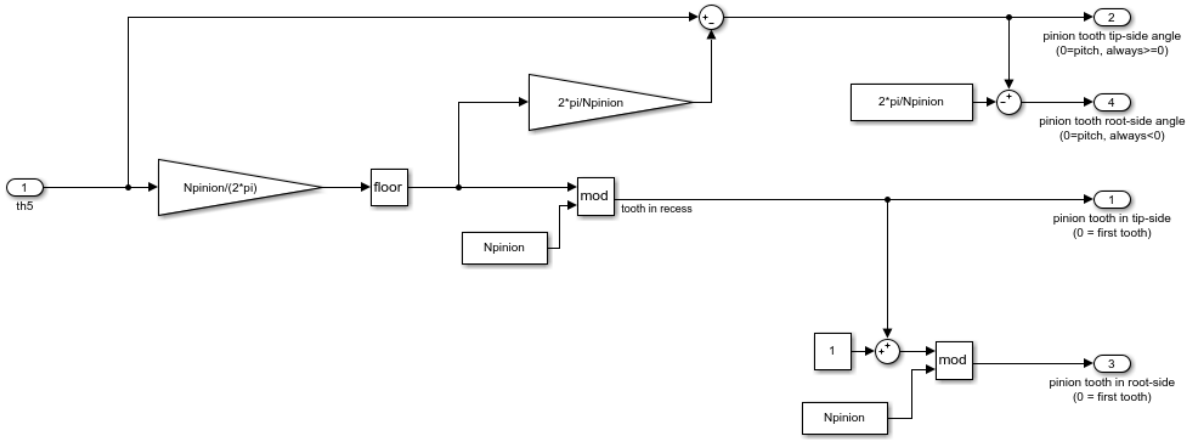

Figure 5.8 Dynamic model in Simulink® simulation environment: single tooth pair contact

ODE 45 is a function that implements a Runge-Kutta method with a variable time step and high computation efficiency, therefore, in this study, ODE45 would be the first choice for solving the dynamic motion equations [41]. In some specific cases, for example, the problem/system is suspected to be stiff [167], ODE15s is the alternative in this study to obtain numerical solutions of the developed dynamic gear transmission system.

5.3 Model validation and calibration

Before using the dynamic model for further analysis, the dynamic model should be validated and calibrated to guarantee the responses from the dynamic model are reliable. In this research, a series of initial tests were performed for the validation and calibration of the dynamic model, including a speed ramp test, impact tests and constant speed tests.

To obtain the natural frequencies/modes of the spur gearbox test rig for comparing with the developed dynamic gear model, a speed ramp test was arranged. This method involves collecting vibration signals over a period when the gearbox is ramping up toward full speed, as shown in Figure 5.9. This particular test uses the vibration of the shaft as a forcing function to provide energy inputting into the gear system. Doing like this will excite resonances as the shaft vibration passes through the critical speed.

Power spectral density (PSD) analysis is a traditional frequency-domain analysis tool to identify the structure modes/natural frequencies of mechanical systems. The reason is that resonance is the amplification of a signal when its frequency is close to the natural frequency of a system. With help of PSD analysis, the resonances in the spectrum are amplified and other components such as background noise are reduced, making the modes of the systems being easily detected. The PSD analysis of the spur gearbox is shown in Figure 5.10.

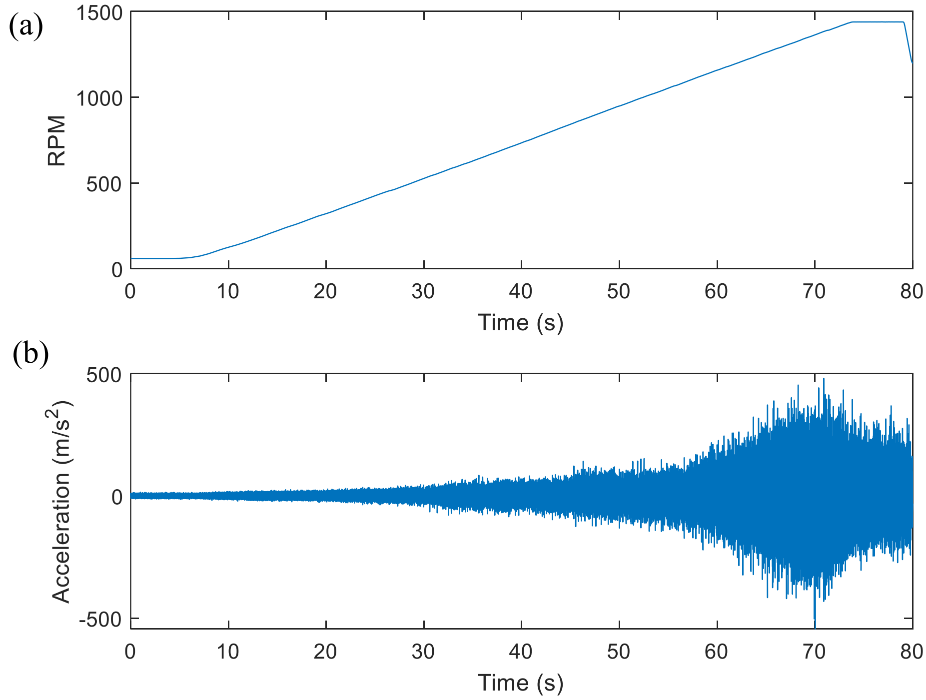

Figure 5.9 Measured vibration during the spur gearbox ramp test: (a) rotational speed; (b) measured vibrations

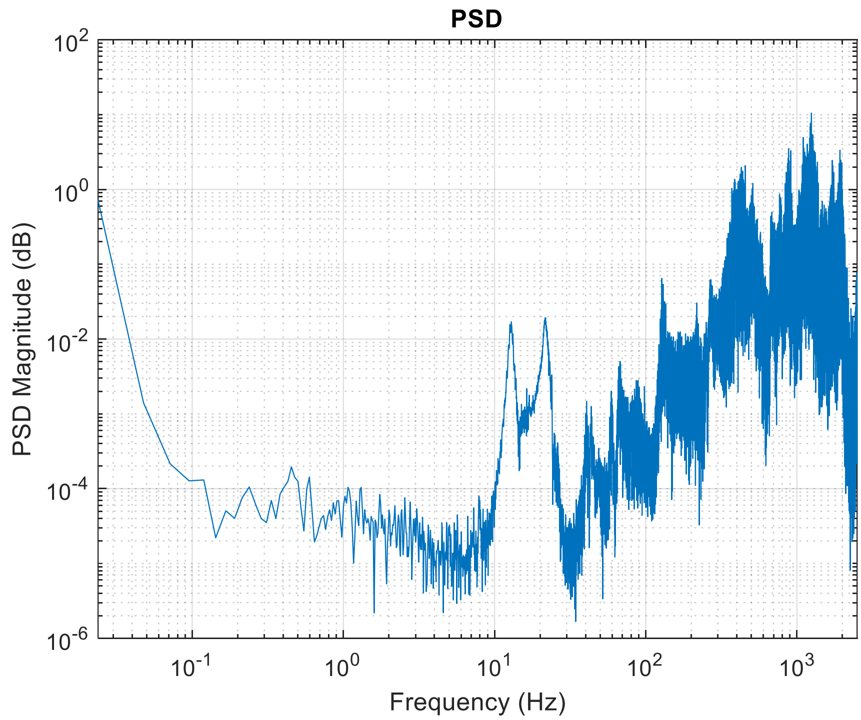

Figure 5.10 PSD analysis of the vibrations of the spur gear system

From Figure 5.10, the modes/natural frequencies of the whole UNSW spur gear system can be identified, which have been summarized in Table 5.4. These natural frequencies can be used as references to help check the validity and reliability of the developed dynamic model. It should be noted that in the developed dynamic model, the foundation of the spur gearbox is not simulated and included, therefore, to make the natural frequency from ramp tests being comparable with the developed dynamic model of the gear system, the foundation of the gearbox's natural frequencies should be excluded from the natural frequencies acquired from ramp tests. With this regard, an impact test was applied to help reveal the natural frequencies of the gearbox's foundation so that it can be subtracted from the whole UNSW spur gear system. Note that a slight load is applied to ensure the gear pairs being in contact, when conducting the hammer test on the foundation of the gearbox.

Table 5.4 Identified natural frequencies from the PSD analysis of experimental measurements

Natural frequencies (Hz)						
13	22	41	59	68	87	128
218	270	430	512	6883	767	880
1103	1167	1248	1367	1471	1714	1927

The quadrature picking method was applied here to determine the natural frequencies/modes and mode shapes of the gearbox's foundation [168], as demonstrated in Figure 5.11. The theory of the quadrature picking method is explained as follows. The Frequency Response Function (FRF) appears to become purely imaginary at the modal frequency. Its amplitude is proportional to the modal displacement, and its sign is positive if displacement is in phase with the excitation. The mode shapes can be determined if a response is fixed, or set an excitation degree of freedom as a reference and then make a set of measurements. The imaginary parts of the measured FRFs can be "picked" at the modal frequencies at which they represent the modal displacement for that specific degree of freedom [168]. This method is based on the assumption that the coupling between the modes is light. In practice, mechanical structures are often very lightly damped (<1%). This implies that the modes are lightly coupled.

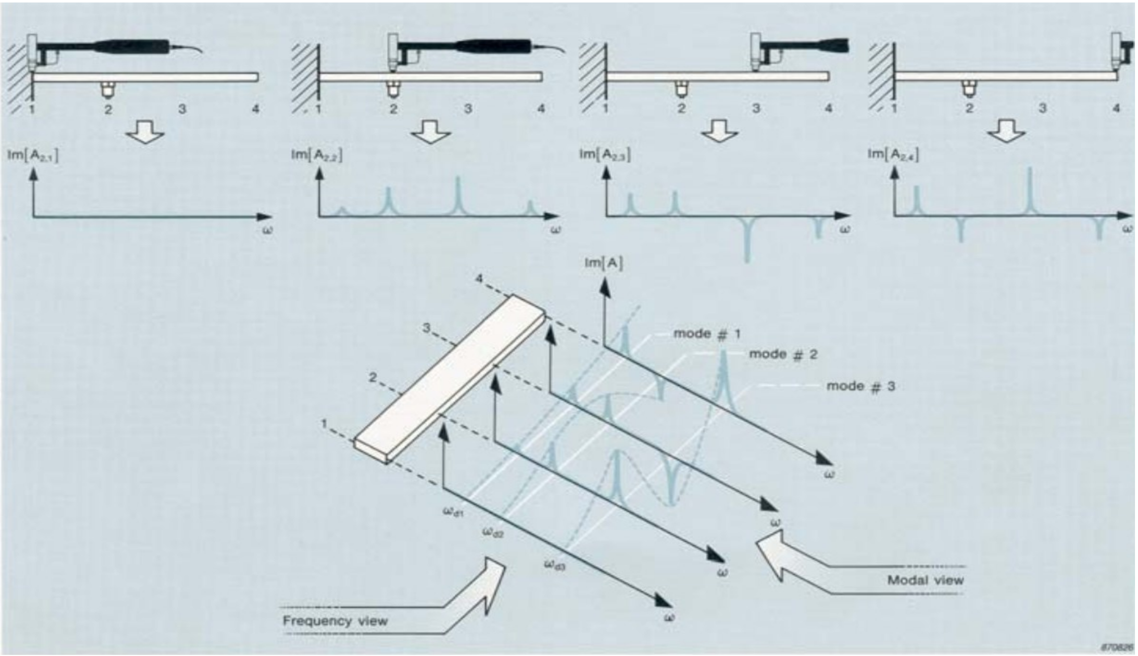

Figure 5.11 Demonstration of quadrature picking method [168]

As for the foundation of the gear system, an accelerometer (B&K 4396) is fixed on the root of the gearbox casing to collect the responses excited by varying inputs generating by impact hammers, as shown in Figure 5.12. The modes of the foundation of the gearbox and its mode shapes can be calculated and extracted through Eq. (5.17)

$$H(\omega) = \frac{X(\omega)}{F(\omega)} \tag{5.17}$$

where $H(\omega)$ is the FRF, $X(\omega)$ is the output of the system and $F(\omega)$ is the input of the system.

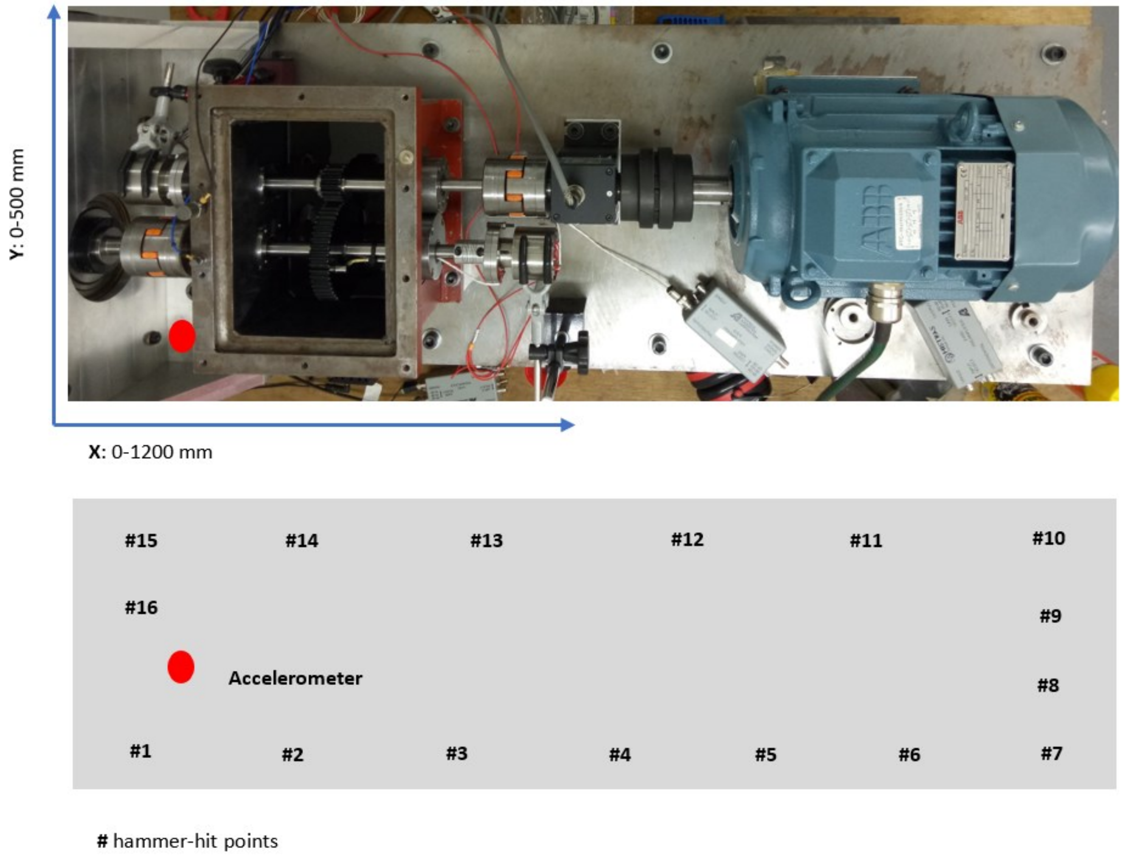

Figure 5.12 Harmer test on gearbox's foundation

Figure 5.13 gives the first four mode shapes for demonstration purposes. Based on Eq. (5.17), the FRF of the gearbox's foundation is shown in Figure 5.14, including the magnitude, phase and coherence. At the modes of the gear system, there would be a peak in the magnitude spectrum, and the corresponding phase would shift 180 degrees. Coherence is a function versus frequency that indicates how much of the output is due to the input in the FRF. It can be an indicator of the quality of the FRF, which evaluates the consistency of the FRF from measurement to repeat of the same measurement: (a) coherence's value is 1 at a particular frequency indicating that the FRF amplitude and phase are very repeatable from measurement to measurement; (b) while coherence's value is 0 indicating that opposite – the measurements are not repeatable, which is a possible "warning flag" that there is an error in the measurement setup.

From the magnitude, phase and coherence spectrums in Figure 5.14, all the modes of the gearbox's foundation can be identified. Subtracting the obtained modes/natural frequencies from the whole gear system's modes (from the speed ramp test), the modes/natural frequencies of the gear system without foundation can be achieved, which are comparable with the developed dynamic model.

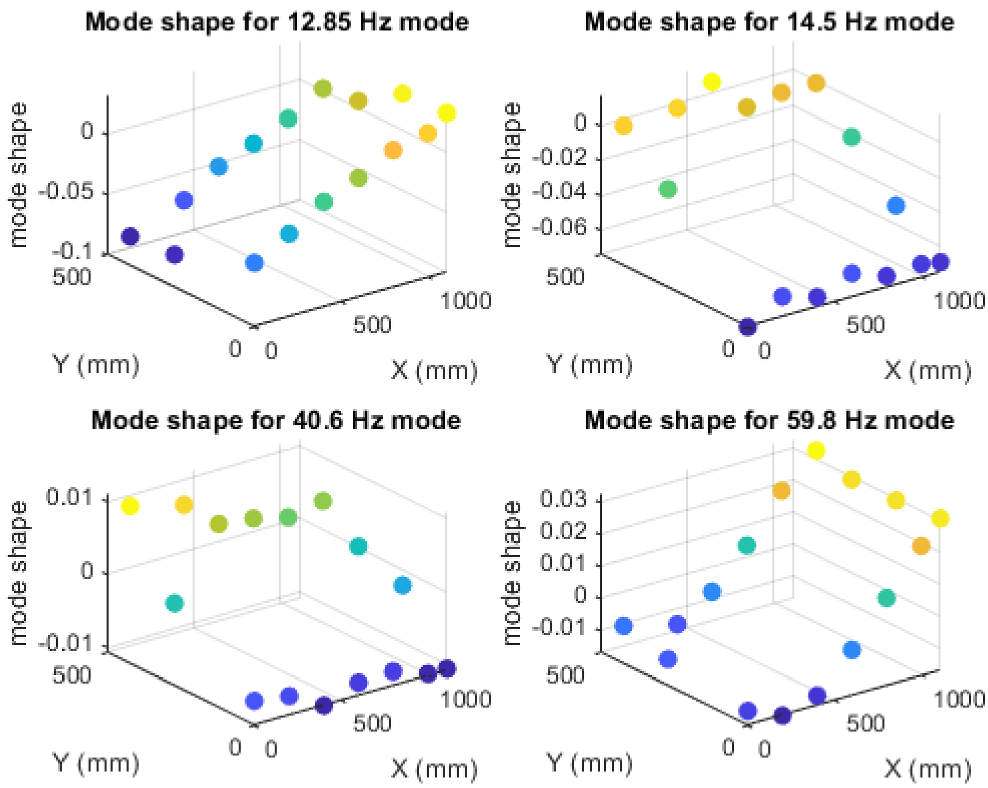

Figure 5.13 The first four mode shapes of the gearbox's foundation

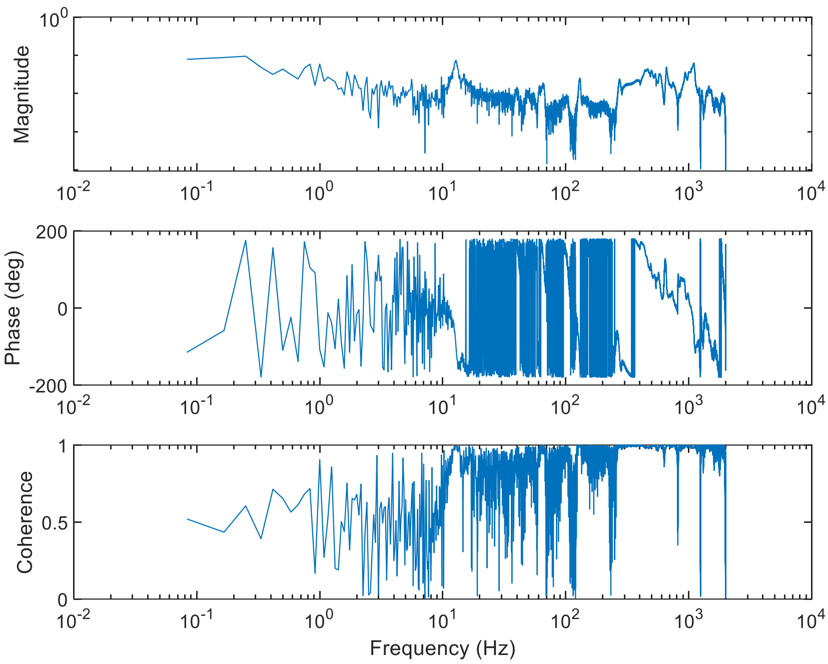

Figure 5.14 Frequency Response Function (FRF) of the gearbox's foundation

The speed ramp and impact tests were used to provide an initial adjustment of the most uncertain model parameters (e.g. stiffness of joints and bearings) with the ultimate aim of obtaining a good match between simulated and experimental natural frequencies in the frequency a range of interest (0-2 kHz). The comparison result is summarised in Table 5.5. And the scaled meshing stiffness is shown in Figure 5.15. Note that the natural frequencies presenting formats (such as accuracy) are set to be the same as the researchers did in Ref. [169]. The reason why scaling the meshing stiffness is explained as follows. In gear transmission systems, various gears are used for different purposes. For example, some gears are surface hardened, while some are not treated with the hardening process. Soft vs hardened gears results in different magnitudes of the meshing stiffness when they have identical gear profiles. To guarantee the responses from the dynamic model are close to the actual measurements from the specific test rig, model calibration is thus necessary. It involves 'scaling' the meshing stiffness of the model so that it is close enough to the gears used in the experiments.

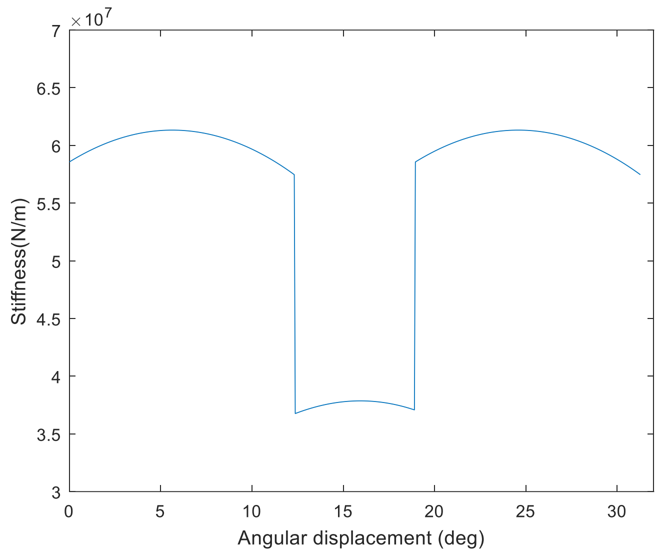

Figure 5.15 Meshing stiffness curve

Table 5.5 Natural frequency comparison results of dynamic model and experimental data

Experiments (Hz)	Dynamic model (Hz)	Difference (%)
22	23	5.1
87	81	-6.7
218	201	-7.8
430	427	-0.8
512	529	3.5
767	740	3.5
1248	1268	1.6
1927	1885	2.2

Table 5.5 shows that the first eight natural frequencies agree between the experiments and the dynamic model within eight percent, which was deemed sufficient to approximate the system response.

Two constant speed tests were then executed to fine-tune a scale factor for the meshing stiffness function k_m and the damping coefficient c_m:

1. 2 Hz rotational speed and 10 Nm motor torque and

2. 2 Hz rotational speed and 20 Nm motor torque.

The encoder signals on the input and output shaft were used in these tests to calculate the static transmission error (STE) of the gearbox system using the phase demodulation method [170] assuming negligible dynamic effects at this low speed. This STE was then used as an input to the dynamic model to simulate a vibration response. After low-pass filtering in the band of interest (0-2 kHz), the RMS of the simulated vibration signal $y_6^{(SIM)}(t)$ was then compared with the experimental results and the meshing stiffness and damping were manually adjusted until good agreement between the results was obtained, as shown in Figure 5.16**.** To examine the rationality of the responses from the developed dynamic model, similar to Ref. [41], the first five gear tooth meshes are expanded and plotted in Figure 5.17. From the comparison between the five gear mesh teeth signals of the experiment and simulation, it can be seen that the characteristics of the gear system are well presented, including the engagement of teeth contact, loading and unloading of teeth, the gear mesh period, and the amplitude of vibration. Note that the wear on each gear tooth is theoretically the same, even though the tooth-to-tooth differences do exist in practice due to manufacturing or mounting error (as shown in Figure 5.16(a) and Figure 5.17(a)), resulting in that modulation phenomenon and sidebands exist in the measured signal. Since uniform wear is simulated in the developed dynamic model, and also because the wear process is the same on each gear tooth, no sidebands around the gear mesh (caused by the modulations behaviours) exist in the simulated signal.

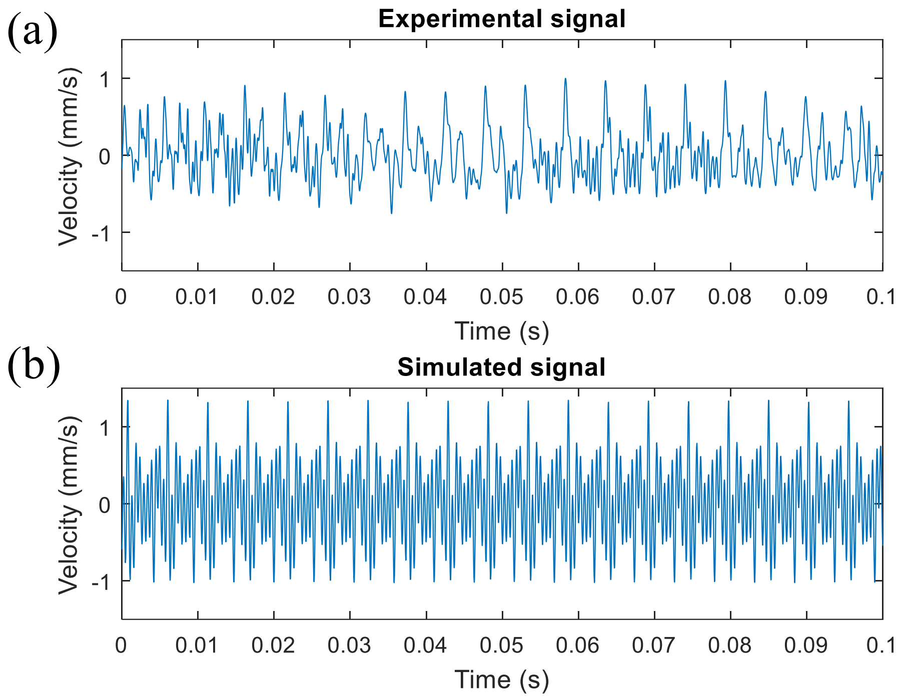

Figure 5.16 Vibration signal: (a) experiment and (b) simulation

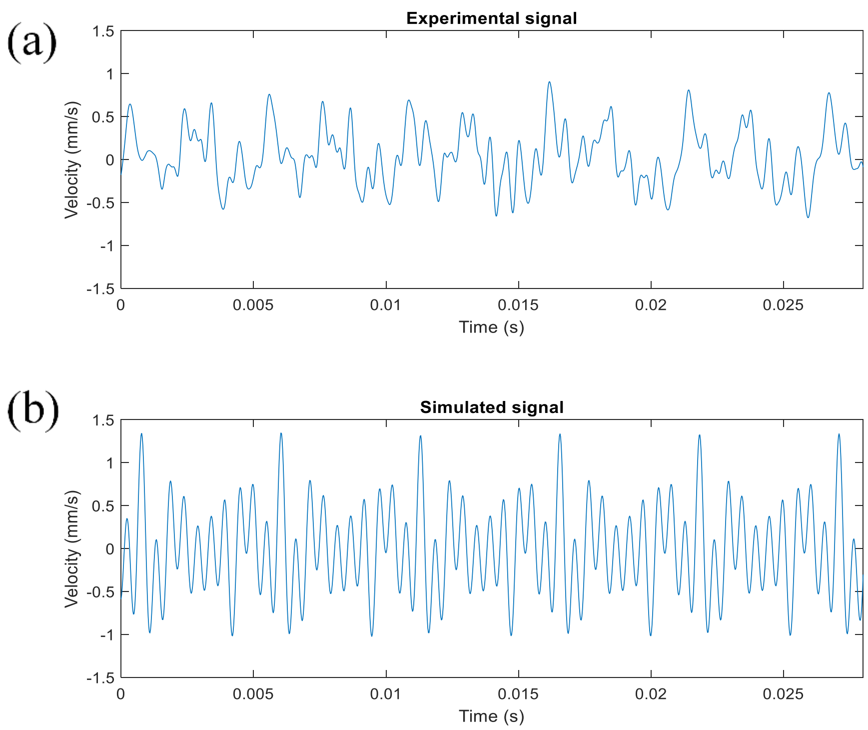

Figure 5.17 Five-gearmesh teeth: (a) experiment and (b) simulation

The low pass filtering was necessary to remove high frequency effects which arise in the simulation from the unrealistic steps in the stiffness function, smoothed in practice by a gradual engagement/disengagement of the teeth. Indeed, even in this limited band the stronger weighting of the higher gear mesh harmonics is apparent in the simulated response in Figure 5.16(b). Nonetheless, the overall magnitudes of the responses were deemed to match the measurements sufficiently for the purposes of the present study.

The dynamic contact force from the developed model is shown in Figure 5.18, and more spikes and fluctuations are observed in the contact force compared with the results shown in Ref. [21]. These spikes and fluctuations are caused by the resonances of the gear system. In Ref. [21], a torsional model (with a single DOF) was established to generate dynamic contact force and the subsequent worn tooth profile. As for the torsional model in Ref. [21], there is only one mode existing in the simulated gear system, therefore, its FRF is simple and only has one peak, resulting in the contact force being in a 'smooth' pattern. However, in practice, the gear system is usually much more complex in terms of potential changes in the dynamic responses under an operating condition, and the single DOF torsional model is not representative anymore. Therefore, the authors in Ref. [60] included the translational effects coming from the shaft bending and bearing radial deflections into the dynamic model, and significantly different characteristics of contact force and the subsequent worn tooth profile were observed, comparing with the results shown in Ref. [21], and more spikes and fluctuations start to appear. Also, the dynamic contact force simulated in Ref. [171] exhibited lots of spikes and fluctuation behaviours due to more degrees of freedom are included in the developed dynamic model.

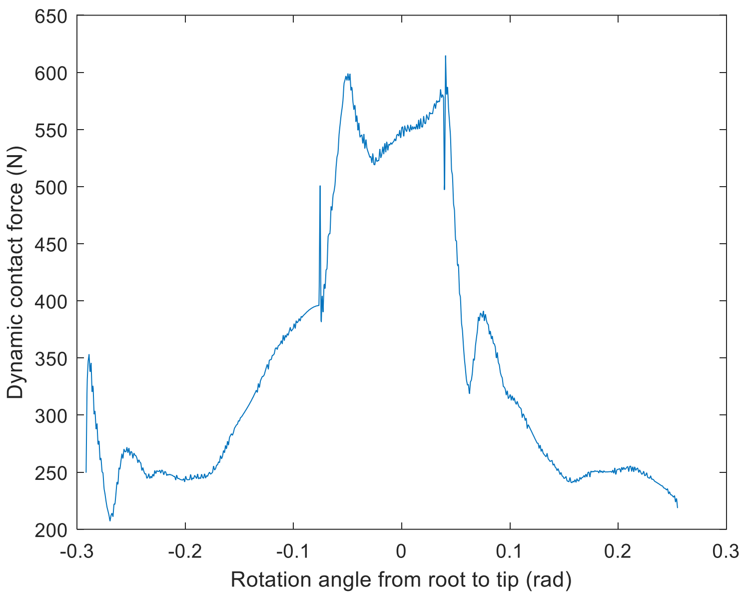

Figure 5.18 Dynamic contact force (from gear root to tip)

This calibrated dynamic model was used both to generate dynamic contact forces (for specified GTEs) for input into the tribological wear model and to simulate responses for comparison with vibration measurements to enable updating of the wear model.

5.4 Summary

This chapter presents the development of a 21-DOFs dynamic model based on the UNSW spur gearbox test rig, including gear meshing stiffness, geometric transmission error evolution, and the solver to acquire numerical solutions. The dynamic model developed in this chapter is a crucial part of the proposed vibration-based wear prediction schemes, which will be introduced in Chapter 6 and Chapter 7. Note that the developed dynamic model is different from previously published research [18, 41, 107] since a new gearbox test rig is used in this thesis. Also, the applications of the developed dynamic model are different from previously published research. To guarantee the dynamic responses of the developed dynamic model is close enough to the actual test rig so that it can provide useful information for further wear analysis, speed ramp test, impact test and several constant speed tests are conducted to validate and calibrate the dynamic model. The natural frequency comparison between experiment and simulation shows that the developed dynamic model match well with the real UNSW spur gearbox test rig. Also, the time waveforms of vibrations from experiments and the dynamic model match each other. It suggests that the developed dynamic model can provide reliable dynamic contact to the tribological (wear) models for further wear analysis. Moreover, the simulated vibration characteristics can be used to compare with actual measurements for updating analysis of wear prediction, which will be introduced in Chapter 6 and Chapter 7.

However, it should be mentioned that the foundation of the gearbox has not been modelled in the developed dynamic model, which might affect the simulated vibrations, especially when it is operating at its resonances range. This issue will be addressed in future work by including the foundation.

Chapter 6 Monitoring and prediction of tooth profile changes during wear progression

The work presented in this chapter is devoted to achieving **objective 3** of this research: **monitoring and prediction of tooth profile changes during wear progression**. This work has been presented in papers titled *"Vibration-based updating of wear prediction for spur gears"* and "*Use of an improved vibration-based updating methodology for gear wear prediction*", which were published in the journals of *Wear* (426-427: 1410-1415, 2019) and *Engineering Failure Analysis* (120: 105066, 2021). The main content of this chapter is identical to the above publications, while the structure of this chapter has been arranged to ensure the consistency of the thesis.

This chapter is organized as follows. In Section 6.1, a brief introduction to this study is presented. Section 6.2 introduces the proposed wear prediction scheme, and then presents the new wear depth distribution calculation approach; Section 6.3 shows the gear wear prediction results using two endurance tests under different lubrication conditions. In Section 6.4, the main outcomes are summarised.

6.1 Introduction

Gear wear is a progressive material loss from contacting gear tooth surfaces due to the combined sliding and rolling motion under boundary or mixed lubrication conditions [13]. During gear service life, wear induced tooth profile change is a common wear phenomenon, and it can result in gear tooth thickness reduction. In general, the wear induced tooth profile alteration non-uniformly distributes from gear tooth root to tip [68]. The reason is that the sliding velocities at the different contact locations of the gear tooth in relation to the pitch line are different and the wear rate is a function of the sliding velocity as well as the pressure [172]. The wear induced tooth profile alteration may lead to a sudden failure of the gearbox transmission system, which can result in unexpected economic loss and serious accidents. Therefore, for the effective management of the health of the transmission system, it is important to be able to monitor the gear profile change and predict its propagation, which is the focus of this chapter.

As reviewed in Chapter 2, the majority of existing research works mainly focused on studying the effects of surface wear processes on gear system dynamic characteristics such as transmission error and dynamic meshing force [31, 72, 173-175], and investigating the effect of gear dynamics on surface wear [21, 59, 60, 176-178]. In contrast, there are only a handful of studies on the prediction of spur gear wear induced tooth profile change under quasi-static operating conditions [57, 68, 84]. But dynamic response characteristics are quite different from those under quasi-static conditions. The dynamic meshing forces are typically larger than the corresponding quasi-static forces and their magnitudes and waveforms are quite different [21].

Theoretically, dynamic response characteristics of a gear pair are sensitive to a profile change, that is, a geometric deviation of the tooth surface profile from a perfect involute, and elastic deformation [25]. Gear surface wear is a material removal process, which can result in a geometric deviation. And, elastic deformation is determined by contact force and meshing stiffness. Based on this theory, the authors in reference [21] used a periodically time-varying meshing stiffness function and an external displacement excitation to represent the effects of dynamic response on the gear wear process. In that research, the authors utilized a torsional model with a single-degree-of-freedom (DOF) and then combined it with a quasi-static wear model [57] to develop a dynamic wear model. This model is capable of investigating the interactions between the surface wear and the spur gear system's dynamic characteristics. Later, to demonstrate the effect of translational deflection on the wear process, one study [60] introduced a 3-DOFs dynamic model to replace the torsional model in Ref. [21], and it found that the translational deflection in the gear system impact the gear progress significantly, therefore, it must be included when analysing gear wear progradation.

It should be noted that both Refs. [21, 60] only investigated the coupling effects between gear dynamics and the wear process through a set of simulations. Gear wear prediction under dynamic conditions, which can bring significant benefits to a wide range of industries, was not included.

The combination of dynamic and wear models, proposed in a few variants in the literature [57, 68, 84], is theoretically able to predict the evolution of wear and its induced tooth profile alteration, considering its interactions with the gearbox dynamics. This prediction will however likely drift away from the actual wear process which is a complex process with multiple factors, especially considering that the parameters governing wear dynamics vary in time (e.g., with the contamination of the lubricant and the change in surface roughness). Increasing the complexity of the wear models to follow these complex trends is an option, but it is likely to result in additional parameters whose quantification for practical applications could be difficult, leading to additional uncertainty in the model predictions.

To accurately and efficiently predict gear tooth profile change in a wear process, a gear-wear prediction methodology is proposed in this research. The following sections will introduce the whole procedure of the proposed vibration-based updating of the wear prediction scheme theoretically and demonstrate the tooth profile change prediction results with accelerated run-to-failure gear wear tests under different lubrication conditions.

6.2 Methodology for monitoring and predicting tooth profile change from wear

6.2.1 The proposed vibration-based approach for monitoring and predicting tooth profile change

In this section, the architecture of the proposed vibration-based prediction scheme for the tooth profile change caused by wear will be introduced briefly.

The overall approach is concisely presented in Figure 6.1. The modelling component of this methodology (on the left of Figure 6.1) is composed of two interacting simulation models: a dynamic model and a wear model. Based on the input of the tooth profile geometry, the dynamic model predicts tooth contact forces, which are passed on to the wear model to estimate gear wear and consequently modify the tooth profile geometry, which is then fed back into the dynamic model. This iterative loop allows a knowledge-based prediction of wear and its induced tooth profile change, which however is likely to be reliable only on a limited timeframe, within which the wear model parameters remain unchanged.

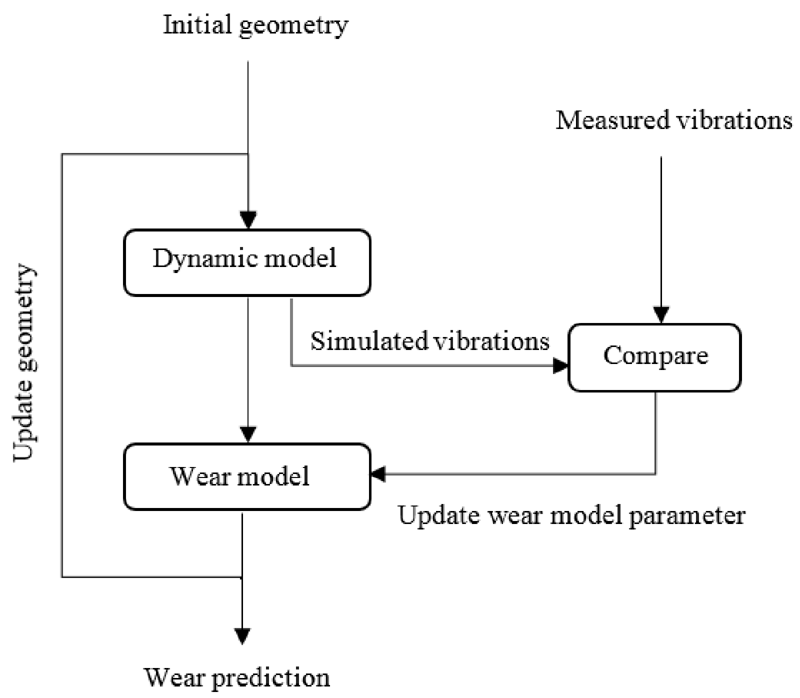

Figure 6.1 Basic procedures of the proposed vibration-based scheme for updating wear predictions

The main novelty of the proposed approach relies on the updating of the wear model parameters based on vibration measurements (on the right of Figure 6.1). The vibrations from the gearbox dynamic model are compared to measured vibration levels to track the quality of the wear model predictions and if necessary update the wear model parameters.

The details of each component of the approach, as outlined in Figure 6.1, will be discussed in depth in the following sections.

6.2.2 Dynamic model

In this section, only a brief introduction of the dynamic model of the spur gearbox will be given since its development has been introduced with details in Chapter 5.

To generate realistic vibrations and contact forces for the wear model, a 21 degree-of-freedom (DOF) lumped parameter dynamic model is established based on the University of New South Wales (UNSW) gearbox test bench, the development of which has been introduced in Chapter 5. The basic motion equations of the dynamic model are as follows

$$\mathbf{M}\ddot{\mathbf{x}} + \mathbf{C}\dot{\mathbf{x}} + \mathbf{K}\mathbf{x} = \mathbf{f} \tag{6.1}$$

where $\mathbf{x}$ represents the angular and translational displacements of the different nodes of the gearbox system, which is in the plane perpendicular to the input and output shaft axes. $\mathbf{K}$, $\mathbf{C}$ and $\mathbf{f}$ are the matrices of corresponding stiffness, damping and force. Further details of this dynamic model development can be found in Chapter 5, also the dynamic model was calibrated using impact tests, some speed ramp tests and several constant speed tests. The calibration ensures that reliable contact force figures are fed into the wear model and that realistic vibration signals are simulated.

6.2.3 Wear model for simulating tooth profile change

Although many advanced wear models have been proposed using different methodologies and parameter sets, the Archard wear model remains the most commonly used for practical applications, and is chosen in this research to simulate the wear induced tooth profile change behaviours. Neglecting changes in the contact area over the meshing cycle, and differentiating the expression of Ref. [21], the Archard wear model is as follows

$$\frac{dh}{dt} = K_{\mathrm{wear}} F v \tag{6.2}$$

where h is the wear depth, F is the normal load and v is the corresponding sliding velocity.

Even though the capability of the Archard wear in simulating wear propagation behaviours has been demonstrated in lots of references [71, 179-181], the Archard wear model can be improved to enhance the gear wear prediction accuracy with consideration of more realistic parameters and factors. First, expressing Eq. (6.2) in terms of contact pressure P rather than contact force would be more physically meaningful [182, 183]. The second point involves the inclusion in the model of the effect from adjacent contact points on the wear depth accumulation at one specific contact point. From the literature review of Chapter 2, it is worth noting that none of the existing works [21, 24, 57, 62, 68, 108] considers the pressure contribution coming from the adjacent contact points to the wear depth accumulation, although the pressure is distributed in a small region and affects the wear distribution.

To address the above-mentioned issues, in this research, the Archard wear model is further improved by considering contact pressure rather than force. Moreover, considering the effect of Hertzian deformation, giving a contact area rather than a line, a new approach is proposed to calculate the wear depth distribution:

$$h(x) = \int K_{\text{wear}} P(x,t) v(t) dt \tag{6.3}$$

where $h(x)$ is the wear depth at contact point x, $P(x,t)$ is the contact pressure distribution at time t, and $v(t)$ is the corresponding sliding velocity.

To clearly explain the new wear depth distribution calculation approach, a simple example is used in Figure 6.2 for demonstration. In Figure 6.2, $\mathrm{P}(5)$, $\mathrm{P}(6)$ and $\mathrm{P}(7)$ represent the instantaneous Hertzian pressure distribution at contact points #5, #6 and #7 respectively. The parameter $\mathrm{P}(5)$_6 represents the consequent pressure at contact point #6 when the gear pairs are engaged at contact point #5, due to the contact area given by Hertzian deformation. A similar meaning holds for P (7)_6. Therefore, in summary, due to the Hertzian deformation, the wear depth at contact point #6 is affected not only when itself is the (theoretical) contact 'point', but also when adjacent points #5 and #7 are the (theoretical) contact points. The sum of them forms the final wear depth at contact point #6, which is demonstrated in Eq. (6.4).

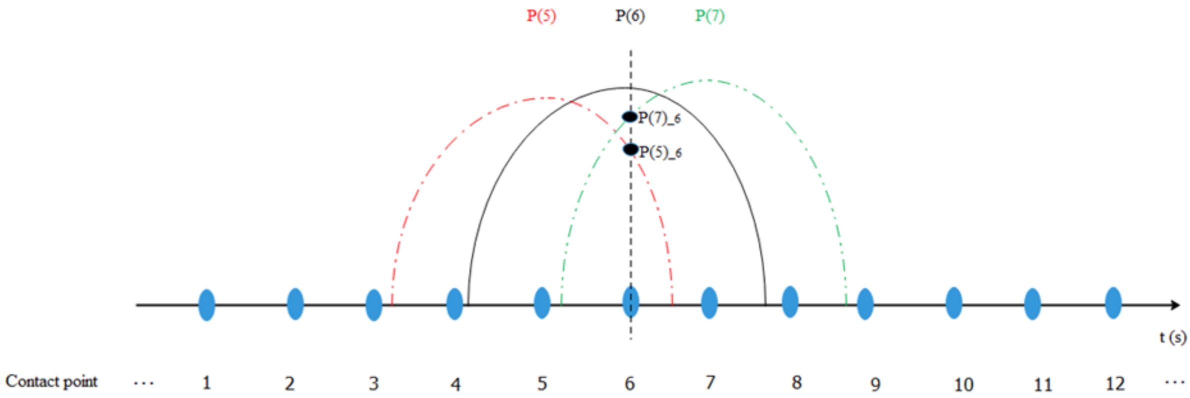

Figure 6.2 The wear depth at contact point #6: including the effects coming from adjacent contact points

$$\Delta h(6) = \left(K_{wear}P_6(6)V(6) + K_{wear}P_5(6)V(5) + K_{wear}P_7(6)V(7)\right) \cdot \Delta t \qquad (6.4)$$

The gear tooth wear depth distribution obtained using the Archard wear model presented in the reference [21] and the improved Archard wear model with the new calculation approach is shown in Figure 6.3. Two differences between the results can be seen:

1) The wear depth at the pitch line (rotation angle zero) is not zero with the new calculation approach, which corresponds more closely with experimental observations (see Figure 6.9 in Section 6.3). The reason is that even though the sliding velocity is theoretically zero at the instant of pitch line contact, due to the Hertzian deformation giving a contact area, the sliding velocity at the pitch line is non-zero during this short instant. This results in mild wear at the pitch line.

2) The curve of the wear depth distribution (from the tooth root to tip) becomes much smoother, which again is more physically meaningful and corresponds with experimental observations (see Figure 6.8 in Section 6.3). In practice, even though dynamic contact pressure distribution has some peaks corresponding to each contact point (see Figure 6.4), it could not cause sharp peaks and troughs in the wear depth distribution when taking into

consideration the effect from the adjacent contact points due to Hertzian deformation. The load altering will rapidly remove any sharp peaks and troughs induced by dynamic forces.

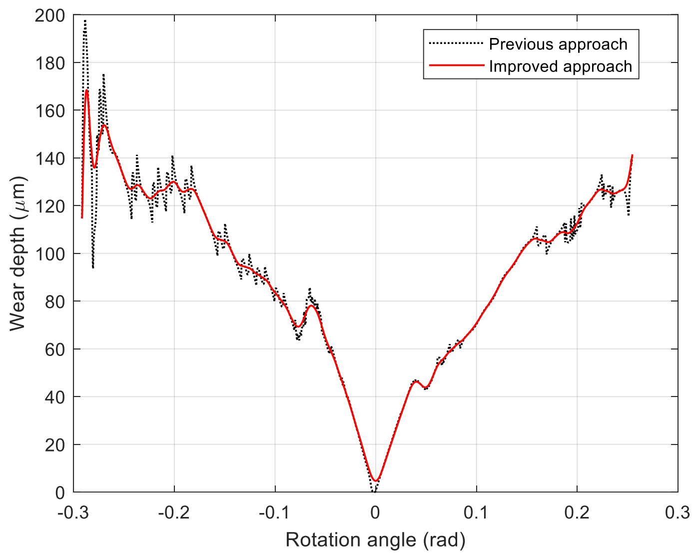

Figure 6.3 Wear depth distribution

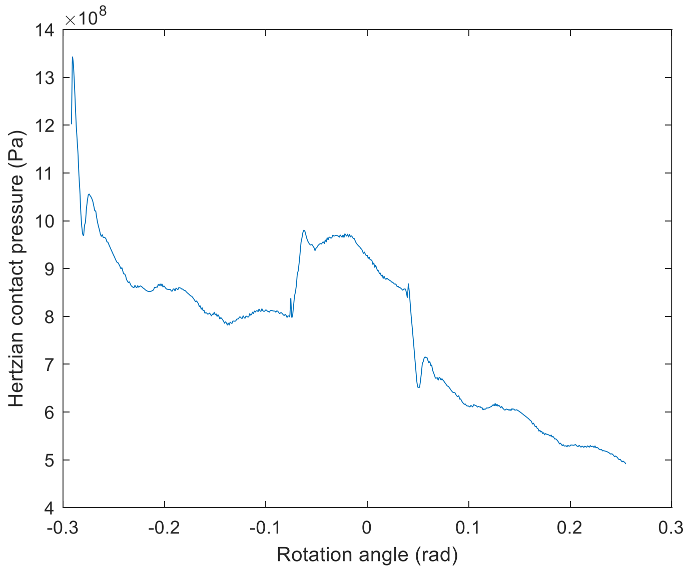

Figure 6.4 Contact pressure distribution: there are some peaks corresponding to each contact point

With consideration of these two factors, the calculated wear profile using the improved Archard wear model with the new calculation approach is more reasonable and realistic compared with the Archard wear model used in Ref. [21], therefore, in this research, the improved Archard wear model is used to simulate the wear propagation behaviours and its induced tooth profile change.

Note that the worn gear tooth profile (the black dot line) shown in Figure 6.3 is different from the results shown in Ref. [21]. More specifically, it is not as 'smooth' as the worn tooth profile presented in Ref. [21]. The reason is that a single DOF torsional model used in Ref. [21] neglects some actual modes (such as translational modes) of gear systems, resulting in a very simple and smooth contact force, which does not represent the actual one. In contrast, a 21 DOFs dynamic model is used in this thesis to account for both translational and torsional modes, and the generated contact force is thus very different to the one obtained from the single DOF torsional model. This difference has been discussed in Section 5.3. Thus, the calculated worn gear tooth profile still has small jags, which is caused by the dynamic interactions from translational and torsional modes of the 21 DOFs dynamic model.

It should note that the wear model parameter K_{wear} (in Eq. (6.3)) is affected by a number of factors including material properties, such as hardness and roughness of the two surfaces, and the lubrication condition, which may evolve in the wear process. Since it is very difficult to estimate or directly measure K_{wear} experimentally, this coefficient is often a major unknown parameter. In this study, K_{wear} is determined experimentally, based on the comparison of simulated and experimental vibrations. The details of this updating methodology will be introduced in the following section.

6.2.4 Updating methodology

The update of the wear coefficient K_{wear} is obtained based on the comparison of the root mean square (RMS) value of simulated and experimental signals. The updating methodology is executed iteratively when the absolute error between the experimental and simulated RMS values exceeds the predefined 5% threshold, and the wear coefficient K_{wear} for the next iteration (i+1) is calculated as follows

$$K_{\mathrm{wear}(i+1)} = D_{(i)} \cdot K_{\mathrm{wear}(i)} \tag{6.5}$$

where $D_{(i)} = \mathrm{RMS}\{y^{(\mathrm{EXP},i)}(t)\}/\mathrm{RMS}\{y^{(\mathrm{SIM},i)}(t)\}$, and $y^{(\mathrm{EXP},i)}(t)$ and $y^{(\mathrm{SIM},i)}(t)$ are the simulated and experimental vibration signals at time t and iteration i. Note that the predefined threshold should be set close to 0 in theory, and the wear coefficient will be updated almost at each step. By doing so, even though the prediction accuracy can be improved slightly, the computation cost will increase significantly. To balance the prediction accuracy and computation cost, a 5% threshold is selected in this research. The iterations are stopped when the absolute error between the simulated and experimental RMS values falls below the predefined threshold. It must be highlighted that the operating conditions of the dynamic model (speed and torque) should be set as close as possible to the actual experimental conditions, to avoid potentially large biases on RMS readings. Luckily, speed measurements and torque estimates (e.g., through current measurements in electromechanical drivetrains) are available in most machines with sufficient criticality to justify a sophisticated condition monitoring system.

6.3 Tooth profile change prediction results

In this section, the wear induced tooth profile change prediction results under dry and lubricated conditions are presented.

6.3.1 Dry test

The dry test was conducted with input shaft speed and torque of 10 Hz and 5 Nm. The wear model parameter K_{wear} was updated (when/if necessary) with the procedure discussed in Section 6.2.4. In total, two updates were executed during the test, when the error between the RMS value of simulated and measured vibration signals exceeded the predefined 5% threshold. The first updating was executed at 0.73×10^4 wear cycles, and the K_{wear} was found to be $1.65 \times 10^{-6}\text{Pa}^{-1}$. The second update occurred at 2.48×10^4 wear cycles, and the updated K_{wear} was $2.17 \times 10^{-6}\text{Pa}^{-1}$. Figure 6.5 shows the evolution of the vibration RMS throughout the dry test. From Figure 6.5, it can be found that the simulated vibrations from the dynamic model match well with the experimental ones after updating the K_{wear}.

To check the effectiveness of the proposed updating scheme (with improved Archard wear model) in wear depth prediction, an estimate of the mean wear depth was calculated based on the wear particles collected using adhesive paper [104]. Figure 6.6 shows the comparison results. It can be found that the wear depths (at 1.29×10^4, 185×10^4, 3.19×10^4 and 3.77×10^4 wear cycles) are well predicted using the proposed updating scheme. Therefore, the proposed updating scheme with the improved Archard wear model has an excellent performance in wear prediction under dry conditions. Note that this and subsequent mean wear depth figures represent the combined wear of the pinion and driven gear tooth profiles, which means that of the pinion alone accounts for about 73% of this wear depth figure. Note too that these wear depth figures were never used in the updating – only the vibration signals (simulated and measured).

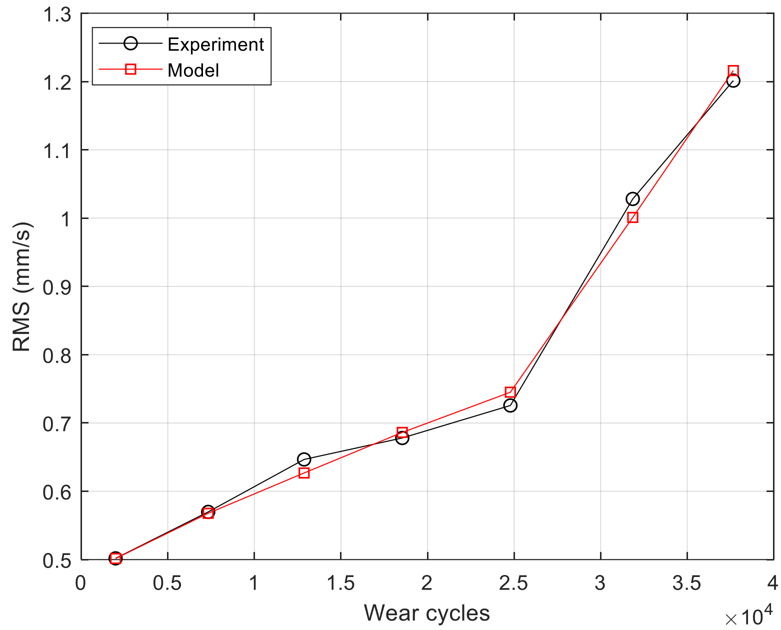

Figure 6.5 Dry test: RMS (in mm/s) versus the number of wear cycles from the experimental testing and the results from simulations (after updating)

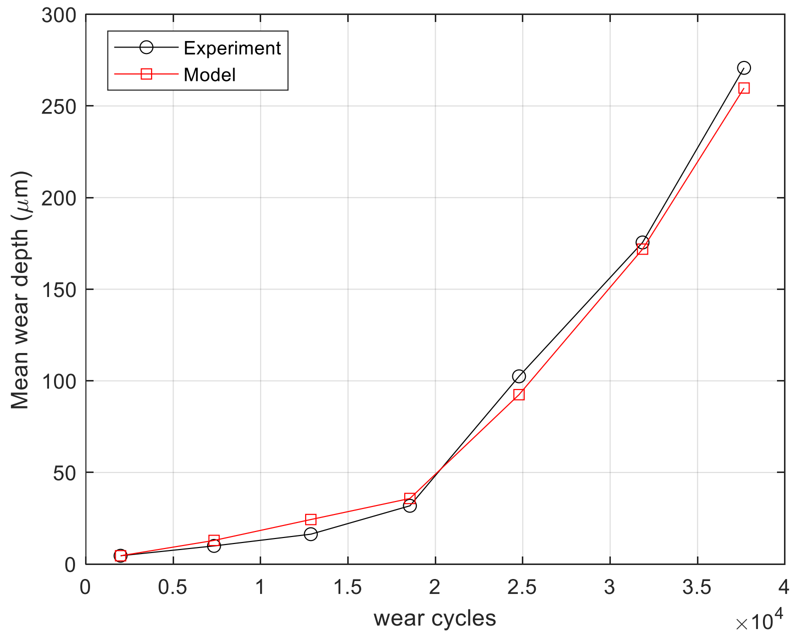

Figure 6.6 Wear depth comparison results of dry test: experiment (from wear particles) and model (after updating)

6.3.2 Lubricated test

In this section, the performance of the updating scheme in wear prediction under lubricated conditions will be examined. The lubricated test was conducted with input shaft speed and torque of $20\ \mathrm{Hz}$ and $20\ \mathrm{Nm}$, respectively. In this case, four updates of the wear coefficient K_{wear} were executed throughout the test (measurements for which the error between the RMS values of simulated and measured vibration signals exceeded the predefined 5% threshold). The updates were applied at 0.57×10^6, 0.82×10^6, 2.19×10^6 and 2.30×10^6 wear cycles. Figure 6.7 shows the RMS comparison results from the model (after updating) and the experiment. The RMS values from the model match well with the experimental ones after updating the K_{wear} values. Note that the manufacturing marks on the driven gear have been significantly removed during [1.41~2.12] million cycles. The same phenomenon was observed in Ref. [128]. Thus, a plateau at $1.4\ \mathrm{mm/s}$ occurs in the RMS trend during this period.

In the lubricated test, it is hard to collect all wear particles in the oil, therefore, the tooth profile change could not be estimated like the dry test using wear particle mass. To obtain reliable wear depth measurements for verifying the effectiveness of the updating scheme in wear prediction, a moulding technique [128] was used to obtain the gear tooth profile change experimentally, see Figure 6.8. Figure 6.9 shows the tooth profile change from 0.36×10^6 wear cycles to 2.58×10^6 wear cycles. Note: the run-in period (the first 0.36×10^6 wear cycles) is excluded.

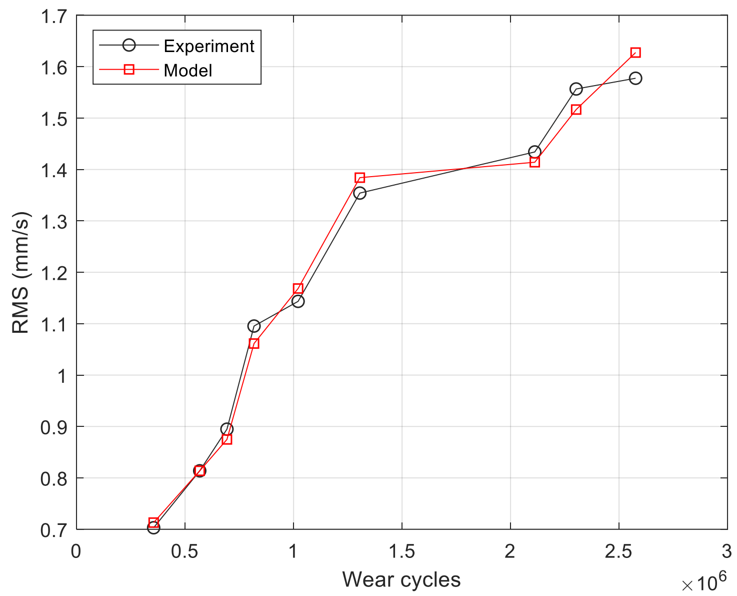

Figure 6.7 Lubricated test: RMS (in mm/s) versus the number of wear cycles from the experimental testing and the results from simulations (after updating)

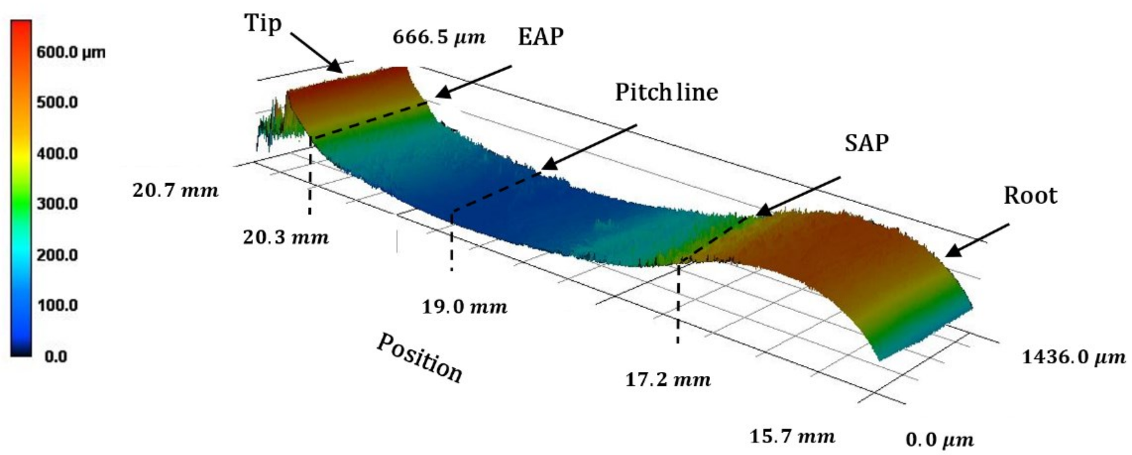

Figure 6.8 3D image of the mould profile collected from pinion (SAP: start of active profile, EAP: end of active profile)

Based on the profile change demonstrated in Figure 6.9, the mean wear depth (from gear root to tip) of the mating gears should be 48.2 µm. The model-based wear depth prediction results compared with the experimental measurement (the latter from only the end of the test) are shown in Figure 6.10. From Figure 6.10, it can be found that the final predicted wear depth is 46.2 µm. Compared with the measured wear depth, a 4.3% error exists, which is acceptable. Therefore, with the improved Archard wear model, the proposed updating methodology is effective in predicting wear depth under lubricated conditions.

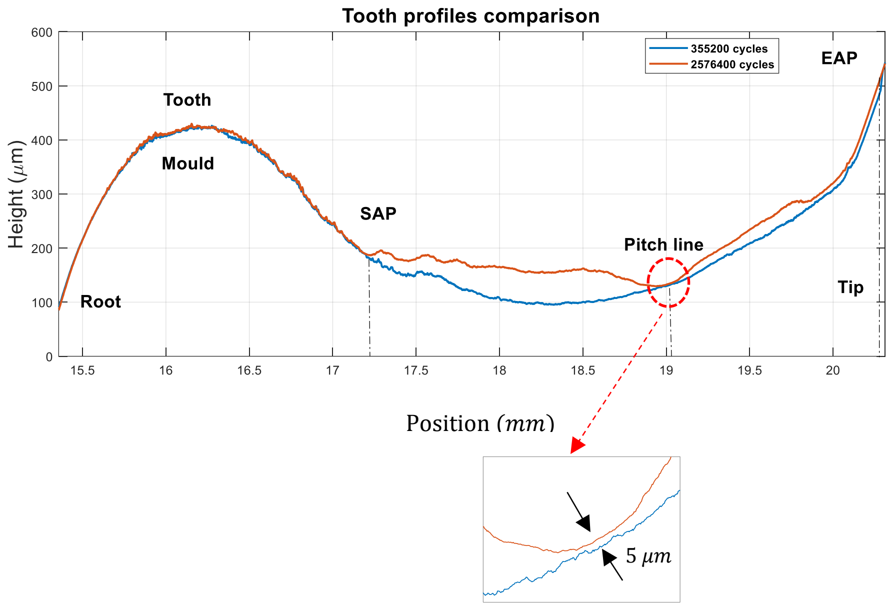

Figure 6.9 The tooth profiles of pinion (SAP: start of active profile, EAP: end of active profile)

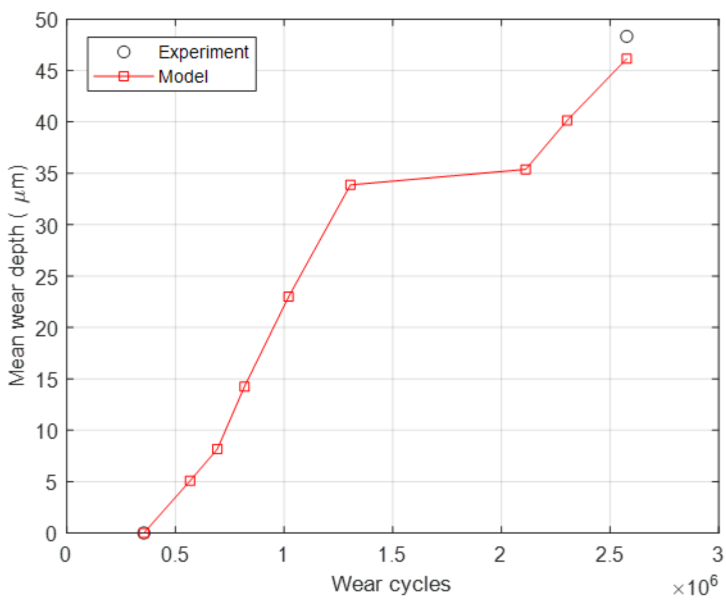

Figure 6.10 Wear depth comparison results of lubricated test: experiment (from moulding technique) and model (after updating)

6.4 Summary

The contribution of the work presented in this chapter is a novel vibration-based updating scheme is proposed to monitor and predict the gear wear process. Unique to previously published work, [21, 92, 184], comparison between simulated vibrations and measurements from the actual test rig is conducted regularly to update the model parameters if necessary. The updating procedure can track and correct for changes in wear rates, thus allowing analysts to obtain reliable wear predictions with relatively simple modelling tools. Also, different to the existing studies in gear-wear prediction, the newly developed wear prediction scheme was applied and validated on both lubricated and dry tests. Reliable and accurate prediction results of the tooth profile change are demonstrated. In addition, unlike Ref. [24], the updating procedure in the proposed scheme does not require gearbox stoppage or disassembly to obtain the wear particle mass. By utilising the advantage of the data acquisition system, the vibration signals can be easily acquired online without disturbing the operation, the proposed method can be applied when the gearbox system is in operating.

In addition, in the developed vibration updating scheme, an improved Archard wear model is also proposed to calculate the wear depth more realistically using the pressure distribution rather than the localised force on the gear surface. The improved Archard wear model implemented in this research includes consideration of the effect of Hertzian deformation, giving a contact area rather than a line, producing qualitatively more realistic and reliable wear induced tooth profile alteration behaviours results in comparison with the original approach used in the reference [21].

However, it should be mentioned that in the lubricated test, significant fatigue pitting propagation was observed, and the proposed vibration-based updating scheme does not have the capability to predict fatigue pitting propagation. Therefore, in the next chapter, Chapter 7, consideration is given to modifying the updating scheme to handle two wear mechanisms (abrasive wear and fatigue pitting) and their consequences on the gear tooth surface (tooth profile change and surface pitting).

Chapter 7 Development of a digital twin approach for monitoring and prediction of surface pitting and tooth profile changes

The work presented in this chapter is devoted to achieving objective 4 of this research: **development of a digital twin approach for monitoring and prediction of surface pitting and tooth profile changes**. This chapter is an improvement of the methodology presented in Chapter 6 by involving multiple wear phenomena: gear tooth profile change and surface pitting. This chapter is a modified version of the paper titled "*Vibration-based monitoring and prediction of surface profile change and pitting density in a spur gear wear process*", which was published in the journal of *Mechanical Systems and Signal Processing* (165: 108319, 2022). The main content of this chapter is identical to the above publication, while the structure of this chapter has been arranged to ensure the consistency of the thesis.

The organisation of this chapter is as follows: Section 7.1 briefly introduces essential background relevant to this study as well as the early work on monitoring and prediction of tooth profile change. Then Section 7.2 presents the relationship between vibration characteristics and wear features, and then vibration indicators for monitoring gear tooth profile change and surface pitting propagation are given. Section 7.3 introduces the proposed vibration-based surface degradation prediction methodology, including the dynamic and tribological models, and novel comparison analysis for model updating. To simulate the surface pitting propagation behaviours, a pitting propagation model is developed and introduced in Section 7.3. Section 7.4 demonstrates and verifies the effectiveness of the proposed surface degradation methodology for wear (gear tooth profile change and surface pitting) monitoring and prediction, with measurements from a laboratory gear rig. A summary of this study is presented in Section 7.5.

7.1 Introduction

In gear systems, wear induced gear tooth surface degradation is an inevitable phenomenon, and it can lead to destructive damage to the gear teeth and a significant reduction in the remaining useful life (RUL) of the gearbox [13, 185-187]. It is, therefore, necessary to monitor and predict the wear propagation process to ensure timely maintenance can be scheduled to avoid catastrophic failure. Tooth profile changes and surface pitting of gear teeth are two common processes during gear service life, and they have different impacts on the degradation rate and RUL of gear systems. During the gear wear process, tooth profile changes and surface pitting can occur simultaneously, and the two wear events can act together leading to a more rapid surface deterioration than if only one acted alone [81, 188-190]. Therefore, the development of an efficient and reliable tool for monitoring and predicting both gear tooth profile changes and surface pitting could bring enormous benefits to the industry.

Based on the literature review in Chapter 2, the Archard wear model [21, 61, 191] is widely used to estimate the wear depth of tooth surfaces. With the help of the Archard wear model, dynamic model and measured vibrations, the prediction of wear induced tooth profile change under dynamic conditions can be realised as presented in Chapter 6. As reviewed in Chapter 2, compared with research on the prediction of abrasive wear and associated tooth profile changes, studies on surface pitting propagation monitoring and prediction are sparser, although there are plenty of publications focusing on explaining the process of surface pitting initiation [76, 77, 192]. With help of the Archard wear model, Dang Van fatigue criterion [193-195] and Lundberg-Palmgren model [80, 196-198], attempts in the surface pitting propagation were made and the coupling effects between abrasion and pitting were investigated in Refs. [81] and [8]. Although promising surface pitting prediction results were demonstrated in these studies, it should be noted that neither study included calibration of the models using actual measurements to accommodate variations in the wear rate. In practice, the pitting propagation rate would be affected by a number of factors, such as lubrication quality and quantity, contact pressure distribution, sliding speed, surface roughness, all of which may change significantly – and so without frequent checking and, if necessary, updating of the wear model parameters, the accuracy of the prediction results cannot be guaranteed and is likely to decrease significantly during the surface pitting propagation.

In short, existing techniques do not have the capability to accurately predict the gear surface degradation, especially when the two wear phenomena (tooth profile change and surface pitting) co-exist. Therefore, it is necessary to develop a reliable and efficient tool, which can utilise the capability of both physics-based models and measurements for predicting both tooth profile change and surface pitting propagation.

A two-step approach is used to achieve the above goal. First, a method for monitoring and predicting the gear tooth profile change is proposed in this project as presented in Chapter 6. This methodology is based on the combination of an Archard wear model, a dynamic model and an updating scheme capable of frequently updating, as necessary, the Archard wear coefficient. By comparing simulated and measured vibrations, reliable predictions of abrasion-induced tooth profile changes were achieved through the proposed methodology. However, the methodology presented in Chapter 6 does not have the ability to monitor and predict surface pitting behaviours. Also, the root mean square (RMS) of the raw vibration signal was the feature used in the comparison analysis, and this could be easily affected by background noise or any number of unrelated machine changes, and could thus drastically reduce prediction accuracy and increase computation cost.

Built upon the work introduced in Chapter 6, a vibration-based methodology for monitoring and predicting both wear induced tooth profile change and surface pitting is then developed in this chapter.

7.2 Relationships of vibration features and wear features

In most applications, with constant or randomly varying speeds and loads, tooth profile change and surface pitting are distributed on all gear teeth uniformly, but the two wear events have different impacts on gear systems [19], and thus result in different vibration characteristics. Tooth profile changes generally cause an increase in the magnitude of gear mesh harmonics [13, 22], and so a suitable indicator for this phenomenon is the RMS of the signal obtained by synchronously averaging over the gearmesh period (giving a signal comprising only gearmesh harmonics), as shown in Eq. (7.1):

$$\mathrm{RMS}_{\mathrm{SA}} = \sqrt{\sum_{i=1}^{N} A_{GMi}^{2}} \tag{7.1}$$

where A_{GMi} is the amplitude of the ith gear mesh harmonic. The merits of using the time-synchronously averaged (TSA) vibration signal are as follows: 1) noise coming from the environment can be reduced significantly; 2) the average level of profile change of all gear teeth can be well indicated. It should be noted that well-lubricated gear systems usually exhibit relative smooth worn tooth profiles characterised by long-wavelength variations from the involute. For such mild wear cases, the first several gear mesh harmonics are sufficient to indicate the level of profile change. In contrast, the severely worn tooth profiles that are more often found in dry or poorly lubricated conditions are more complex, and therefore more gear mesh harmonics are required to properly reflect such profiles. This difference will be demonstrated with a lubricated test and a dry test in the results section.

As for surface pitting, it is fatigue-induced material loss, after which the effective working tooth profile (considered across the entire face width) often remains unchanged (unless pitting is extremely severe). Therefore, gear mesh harmonics often change negligibly during this process. To indicate the surface pitting propagation, ICS2, a measure of the degree of second-order cyclostationarity in a signal [37] and shown in Eq. (7.2), was investigated for tracking surface pitting propagation in Chapter 4, with consideration of the underlying physics of the gear meshing process:

$$\mathrm{ICS2}^{\mathcal{A}_\mathrm{h},\mathrm{H}} = \frac{\sum_{\mathrm{h}=1:\mathrm{H}} \max\limits_{\mathrm{n}\in\mathcal{A}_\mathrm{h}} (\mathrm{SES}[\mathrm{n}]^2)}{\mathrm{SES}[0]^2} \tag{7.2}$$

where h is the harmonic order of the gearmesh frequency, and $\mathcal{A}_h$ $(h = 1, 2, \ldots, \mathrm{H})$ represents the equivalent sets for the corresponding harmonics (with a tolerance band in the case of expected cyclic frequency deviations, to account for imperfect order tracking for example). SES is the (amplitude) spectrum of the squared envelope, obtained by amplitude demodulating the signal. A bandpass filtered version of the signal can be used to obtain the SES, giving an ICS2 enhanced by targeting not just the desired cyclic frequency(ies) but also the desired carrier frequency range(s). ICS2 obtained in this way has proven successful in difficult bearing diagnostic cases [199], and the experimental results presented in Chapter 4 demonstrate that ICS2 has an excellent performance in tracking surface pitting propagation when based on a low (carrier) frequency band. Therefore, in this study, ICS2 based on a low frequency band will be employed as the vibration feature to conduct the comparison analysis for surface pitting propagation monitoring and prediction (see details in Section 7.3).

7.3 Methodology for monitoring and predicting surface pitting and tooth profile change

In this section, the proposed vibration-based surface degradation monitoring and prediction methodology is presented. The details of the dynamic and tribological/wear models' development are provided, followed by the approaches of model updating using measured vibrations.

7.3.1 Structure of the proposed vibration-based surface degradation prediction methodology

Figure 7.1 shows the architecture of the proposed methodology. It consists of a dynamic model, wear models (Archard wear model and surface pitting model) and comparison analysis with measured vibrations for updating wear coefficients.

A dynamic model is established to simulate the actual spur gearbox. The dynamic model development has been introduced in Chapter 5, therefore, it will not be introduced in this chapter to avoid repetition. Based on the inputs of gear tooth profile geometry and operating conditions, the dynamic model can provide dynamic contact forces and simulated vibrations of the gear system. The contact pressure can then be calculated using the Hertzian contact theory. With the contact pressure as an input, the Archard wear model can estimate the abrasive wear rate and consequently predict the gear tooth profile geometry at a specified future point in time, and this is then fed back into the dynamic model. Meanwhile, the contact pressure is passed on to a surface pitting model to predict the surface pitting density, which consequently modifies the contact area and then alters the Hertzian contact pressure. Further information about the wear models can be found in Section 7.3.2. Both the profile change and surface pitting can affect the contact pressure, through modifying gear tooth profile geometry and contact area respectively, and therefore, there is an interaction between tooth profile change and surface pitting propagation.

In the proposed methodology, the contact pressure from the dynamic model is provided to the two wear models (Archard wear model and surface pitting model), and wear depth and surface pitting density are predicted simultaneously. In Figure 7.1, this part of the methodology is represented mostly in black, with the blue part indicating the updating of the contact area and tooth profile geometry, both of which can be conducted as often as required (without measurements).

In practice, there are many factors that can affect the dominant wear mechanisms and wear rate, such as the quality of lubrication and changes in the surface roughness and operating conditions. Therefore, using a constant wear coefficient K in each wear model could result in significant prediction errors. To guarantee accurate predictions, regular updating of the wear coefficients is implemented by comparing measured vibrations ($\mathrm{RMS_{SA}}$ and ICS2 in Section 7.2), when available, with the simulations. In this updating process, indicated in purple in Figure 7.1, the $\mathrm{RMS_{SA}}$ of the measured and simulated vibrations is compared directly. ICS2, on the other hand, is not compared directly; rather, ICS2 from the measurements is used to estimate pitting density, which is then compared with the simulation. This is because it is very difficult to accurately model the effect on vibration of fatigue pitting as it would require a very complex contact model and a much more detailed dynamic model to replicate vibration responses over the required frequency range.

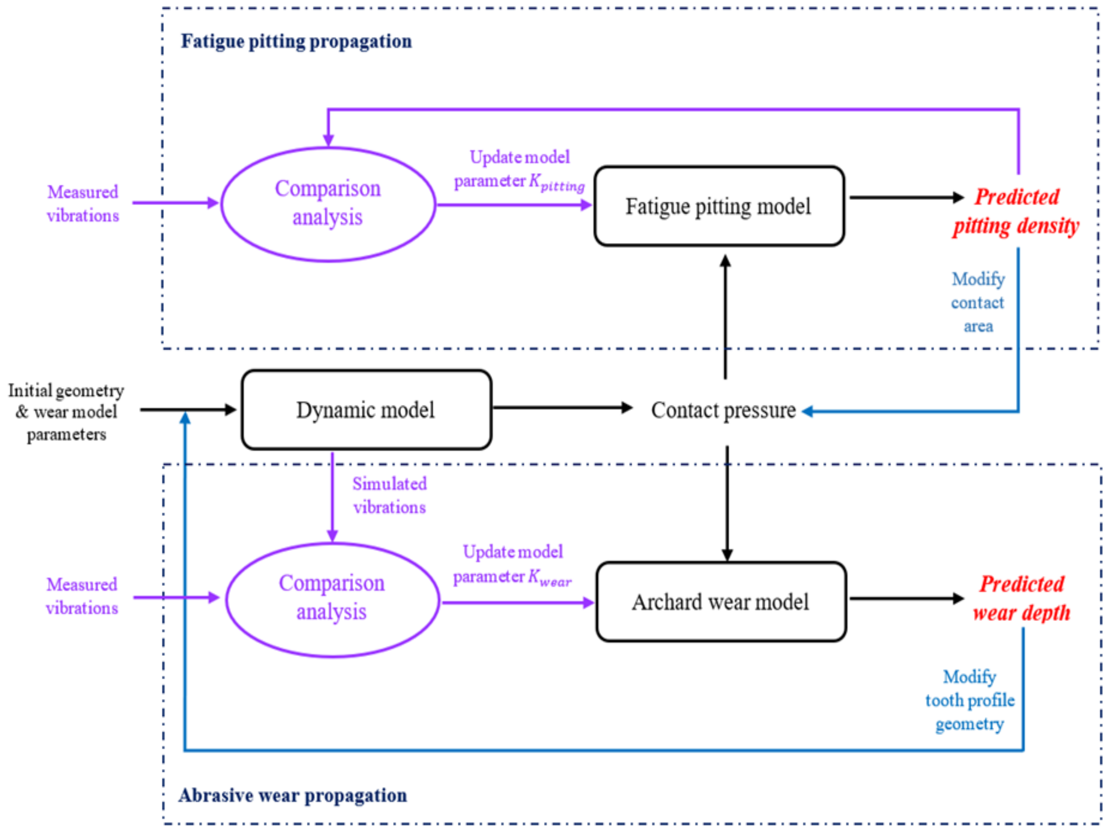

Figure 7.1 Basic procedure of vibration-based updating methodology for gear wear prediction

In summary, once the simulations start to drift away from actual measurements, two separate updating procedures are executed on the wear coefficients in the two models. The approaches for updating wear coefficients will be introduced in Section 7.3.3.

7.3.2 Wear models: modelling surface pitting behaviours

The Archard wear model and its improvement for simulating wear induced tooth profile change have been introduced in Chapter 6. Therefore, in this section, only the newly developed surface pitting model is introduced.

The Lundberg-Palmgren fatigue model (Eq. (7.3)) proposed in Ref. [80] is a commonly accepted theory for determining the fatigue life of rolling element bearings, with its advantages including excellent performance and high computational efficiency. It has also been applied to gear systems [200-202] to determine the gear RUL when surface pitting propagates. It can be expressed as

$$ln\frac{1}{S(N,\theta)}\sim\frac{\tau_0(\theta)^c N^m}{z_0(\theta)^h}V(\theta) \tag{7.3}$$

where $S(N,\theta)$ is the survival probability of the gear tooth at specific rotation angle θ after N running cycles, and c, m and h are the material coefficients, which are determined by gear material properties [27]. Some parameters are determined through Hertzian contact theory, like maximum shear stress τ_0, stressed volume V and depth of the maximum shear stress z_0 [27, 203, 204], defined as

$$\tau_0(\theta) = 0.3 \times P_{\max}(\theta) \tag{7.4}$$

$$z_0(\theta) = 0.786 \times b(\theta) \tag{7.5}$$

$$V(\theta) = 2b(\theta) \times z_0(\theta) \times 2\pi \times R(\theta) \tag{7.6}$$

where $P_{\max}$ is the maximum Hertzian contact pressure at the specific rotation angle θ, and, b and R are Hertzian contact radius and equivalent radius, respectively.

However, from the literature review in Chapter 2, it can be found that the model has not been developed for simulating pitting propagation behaviours. To address this issue, in recently published research [81], the level of surface pitting damage was assumed to be the reciprocal of S, and the distribution of fatigue pitting on the gear tooth was modelled, but its severity was not simulated or assessed. Inspired by this research, and furthermore considering that the range of S is $[0,1]$, we propose instead to approximate surface pitting density as:

$$D(N,\theta) \sim 1 - S(N,\theta) \tag{7.7}$$

With this assumption, the fatigue pitting propagation behaviour can be simulated and predicted. However, two issues remain with respect to Eq. (7.7):

1) The pitting propagation behaviour is determined by the initial contact stresses, and any changes in these stresses due to abrasive wear are not taken into account.
2) There is no feedback mechanism to account for the fact that prior pitting significantly affects the pitting propagation rate.

In practice, the pitting propagation rate would be affected by a number of factors, such as lubrication quality and quantity, contact pressure distribution, surface roughness and operating conditions, and the previous pitting density would indeed influence the rate and nature of further pitting propagation. To address these issues, K_{pitting}, the surface pitting coefficient, is introduced to update the surface pitting propagation rate based on actual measurements. The surface pitting propagation model in Eq. (7.7) is thus further developed into Eq. (7.8):

$$D(N,\theta) = 1 - \frac{1}{\exp\left(\frac{K_{\text{pitting}} \cdot \tau_0(\theta)^c \cdot N^m \cdot V(\theta)}{z_0(\theta)^h}\right)} \tag{7.8}$$

To realise the accumulated pitting propagation behaviour, the surface pitting propagation rate $D'(N,\theta)$ is calculated as follows:

$$D'(N,\theta) = \frac{dD(N,\theta)}{dN}$$
$$= \frac{K_{\text{pitting}} \times \tau_0(\theta)^c \times m \times V(\theta) \times N^{m-1} \times \exp\left(-\frac{K_{\text{pitting}} \times \tau_0(\theta)^c \times V(\theta) \times N^m}{z_0(\theta)^h}\right)}{z_0(\theta)^h} \quad (7.9)$$

The surface pitting increment ΔD during ΔN running cycles is shown in Eq. (7.10):

$$\Delta D(\Delta N,\theta) = \int_N^{N+\Delta N} D'(N,\theta)\, dN$$
$$= \exp\left(-\frac{K_{\text{pitting}} \times \tau_0(\theta)^c \times V(\theta) \times N^m}{z_0(\theta)^h}\right)$$
$$-\exp\left(-\frac{K_{\text{pitting}} \times \tau_0(\theta)^c \times V(\theta) \times (N+\Delta N)^m}{z_0(\theta)^h}\right) \quad (7.10)$$

The accumulated pitting density D_{i+1} at $N + \Delta N$ running cycles is

$$D_{i+1} = D_i + (\exp(-\frac{K_{\text{pitting}} \times \tau_0(\theta)^c \times V(\theta) \times N^m}{z_0(\theta)^h})$$
$$-\exp\left(-\frac{K_{\text{pitting}} \times \tau_0(\theta)^c \times V(\theta) \times (N+\Delta N)^m}{z_0(\theta)^h}\right) \quad (7.11)$$

where D_i is the pitting density at N running cycles. It should be noted that $\tau_0(\theta)$, $V(\theta)$ and $z_0(\theta)$ will be updated based on the pitting density D_i, which will be introduced below.

The surface pitting can reduce the actual contact length (B), and then affect further surface pitting propagation, which is defined in Eq. (7.12)

$$B(N_{i+1}) = B_{\text{initial}} \times \left(1 - D(N_i)\right) \quad (7.12)$$

where B_{initial} is the designed gear tooth width.

Then $\tau_0(N_{i+1})$, $V(N_{i+1})$ and $z_0(N_{i+1})$ will be calculated with previous pitting density $D(N_i)$ based on Hertzian theory, and the pitting density $D(N_{i+1})$ can be obtained.

With Equations (7.11) and (7.12), the accumulated pitting propagation process can be simulated. Using accumulated pitting density as in Equation (7.11), in which τ_0, V and z_0 are functions of the number of running cycles N, allows for the fact that existing pitting (and indeed any existing changes in the tooth profile from abrasive wear) would definitely promote and affect future pitting propagation. This feedback effect of both abrasive wear and fatigue pitting can be conducted without vibration measurements, and is shown in the blue parts of Figure 7.1.

7.3.3 Model updating procedures using measured vibrations

As introduced in the purple part of Figure 7.1, to deliver an accurate wear prediction result in the proposed methodology, measured vibration signals are used to determine whether any updating of the wear model coefficient *K* is required. The model updating procedures for gear tooth profile change and surface pitting propagation will be introduced in this section.

To determine whether the wear coefficient K_{wear} in Archard's model requires updating, the simulated and measured vibration signals are compared as introduced in Chapter 6. The updating methodology is executed iteratively when the absolute error between the simulated and experimental RMS_{SA} values exceeds the predefined 5% threshold, and the wear coefficient for the next iteration is calculated as follows:

$$K_{\text{wear}_{(j+1)}} = G_{(j)}^{-1} \cdot K_{\text{wear}_{(j)}} \tag{7.13}$$

where

$$G_{(j)} = RMS_{SA}\{y^{(\text{SIM},j)}(t)\}/RMS_{SA}\{y^{(\text{EXP},j)}(t)\} \tag{7.14}$$

in which, $y^{(\text{SIM})}(t)$ and $y^{(\text{EXP})}(t)$ are the simulated and experimental vibration signals. This iterative loop permits a knowledge-based monitoring and prediction of the tooth profile change. Note that the index *j* relating to running cycles here differs from *i* used in Equations (7.11) and (7.12). While *i* relates to the frequency of 'blue loop' updates (Figure 7.1) – the wear feedback effects contained entirely within the simulation model –

which can be executed as often as desired, j refers to the frequency of 'purple loop' updates, which are executed based on measurement availability.

Since pitting severity can be estimated based on instantaneous measurements, the pitting coefficient K_{pitting} can be periodically updated to account for changes in the pitting growth rate, which might be caused by lubrication contamination or surface contact temperature changes. In the following, the updating procedure will be introduced.

The ICS2 of measured vibrations in the low frequency region has been found to perform very well in tracking surface pitting propagation in Chapter 4; therefore, ICS2 is employed here as the vibration feature for the updating procedure. If the surface pitting model performs well, the predicted pitting density should also have a high correlation with ICS2. Otherwise, the surface pitting model parameter K_{pitting} should be updated to deliver improved pitting predictions. Note that although a good correlation between ICS2 (in the low frequency region) and pitting density (area) was found in Chapter 4, the 'scale factor' is still missing, meaning the actual pitting level cannot be reliably determined through measurements directly. At least one detailed inspection of the gear surface is therefore required to find this 'scale factor', which will be introduced in the updating procedure below.

In Chapter 4, the coefficient of determination R^2 is used to quantify the correlation between measured pitting density and ICS2 of measured vibrations, and a linear relationship was found. In the case of a single regressor, fitted by least squares, the coefficient of determination R^2 is the square of Pearson's correlation coefficient C [205]. Thanks to its clear analytical expression and simple computational procedure, Pearson's correlation coefficient [206] is used in this study to find the optimal K_{pitting}, ensuring the ICS2 of measured vibrations and predicted pitting density are well correlated.

The predicted pitting density array can be defined as $\mathbf{X} = [D_{j-1}, D_j, D_{j+1}]$ and measured ICS2 array as $\mathbf{Y} = [ICS_{j-1}, ICS2_j, ICS2_{j+1}]$. Taking $\bar{x} = \frac{D_{j-1}+D_j+ D_{j+1}}{3}$ and $\bar{y} = \frac{ICS_{j-1}+ICS2_j+ICS2_{j+1}}{3}$, the correlation coefficient C between **X** and **Y** is given by:

$$C = \frac{(D_{j-1} - \bar{x})(ICS2_{j-1} - \bar{y}) + (D_j - \bar{x})(ICS2_j - \bar{y}) + (D_{j+1} - \bar{x})(ICS2_{j+1} - \bar{y})}{\sqrt{(D_{j-1} - \bar{x})^2 + (D_j - \bar{x})^2 + (D_{j+1} - \bar{x})^2}\sqrt{(ICS2_{j-1} - \bar{y})^2 + (ICS2_j - \bar{y})^2 + (ICS2_{j+1} - \bar{y})^2}} \quad (7.15)$$

Now define correlation coefficient C as a function of K_{pitting}:

$$C(K_{\text{pitting}}) = f(K_{\text{pitting}}), K_{\text{pitting}} \in [0, +\infty) \quad (7.16)$$

If the surface pitting model needs to be updated due to changes in the pitting propagation rate, the updated $K_{\text{pitting}_{\textbf{updated}}}$ should maximise the correlation coefficient C, at which point the derivative of C should be 0:

$$C'\left(K_{\text{pitting}_{\textbf{updated}}}\right) = 0 \quad (7.17)$$

It should be noted that only three ICS2_j values and predicted surface pitting densities D_j are used to conduct the correlation analysis, which ensures the correlation coefficient C is highly sensitive to changes in the pitting growth rate so that the optimal pitting coefficient K_{pitting} can be obtained.

The detailed updating procedure for K_{pitting} is summarised as follows:

Step 1: measure ICS2 to identify the specific pitting occurrence time and define it as $j = 0$. Note: after the run-in period, the propagation of surface pitting should lead to an increase in ICS2 of measured vibrations as presented in Chapter 4;

Step 2: use mould image [128] if possible (or visual inspection) to obtain the actual pitted density: $D_{\text{actual}}(N_0)$ and $D_{\text{actual}}(N_1)$;

Step 3: procedures to determine the simulated pitting density $D(N_2)$ and predict pitting density $D(N_3)$ are as follows:

1) Build vibration reference $[ICS2_0, ICS2_1, ICS2_2]$;
2) Use surface pitting model to obtain the simulated pitting density $D(N_2)$ with an initial pitting coefficient $K_{\text{pitting}}(2)$;
3) If the Pearson's correlation coefficient C between $[ICS2_0, ICS2_1, ICS2_2]$ and $[D_{\text{actual}}(N_0), D_{\text{actual}}(N_1), D(N_2)]$ is greater than 0.95, it means the surface pitting model at time $j = 2$ performs well, and so $K_{\text{pitting}}(3) = K_{\text{pitting}}(2)$ can be used to predict surface pitting density $D(N_3)$ at time $j = 3$;
4) If the Pearson's correlation coefficient C between $[ICS2_0, ICS2_1, ICS2_2]$ and $[D_{\text{actual}}(N_0), D_{\text{actual}}(N_1), D(N_2)]$ is less than 0.95, it means the simulated surface pitting density $D(N_2)$ is not correct, and the surface pitting coefficient needs to be updated to obtain $K_{\text{pitting}}(2)$.

With the above-mentioned updating approach (see Eq. (7.17)), the optimal $K_{\text{pitting}}(2)$ can be determined (then obtain updated $D(N_2)$), which produces a strong correlation between $[ICS2_0, ICS2_1, ICS2_2]$ and $[D_{actual}(N_0), D_{actual}(N_1), D(N_2)]$. After that, set $K_{\text{pitting}}(3) = K_{\text{pitting}}(2)_{\textbf{updated}}$ to predict pitting density $D(N_3)$ at time $j = 3$;

Step 4: Repeat the above-mentioned process. At time j, current surface pitting coefficient $K_{\text{pitting}}(j) = K_{\text{pitting}}(j-1)$, and the predicted pitting density is $D(N_j)$. If the correlation coefficient C between $[D(N_{j-2}), D(N_{j-1}), D(N_j)]$ and $[ICS2_{j-2}, ICS2_{j-1}, ICS2_j]$ is greater than 0.95, it means the current predicted pitting density $D(N_j)$ is correct. And then set $K_{\text{pitting}}(j+1) = K_{\text{pitting}}(j)$ to predict the pitting density $D(N_{j+1})$ at time $j+1$.

Otherwise, the above-mentioned updating approach (see Eq. (7.17)) is used to obtain the updated pitting coefficient $K_{\text{pitting}}(j)_{\mathbf{updated}}$ and the corresponding new predicted pitting density $D(N_j)$. After that, set $K_{\text{pitting}}(j+1) = K_{\text{pitting}}(j)_{\mathbf{updated}}$ to predict the surface pitting density at time $j+1$.

Note that after attempts to update, the 95% threshold for the correlation coefficient between measured ICS2 and predicted surface pitting density cannot be achieved, $K_{\text{pitting}}(j)$ and $K_{\text{pitting}}(j+k)$ will be set to 0. This condition would likely be caused by a reduction in ICS2, but the proposed pitting model assumes ever-increasing pitting density. In reality, when surface pitting density starts to decrease, it means the gear should be replaced due to the presence of severe surface pitting [207]. This will be demonstrated in the results in Section 7.4.1.

7.4 Test and Results

Two run-to-failure experiments were conducted under different lubrication conditions (lubricated and dry test) to demonstrate and verify the effectiveness of the proposed methodology in wear prediction.

The details of test programs and experimental data collection have been presented in Chapter 3, therefore, these two tests will not be introduced in this chapter to avoid repetition.

7.4.1 Monitoring and prediction of surface pitting and mild tooth profile change during the lubricated test

Two wear events presented in the lubricated test: surface pitting propagation and mild abrasive wear, leading to modest gear tooth profile changes. This allows for testing of the proposed method on both wear types using the same dataset. The collected moulds during the tests were imaged using a laser scanning confocal microscope (LSCM). The tooth profile change (see Figure 7.2 and Figure 7.3) and the actual pitting density (see Figure 7.4) were then quantified using the images and used as references to check the monitoring and prediction results [128]. Note that both the tooth profile change and pitting density in Figure 7.2, Figure 7.3 and Figure 7.4 are obtained from the pinion's mould images. The combined tooth profile change can be calculated based on the gear ratio (the pinion's profile change accounts for 73% of the combined tooth profile change). As for the surface pitting propagation, much less pitting was observed on the driven gear surface, and the occurrence of pitting on the driven gear was greatly delayed. Thus, the total pitting density of the gear pair can be represented by the pinion's pitting density. The measured pitting density will be used to check the effectiveness of the proposed method in surface pitting propagation monitoring and prediction. A run-in period took place from 0 to 0.12 million cycles, during which the roughening marks were worn away. From Figure 7.4, it can be found that surface pitting started to propagate from 0.12 million cycles, and the pitting density mainly kept increasing until 2.12 million cycles. From 2.12 million cycles to 3.25 million cycles, the pitting density started to decrease. It appears that in this period the generation of new pits was outweighed by the filling-in of existing cavities, perhaps from wear debris pressed into the cavities under the meshing load [142].

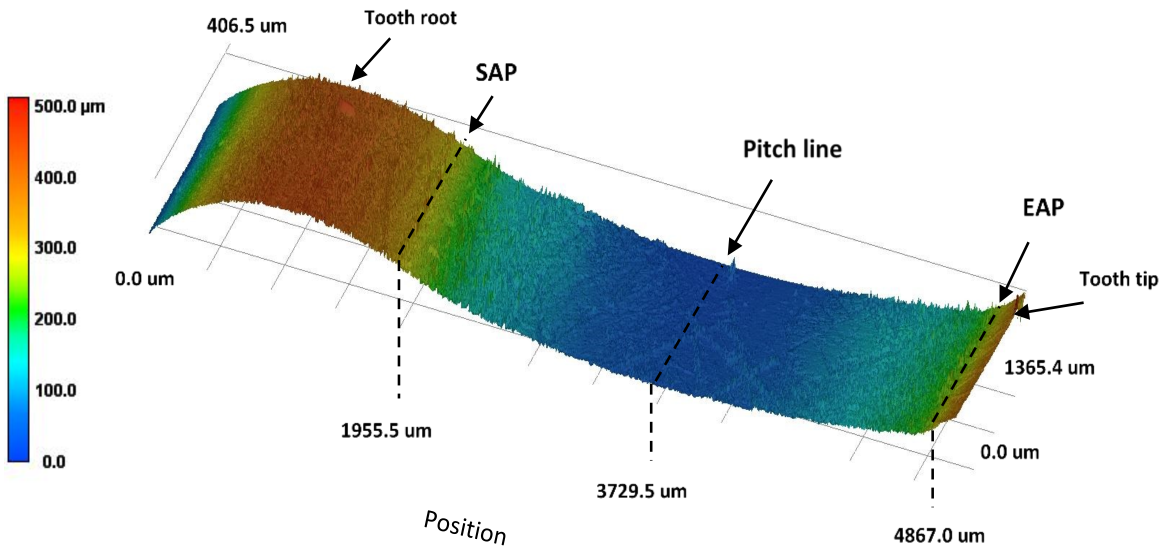

Figure 7.2 3D image of the mould profile collected from pinion at 0.35 million cycles (SAP: start of active profile, EAP: end of active profile) during the lubricated test

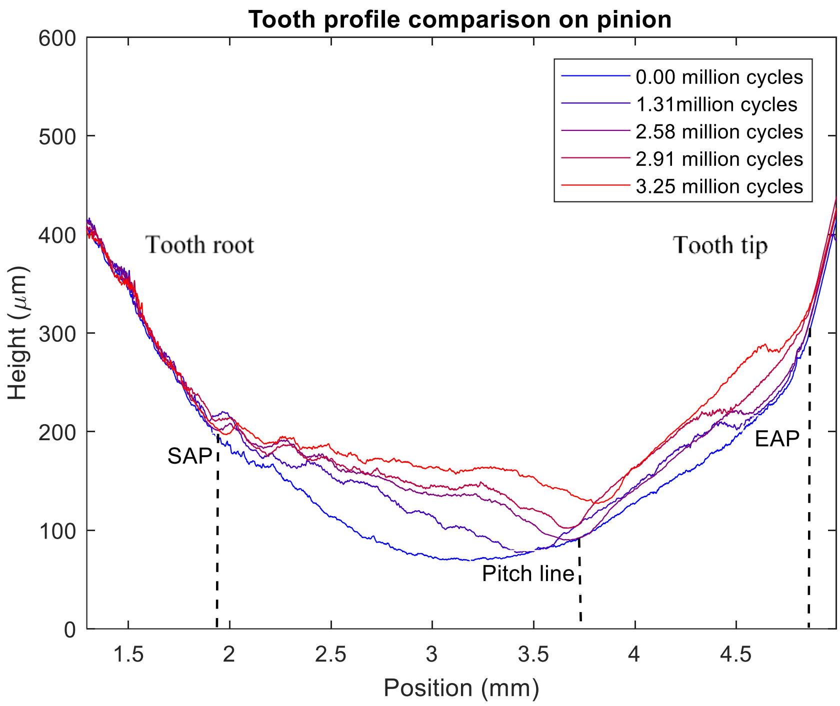

Figure 7.3 Lubricated test: The average profiles of pinion at different running cycles (see the locations of SAP and EAP in Figure 7.2)

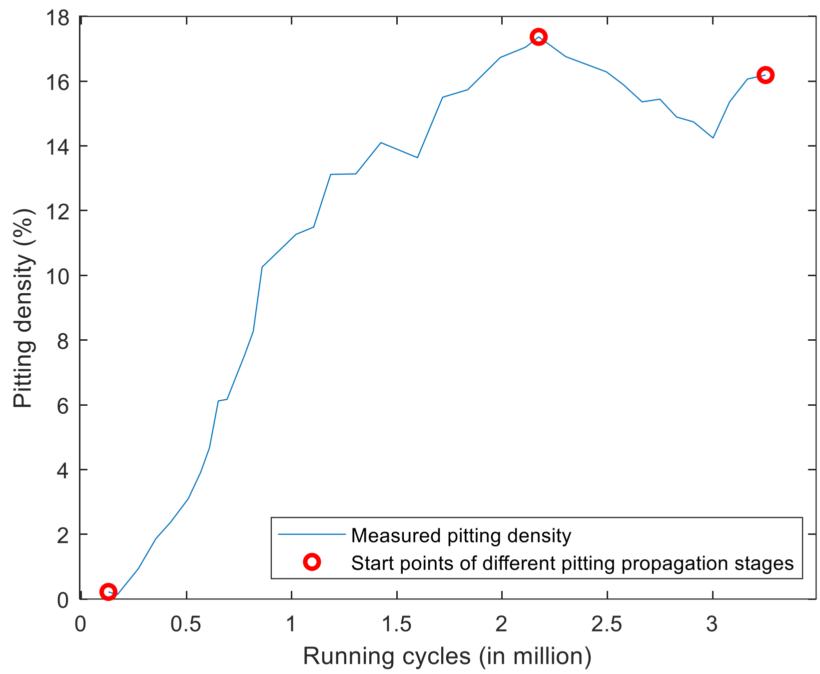

Figure 7.4 Lubricated test: Pitting density of pinion obtained from moulds: red dots represent: 0.12 million cycles, when surface pitting was detected; 2.12 million cycles, the point of maximum pitting density; and 3.25 million cycles, the end of the test

<u>Monitoring and prediction of change in tooth profile</u>

This sub-section investigates the application and performance of the proposed methodology in monitoring and predicting wear induced tooth profile changes. First, to determine the best vibration feature for tracking mild profile changes under lubricated conditions, the number of gear mesh harmonics included in RMS_{SA} (Eq. (7.1)) is investigated. Then, with the help of the selected wear-relevant vibration feature, the profile change monitoring and prediction results are presented and compared with the actual measurements.

Due to the continual lubrication provided by the oil bath, this test was characterised by a low wear rate and a relatively smooth worn tooth profile, as shown in Figure 7.3. Gear teeth with different profile shapes can affect different gear mesh harmonics directly [25], and here the required number of harmonics to sufficiently represent the profile change is investigated. Figure 7.5 shows the change in gear mesh harmonics of measured vibrations throughout the test. It shows that the first two harmonics change more significantly than the others. To determine the optimal number of harmonics to be used, correlation analysis between the vibration indicator RMS_{SA} and the wear depth (calculated based on mould images shown in Figure 7.3) with different numbers of gear mesh harmonics included (see Eq. (7.1)) was conducted. More specifically, the Pearson correlation coefficient is used to quantify the similarity between the two variables: RMS_{SA} and wear depth. The results show that tooth profile change can be represented with the first two gear mesh harmonics, and Figure 7.6 demonstrates a strong relationship between RMS_{SA} $(N = 2)$ of measured vibration and wear depth. Therefore, in this study, RMS_{SA} $(N = 2)$ will be used as the vibration feature to be compared with measured vibrations for the monitoring and prediction of tooth profile changes in the lubricated test.

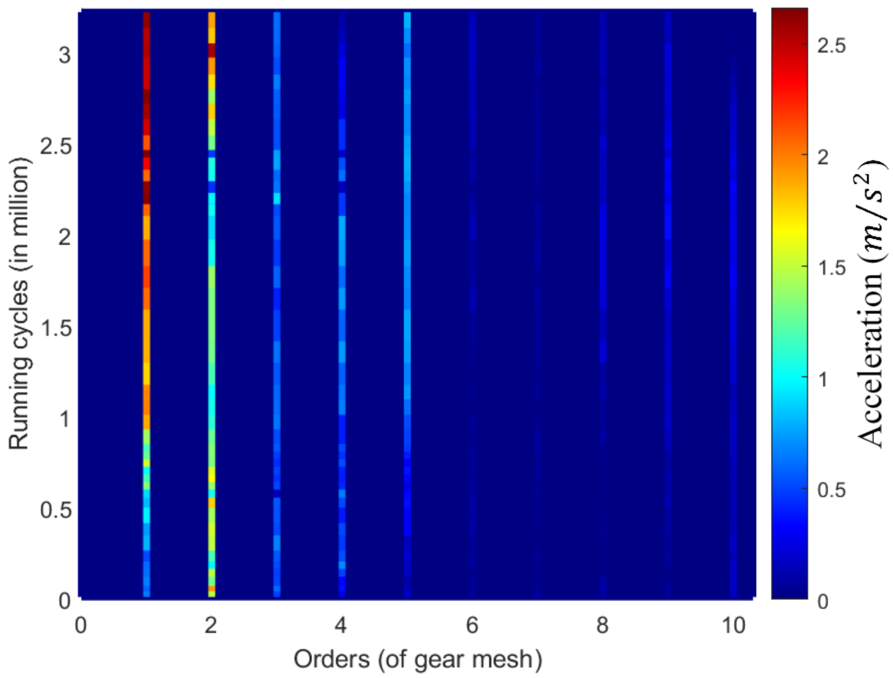

Figure 7.5 Changes in gear mesh harmonics of measured vibrations during the lubricated test (the first ten gear mesh harmonics)

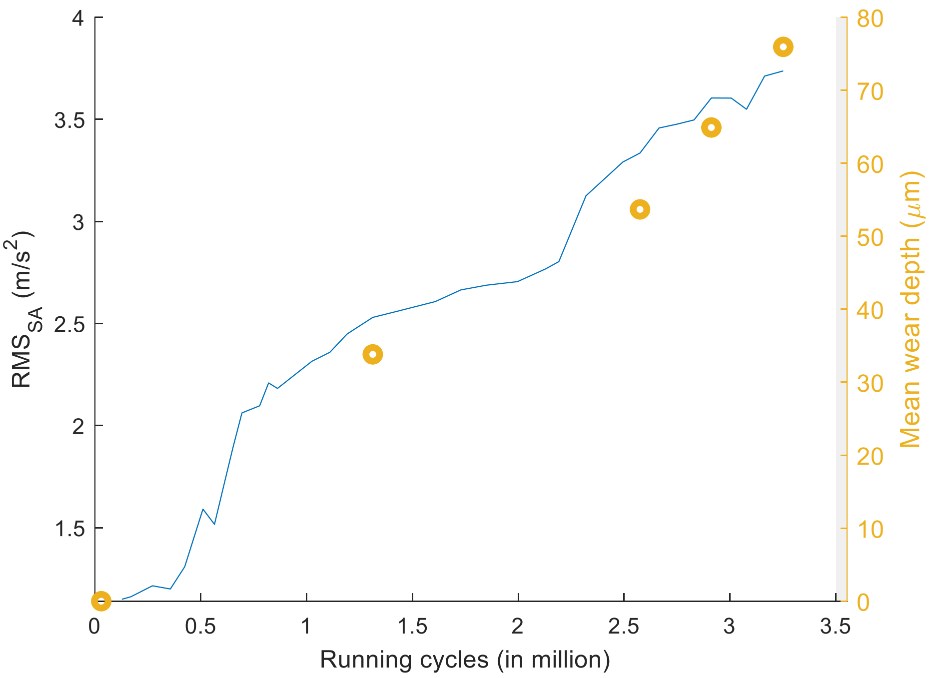

Figure 7.6 Lubricated test: RMS_{SA} ($N = 2$) of measured vibrations and wear depth change obtained from mould images as shown in Figure 7.3

For comparison purposes, the relationship between RMS_{SA} ($N = 2$) of measured vibration and measured pitting density also presented in Figure 7.7. From Figure 7.7, it can be found that there is a poor relationship between RMS_{SA} ($N = 2$) and measured pitting density. Therefore, ICS2 will be used as the vibration feature in the proposed method to help monitor and predict the pitting propagation, which will be introduced in this section later.

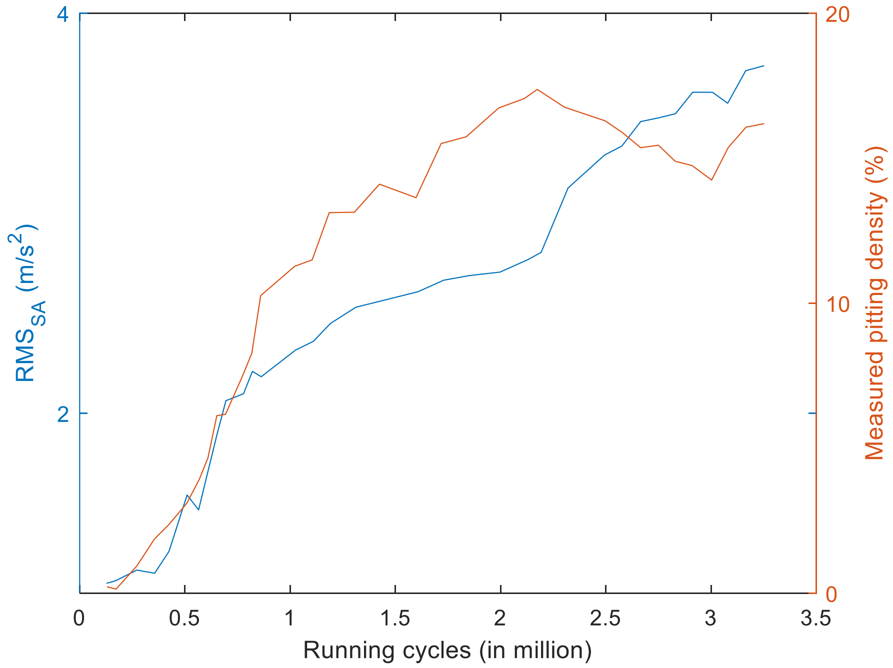

Figure 7.7 Lubricated test: $\mathrm{RMS_{SA}}$ ($\mathrm{N} = 2$) of measured vibrations and measured pitting density as shown in Figure 7.4

As introduced in Chapter 5, with the help of measured vibrations, the dynamic model was first calibrated at 0.12 million cycles (after the run-in period) to guarantee the simulated vibration signal and contact forces are sufficiently close to those of the actual test rig. Then, the initial wear coefficient K_{wear} in the Archard wear model was calibrated to be $3.55 \times 10^{-10}\mathrm{Pa}^{-1}$, with the help of the measured vibration signal at 0.27 million cycles. This wear coefficient calibration step can be recognised as the execution of the first updating of the wear coefficient K_{wear}.

In the further wear propagation process, because the error between the $\mathrm{RMS_{SA}}$ value of the simulated and that of the measured vibration signals exceeds the predefined 5% threshold, three more updates of K_{wear} were executed, at 0.57, 1.43 and 2.19 million cycles. The updated wear coefficients are 4.03×10^{-10}, 1.44×10^{-10} and $3.97 \times 10^{-10}\mathrm{Pa}^{-1}$, respectively. The relationship between measured $\mathrm{RMS_{SA}}$ and simulated $\mathrm{RMS_{SA}}$ is given in Figure 7.8, showing that the error between them remains within 5.0%

after necessary updating of the wear coefficient. The tooth profile change monitoring and prediction results are plotted in Figure 7.9, illustrating that the maximum error between predicted and measured wear depth is 4.7 %. The specific points when updates were executed are indicated using grey dashed lines in Figure 7.9. The tooth profile change is therefore well monitored and predicted using the proposed methodology.

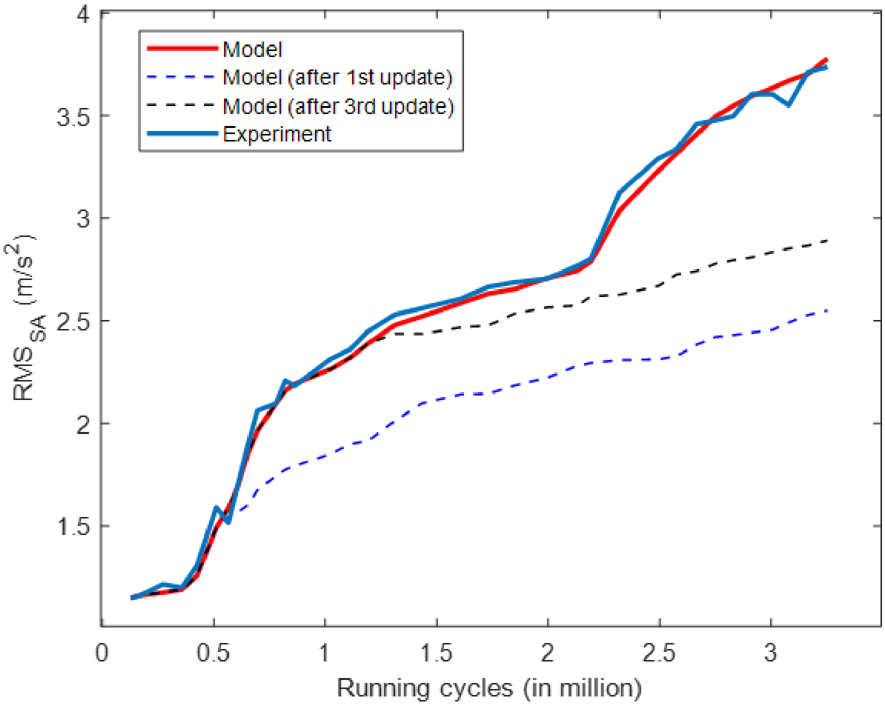

Figure 7.8 RMS_{SA} (N=2) comparison results of the lubricated test: experiment and model

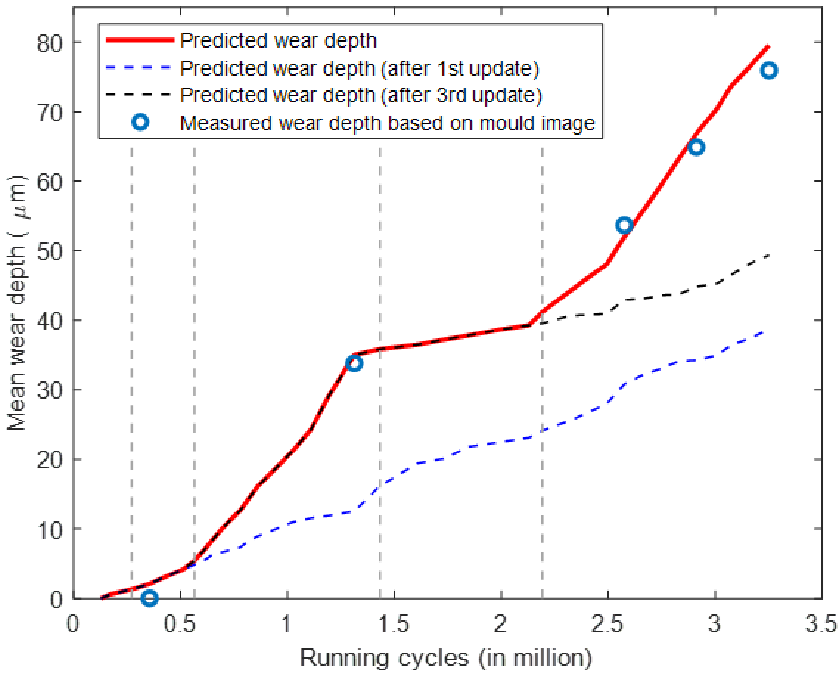

Figure 7.9 Mean wear depth comparison results of the lubricated test: experiment and model. Note: grey dashed lines indicate when updates are executed

Note that there are two wear rate changes observed in Figure 7.9. Possible explanations for these changes are as follows. The manufacturing marks on the driven gear have been significantly removed during [1.41~2.12] million cycles. The same phenomenon was observed in Ref. [128]. Thus, a plateau wear rate occurs during this period. After 2.12 million cycles, the involute profile of the gear tooth becomes flat, and the contact area of engaging tooth pairs increased. As a result, the tooth profile change rate might increase significantly [208].

The monitoring and prediction results with several limited wear coefficient updates (not all necessary updates) are also demonstrated in Figure 7.9, i.e., the first and third updates of K_{wear}. It can be seen that the abrasive wear rate changed significantly during the lubricated test, and that if the wear coefficient were not able to be updated it would lead to very large errors in wear depth prediction. In general, with more wear coefficient updates, increasingly accurate prediction results can be achieved. Therefore, to guarantee accurate wear prediction results, regular comparisons with measurements and (where required) updates to the wear coefficient are recommended.

Surface pitting propagation monitoring and prediction

Based on observations during the lubricated test, the surface pitting initiates at the dedendum of the gear tooth, and then propagates to the pitch line and finally to the addendum, as shown in Figure 7.10. In the proposed methodology, with the dynamic contact force outputted from the dynamic model, the pitting propagation behaviour can be simulated using the developed surface pitting model, as shown in Figure 7.11. From Figure 7.11, it can be seen that according to the developed model, the surface pitting also initiates at the gear tooth root and then propagates to the pitch line. The trends shown in Figure 7.11 match the actual pitting propagation trends shown in Figure 7.10, suggesting the developed surface pitting model has the ability to simulate accurately the surface pitting propagation behaviour. Note that the dynamic force has several spikes, it is caused by the resonances of the gear system and a similar phenomenon was observed in Ref. [171]. More explanations on this phenomenon can refer to Section 5.3.

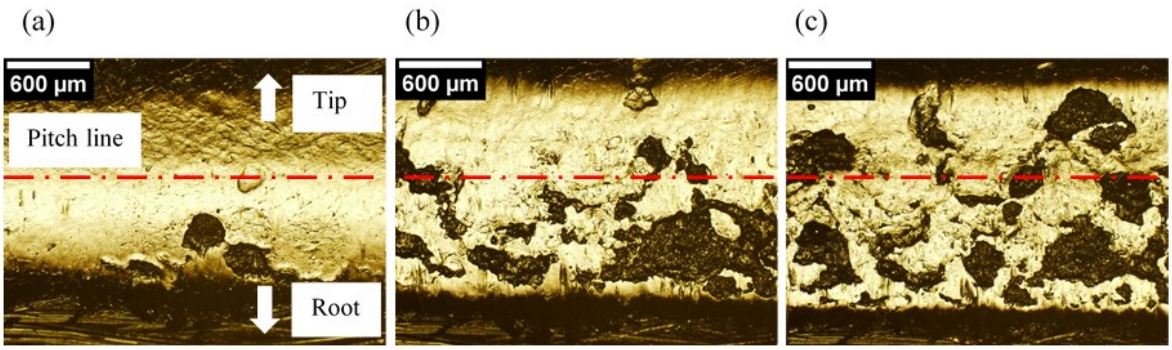

Figure 7.10 Lubricated test: Optical images of pinion tooth surfaces taken from moulds by optical microscope with a 5× magnification objective lens. Image size: 2.8mm ×2.11 mm (a) 0.1296 million cycles, (b) 0.8178 million cycles, (c) 1.7175 million cycles [142]

Using the developed surface pitting model and the proposed wear monitoring methodology, the surface pitting propagation can be monitored and predicted. The relationship between predicted pitting density and ICS2 is shown in Figure 7.12. It can be seen that the ICS2 of measured vibration correlates well with the predicted pitting density (after the run-in period, from 0.12 million cycles to 2.00 million cycles). The magnitude of surface pitting coefficient K_{pitting} is first calibrated to be 5.64×10^{-15} using the mould images captured at 0.12 and 0.27 million cycles. This calibration of K_{pitting} can be recognised as the first update.

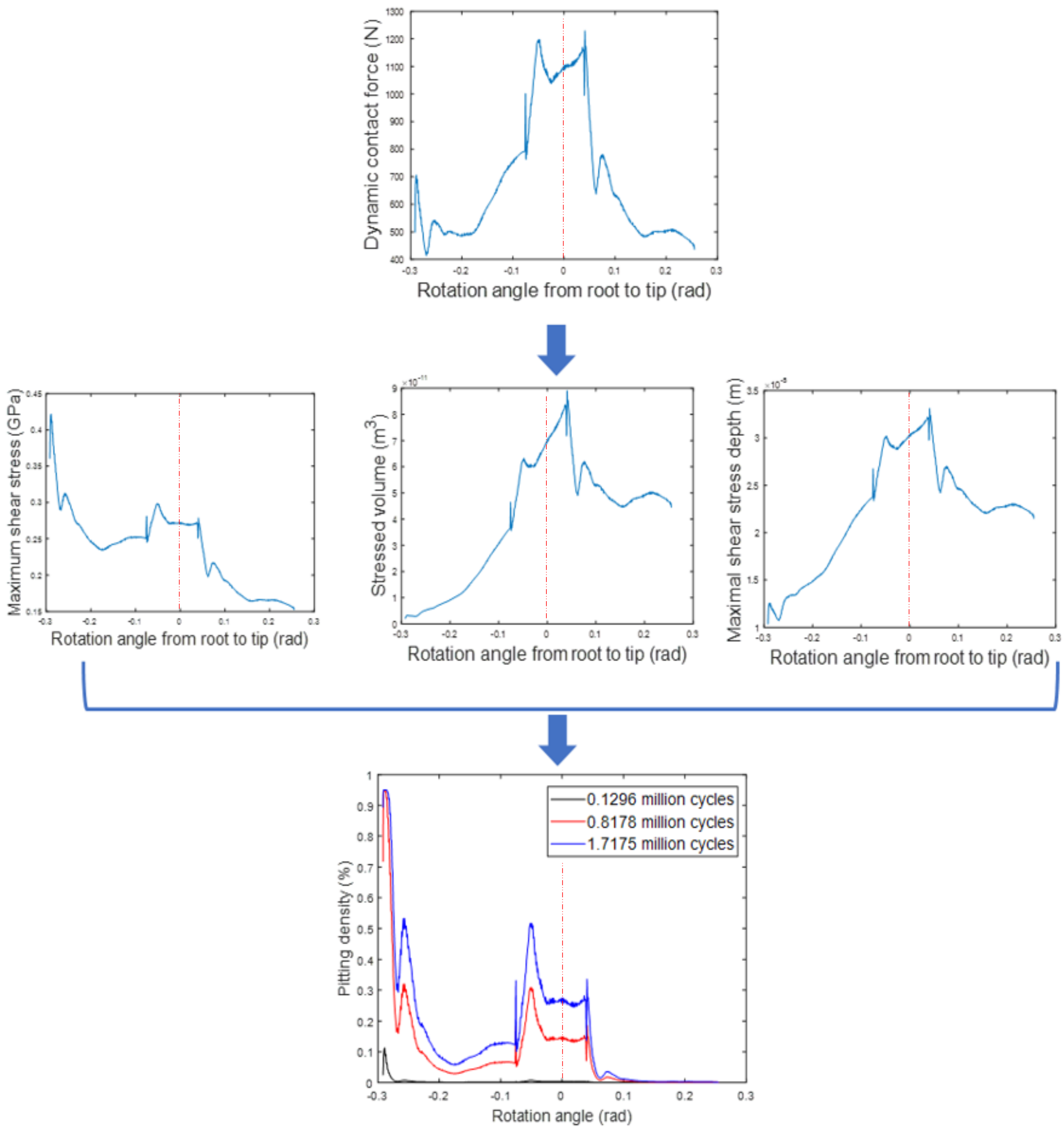

Figure 7.11 Diagram of pitting density calculation using surface pitting model: pitch line is at 0 rad and indicated by red vertical dash line

During the further pitting propagation process, six more updates of $K_{pitting}$ were executed, prompted by Pearson's correlation coefficient C between measured ICS2 and predicted pitting density falling below the predefined 95% threshold. These updates were at 0.51, 0.56, 1.02, 1.11, 1.97 and 2.12 million cycles, respectively. The final update at 2.12 million cycles sets K_{pitting} to 0 because the 95% threshold for C cannot be achieved. Figure 7.13 shows the pitting prediction results compared with the actual measured pitting densities using mould images. From the comparison, it can be seen that the surface pitting propagation is very well monitored and predicted after all necessary updating (before 2.00 million cycles).

Note that from 2.00 million cycles to 3.25 million cycles, the measured pitting density decreased slightly. The tooth profile started to change rapidly in this period, caused by increased abrasive wear. Because the developed surface pitting model is designed to represent accumulated pitting behaviour on the assumption that pitting density cannot decrease, therefore, the stabilisation stage (2.00 million cycles to 3.25 million cycles) was not simulated and predicted in this study. During this stage, the pitting coefficient is set to 0 automatically, and the predicted surface pitting density remains a constant value. Moreover, at 2.00 million cycles the pitting density is already 17.4%, and according to the ASM Handbook [207], the gear should be scrapped, and could thus be considered already to have failed. That is, the proposed method delivers excellent pitting prediction results over the most meaningful phase of the gear's degradation, from 0.12–2.00 million cycles.

Figure 7.13 shows the prediction results if only earlier updates of the pitting coefficient, the first and the fourth, were used. Here it turns out that the 'point of failure' (~2 million cycles) is in fact better predicted using the fourth update of K_{pitting} than the first, and a more accurate prediction result can be expected with more updates.

Note that in the proposed methodology, the tooth profile is continually updated through the improved Archard wear model (introduced in Chapter 6) to provide updated contact pressure to the surface pitting model, which is used for predicting pitting propagation. In turn, the occurrence of surface pitting affects the effective contact width, resulting in a change in the contact pressure. This is a two-way relationship between surface pitting propagation and tooth profile change. The comparison analysis between measurements and simulations can guarantee accurate tooth profile change prediction and surface pitting propagation prediction results, as shown in Figure 7.9 and Figure 7.13.

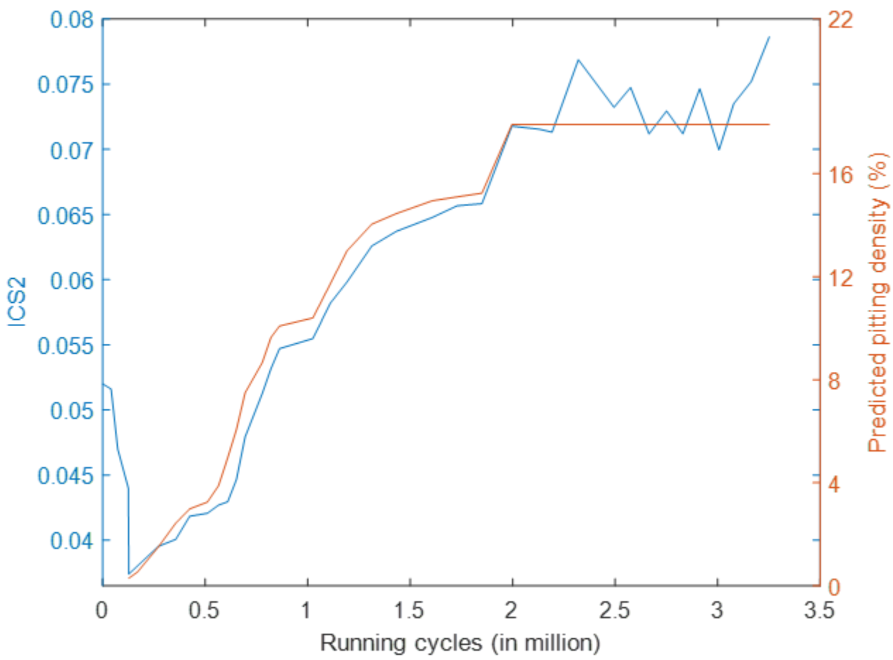

Figure 7.12 Comparison results: ICS2 of measured vibration and predicted pitting density based on model (after updating)

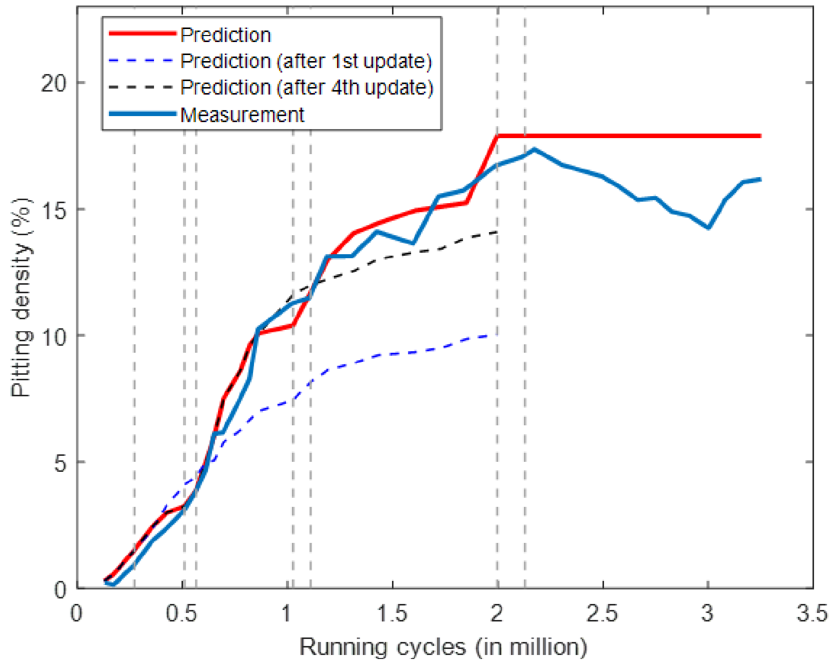

Figure 7.13 Pitting density comparison results: experiment and model-based prediction. Note: grey dashed lines indicate when updates are executed

7.4.2 Monitoring and prediction of severe tooth profile change during the dry test

Compared with the lubricated test, the dry test represents an extreme case, with severe abrasive wear and a correspondingly large change in the tooth profile, but very little surface pitting propagation (as demonstrated in Figure 7.14). The proposed approach is however still effective under dry conditions, as will be demonstrated in this section.

As with the lubricated test, this section first investigates the number of gear mesh harmonics required in the vibration feature to accurately track the severe tooth profile changes. Figure 7.15 shows the evolution in the amplitudes of measured acceleration signal of the first 10 gear mesh harmonics during the test, from which it can be seen that the first six harmonics change significantly. To find the required number of harmonics for tracking profile changes in this test, correlation analysis between the wear depth (calculated based on the weight of collected wear particles) and the vibration indicator RMS_{SA} with different numbers of gear mesh harmonics (absolute values) was conducted.

The results show that severe tooth profile changes can be represented with the first six-gear mesh harmonics, and Figure 7.15 demonstrates this by showing the strong relationship between measured RMS_{SA} $(N = 6)$ and measured wear depth based on collected wear particles. Therefore, for this test, RMS_{SA} $(N = 6)$ was used as the vibration feature to compare the measured and simulated vibrations for tooth profile change monitoring and prediction. Compared with the lubricated test, severer tooth profile change occurs during the dry test, therefore, more gear mesh harmonics (the first six) are required to represent the worn tooth profile, while, only the first two gear mesh harmonics are required to represent the tooth profile change during lubricated tests. This phenomenon also has been discussed in Section 7.2.

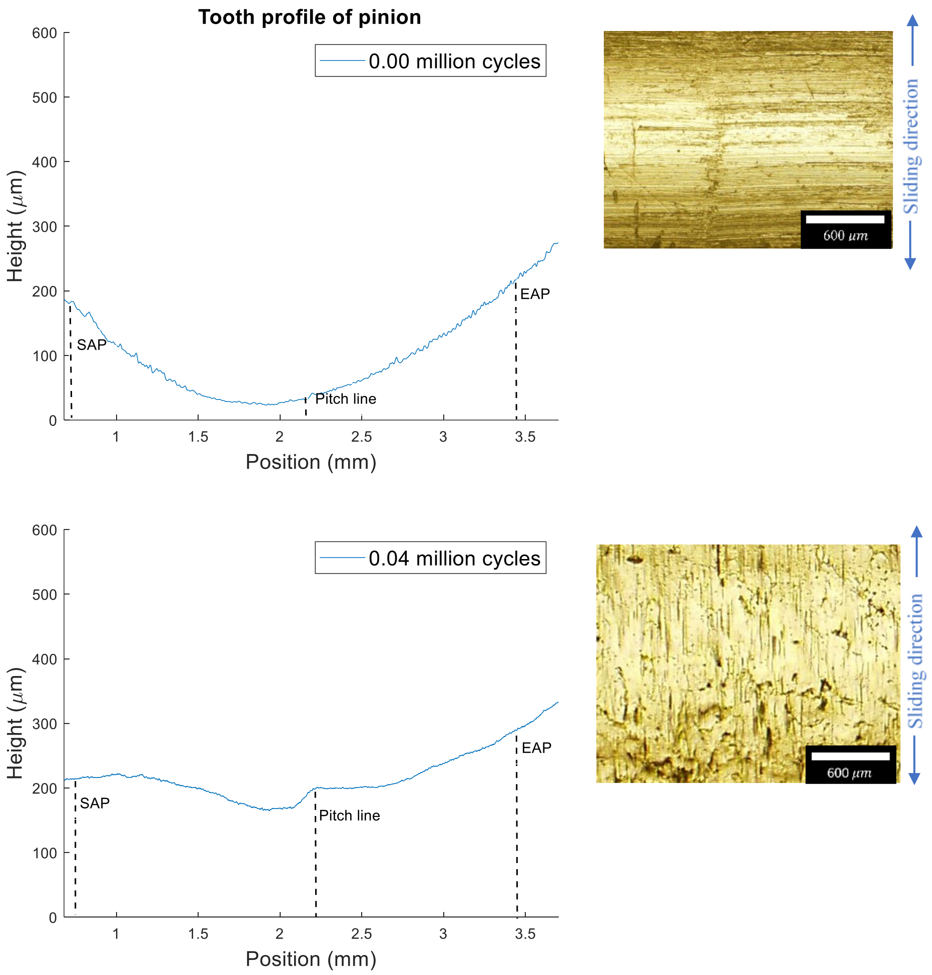

Figure 7.14 Gear tooth profile and surface morphology of the dry test at 0 and 0.04 million cycles (SAP: start of active profile, EAP: end of active profile)

The Archard wear model parameter K_{wear} can be updated (if necessary) with the procedure discussed in Section 7.3.3 at each measured time. The trends of RMS_{SA} and mean wear depth vs wear cycles (rotations of the pinion) are plotted in Figure 7.17 and Figure 7.18, respectively. Two updates were executed during the short dry test, when the error between the RMS_{SA} value of the simulated and measured vibration signals exceeded the predefined 5% threshold. With the help of measured vibration at 0.007 million running cycles, the wear model parameter was found/calibrated to be $1.65 \times 10^{-6}\text{Pa}^{-1}$, and the predicted mean wear depth was estimated at 12.92 μm. This calibration can be considered the first update. After that, the simulated RMS_{SA} and estimated wear depth match well with experiments until the second update was triggered at 0.025 million cycles, and the wear model parameter K_{wear} was updated to $2.19 \times 10^{-6}\text{Pa}^{-1}$, after which the wear model gives good prediction results for the remainder of the test. From Figure 7.17, it can be found that the maximum error between predicted wear depth and measured wear depth is 4.5%. Therefore, with a vibration feature based on gear mesh harmonics combined with an improved Archard model, the proposed surface degradation monitoring and prediction methodology has an excellent performance in tracking and predicting the tooth profile change (in terms of wear depth) under dry conditions.

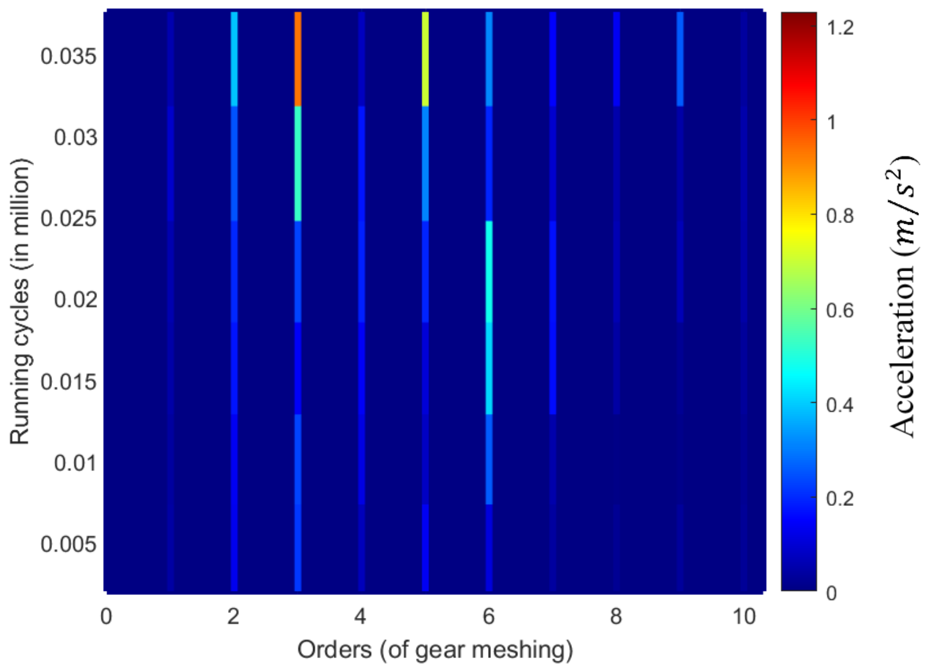

Figure 7.15 Changes in gear mesh harmonics during the dry test (the first ten gear mesh harmonics)

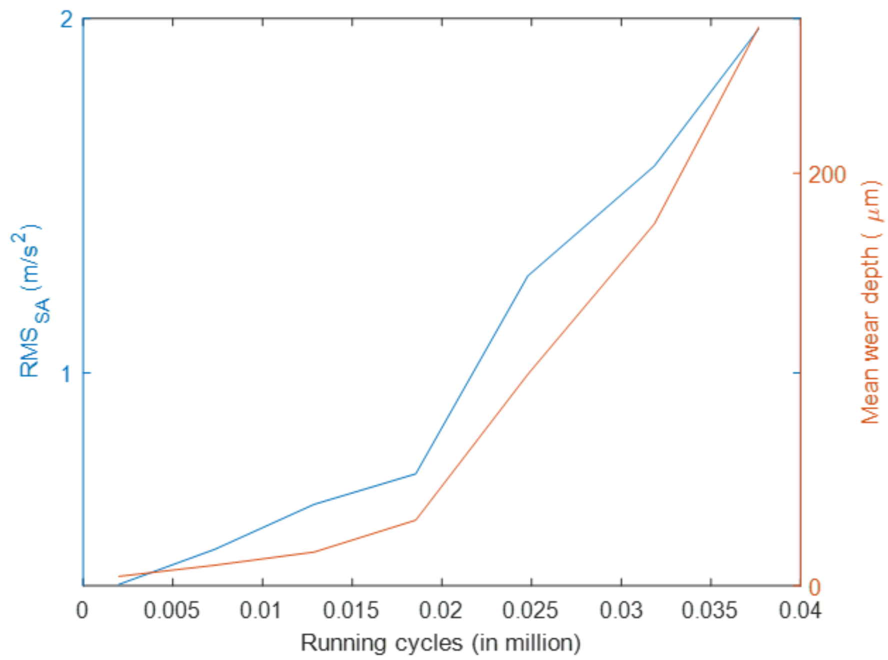

Figure 7.16 Dry test: measured RMS_{SA} ($N = 6$) and measured wear depth based on collected wear particles

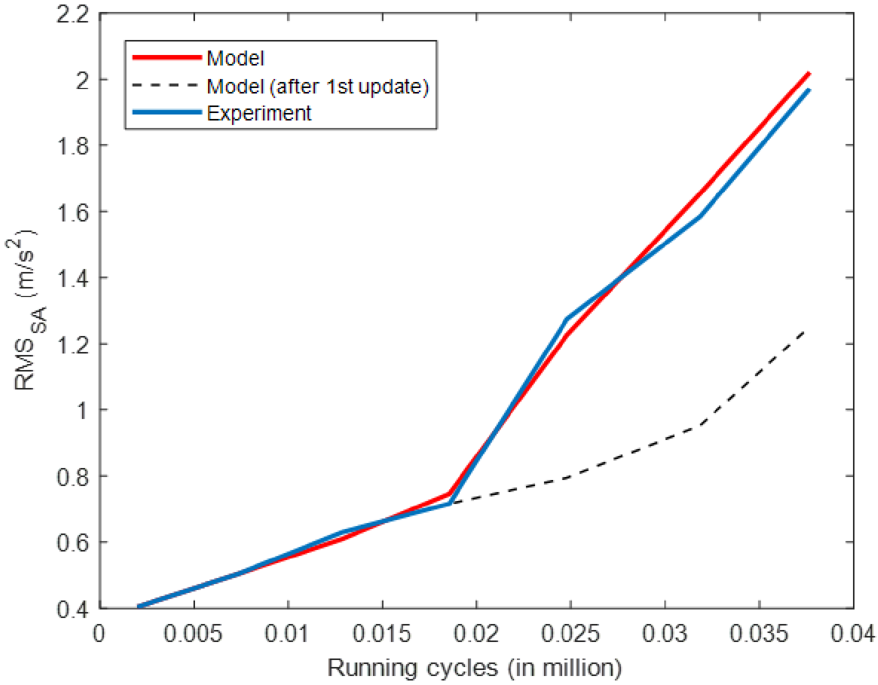

Figure 7.17 RMS$_{SA}$ comparison results of the dry test: experiment and model (after updating)

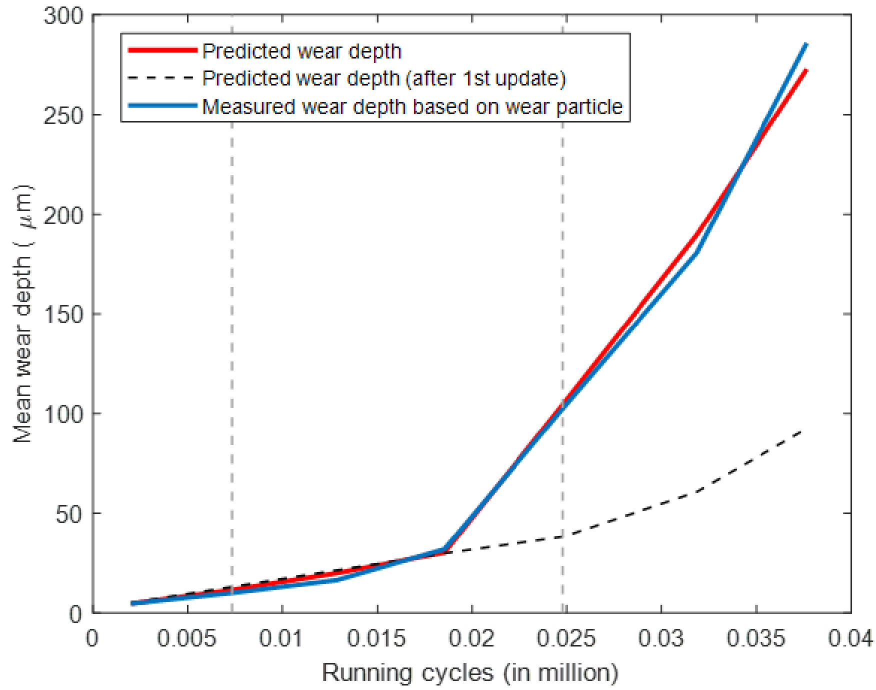

Figure 7.18 Mean wear depth comparison results of the dry test: experiment and model. Note: grey dashed lines indicate when updates are executed

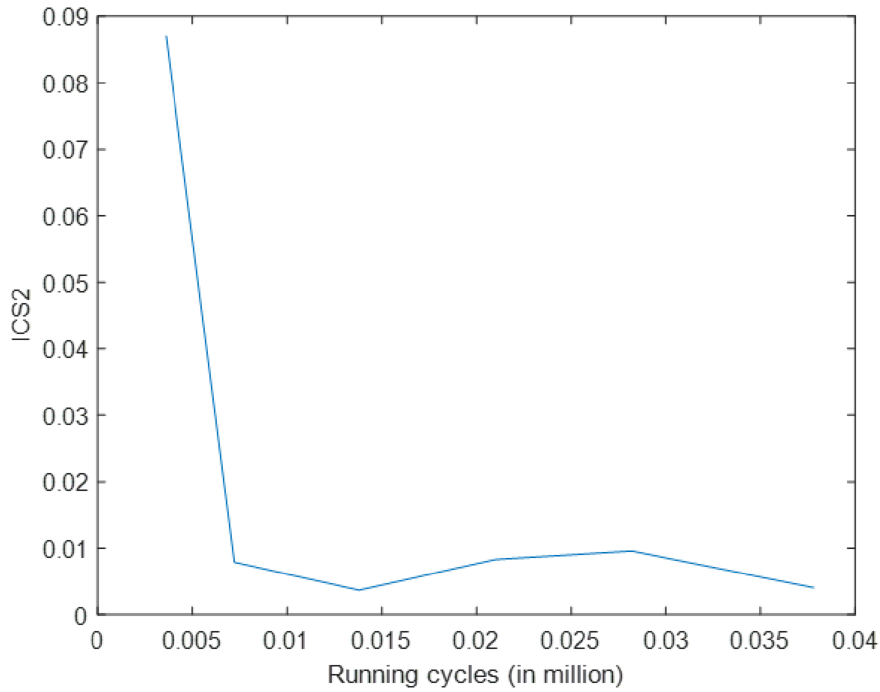

Figure 7.19 Dry test: ICS2 of measured vibrations

The tooth profile prediction results with one update/calibration of K_{wear} are also shown in Figure 7.18 for comparison purposes. It can be seen that the wear rate changes significantly around 0.018 million cycles, and so without the second updating of K_{wear}, there would be a significant under-estimation of the future wear level.

During the dry test, almost no surface pitting was observed from the mould images (as shown in Figure 7.14), and ICS2 of the measured vibrations keeps fluctuating during the wear propagation, as shown in Figure 7.19. Based on the rules introduced in Sections 7.3.3, the surface pitting coefficient was set to zero, and the predicted pitting density is 0% during the dry test. This is consistent with the observation in Ref. [82] that the dominant wear phenomenon in this test is tooth profile change, and very little or no surface pitting occurs.

7.5 Summary

In this chapter, a vibration-based surface degradation monitoring and prediction methodology was proposed to monitor and predict the two common wear events in gears: gear tooth profile change, and surface pitting propagation. Based on the literature review and discussion in Section 7.1, there is no digital twin approach that can monitor and predict the two wear events simultaneously. In the proposed methodology, a simple vibration feature based on a few gear mesh harmonics is used for tracking gear tooth profile changes under different lubrication conditions, and an improved version of Archard's wear model (introduced in Chapter 6) is used in combination with a gearbox dynamic model to predict future worn tooth profiles. An effective and efficient surface pitting model was also proposed in this chapter, and the level of second-order cyclostationarity (ICS2) in the measured vibration signal was used for tracking surface pitting progression.

A key component of the methodology is that through regular and intelligent use of measured vibration signals, the parameters of the two wear models can be updated as necessary, ensuring wear predictions that tend to improve over time. Unique among existing studies in gear-wear prediction, the interaction of the developed dynamic and wear models, along with this updating capability, deliver an approach that is able to monitor and predict the two common wear events (profile change and surface pitting) simultaneously and under different lubrication conditions. Although two calibration steps are required by the approach – one for the dynamic model and one for relating ICS2 to the pitting level – the models are relatively simple. The flexible and evolving nature of the prediction approach means that it could be easily deployed within existing digital twin frameworks, bringing significant potential benefits to gear prognostics in practice. In summary, in this chapter, novel gear surface degradation prediction models and schemes are proposed. Through regular and intelligent use of measured vibration signals, the models can be updated as necessary, ensuring accurate predictions of gear wear propagation can be delivered.

The main limitation of the method in its current form is that a scan (or perhaps a close visual inspection) of the gear surface is required to find the 'scale factor' between ICS2 and the actual pitting level, and this requires that the gearbox be stopped and partially dismantled. Another option is that the scan could presumably be done by endoscopic examination, with almost no dismantling, just access through a small inspection cover; this is widely practised with wind turbine gearboxes [209]. It has also been found that ICS2 tends not to track pitting levels well in the initial stages. To deliver improved pitting propagation predictions, a good future contribution would therefore be to establish a more definitive relationship between ICS2 and pitting level or in developing a more reliable pitting-sensitive vibration indicator.

Chapter 8 Conclusions and future work

The conclusions and recommendations for future research work are presented in this chapter. The chapter begins with a summary of the outcomes of this thesis, regarding the proposed research objectives. Then, the limitations of the studies are discussed, followed by suggested future research directions that would improve the presented work in this thesis.

8.1 Summary of findings and contribution to research

This thesis investigated the interconnection between vibration characteristics and gear wear through signal processing algorithms and modelling techniques to realize accurate gear wear monitoring and prediction using vibration-based techniques. This section summarises the main outcomes of this thesis guided by research objectives.

- **Identification of gear wear mechanism and tracking wear evolution using cyclostationary properties of measured vibrations (Objective 1)**

A novel relationship is proposed in Chapter 4 to represent the internal connection between vibration characteristics and gear surface features. More specifically, the link between the carrier frequency of vibrations f_v and spatial frequency of gear surface f_s was built. The proposed relationship is validated through the cyclostationarity analysis of vibrations and power spectral density (PSD) analysis of the scanned gear surface images.

Based on the achieved understanding from the derived equation, a vibration-based gear wear mechanism identification approach is proposed. More specifically, through the use of cyclostationary properties of vibrations, the abrasive wear and fatigue pitting are separated and identified via spectral coherence map and ICS2-based band selection results. This developed novel online gear wear mechanism identification approach avoids interruption of the operation of the gearbox (in the case of visual inspection, which is the most widely used approach for identification of wear mechanism at present) or a delay in analysing wear debris generated from gear surface, making it be a more practical tool in industry practice.

Moreover, with help of the derived equation and indicator of vibration cyclosationarity, an informative vibration frequency band can be determined, then the fatigue pitting and abrasive wear propagation can be well tracked and monitored using ICS2 of vibration in the corresponding selected appropriate frequency bands. Differently from previous works, the carrier frequencies (spectral content) of the gearmesh-cyclic CS2 components are analysed and used in this research to distinguish and track the two wear phenomena.

- **Dynamic model development (Objective 2)**

A comprehensive dynamic model is developed in Chapter 5, based on the UNSW spur gearbox test rig. And there is no published work on modelling this test rig, whose layout is shown in Figure 3.2. After a series of necessary model validations and calibrations, the natural frequencies of the developed dynamic model and time waveforms match well with the measurements from the actual gearbox transmission system. Thus, the dynamic model can generate contact force and vibration responses, which are close enough to the actual test rig. The developed dynamic model can provide insights into the coupling effects between gear wear and gear dynamic characteristics (e.g., contact force and vibrations). This can benefit the gear maintenance schedule to minimize the consequences of gear wear on the service life of the gear system.

- **Monitoring and prediction of tooth profile changes during wear progression (Objective 3)**

A novel vibration-based updating scheme is developed in Chapter 6 to monitor and predict the gear tooth profile change during gear wear propagation. Unique to previously published work, such as Refs. [21, 92, 184], in the developed vibration-based updating scheme, measured vibrations are compared with simulated vibrations from the dynamic model, to update the coefficient K_{wear} when a deviation from predictions is detected. The developed methodology can track and correct for changes in the gear wear rates, thus allowing reliable gear wear prediction. In addition, the vibration signals can be easily acquired without disturbing the operation of the gearbox, and no gearbox stoppage or disassembly is required to obtain the wear mass (as presented in Ref. [24]).

In the proposed wear prediction scheme, the Archard wear model is improved with consideration of the effect of Hertzian deformation, giving a contact area rather than a line. The improvement makes the calculated wear profile distribution is more reasonable and realistic compared with the original Archard wear model used in the study [21].

- **Development of a digital twin approach for monitoring and prediction of surface pitting and tooth profile changes (Objective 4)**

  A vibration-based surface degradation monitoring and prediction methodology is proposed in Chapter 7 to monitor and predict the two common wear events in gears: gear profile change (e.g., from abrasive wear), and surface pitting propagation. Through regular and intelligent use of measured vibration signals, the parameters of the wear models can be updated as necessary, ensuring wear predictions that tend to improve over time. It is a novel work since no research have been published to report a digital twin methodology that can predict two wear events propagation and validated its effectiveness using measurements from gearbox tests rig.

  To simulate the surface pitting propagation behaviours, an efficient pitting propagation model is also developed based on the Lundberg Palmgren model [80] and presented in Chapter 7. With the developed fatigue pitting model, the accumulated pitting propagation process can be simulated and the impacts on pitting propagation rate from the prior pitting are also taken into consideration.

To conclude, in this research, the wear propagation phenomenon and its consequences on gear tooth surface have been comprehensively investigated and studied with the use of vibration analysis techniques, including signal processing algorithms and modelling methodology. To realize gear wear monitoring, a vibration-based integrated system is developed. With the developed integrated system, the gear wear mechanism can be identified on-line and then its propagation can be well tracked using the developed digital twin approach, so that the remaining useful life of the gear system can be predicted. The developments for gear wear monitoring and prediction in this research bring significant benefits to the research community and industrial practices.

8.2 Recommendations for future work

In this research, vibration-based gear wear monitoring techniques are developed and applied to wear mechanism identification and wear prediction of the fixed-axis gearbox. Considering the kinematic characteristics of the gearbox transmission systems are similar, therefore, the techniques developed in this research should be tested on other gear types and gearing arrangements, including planetary gearboxes, and industrial practices.

Even though the theoretical developments in this research are validated through the relevant experimental investigations, some limitations still exist in the developed techniques presented in this thesis, which will be pointed out as follows, together with corresponding recommendations for future improvements.

1. The limitation of using ICS2 to monitor the fatigue pitting and abrasive wear propagation is that the real wear severity can not be directly assessed from the ICS2 trend, since the mathematical relationship between ICS2 trends and the real severity of gear wear has not been derived in Chapter 4. Therefore, future work will focus on establishing the mathematical relationship between ICS2 and wear severity using the regression analysis theory [210, 211], so that the real wear severity can be quantified once the measured vibration is acquired.

2. There is a limitation of using the Archard wear model to present the wear induced tooth profile change. The Archard model is modelling a significant component of the geographical variation of wear along the tooth flank, more complex dynamics can contribute significantly to the evolution of the wear profile geometry. Therefore, in future work, model development that has the capability of modelling complex wear profile geometry will be considered, such as using Legendre Polynomials [25].
3. In the vibration-based gear wear monitoring and prediction methodology developed in Chapter 7, the ICS2 of measured vibration is used to compare with the predicted fatigue pitting density, and then update the surface pitting coefficient $K_{pitting}$ if necessary. This approach should deliver an accurate prediction of overall surface pitting severity representing an average across the whole surface; however, it can not provide information on the pitting distribution on the gear tooth (from root to tip). Therefore, vibration features that can accurately represent the surface pitting distribution are extremely valuable and should be studied in the future.

References

[1] A. Ramalho, J.C. Miranda, The relationship between wear and dissipated energy in sliding systems, Wear, 260 (2006) 361-367. https://doi.org/10.1016/j.wear.2005.02.121.

[2] K. Mao, Gear tooth contact analysis and its application in the reduction of fatigue wear, Wear, 262 (2007) 1281-1288. https://doi.org/10.1016/j.wear.2006.06.019.

[3] H. Wang, C. Zhou, H. Wang, B. Hu, Z. Liu, A novel contact model for rough surfaces using piecewise linear interpolation and its application in gear wear, Wear, (2021) 203685. https://doi.org/10.1016/j.wear.2021.203685.

[4] P.J.L. Fernandes, C. McDuling, Surface contact fatigue failures in gears, Engineering Failure Analysis, 4 (1997) 99-107. https://doi.org/10.1016/S1350-6307(97)00006-X.

[5] P.K. Singh, Siddhartha, A.K. Singh, An investigation on the thermal and wear behavior of polymer based spur gears, Tribology International, 118 (2018) 264-272. https://doi.org/10.1016/j.triboint.2017.10.007.

[6] R. Shao, W. Hu, Y. Wang, X. Qi, The fault feature extraction and classification of gear using principal component analysis and kernel principal component analysis based

on the wavelet packet transform, Measurement, 54 (2014) 118-132. https://doi.org/10.1016/j.measurement.2014.04.016.

[7] K.F. Brethee, D. Zhen, F. Gu, A.D. Ball, Helical gear wear monitoring: Modelling and experimental validation, Mechanism and Machine Theory, 117 (2017) 210-229. https://doi.org/10.1016/j.mechmachtheory.2017.07.012.

[8] G.E. Morales-Espejel, P. Rycerz, A. Kadiric, Prediction of micropitting damage in gear teeth contacts considering the concurrent effects of surface fatigue and mild wear, Wear, 398-399 (2018) 99-115. https://doi.org/10.1016/j.wear.2017.11.016.

[9] J.A. Williams, A.M. Hyncica, Mechanisms of abrasive wear in lubricated contacts, Wear, 152 (1992) 57-74. https://doi.org/10.1016/0043-1648(92)90204-L.

[10] R.B. Randall, Vibration-based condition monitoring: industrial, aerospace and automotive applications, John Wiley & Sons, 2011.

[11] Z. Peng, T.B. Kirk, Automatic wear-particle classification using neural networks, Tribology Letters, 5 (1998) 249-257. https://doi.org/10.1023/A:1019126732337.

[12] G. Liu, R.G. Parker, Dynamic Modeling and Analysis of Tooth Profile Modification for Multimesh Gear Vibration, Journal of Mechanical Design, 130 (2008). https://doi.org/10.1115/1.2976803.

[13] C. Hu, W.A. Smith, R.B. Randall, Z. Peng, Development of a gear vibration indicator and its application in gear wear monitoring, Mechanical Systems and Signal Processing, 76-77 (2016) 319-336. https://doi.org/10.1016/j.ymssp.2016.01.018.

[14] X. Zhang, W.A. Smith, P. Borghesani, Z. Peng, R.B. Randall, Use of Cyclostationarity to Detect Changes in Gear Surface Roughness Using Vibration

Measurements, Asset Intelligence through Integration and Interoperability and Contemporary Vibration Engineering Technologies, Springer, 2019, pp. 763-771.

[15] Y. Yang, W.A. Smith, P. Borghesani, Z. Peng, R.B. Randall, Detecting changes in gear surface roughness using vibration signals, Acoustics 2015 Hunter Valley, (2015) 1-10.

[16] K. Feng, W.A. Smith, P. Borghesani, R.B. Randall, Z. Peng, Use of cyclostationary properties of vibration signals to identify gear wear mechanisms and track wear evolution, Mechanical Systems and Signal Processing, 150 (2021) 107258. https://doi.org/10.1016/j.ymssp.2020.107258.

[17] P. Rycerz, A. Kadiric, The Influence of Slide–Roll Ratio on the Extent of Micropitting Damage in Rolling–Sliding Contacts Pertinent to Gear Applications, Tribology Letters, 67 (2019) 63. 10.1007/s11249-019-1174-7.

[18] H. Endo, Simulation of gear faults and its application to the development of differential diagnostic technique, School of Mechanical and Manufacturing Engineering, The University of New South Wales, Australia, 2005.

[19] A.A.T. Committee, Appearance of Gear Teeth: Terminology of Wear and Failure, American Gear Manufacturers Association, 40 (1995).

[20] B. Bhushan, Modern tribology handbook, two volume set, CRC press, 2000.

[21] H. Ding, A. Kahraman, Interactions between nonlinear spur gear dynamics and surface wear, Journal of Sound and Vibration, 307 (2007) 662-679. https://doi.org/10.1016/j.jsv.2007.06.030.

[22] R.B. Randall, A New Method of Modeling Gear Faults, Journal of Mechanical Design, 104 (1982) 259-267. 10.1115/1.3256334.

[23] I. Barányi, G. Kalácska, P. De Baets, Characterisation of abrasive worn surfaces by surface microtopography parameters, International Journal Sustainable Construction & Design, 4 (2013).

[24] F. Zhao, Z. Tian, X. Liang, M. Xie, An Integrated Prognostics Method for Failure Time Prediction of Gears Subject to the Surface Wear Failure Mode, IEEE Transactions on Reliability, 67 (2018) 316-327. 10.1109/TR.2017.2781147.

[25] W.D. Mark, Performance-based gear metrology, Wiley Online Library, 2012.

[26] R. Zhang, X. Gu, F. Gu, T. Wang, A.D. Ball, Gear Wear Process Monitoring Using a Sideband Estimator Based on Modulation Signal Bispectrum, Applied Sciences, 7 (2017) 274. https://doi.org/10.3390/app7030274.

[27] G.E. Totten, ASM handbook, Volume 18: friction, lubrication, and wear technology, ASM international, Cleveland, (1992).

[28] Z.K. Zhu, Z.H. Feng, F.R. Kong, Cyclostationarity analysis for gearbox condition monitoring: Approaches and effectiveness, Mechanical Systems and Signal Processing, 19 (2005) 467-482. https://doi.org/10.1016/j.ymssp.2004.02.007.

[29] X. Zhang, J. Kang, J. Zhao, D. Cao, Features for fault diagnosis and prognosis of gearbox, Chemical Engineering Transactions, 33 (2013) 1027-1032.

[30] M. Amarnath, S.-K. Lee, Assessment of surface contact fatigue failure in a spur geared system based on the tribological and vibration parameter analysis, Measurement, 76 (2015) 32-44. https://doi.org/10.1016/j.measurement.2015.08.020.

[31] I. Yesilyurt, F. Gu, A.D. Ball, Gear tooth stiffness reduction measurement using modal analysis and its use in wear fault severity assessment of spur gears, Ndt & E International, 36 (2003) 357-372. https://doi.org/10.1016/S0963-8695(03)00011-2.

[32] J. Mathew, J. Stecki, Comparison of vibration and direct reading ferrographic techniques in application to high-speed gears operating under steady and varying load conditions, Lubrication engineering, 43 (1987) 646-653.

[33] S. Ziaran, R. Darula, Determination of the State of Wear of High Contact Ratio Gear Sets by Means of Spectrum and Cepstrum Analysis, Journal of Vibration and Acoustics, 135 (2013). 10.1115/1.4023208.

[34] C.J. Li, J.D. Limmer, Model-based condition index for tracking gear wear and fatigue damage, Wear, 241 (2000) 26-32. https://doi.org/10.1016/S0043-1648(00)00356-2.

[35] P. Kundu, A.K. Darpe, M.S. Kulkarni, A correlation coefficient based vibration indicator for detecting natural pitting progression in spur gears, Mechanical Systems and Signal Processing, 129 (2019) 741-763. https://doi.org/10.1016/j.ymssp.2019.04.058.

[36] F. Combet, L. Gelman, Novel adaptation of the demodulation technology for gear damage detection to variable amplitudes of mesh harmonics, Mechanical Systems and Signal Processing, 25 (2011) 839-845. https://doi.org/10.1016/j.ymssp.2010.07.008.

[37] A. Raad, J. Antoni, M. Sidahmed, Indicators of cyclostationarity: Theory and application to gear fault monitoring, Mechanical Systems and Signal Processing, 22 (2008) 574-587. https://doi.org/10.1016/j.ymssp.2007.09.011.

[38] H. Ozturk, I. Yesilyurt, M. Sabuncu, Detection and Advancement Monitoring of Distributed Pitting Failure in Gears, Journal of Nondestructive Evaluation, 29 (2010) 63-73. 10.1007/s10921-010-0066-4.

[39] A. Hase, H. Mishina, M. Wada, Correlation between features of acoustic emission signals and mechanical wear mechanisms, Wear, 292-293 (2012) 144-150. https://doi.org/10.1016/j.wear.2012.05.019.

[40] X. Chen, S. Wang, B. Qiao, Q. Chen, Basic research on machinery fault diagnostics: Past, present, and future trends, Frontiers of Mechanical Engineering, 13 (2018) 264-291. 10.1007/s11465-018-0472-3.

[41] N. Sawalhi, R.B. Randall, Simulating gear and bearing interactions in the presence of faults: Part I. The combined gear bearing dynamic model and the simulation of localised bearing faults, Mechanical Systems and Signal Processing, 22 (2008) 1924-1951. https://doi.org/10.1016/j.ymssp.2007.12.001.

[42] A. Al-Shyyab, A. Kahraman, A non-linear dynamic model for planetary gear sets, Proceedings of the Institution of Mechanical Engineers, Part K: Journal of Multi-body Dynamics, 221 (2007) 567-576. https://doi.org/10.1243/14644193JMBD92.

[43] M. Machado, P. Moreira, P. Flores, H.M. Lankarani, Compliant contact force models in multibody dynamics: Evolution of the Hertz contact theory, Mechanism and Machine Theory, 53 (2012) 99-121. https://doi.org/10.1016/j.mechmachtheory.2012.02.010.

[44] C. Zhou, H. Wang, An adhesive wear prediction method for double helical gears based on enhanced coordinate transformation and generalized sliding distance model, Mechanism and Machine Theory, 128 (2018) 58-83. https://doi.org/10.1016/j.mechmachtheory.2018.05.010.

[45] H. Wang, C. Zhou, Y. Lei, Z. Liu, An adhesive wear model for helical gears in line-contact mixed elastohydrodynamic lubrication, Wear, 426-427 (2019) 896-909. https://doi.org/10.1016/j.wear.2019.01.104.

[46] J. Wei, A. Zhang, P. Gao, A study of spur gear pitting under EHL conditions: Theoretical analysis and experiments, Tribology International, 94 (2016) 146-154. https://doi.org/10.1016/j.triboint.2015.08.037.

[47] A. Fernandez del Rincon, F. Viadero, M. Iglesias, P. García, A. de-Juan, R. Sancibrian, A model for the study of meshing stiffness in spur gear transmissions, Mechanism and Machine Theory, 61 (2013) 30-58. https://doi.org/10.1016/j.mechmachtheory.2012.10.008.

[48] K. HAYASHI, Load distribution on the contact line of helical gear teeth: part 1 fundamental concept, Bulletin of JSME, 6 (1963) 336-343.

[49] J. Boerner, Very efficient calculation of the load distribution on external gear sets—the method and applications of the program LVR, Proc. of the 7th International Power Transmission and Gearing Conference, ASME San Diego, 1996, pp. 219-225.

[50] M. Pimsarn, K. Kazerounian, Efficient evaluation of spur gear tooth mesh load using pseudo-interference stiffness estimation method, Mechanism and Machine Theory, 37 (2002) 769-786. https://doi.org/10.1016/S0094-114X(02)00022-8.

[51] J.I. Pedrero, M. Pleguezuelos, M. Artés, J.A. Antona, Load distribution model along the line of contact for involute external gears, Mechanism and Machine Theory, 45 (2010) 780-794. https://doi.org/10.1016/j.mechmachtheory.2009.12.009.

[52] S. Li, Effect of addendum on contact strength, bending strength and basic performance parameters of a pair of spur gears, Mechanism and Machine Theory, 43 (2008) 1557-1584. https://doi.org/10.1016/j.mechmachtheory.2007.12.010.

[53] M. Arafa, M. Megahed, Evaluation of spur gear mesh compliance using the finite element method, Proceedings of the Institution of Mechanical Engineers, Part C: Journal of Mechanical Engineering Science, 213 (1999) 569-579.

[54] Y. Temis, E. Kozharinov, D. Kalinin, Simulation of Gear Systems with Dynamic Analysis, Proceedings of the 14th IFToMM World Congress, 2015, pp. 313-317.

[55] Z. Chen, Y. Shao, Mesh stiffness calculation of a spur gear pair with tooth profile modification and tooth root crack, Mechanism and Machine Theory, 62 (2013) 63-74. https://doi.org/10.1016/j.mechmachtheory.2012.10.012.

[56] J. Lin, C. Teng, E. Bergstedt, H. Li, Z. Shi, U. Olofsson, A quantitatively distributed wear-measurement method for spur gears during micro-pitting and pitting tests, Tribology International, 157 (2021) 106839. https://doi.org/10.1016/j.triboint.2020.106839.

[57] P. Bajpai, A. Kahraman, N.E. Anderson, A surface wear prediction methodology for parallel-axis gear pairs, Journal of Tribology, 126 (2004) 597-605. 10.1115/1.1691433.

[58] J. Brauer, S. Andersson, Simulation of wear in gears with flank interference—a mixed FE and analytical approach, Wear, 254 (2003) 1216-1232. https://doi.org/10.1016/S0043-1648(03)00338-7.

[59] A. Kahraman, H. Ding, A Methodology to Predict Surface Wear of Planetary Gears Under Dynamic Conditions#, Mechanics Based Design of Structures and Machines, 38 (2010) 493-515. 10.1080/15397734.2010.501312.

[60] X. Liu, Y. Yang, J. Zhang, Investigation on coupling effects between surface wear and dynamics in a spur gear system, Tribology International, 101 (2016) 383-394. https://doi.org/10.1016/j.triboint.2016.05.006.

[61] J. Archard, Contact and rubbing of flat surfaces, Journal of applied physics, 24 (1953) 981-988.

[62] T. Osman, P. Velex, Static and dynamic simulations of mild abrasive wear in wide-faced solid spur and helical gears, Mechanism and Machine Theory, 45 (2010) 911-924. https://doi.org/10.1016/j.mechmachtheory.2010.01.003.

[63] M. Priest, C.M. Taylor, Automobile engine tribology — approaching the surface, Wear, 241 (2000) 193-203. https://doi.org/10.1016/S0043-1648(00)00375-6.

[64] J.A. Brandão, P. Cerqueira, J.H.O. Seabra, M.J.D. Castro, Measurement of mean wear coefficient during gear tests under various operating conditions, Tribology International, 102 (2016) 61-69. https://doi.org/10.1016/j.triboint.2016.05.008.

[65] S. Wu, H.S. Cheng, Sliding Wear Calculation in Spur Gears, Journal of Tribology, 115 (1993) 493-500. 10.1115/1.2921665.

[66] M. Amarnath, C. Sujatha, S. Swarnamani, Experimental studies on the effects of reduction in gear tooth stiffness and lubricant film thickness in a spur geared system, Tribology International, 42 (2009) 340-352. https://doi.org/10.1016/j.triboint.2008.07.008.

[67] S. Li, Lubrication and contact fatigue models for roller and gear contacts, The Ohio State University, 2009.

[68] A. Flodin, S. Andersson, Simulation of mild wear in spur gears, Wear, 207 (1997) 16-23. https://doi.org/10.1016/S0043-1648(96)07467-4.

[69] A. Flodin, S. Andersson, Simulation of mild wear in helical gears, Wear, 241 (2000) 123-128. https://doi.org/10.1016/S0043-1648(00)00384-7.

[70] A. Flodin, S. Andersson, A simplified model for wear prediction in helical gears, Wear, 249 (2001) 285-292. https://doi.org/10.1016/S0043-1648(01)00556-7.

[71] A. Kahraman, P. Bajpai, N.E. Anderson, Influence of Tooth Profile Deviations on Helical Gear Wear, Journal of Mechanical Design, 127 (2004) 656-663. 10.1115/1.1899688.

[72] C. Yuksel, A. Kahraman, Dynamic tooth loads of planetary gear sets having tooth profile wear, Mechanism and Machine Theory, 39 (2004) 695-715. https://doi.org/10.1016/j.mechmachtheory.2004.03.001.

[73] S. Li, A. Kahraman, A Transient Mixed Elastohydrodynamic Lubrication Model for Spur Gear Pairs, Journal of Tribology, 132 (2009). 10.1115/1.4000270.

[74] S. Li, A. Kahraman, M. Klein, A fatigue model for spur gear contacts operating under mixed elastohydrodynamic lubrication conditions, Journal of Mechanical Design, 134 (2012). 10.1115/1.4005655.

[75] S. Li, A. Kahraman, A physics-based model to predict micro-pitting lives of lubricated point contacts, International Journal of Fatigue, 47 (2013) 205-215. https://doi.org/10.1016/j.ijfatigue.2012.09.002.

[76] K. Aslantaş, S. Taşgetiren, A study of spur gear pitting formation and life prediction, Wear, 257 (2004) 1167-1175. https://doi.org/10.1016/j.wear.2004.08.005.

[77] C.H. Chue, H.H. Chung, Pitting formation under rolling contact, Theoretical and Applied Fracture Mechanics, 34 (2000) 1-9. https://doi.org/10.1016/S0167-8442(00)00019-7.

[78] Y. Yin, Y.-X. Chen, L. Liu, Lifetime prediction for the subsurface crack propagation using three-dimensional dynamic FEA model, Mechanical Systems and Signal Processing, 87 (2017) 54-70. https://doi.org/10.1016/j.ymssp.2016.09.033.

[79] S. Li, A. Kahraman, A micro-pitting model for spur gear contacts, International Journal of Fatigue, 59 (2014) 224-233. https://doi.org/10.1016/j.ijfatigue.2013.08.015.

[80] G. Lundberg, Dynamic capacity of rolling bearings, IVA Handlingar, 196 (1947) 12.

[81] M. Weibring, L. Gondecki, P. Tenberge, Simulation of fatigue failure on tooth flanks in consideration of pitting initiation and growth, Tribology International, 131 (2019) 299-307. https://doi.org/10.1016/j.triboint.2018.10.029.

[82] S. Dhanasekaran, R. Gnanamoorthy, Gear tooth wear in sintered spur gears under dry running conditions, Wear, 265 (2008) 81-87. https://doi.org/10.1016/j.wear.2007.08.025.

[83] K.J. Sharif, H.P. Evans, R.W. Snidle, Prediction of the wear pattern in worm gears, Wear, 261 (2006) 666-673. https://doi.org/10.1016/j.wear.2006.01.018.

[84] M. Masjedi, M.M. Khonsari, On the prediction of steady-state wear rate in spur gears, Wear, 342-343 (2015) 234-243. https://doi.org/10.1016/j.wear.2015.08.010.

[85] M. Masjedi, M.M. Khonsari, Film Thickness and Asperity Load Formulas for Line-Contact Elastohydrodynamic Lubrication With Provision for Surface Roughness, Journal of Tribology, 134 (2012). https://doi.org/10.1115/1.4005514.

[86] S. Li, Effects of machining errors, assembly errors and tooth modifications on loading capacity, load-sharing ratio and transmission error of a pair of spur gears, Mechanism and Machine Theory, 42 (2007) 698-726. https://doi.org/10.1016/j.mechmachtheory.2006.06.002.

[87] C. Xie, L. Hua, J. Lan, X. Han, X. Wan, X. Xiong, Improved analytical models for mesh stiffness and load sharing ratio of spur gears considering structure coupling effect, Mechanical Systems and Signal Processing, 111 (2018) 331-347. https://doi.org/10.1016/j.ymssp.2018.03.037.

[88] M.B. Sánchez, M. Pleguezuelos, J.I. Pedrero, Approximate equations for the meshing stiffness and the load sharing ratio of spur gears including hertzian effects,

Mechanism and Machine Theory, 109 (2017) 231-249. https://doi.org/10.1016/j.mechmachtheory.2016.11.014.

[89] V. Hegadekatte, J. Hilgert, O. Kraft, N. Huber, Multi time scale simulations for wear prediction in micro-gears, Wear, 268 (2010) 316-324. https://doi.org/10.1016/j.wear.2009.08.017.

[90] H. Zhang, X. Shen, A dynamic tooth wear prediction model for reflecting "two-sides" coupling relation between tooth wear accumulation and load sharing behavior in compound planetary gear set, Proceedings of the Institution of Mechanical Engineers, Part C: Journal of Mechanical Engineering Science, 234 (2020) 1746-1763. 10.1177/0954406219900085.

[91] G. Muthuveerappan, R. Thirumurugan, Prediction of theoretical wear in high contact ratio spur gear drive, 15th National Conference on Machines and Mechanisms, 2011.

[92] D. Park, M. Kolivand, A. Kahraman, Prediction of surface wear of hypoid gears using a semi-analytical contact model, Mechanism and Machine Theory, 52 (2012) 180-194. https://doi.org/10.1016/j.mechmachtheory.2012.01.019.

[93] D. Park, M. Kolivand, A. Kahraman, An approximate method to predict surface wear of hypoid gears using surface interpolation, Mechanism and Machine Theory, 71 (2014) 64-78. https://doi.org/10.1016/j.mechmachtheory.2013.09.002.

[94] S. Sun, S. Wang, Y. Wang, T.C. Lim, Y. Yang, Prediction and optimization of hobbing gear geometric deviations, Mechanism and Machine Theory, 120 (2018) 288-301. https://doi.org/10.1016/j.mechmachtheory.2017.09.002.

[95] S. Raadnui, K. Wangwira, Abrasive Spur Gear Wear Prediction Model: Utilization of the Statistical Design Experiments, The 30th International Congress on Condition Monitoring and Diagnostic Engineering Management, Preston, United Kingdom.

[96] X. Zhao, X. Xu, W. Zhao, Z. Jiang, X. Liu, Trend prediction of wear fault of wind generator high-speed gear using a fusion of UICA and PE method, Cluster Computing, 20 (2017) 427-437. 10.1007/s10586-017-0733-7.

[97] R. Guilbault, S. Lalonde, A stochastic prediction of roughness evolution in dynamic contact modelling applied to gear mild wear and contact fatigue, Tribology International, 140 (2019) 105854. https://doi.org/10.1016/j.triboint.2019.105854.

[98] A. Krishnakumari, A. Perumal, R.C. Panda, Prediction for condition monitoring of wear and film thickness in a gear box, 2013.

[99] P. Kumar, H. Hirani, A. Agrawal, Fatigue failure prediction in spur gear pair using AGMA approach, Materials Today: Proceedings, 4 (2017) 2470-2477. https://doi.org/10.1016/j.matpr.2017.02.099.

[100] I.S. Al-Tubi, H. Long, Prediction of wind turbine gear micropitting under variable load and speed conditions using ISO/TR 15144-1: 2010, Proceedings of the Institution of Mechanical Engineers, Part C: Journal of Mechanical Engineering Science, 227 (2013) 1898-1914. 10.1177/0954406212469593.

[101] H. Jiang, S. Qin, J. Fu, J. Zhang, G. Ding, How to model and implement connections between physical and virtual models for digital twin application, Journal of Manufacturing Systems, 58 (2021) 36-51. https://doi.org/10.1016/j.jmsy.2020.05.012.

[102] Q. Qi, F. Tao, T. Hu, N. Anwer, A. Liu, Y. Wei, L. Wang, A.Y.C. Nee, Enabling technologies and tools for digital twin, Journal of Manufacturing Systems, 58 (2021) 3-21. https://doi.org/10.1016/j.jmsy.2019.10.001.

[103] J. Ma, H. Chen, Y. Zhang, H. Guo, Y. Ren, R. Mo, L. Liu, A digital twin-driven production management system for production workshop, The International Journal of

Advanced Manufacturing Technology, 110 (2020) 1385-1397. https://doi.org/10.1007/s00170-020-05977-5.

[104] Z.Y. Chin, W.A. Smith, P. Borghesani, R.B. Randall, Z. Peng, Absolute transmission error: A simple new tool for assessing gear wear, Mechanical Systems and Signal Processing, 146 (2021) 107070. https://doi.org/10.1016/j.ymssp.2020.107070.

[105] A. Soom, J.-W. Chen, Simulation of Random Surface Roughness-Induced Contact Vibrations at Hertzian Contacts During Steady Sliding, Journal of Tribology, 108 (1986) 123-127. https://doi.org/10.1115/1.3261131.

[106] S. Li, A. Kahraman, A tribo-dynamic model of a spur gear pair, Journal of Sound and Vibration, 332 (2013) 4963-4978. https://doi.org/10.1016/j.jsv.2013.04.022.

[107] L. Deshpande, N. Sawalhi, R. Randall, Gearbox fault simulation using finite element model reduction technique, Proceedings of Acoustics, Gold Coast, Australia, 2011, pp. 111.

[108] Z. Shen, B. Qiao, L. Yang, W. Luo, X. Chen, Evaluating the influence of tooth surface wear on TVMS of planetary gear set, Mechanism and Machine Theory, 136 (2019) 206-223. https://doi.org/10.1016/j.mechmachtheory.2019.03.014.

[109] S. Glodež, Z. Ren, G. Fajdiga, Computational modelling of the surface fatigue crack growth on gear teeth flanks, Communications in Numerical Methods in Engineering, 17 (2001) 529-541. https://doi.org/10.1002/cnm.427.

[110] Q. Ni, J.C. Ji, K. Feng, B. Halkon, A novel correntropy-based band selection method for the fault diagnosis of bearings under fault-irrelevant impulsive and cyclostationary interferences, Mechanical Systems and Signal Processing, 153 (2021) 107498. https://doi.org/10.1016/j.ymssp.2020.107498.

[111] Y.-F. Li, M. Zuo, K. Feng, Y.-J. Chen, Detection of Bearing Faults Using a Novel Adaptive Morphological Update Lifting Wavelet, Chinese Journal of Mechanical Engineering, 30 (2017) 1305-1313. https://doi.org/10.1007/s10033-017-0186-1.

[112] Q. Ni, K. Feng, K. Wang, B. Yang, Y. Wang, A case study of sample entropy analysis to the fault detection of bearing in wind turbine, Case Studies in Engineering Failure Analysis, 9 (2017) 99-111. https://doi.org/10.1016/j.csefa.2017.10.002.

[113] K. Feng, K. Wang, P. Chen, A signal selection scheme through order tracking techniques for planetary gearbox condition monitoring, 2016 Prognostics and System Health Management Conference (PHM-Chengdu), IEEE, 2016, pp. 1-5.

[114] T. Barszcz, R.B. Randall, Application of spectral kurtosis for detection of a tooth crack in the planetary gear of a wind turbine, Mechanical Systems and Signal Processing, 23 (2009) 1352-1365. https://doi.org/10.1016/j.ymssp.2008.07.019.

[115] K. Feng, K. Wang, M. Zhang, Q. Ni, M.J. Zuo, A diagnostic signal selection scheme for planetary gearbox vibration monitoring under non-stationary operational conditions, Measurement Science and Technology, 28 (2017) 035003. https://doi.org/10.1088/1361-6501/aa543e.

[116] H. Endo, R.B. Randall, C. Gosselin, Differential diagnosis of spall vs. cracks in the gear tooth fillet region: Experimental validation, Mechanical Systems and Signal Processing, 23 (2009) 636-651. https://doi.org/10.1016/j.ymssp.2008.08.015.

[117] D. Peng, W.A. Smith, P. Borghesani, R.B. Randall, Z. Peng, Comprehensive planet gear diagnostics: Use of transmission error and mesh phasing to distinguish localised fault types and identify faulty gears, Mechanical Systems and Signal Processing, 127 (2019) 531-550. https://doi.org/10.1016/j.ymssp.2019.03.024.

[118] R. Ma, Y. Chen, Research on the dynamic mechanism of the gear system with local crack and spalling failure, Engineering Failure Analysis, 26 (2012) 12-20. https://doi.org/10.1016/j.engfailanal.2012.05.022.

[119] Y. Li, K. Ding, G. He, H. Lin, Vibration mechanisms of spur gear pair in healthy and fault states, Mechanical Systems and Signal Processing, 81 (2016) 183-201. https://doi.org/10.1016/j.ymssp.2016.03.014.

[120] M.J. Roan, J.G. Erling, L.H. Sibul, A new, non-linear, adaptive, blind source separation approach to gear tooth failure detection and analysis, Mechanical Systems and Signal Processing, 16 (2002) 719-740. https://doi.org/10.1006/mssp.2002.1504.

[121] K. Feng, K. Wang, Q. Ni, M.J. Zuo, D. Wei, A phase angle based diagnostic scheme to planetary gear faults diagnostics under non-stationary operational conditions, Journal of Sound and Vibration, 408 (2017) 190-209. https://doi.org/10.1016/j.jsv.2017.07.030.

[122] C. Kar, A.R. Mohanty, Monitoring gear vibrations through motor current signature analysis and wavelet transform, Mechanical Systems and Signal Processing, 20 (2006) 158-187. https://doi.org/10.1016/j.ymssp.2004.07.006.

[123] P.V. Kane, A.B. Andhare, Critical evaluation and comparison of psychoacoustics, acoustics and vibration features for gear fault correlation and classification, Measurement, 154 (2020) 107495. https://doi.org/10.1016/j.measurement.2020.107495.

[124] K. Feng, P. Borghesani, W.A. Smith, R.B. Randall, Z.Y. Chin, J. Ren, Z. Peng, Vibration-based updating of wear prediction for spur gears, Wear, 426-427 (2019) 1410-1415. https://doi.org/10.1016/j.wear.2019.01.017.

[125] R.F. Handschuh, A.J. Zakrajsek, High-Pressure Angle Gears: Comparison to Typical Gear Designs, Journal of Mechanical Design, 133 (2011). https://doi.org/10.1115/1.4004458.

[126] C. Capdessus, M. Sidahmed, J.L. Lacoume, Cyclostationary processes: application in gear faults early diagnosis, Mechanical Systems and Signal Processing, 14 (2000) 371-385. https://doi.org/10.1006/mssp.1999.1260.

[127] R. Zimroz, W. Bartelmus, Gearbox Condition Estimation Using Cyclo-Stationary Properties of Vibration Signal, Key Engineering Materials, 413-414 (2009) 471-478. https://doi.org/10.4028/www.scientific.net/KEM.413-414.471.

[128] H. Chang, P. Borghesani, W.A. Smith, Z. Peng, Application of surface replication combined with image analysis to investigate wear evolution on gear teeth – A case study, Wear, 430-431 (2019) 355-368. https://doi.org/10.1016/j.wear.2019.05.024.

[129] P. Velex, V. Cahouet Experimental and Numerical Investigations on the Influence of Tooth Friction in Spur and Helical Gear Dynamics, Journal of Mechanical Design, 122 (2000) 515-522. https://doi.org/10.1115/1.1320821.

[130] J. Antoni, G. Xin, N. Hamzaoui, Fast computation of the spectral correlation, Mechanical Systems and Signal Processing, 92 (2017) 248-277. https://doi.org/10.1016/j.ymssp.2017.01.011.

[131] R.W. Bruce, Handbook of lubrication and tribology, volume II: Theory and design, CRC Press, 2012.

[132] F. Combet, L. Gelman, Optimal filtering of gear signals for early damage detection based on the spectral kurtosis, Mechanical Systems and Signal Processing, 23 (2009) 652-668. https://doi.org/10.1016/j.ymssp.2008.08.002.

[133] Y. Chen, X. Liang, M.J. Zuo, Sparse time series modeling of the baseline vibration from a gearbox under time-varying speed condition, Mechanical Systems and Signal Processing, 134 (2019) 106342. https://doi.org/10.1016/j.ymssp.2019.106342.

[134] J.M. Ha, B.D. Youn, H. Oh, B. Han, Y. Jung, J. Park, Autocorrelation-based time synchronous averaging for condition monitoring of planetary gearboxes in wind turbines, Mechanical Systems and Signal Processing, 70-71 (2016) 161-175. https://doi.org/10.1016/j.ymssp.2015.09.040.

[135] S. Braun, The synchronous (time domain) average revisited, Mechanical Systems and Signal Processing, 25 (2011) 1087-1102. https://doi.org/10.1016/j.ymssp.2010.07.016.

[136] J. Antoni, R.B. Randall, Unsupervised noise cancellation for vibration signals: part II—a novel frequency-domain algorithm, Mechanical Systems and Signal Processing, 18 (2004) 103-117. https://doi.org/10.1016/S0888-3270(03)00013-X.

[137] J. Antoni, F. Bonnardot, A. Raad, M. El Badaoui, Cyclostationary modelling of rotating machine vibration signals, Mechanical Systems and Signal Processing, 18 (2004) 1285-1314. https://doi.org/10.1016/S0888-3270(03)00088-8.

[138] Z. Feng, M.J. Zuo, R. Hao, F. Chu, M.E. Badaoui, Gear Damage Assessment Based on Cyclic Spectral Analysis, IEEE Transactions on Reliability, 60 (2011) 21-32. https://doi.org/10.1109/TR.2010.2104017.

[139] W.A. Smith, P. Borghesani, Q. Ni, K. Wang, Z. Peng, Optimal demodulation-band selection for envelope-based diagnostics: A comparative study of traditional and novel tools, Mechanical Systems and Signal Processing, 134 (2019) 106303. https://doi.org/10.1016/j.ymssp.2019.106303.

[140] Q. Ni, K. Wang, J. Zheng, Rolling Element Bearings Fault Diagnosis Based on a Novel Optimal Frequency Band Selection Scheme, IEEE Access, 7 (2019) 80748-80766. https://doi.org/10.1109/ACCESS.2019.2921409.

[141] Jerome Antoni (2021). Fast_SC(x,Nw,alpha_max,Fs,opt) (https://www.mathworks.com/matlabcentral/fileexchange/60561-fast_sc-x-nw-alpha_max-fs-opt), MATLAB Central File Exchange. Retrieved June 14, 2021.

[142] P. Feng, P. Borghesani, H. Chang, W.A. Smith, R.B. Randall, Z. Peng, Monitoring gear surface degradation using cyclostationarity of acoustic emission, Mechanical Systems and Signal Processing, 131 (2019) 199-221. https://doi.org/10.1016/j.ymssp.2019.05.055.

[143] J. Michalski, Surface topography of the cylindrical gear tooth flanks after machining, The International Journal of Advanced Manufacturing Technology, 43 (2008) 513. https://doi.org/10.1007/s00170-008-1737-5.

[144] G.M. Krolczyk, R.W. Maruda, P. Nieslony, M. Wieczorowski, Surface morphology analysis of Duplex Stainless Steel (DSS) in Clean Production using the Power Spectral Density, Measurement, 94 (2016) 464-470. https://doi.org/10.1016/j.measurement.2016.08.023.

[145] J. Michalski, P. Pawlus, W. Żelasko, Surface topography of cylindrical gear wheels after smoothing in abrasive mass, honing and shot peening, Journal of Physics: Conference Series, 311 (2011) 012022. https://doi.org/10.1088/1742-6596/311/1/012022.

[146] S. Li, Finite element analyses for contact strength and bending strength of a pair of spur gears with machining errors, assembly errors and tooth modifications, Mechanism and Machine Theory, 42 (2007) 88-114. https://doi.org/10.1016/j.mechmachtheory.2006.01.009.

[147] J. Hedlund, A. Lehtovaara, Modeling of helical gear contact with tooth deflection, Tribology International, 40 (2007) 613-619. https://doi.org/10.1016/j.triboint.2005.11.004.

[148] V. Simon, FEM stress analysis in hypoid gears, Mechanism and Machine Theory, 35 (2000) 1197-1220. https://doi.org/10.1016/S0094-114X(99)00071-3.

[149] X. Liang, M.J. Zuo, Z. Feng, Dynamic modeling of gearbox faults: A review, Mechanical Systems and Signal Processing, 98 (2018) 852-876. https://doi.org/10.1016/j.ymssp.2017.05.024.

[150] Y. Huangfu, K. Chen, H. Ma, X. Li, H. Han, Z. Zhao, Meshing and dynamic characteristics analysis of spalled gear systems: A theoretical and experimental study, Mechanical Systems and Signal Processing, 139 (2020) 106640. https://doi.org/10.1016/j.ymssp.2020.106640.

[151] C.J. Li, H. Lee, Gear fatigue crack prognosis using embedded model, gear dynamic model and fracture mechanics, Mechanical Systems and Signal Processing, 19 (2005) 836-846. https://doi.org/10.1016/j.ymssp.2004.06.007.

[152] X. Liang, M.J. Zuo, M. Pandey, Analytically evaluating the influence of crack on the mesh stiffness of a planetary gear set, Mechanism and Machine Theory, 76 (2014) 20-38. https://doi.org/10.1016/j.mechmachtheory.2014.02.001.

[153] X. Liang, M.J. Zuo, T.H. Patel, Evaluating the time-varying mesh stiffness of a planetary gear set using the potential energy method, Proceedings of the Institution of Mechanical Engineers, Part C: Journal of Mechanical Engineering Science, 228 (2013) 535-547. https://doi.org/10.1177/0954406213486734.

[154] Z. Wan, H. Cao, Y. Zi, W. He, Y. Chen, Mesh stiffness calculation using an accumulated integral potential energy method and dynamic analysis of helical gears, Mechanism and Machine Theory, 92 (2015) 447-463. https://doi.org/10.1016/j.mechmachtheory.2015.06.011.

[155] D.C.H. Yang, J.Y. Lin, Hertzian Damping, Tooth Friction and Bending Elasticity in Gear Impact Dynamics, Journal of Mechanisms, Transmissions, and Automation in Design, 109 (1987) 189-196. https://doi.org/10.1115/1.3267437.

[156] K. Chen, Y. Huangfu, H. Ma, Z. Xu, X. Li, B. Wen, Calculation of mesh stiffness of spur gears considering complex foundation types and crack propagation paths, Mechanical Systems and Signal Processing, 130 (2019) 273-292. https://doi.org/10.1016/j.ymssp.2019.05.014.

[157] Y. Pandya, A. Parey, Experimental investigation of spur gear tooth mesh stiffness in the presence of crack using photoelasticity technique, Engineering Failure Analysis, 34 (2013) 488-500. https://doi.org/10.1016/j.engfailanal.2013.07.005.

[158] D.C.H. Yang, Z.S. Sun, A Rotary Model for Spur Gear Dynamics, Journal of Mechanisms, Transmissions, and Automation in Design, 107 (1985) 529-535. https://doi.org/10.1115/1.3260759.

[159] X. Liang, H. Zhang, L. Liu, M.J. Zuo, The influence of tooth pitting on the mesh stiffness of a pair of external spur gears, Mechanism and Machine Theory, 106 (2016) 1-15. https://doi.org/10.1016/j.mechmachtheory.2016.08.005.

[160] L. Liu, X. Liang, M.J. Zuo, Vibration signal modeling of a planetary gear set with transmission path effect analysis, Measurement, 85 (2016) 20-31. https://doi.org/10.1016/j.measurement.2016.02.006.

[161] Y. Pandya, A. Parey, Failure path based modified gear mesh stiffness for spur gear pair with tooth root crack, Engineering Failure Analysis, 27 (2013) 286-296. https://doi.org/10.1016/j.engfailanal.2012.08.015.

[162] M. Amabili, A. Rivola, Dynamic analysis of spur gear pairs: steady-state response and stability of the SDOF model with time-varying meshing damping, Mechanical

Systems and Signal Processing, 11 (1997) 375-390. https://doi.org/10.1006/mssp.1996.0072.

[163] A.S. Kumar, T.S. Sankar, M.O.M. Osman, On Dynamic Tooth Load and Stability of a Spur-Gear System Using the State-Space Approach, Journal of Mechanisms, Transmissions, and Automation in Design, 107 (1985) 54-60. https://doi.org/10.1115/1.3258695.

[164] H. Nevzat Özgüven, D.R. Houser, Mathematical models used in gear dynamics—A review, Journal of Sound and Vibration, 121 (1988) 383-411. https://doi.org/10.1016/S0022-460X(88)80365-1.

[165] L. Yutao, T. Di, Dynamics Modeling of Planetary Gear Set Considering Meshing Stiffness Based on Bond Graph, Procedia Engineering, 24 (2011) 850-855. https://doi.org/10.1016/j.proeng.2011.11.2749.

[166] N. Sawalhi, Diagnostics, prognostics and fault simulation for rolling element bearings, School of Mechanical and Manufacturing Engineering, The University of New South Wales, Australia, 2007.

[167] X. Tian, Dynamic simulation for system response of gearbox including localized gear faults, Master of Science Thesis, Department of Mechanical Engineering, University of Alberta Edmonton, Canada, 2004.

[168] Brüel and Kjær. Modal Analysis and Simulation: Structural Testing - Part II. Accessed on https://www.bksv.com/en/Knowledge-center/blog/articles/vibration/structural-testing-part-two. Retreved June 14, 2021.

[169] Y. Guo, T. Eritenel, T.M. Ericson, R.G. Parker, Vibro-acoustic propagation of gear dynamics in a gear-bearing-housing system, Journal of Sound and Vibration, 333 (2014) 5762-5785. https://doi.org/10.1016/j.jsv.2014.05.055.

[170] P.J. Sweeney, R.B. Randall, Gear Transmission Error Measurement Using Phase Demodulation, Proceedings of the Institution of Mechanical Engineers, Part C: Journal of Mechanical Engineering Science, 210 (1996) 201-213. https://doi.org/10.1243/pime_proc_1996_210_190_02.

[171] H. Dai, F. Chen, C. Xun, X. Long, Numerical calculation and experimental measurement for gear mesh force of planetary gear transmissions, Mechanical Systems and Signal Processing, 162 (2022) 108085. https://doi.org/10.1016/j.ymssp.2021.108085.

[172] Y. Huangfu, Z. Zhao, H. Ma, H. Han, K. Chen, Effects of tooth modifications on the dynamic characteristics of thin-rimmed gears under surface wear, Mechanism and Machine Theory, 150 (2020) 103870. https://doi.org/10.1016/j.mechmachtheory.2020.103870.

[173] J. Wojnarowski, V. Onishchenko, Tooth wear effects on spur gear dynamics, Mechanism and Machine Theory, 38 (2003) 161-178. https://doi.org/10.1016/S0094-114X(02)00091-5.

[174] F.K. Choy, V. Polyshchuk, J.J. Zakrajsek, R.F. Handschuh, D.P. Townsend, Analysis of the effects of surface pitting and wear on the vibration of a gear transmission system, Tribology International, 29 (1996) 77-83. https://doi.org/10.1016/0301-679X(95)00037-5.

[175] J.H. Kuang, A.D. Lin, The Effect of Tooth Wear on the Vibration Spectrum of a Spur Gear Pair, Journal of Vibration and Acoustics, 123 (2001) 311-317. https://doi.org/10.1115/1.1379371.

[176] Z. Shen, B. Qiao, L. Yang, W. Luo, Z. Yang, X. Chen, Fault mechanism and dynamic modeling of planetary gear with gear wear, Mechanism and Machine Theory, 155 (2021) 104098. https://doi.org/10.1016/j.mechmachtheory.2020.104098.

[177] B. Hu, C. Zhou, H. Wang, S. Chen, Nonlinear tribo-dynamic model and experimental verification of a spur gear drive under loss-of-lubrication condition, Mechanical Systems and Signal Processing, 153 (2021) 107509. https://doi.org/10.1016/j.ymssp.2020.107509.

[178] W. Chen, Y. Lei, Y. Fu, L. Hou, A study of effects of tooth surface wear on time-varying mesh stiffness of external spur gear considering wear evolution process, Mechanism and Machine Theory, 155 (2021) 104055. https://doi.org/10.1016/j.mechmachtheory.2020.104055.

[179] T.L. Krantz, A. Kahraman, An Experimental Investigation of the Influence of the Lubricant Viscosity and Additives on Gear Wear, Tribology Transactions, 47 (2004) 138-148. https://doi.org/10.1080/05698190490278949.

[180] M.Ş. Tunalioğlu, B. Tuç, Theoretical and experimental investigation of wear in internal gears, Wear, 309 (2014) 208-215. https://doi.org/10.1016/j.wear.2013.11.016.

[181] K. Mao, W. Li, C.J. Hooke, D. Walton, Friction and wear behaviour of acetal and nylon gears, Wear, 267 (2009) 639-645. https://doi.org/10.1016/j.wear.2008.10.005.

[182] J. Andersson, A. Almqvist, R. Larsson, Numerical simulation of a wear experiment, Wear, 271 (2011) 2947-2952. https://doi.org/10.1016/j.wear.2011.06.018.

[183] D. Park, A. Kahraman, A surface wear model for hypoid gear pairs, Wear, 267 (2009) 1595-1604. https://doi.org/10.1016/j.wear.2009.06.017.

[184] Z. Zhang, C. Zheng, M. Wen, S. Yang, H. Li, Q. Du, A Wear Prediction Model for Spur Gears Based on the Dynamic Meshing Force and Tooth Profile Reconstruction, 2nd International Conference on Computer Engineering, Information Science & Application Technology (ICCIA 2017), Atlantis Press, 2016.

[185] Y. Pan, R. Hong, J. Chen, J. Singh, X. Jia, Performance degradation assessment of a wind turbine gearbox based on multi-sensor data fusion, Mechanism and Machine Theory, 137 (2019) 509-526. https://doi.org/10.1016/j.mechmachtheory.2019.03.036.

[186] Y. Pan, R. Hong, J. Chen, W. Wu, A hybrid DBN-SOM-PF-based prognostic approach of remaining useful life for wind turbine gearbox, Renewable Energy, 152 (2020) 138-154. https://doi.org/10.1016/j.renene.2020.01.042.

[187] J.P. Salameh, S. Cauet, E. Etien, A. Sakout, L. Rambault, Gearbox condition monitoring in wind turbines: A review, Mechanical Systems and Signal Processing, 111 (2018) 251-264. https://doi.org/10.1016/j.ymssp.2018.03.052.

[188] S.M. Evans, P.S. Keogh, Wear mechanisms in polyoxymethylene spur gears, Wear, 428-429 (2019) 356-365. https://doi.org/10.1016/j.wear.2019.03.027.

[189] A.C. Petare, N. Kumar Jain, On simultaneous improvement of wear characteristics, surface finish and microgeometry of straight bevel gears by abrasive flow finishing process, Wear, 404-405 (2018) 38-49. https://doi.org/10.1016/j.wear.2018.03.002.

[190] R.I. Trezona, D.N. Allsopp, I.M. Hutchings, Transitions between two-body and three-body abrasive wear: influence of test conditions in the microscale abrasive wear test, Wear, 225-229 (1999) 205-214. https://doi.org/10.1016/S0043-1648(98)00358-5.

[191] D. Huang, Z. Wang, A. Kubo, Hypoid gear integrated wear model and experimental verification design and test, International Journal of Mechanical Sciences, 166 (2020) 105228. https://doi.org/10.1016/j.ijmecsci.2019.105228.

[192] S. Li, A. Kahraman, A fatigue model for contacts under mixed elastohydrodynamic lubrication condition, International Journal of Fatigue, 33 (2011) 427-436. https://doi.org/10.1016/j.ijfatigue.2010.09.021.

[193] E. Charkaluk, A. Constantinescu, H. Maïtournam, K. Dang Van, Revisiting the Dang Van criterion, Procedia Engineering, 1 (2009) 143-146. https://doi.org/10.1016/j.proeng.2009.06.033.

[194] E. Charkaluk, A. Bignonnet, A. Constantinescu, K. Dang Van, Fatigue design of structures under thermomechanical loadings, Fatigue & Fracture of Engineering Materials & Structures, 25 (2002) 1199-1206. https://doi.org/10.1046/j.1460-2695.2002.00612.x.

[195] K.D. Van, M.H. Maitournam, On some recent trends in modelling of contact fatigue and wear in rail, Wear, 253 (2002) 219-227. https://doi.org/10.1016/S0043-1648(02)00104-7.

[196] B. Jalalahmadi, F. Sadeghi, V. Bakolas, Material Inclusion Factors for Lundberg-Palmgren–Based RCF Life Equations, Tribology Transactions, 54 (2011) 457-469. https://doi.org/10.1080/10402004.2011.560412.

[197] T.E. Tallian, Simplified Contact Fatigue Life Prediction Model—Part I: Review of Published Models, Journal of Tribology, 114 (1992) 207-213. https://doi.org/10.1115/1.2920875.

[198] E.V. Zaretsky, J.V. Poplawski, S.M. Peters, Comparison of Life Theories for Rolling-Element Bearings, Tribology Transactions, 39 (1996) 237-248. https://doi.org/10.1080/10402009608983525.

[199] W.A. Smith, R.B. Randall, X.d.C. du Mée, P. Peng, Use of cyclostationary properties to diagnose planet bearing faults in variable speed conditions, 10th DST group international conference on health and usage monitoring systems, 17th Australian Aerospace Congress, 2017, pp. 26-28.

[200] H. Liu, H. Liu, C. Zhu, J. Tang, Study on gear contact fatigue failure competition mechanism considering tooth wear evolution, Tribology International, 147 (2020) 106277. https://doi.org/10.1016/j.triboint.2020.106277.

[201] J.J. Coy, D.P. Townsend, E.V. Zaretsky, An update on the life analysis of spur gears, NASA Techanical Report, 1983.

[202] D. Zhu, N. Ren, Q.J. Wang, Pitting life prediction based on a 3D line contact mixed EHL analysis and subsurface von mises stress calculation, Journal of Tribology, 131 (2009) 041501. https://doi.org/10.1115/1.3195040.

[203] T.A. Harris, M.N. Kotzalas, Rolling bearing analysis: essential concepts of bearing technology, CRC Press, 2007.

[204] E. Ioannides, T.A. Harris, A new fatigue life model for rolling bearings, Journal of Tribology, 107 (1985) 367-377. https://doi.org/10.1115/1.3261081.

[205] A.G. Asuero, A. Sayago, A. Gonzalez, The correlation coefficient: An overview, Critical Reviews in Analytical Chemistry, 36 (2006) 41-59. https://doi.org/10.1080/10408340500526766.

[206] P. Sedgwick, Pearson's correlation coefficient, Bmj, 345 (2012). https://doi.org/10.1136/bmj.e4483.

[207] F.C. Campbell, Fatigue and fracture: understanding the basics, ASM International, 2012.

[208] H. Chang, P. Borghesani, Z. Peng, Investigation on the relationship between macropits and wear particles in a gear fatigue process, Wear, (2021) 203724. https://doi.org/10.1016/j.wear.2021.203724.

[209] R. Zimroz, W. Bartelmus, T. Barszcz, J. Urbanek, Diagnostics of bearings in presence of strong operating conditions non-stationarity—A procedure of load-dependent features processing with application to wind turbine bearings, Mechanical Systems and Signal Processing, 46 (2014) 16-27. https://doi.org/10.1016/j.ymssp.2013.09.010.

[210] S. Chatterjee, A.S. Hadi, Regression analysis by example, John Wiley & Sons, 2015.

[211] E. Uludamar, E. Tosun, K. Aydın, Experimental and regression analysis of noise and vibration of a compression ignition engine fuelled with various biodiesels, Fuel, 177 (2016) 326-333. https://doi.org/10.1016/j.fuel.2016.03.028.